UNIVERSIDADE FEDERAL DE SANTA CATARINA
CAMPUS FLORIANÓPOLIS
PROGRAMA DE PÓS-GRADUAÇÃO EM ENGENHARIA DE AUTOMAÇÃO E SISTEMAS

Diogo Ortiz Machado

Contributions to Exergy-Based Model Predictive Control of Renewable Energy Systems

Florianópolis - SC - Brazil
2022

Diogo Ortiz Machado

Contribuições ao Controle Preditivo Baseado em Exergia em Sistemas de Energias Renováveis

Tese submetida ao Programa de Pós-Graduação em Engenharia de Automação e Sistemas da Universidade Federal de Santa Catarina e ao Programa de Doutorado em Engenharia Automática, Eletrônica e de Telecomunicações da Universidade de Sevilha em cotutela para a obtenção do título duplo de Doutor em Engenharia de Automação e Sistemas e Doutor em Engenharia de Automática, Eletrônica e Telecomunicações.
Orientadores: Prof. Julio Elias Normey-Rico, Dr. (UFSC) e Prof. Carlos Bordons (US)
Coorientador: Prof. Gustavo Artur de Andrade, Dr.

Florianópolis – SC - Brasil/ Sevilha - Espanha
2022

Diogo Ortiz Machado

Contribuciones al Control Predictivo Basado en Exergia en Sistemas de Energías Renovables

Tesis sometida al Programa de Pos Graduación en Ingeniería de Automatización y Sistemas de la Universidad Federal de Santa Catarina y al Programa de Doctorado em Ingeniería Automática, Electrónica y de Telecomunicación de la Universidad de Sevilla en régimen de cotutela para la obtención del título doble de Doctor en Ingeniería de Automatización y Sistemas y Doctor em Ingeniería Automática, Electrónica y de Telecomunicación.
Orientadores: Prof. Julio Elias Normey-Rico, Dr. (UFSC) e Prof. Carlos Bordons (US)
Coorientador: Prof. Gustavo Artur de Andrade, Dr.

Florianópolis – SC - Brasil/ Sevilla - España
2022

Diogo Ortiz Machado

Contributions to Exergy-Based Model Predictive Control of Renewable Energy Systems

Doctoral Dissertation submitted to the Postgraduate Program in Automation and Systems Engineering at Santa Catarina Federal University and to the Doctorate Program in Automation, Electronics and Telecomunications at Seville University in co-supervision to obtain double title of Doctor in Automation and Systems Engineering, and Doctor in Automation, Electronics and Telecomunications Engineering.
Supervisors: Prof. Julio Elias Normey-Rico, Dr. (UFSC) and Prof. Carlos Bordons (US)
Co-supervisor: Prof. Gustavo Artur de Andrade, Dr.

Florianopolis – SC - Brazil/ Seville - Spain
2022

Ficha de identificação da obra elaborada pelo autor,
através do Programa de Geração Automática da Biblioteca Universitária da UFSC.

Machado, Diogo Ortiz
Contributions to Exergy-Based Model Predictive Control of Renewable Energy Systems / Diogo Ortiz Machado ; orientador, Julio Normey-Rico, orientador, Carlos Bordons, coorientador, Gustavo Artur de Andrade, 2022.
166 p.

Tese (doutorado) - Universidade Federal de Santa Catarina, Centro Tecnológico, Programa de Pós-Graduação em Engenharia de Automação e Sistemas, Florianópolis, 2022.

Inclui referências.

Trabalho elaborado em regime de co-tutela.

1. Engenharia de Automação e Sistemas. 2. Control. 3. Model Predictive Control. 4. Exergy. 5. Renewable energy. I. Normey-Rico, Julio. II. Bordons, Carlos. III. Artur de Andrade, Gustavo. IV. Universidade Federal de Santa Catarina. Programa de Pós-Graduação em Engenharia de Automação e Sistemas. V. Título.

Diogo Ortiz Machado

Contributions to Exergy-Based Model Predictive Control of Renewable Energy Systems

O presente trabalho em nível de Doutorado foi avaliado e aprovado, em 08 de novembro de 2022 pela banca examinadora composta pelos seguintes membros:

El presente trabajo a nivel de Doctorado fue evaluado y aprobado el 8 de noviembre de 2022 por el tribunal examinador integrado por los siguientes miembros:

Prof. Julio Normey-Rico, Dr.
Universidade Federal de Santa Catarina (UFSC)

Prof. Carlos Bordons, Dr.
Universidad de Sevilla (US)

Prof. Manuel Berenguel, Dr.
Universidad de Almería

Prof. Daniel Coutinho, Dr.
Universidade Federal de Santa Catarina (UFSC)

Prof. Darci Odloak, Dr.
Universidade de São Paulo

Certificamos que esta é a versão original e final do trabalho de conclusão em cotutela que foi julgado adequado para obtenção do duplo título de Doutor em Engenharia de Controle e Sistemas pela UFSC e Doutor em Engenharia de Automação, Eletrônica e Telecomunicações pela US.

Certificamos que esta es la versión original y final del trabajo de conclusión en cotutela que se consideró apta para la obtención del doble título de Doctor en Ingeniería de Control y Sistemas de la UFSC y Doctor en Ingeniería Automática, Electrónica y Telecomunicación de la US.

_____

Prof. Júlio Normey-Rico, Dr.
Orientador e Coordenador PPGEAS (UFSC)

_____

Prof. Carlos Bordons Dr.
Orientador (US)

Florianópolis – SC - Brasil/ Sevilla – España - 2022

Este trabalho é dedicado aos meus queridos pais e
irmãos, à Fernanda e ao IFRS.

ACKNOWLEDGEMENTS

To Prof. Júlio, probably my last professor in formal education, thank you for your guidance and advice. In those moments, I learned that your excellence comes from efficiency, work, trust, and paving the way for his advisees. Obviously, I must thank you for your kindness and generosity in teaching both the control and the preparation of paellas. To Prof. Gustavo, thank you for your technical contributions and the good conversations and discussions about teaching, which I will cherish in my work. To Paulo Mendes, I am eternally grateful for his dedication and affection during my reception, setting with the work group at UFSC, and during my stay, through tours and churrascos in Florianópolis. I sincerely thank UFSC and PGEAS, the professors and staff, especially Werner, Lívia, and Ênio, for their work and competence. I would also like to thank my laboratory colleagues, José Vergara and his family, Adriano Brandão, Thamiris Lima Costa, Feres Salem, and Alan Kunz Cechinel, for their support, laughter, and the enormous amount of coffee with grounds consumed. What remains are friendships that exceed the excellence of PGEAS.

I am deeply grateful for the guidance of Prof. Carlos during my stay at the University of Seville. The international exchange during the COVID-19 pandemic was made possible by your affection and attention in suggesting I live with the dear Yago Llopart and Maria Esther, for taking me to know Seville, the tapas, and the oloroso de Jerez soon after my arrival. Despite being out of luggage after an unexpected landing in Malaga. Due to the closure of Madrid by the Filomena blizzard (the worst of the century). I thank Prof. Juan Manuel and Prof. Eduardo for welcoming me into the respective research groups they lead and for their contributions and knowledge sharing. For the opportunities to study in the thermosolar absorption plant of the school of engineers and for the support of researchers Adolfo, Antonio, and Kumars Rouzbehi. I thank William for the fruitful friendship, conversations, and tours at Seville and for not letting me forget the most important. I thank Javier Gómes and his family for the invitation and affection during his graduation. Many thanks to all colleagues in the US who contributed to this journey.

To Nubia, my mother and first professor, I thank her life and her professional example. I thank my father and brothers for their affection and trust in this life. I thank Fernanda Bratz for her love, patience, and positive contributions that brought us here. To IFRS for the opportunity to study for a doctorate. To colleagues from the Industrial Automation course for the partnership. The doctoral journey was long, challenging, in the same measure, rich, and fruitful. Between departures and arrivals, I hope my doctorate will contribute and be one more link in these work and research chains for a prosperous future.

AGRADECIMENTOS

Ao Prof. Júlio, provavelmente meu último Professor na educação formal, obrigado pela orientação e pelo convívio. Nesses momentos, aprendi que sua excelência vem da eficiência, trabalho, confiança e por pavimentar o caminho para seus orientandos. Obviamente, devo agradecer a sua simpatia e generosidade em ensinar tanto o controle quanto o preparo de paellas. Ao Prof. Gustavo, agradeço por suas contribuições técnicas e pelas boas conversas e discussões sobre a docência, às quais levarei com carinho na minha atuação. Ao Paulo Mendes, sou eternamente grato pela sua dedicação e afeto tanto durante minha recepção e ambientação com o grupo de trabalho na UFSC, quanto para minha permanência, através de passeios e churrascos em Florianópolis. Agradeço profundamente à UFSC e ao PGEAS, aos professores e servidores, especialmente, ao Werner, Lívia e Ênio, pelo trabalho e pela competência. Agradeço, ainda aos colegas de laboratório, José Vergara e sua família, Adriano Brandão, Thamiris Lima Costa, Feres Salem e Alan Kunz Cechinel pelo apoio, pelas risadas e pela enorme quantidade consumida de café com borra. O que permanece são amizades que perpassam a excelência do PGEAS.

Agradeço profundamente à orientação do Prof. Carlos durante minha estada na Universidade de Sevilha. O intercâmbio internacional durante a pandemia de COVID-19 foi possível por seu carinho e atenção em me sugerir morar com os queridos Yago Llopart e a Maria Esther, por me levar conhecer Sevilha, as tapas, e o olorozo de jerez logo após minha chegada. Isso apesar de estar sem bagagens após um pouso inesperado em Málaga, devido ao fechamento de Madrid pela nevasca Filomena (a pior do século). Agradeço aos Prof. Juan Manuel e Prof. Eduardo por me acolherem nos respectivos grupos de pesquisa que lideram, pelas contribuições e compartilhamento de conhecimento. Pelas oportunidades de estudo na planta de absorção termossolar da escola de engenheiros, e pelo apoio dos pesquisadores Adolfo, Antonio e Kumars Rouzbehi. Agradeço ao William, pela amizade frutífera, pelas conversas, passeios por Sevilha e por não me deixar esquecer do principal. Agradeço ao Javier Gómes e sua família pelo convite e carinho durante a sua formatura. Meu muito obrigado a todos os colegas da US que contribuíram nessa caminhada.

À Dona Nubia, minha mãe e primeira professora, agradeço à vida e ao exemplo profissional. Ao meu pai e meus irmãos agradeço o afeto e confiança nessa vida. Agradeço à Fernanda Bratz pelo amor, paciência e todas as suas contribuições positivas às quais nos trouxeram até aqui. Ao IFRS pela oportunidade de afastamento para doutorado e aos colegas do curso de Automação Industrial pela parceria. A jornada do doutorado foi longa, desafiadora, na mesma proporção que rica e frutífera. Entre partidas e chegadas, espero que o meu doutorado contribua e seja mais um elo nessas correntes de trabalho em prol de um futuro prospero.

“Scientia potentia est”

RESUMO

A unidade temática desta tese é o controle de plantas termossolares de concentração. O trabalho é dividido em três partes. A **Parte I** desenvolve modelos adaptativos neuro difusos para integrar os gêmeos digitais da planta de absorção solar construída na Universidade de Sevilha para futuras aplicações de otimização e controle. Os modelos desenvolvidos descrevem dinamicamente a máquina de absorção e o coletor de concentração solar Fresnel. Ambos processos são complexos e apresentam desafios para a modelagem fenomenológica. Além disso, os dados medidos e disponíveis da planta são incompletos e ruidosos. Assim, *Adaptive Neuro-Fuzzy Inference Systems* (ANFIS) foram utilizados pois eles são capazes de descrever sistemas dinâmicos complexos mesmo com dados de treinamentos incompletos e ruidosos. A quantidade de dados para treinamento e validação foi massiva, gerando modelos generalizados com erros relativos menores que 3% com operação contínua entre o dia e a noite. Além disso, os modelos do coletor Fresnel são inéditos pois descrevem dinamicamente o efeito do desenfoque dos espelhos do coletor na sua temperatura de saída. A **Parte II** apresenta o projeto de controladores na camada regulatória considerando tanto o desfoque proporcional dos espelhos quanto a vazão como atuadores para regulação normal da temperatura de saída. Na literatura, o desenfoque é visto como um último esforço de controle para segurança do coletor solar pois significa desperdício de energia solar. Porém, percebeu-se que o desenfoque é necessário para a operação normal de plantas de concentração solar com múltiplo solar maior que um. Além disso, os controles que consideram desenfoque normalmente utilizam controles MPC híbridos ou máquinas de estados computacionalmente custosos. Nesta tese propõe-se utilizar o sistema de seguimento solar do coletor solar não só para mirar os raios solares para coincidir com a posição do tubo absorvedor mas também variar proporcionalmente o ponto focal da irradiação solar. A ideia básica é manipular o conjunto de espelhos do coletor fresnel como se fossem um espelho parabólico com foco e diretriz variáveis, criando-se, assim, um novo atuador proporcional. Duas técnicas de controle são utilizadas para testar o conceito: split-range e PNMPC com seguimento de referência dos atuadores. Os controladores são simples, apresentam minimização do desperdício de energia com prevenção de superaquecimento, e reduzem eventos de segurança. A **Parte III** desenvolve o controle preditivo baseado em exergia, considerado como a principal contribuição científica desta tese devido ao ineditismo e escassas publicações sobre o tema. O controle baseado em exergia tem o objetivo de obter vantagens em ambas a performance dinâmica e a performance energética em sistemas térmicos de concentração solar. O controle hierárquico utiliza a técnica *Practical Non-linear Model Predictive Control* (PNMPC) na camada regulatória e incorpora a maximização da produção líquida de exergia na camada de otimização. O controle hierárquico baseado em exergia é comparado com abordagens utilizadas na literatura como a maximização da energia líquida produzida e a maximização da temperatura de saída. Os balanços de energia consideram o custo energético de bombeamento, da perda de carga nas tubulações, e a operação intermitente da operação entre dia e noite. O controle baseado em exergia apresenta o melhor desempenho no que tange a produção de energia útil, conforme a segunda lei da termodinâmica, e pode ser aplicado a qualquer sistema de energia renovável.

Palavras-chave: Controle Preditivo. Plantas térmicas de concentração solar. Exergia

RESUMO EXPANDIDO

Introdução

Nossa sociedade está passando eventos disruptivos como a transição energética e a revolução industrial da informação e comunicação. Enquanto a primeira diz respeito às relações entre a humanidade, natureza, mudança climática, consumo e geração responsável de energia, a segunda trata de mais uma onda de rápido desenvolvimento tecnológico humano. Nesse contexto, a ideia dessa tese é escolher uma variável termodinâmica bem definida para quantificar a operação de sistemas de energias renováveis, naturalmente intermitentes e heterogêneas. Posteriormente, incorporar essa variável nos sistemas de controle e automação para determinar sua operação ótima.

A energia solar é limpa e a fonte mais abundante de energia renovável. Plantas de concentração solar podem aproveitar a energia do sol direcionando a irradiação solar em um dispositivo absorvedor, aumentando a energia interna de um dado fluido de trabalho que pode ser utilizado para gerar eletricidade, calor de processo ou climatização. Esse trabalho foca-se no controle supervisório de plantas de concentração, considerando a intermitência natural entre o dia e a noite e as não-linearidades do processo. Para isso, são necessários um modelo dinâmico acurado e uma camada de controle regulatório adequado. O problema é que tais modelos detalhados não estão disponíveis na literatura por causa de complexidades fenomenológicas, não-linearidades, dados ruidosos, incompletos e escassos. Ademais, o projeto de controladores regulatórios das plantas de concentração solar é desafiador devido a gradientes de temperatura, atrasos de transporte, e operação intermitente. Considerando o exposto, esse trabalho desenvolve o modelo de uma planta de absorção solar usando técnicas de soft-computing (**Parte I**), propõe o projeto inovador dos controladores regulatórios de coletores solares do tipo Fresnel utilizando desfoque (**Parte II**) e apresenta um controle supervisório baseado em exergia utilizando-se técnicas de controle preditivo (MPC) (**Parte III**).

A exergia é uma quantidade termodinâmica bem definida que pode ser utilizada como métrica comum para integrar sistemas de energias renováveis. MPC é uma técnica de controle multivariável flexível capaz de incorporar a exergia em sua formulação, entregando uma solução de controle ótimo ao mesmo tempo respeitando restrições do processo. Uma revisão da literatura sobre controle MPC baseado em exergia resultou em dezessete artigos e três teses, iniciando em 2014, indicando que a ideia é nova e o tema tem inúmeras oportunidades. Assim, essa pesquisa doutoral busca responder a seguinte pergunta de investigação “é possível integrar exergia, MPC e energias renováveis em uma estrutura de controle hierárquica?” A hipótese é que sim, e o autor propõe usar uma abordagem hierárquica para testar a ideia.

Objetivos

Estudar e desenvolver um controle hierárquico baseado em exergia para sistemas de concentração solar utilizando técnicas MPC.

1. Desenvolver modelos confiáveis para prova de conceito;
2. Desenvolver controles regulatórios inovadores;
3. Desenvolver controle hierárquico com exergia e MPC;
4. Analisar e comparar a proposta em relação a abordagens tradicionais.

Metodologia

A Parte I desenvolve os gêmeos digitais da planta de climatização por concentração solar instalada no prédio da Escola de Engenheiros da Universidade de Sevilha. O principal objetivo da planta é reduzir a emissão de gases do efeito estufa e o consumo de energia elétrica do sistema de ar-condicionado. Na Parte I, são desenvolvidos e validados modelos adaptativos capazes de descrever dinamicamente a planta durante o dia e a noite, em operação intermitente. A planta é composta por uma máquina de absorção e por um coletor solar de concentração Fresnel. A máquina de absorção utiliza o calor oriundo do coletor solar para gerar frio através de um ciclo termodinâmico de absorção composta por 4 subsistemas. Cabe salientar que uma máquina de absorção é um sistema bastante complexo com efeitos termodinâmicos e fluidodinâmicos complexos. Tal complexidade resulta em modelos fenomenológicos ou com grandes erros no caso de descrever uma ampla faixa de operação, e com erros menores para o caso de uma descrição dinâmica no ponto de operação. O problema da última é que para o caso da planta solar intermitente é insuficiente. Uma grande quantidade de dados de operação da planta estava disponível. Por isso a técnica baseada em dados de soft-computing Adaptive Neuro Fuzzy Inference System (ANFIS) foi escolhida para modelar o sistema, já que é capaz de descrever dinamicamente sistemas complexos mesmo com dados não perfeitos e incompletos, gerando modelos caixa-cinza. Ademais, os dados eram incompletos, ruidosos e descontínuos, por isso realizou-se um pré-tratamento, retirando-se outliers, aplicando-se filtros gaussianos e de média móvel, e preenchendo-se intervalos descontínuos através de interpolação linear. O tempo de adaptação e simulação das redes ficou elevado, assim utilizou-se uma a técnica PCA para redução da matriz de dados de entrada. A saída do PCA foi então alimentada para treinamento e validação dos ANFIS para cada um dos 4 subsistemas da máquina de absorção. Os ANFIS também foram aplicados na modelagem do coletor solar Fresnel. As diferenças com a modelagem da máquina de absorção foram a não utilização de PCA devido à menor dimensão dos dados de entrada, e a comparação do modelo baseado em dados com o modelo fenomenológico utilizado na literatura. O desenvolvimento do modelo fenomenológico do coletor baseou-se nas Equações diferenciais Parciais e identificação dos parâmetros com mínimos quadrados. Então, utiliza-se uma série de dados de três dias contínuos para a validação e análise dos modelos. A Parte II, desenvolve o controle regulatório de plantas de concentração solar partindo-se da proposta de um coletor solar do tipo Fresnel capaz de variar proporcionalmente o ângulo dos espelhos e, assim, o ponto focal dos raios solares. Logo, se torna possível variar a entrada de energia no coletor, disponibilizando-se uma nova variável manipulada contínua para o projetista destes tipos de processos. Dois controladores são implementados e testados com a ideia de manipular tanto a vazão quando o desfoque dos espelhos. O primeiro é um PNMPC que contém os termos do esforço de controle e do valor desejado dos atuadores. Desse modo é possível minimizar a utilização do desfoque para não causar desperdício de energia solar, ao mesmo tempo que é possível reduzir a potência térmica do coletor mantendo-se a temperatura de saída. O segundo controlador proposto é um split-range que utiliza uma lei de controle proporcional integral cujo sinal de controle é dividido em uma faixa. Na primeira metade da faixa o desfoque se mantém zero e a vazão varia até saturação, na segunda metade da faixa a vazão fica saturada em seu máximo e o desfoque é manipulado. A Parte III é considerada a principal contribuição desta tese e apresenta um controlador hierárquico baseado em exergia. A estrutura de controle contém duas camadas: uma de otimização não linear da produção líquida de exergia

e outra de controle não-linear para seguir as referências enviadas pela camada de otimização desde o ligamento até o desligamento. A camada de otimização utiliza o solver fmincon do matlab maximizando 5 funções custo distintas para fins de comparação: energia, exergia, temperatura de saída, energia líquida e exergia líquida. As produções líquidas significam que o custo energético do bombeamento e da perda de carga nas tubulações são subtraídas da produção térmica na saída do coletor. Um controlador PNMPC foi implementado na camada de controle regulatório a fim de seguir a referência dada pela camada de otimização de temperatura tanto na partida, a temperatura ambiente, até a produção, no ponto de operação próximo ao valor máximo de temperatura. Tanto a análise em regime permanente quanto a dinâmica são realizadas.

Resultados e Discussão

Os resultados da **Parte I** indicam que a modelagem baseada em dados da planta solar de absorção com a utilização de técnicas de PCA com ANFIS descrevem adequadamente os processos. Apesar da complexidade e intermitência, os modelos da máquina de absorção apresentam um erro médio absoluto percentual menor que 3,30%, um tempo médio de treinamento por amostra de 121ms, e um tempo médio de simulação por amostra menor que 0.20ms para os ANFIS, considerando cada modelo separadamente. Ademais, a validação dos modelos é realizada com dados de três dias de operação continua com tempos de amostragem de 20s. Portanto, são validações confiáveis sendo os modelos genéricos e adequados para aplicações de controle e otimização. Na **Parte II**, a utilização de um desfoque proporcional resulta em um novo atuador a disposição para o projetista de controle. A sua utilização com a técnica de controle MPC ou split-range gera um controle de coletores solares por concentração segura, pois evita sobreaquecimento, energeticamente ótima, pois desfoca apenas o necessário, sendo ainda capaz de operar nos casos de redução de potência térmica. Assim, ambos os controladores obtêm resultados satisfatórios operando com minimização de desfoque, menores erros de seguimento de referência, reduzindo eventos de segurança do coletor. O controle hierárquico baseado em exergia apresentado na **Parte III** é uma metodologia que pode ser estendida a quaisquer coletores solar de concentração ou sistema de energia renovável. Sua aplicação em um coletor solar de concentração parabólico aumenta a produção de exergia líquida, apresenta o melhor desempenho conforme a segunda lei da termodinâmica e indica que a otimização da produção de energia líquida não é indicada, e que a maximização da temperatura de saída do coletar é uma técnica quase ótima.

Considerações Finais

Ante todo o exposto, esta tese contribui com o corpo de conhecimento de sistemas de controle aplicados a sistemas de energia renovável. Especificamente a aplicação de diversas técnicas de modelagem, controle regulatório e controle supervisório de planta térmicas de concentração solar.

Palavras-chave: Controle Preditivo. Plantas térmicas de concentração solar. Exergia

RESUMEN

La unidad temática de esta tesis es el control de plantas de concentración solar térmica. La obra se divide en tres partes. **Parte I** desarrolla modelos neuro adaptativos difusos para integrar los gemelos digitales de la planta de absorción solar construida en la Universidad de Sevilla para futuras aplicaciones de optimización y control. Los modelos desarrollados describen dinámicamente la máquina de absorción y el colector solar de concentración Fresnel. Ambos procesos son complejos y presentan desafíos para el modelado fenomenológico. Además, los datos medidos y disponibles de planta son incompletos y ruidosos. Por lo tanto, se utilizó *Adaptive Neuro-Fuzzy Inference Systems* (ANFIS) porque son capaces de describir sistemas dinámicos complejos incluso con datos de entrenamiento incompletos y ruidosos. La cantidad de datos para entrenamiento y validación fue masiva, generando modelos generalizados con errores relativos inferiores al 3% con operación continua entre el día y la noche. Además, los modelos del colector fresnel son novedosos porque describen dinámicamente el efecto del desenfoque de los espejos colectores en su temperatura de salida. **Parte II** presenta el diseño de los controladores en la capa reguladora considerando tanto el desenfoque proporcional de los espejos como el flujo como actuadores para la regulación normal de la temperatura de salida. En la literatura, el desenfoque se ve como un último esfuerzo de control para la seguridad del colector solar porque significa desperdicio de energía solar. Sin embargo, se notó que el desenfoque es necesario para el funcionamiento normal de las plantas de concentración solar con múltiplos solares mayores que uno. Además, los controles que consideran el desenfoque suelen utilizar controles MPC híbridos o máquinas de estado computacionalmente costosas. En esta tesis se propone utilizar el sistema de seguimiento solar del colector solar no solo para apuntar los rayos del sol para que coincidan con la posición del tubo absorbente sino también para variar proporcionalmente el punto focal de la irradiación solar. La idea básica es manipular el conjunto de espejos del colector fresnel como si fueran un espejo parabólico con enfoque y directriz variables, creando así un nuevo actuador proporcional. Se utilizan dos técnicas de control para probar el concepto: rango dividido y PNMPC con seguimiento de referencia de los actuadores. Los controladores son simples, minimizan el desperdicio de energía con la prevención del sobrecalentamiento y reducen los eventos de seguridad. **Parte III** desarrolla el control predictivo basado en exergía, considerado como el principal aporte científico de esta tesis debido a la novedad y escasas publicaciones sobre el tema. El control basado en exergía tiene como objetivo obtener ventajas tanto en el rendimiento dinámico como en el rendimiento energético en los sistemas solares térmicos. El control jerárquico basado en exergía se compara con enfoques utilizados en la literatura como la maximización de la energía líquida producida y la maximización de la temperatura de salida. Los balances de energía consideran el costo de energía de bombeo, la pérdida de carga en las tuberías y el funcionamiento intermitente de la operación entre el día y la noche. El control basado en exergía funciona mejor en términos de producción de energía útil, de acuerdo con la segunda ley de la termodinámica, y se puede aplicar a cualquier sistema de energía renovable.

Palabras clave: Control predictivo. Plantas térmicas de concentración solar. Exergía.

ABSTRACT

The thematic unit of this thesis is the control of solar thermal concentrating plants. The work is divided into three parts. **Part I** develops neuro-fuzzy models to integrate the digital twins of the solar absorption plant built at the University of Seville intending further applications to optimization and control. The models dynamically describe the Fresnel solar absorption machine and the Fresnel concentrating collector. Both processes are complex and present challenges for phenomenological modeling. In addition, the measured and available plant data are incomplete and noisy. This study employs *Adaptive Neuro-Fuzzy Inference Systems* (ANFIS) because they can describe complex dynamic systems even with incomplete and noisy training data. The data for training and validation was massive, generating generalized models with relative errors lower than 3% with continuous operation between day and night. In addition, Fresnel collector models are the first to dynamically describe the effect of the defocus of the collector mirrors on their output temperature. **Part II** presents the design of controllers in the regulatory layer considering both the proportional defocus of the mirrors and the flow as actuators for normal regulation of the output temperature. In the literature, the defocus is seen as the last control effort for the safety of the solar collector because it means a waste of solar energy. However, the author noticed that the defocus is necessary for the regular operation of solar concentration plants with solar multiple greater than one. In addition, controls that consider defocusing use computationally costly hybrid MPC controls or state machines. This dissertation proposes using the solar collector's solar tracking system not only to aim the sunbeam to match the position of the absorber tube but also to vary the focal point of solar irradiation proportionally. The basic idea is to manipulate the set of mirrors of the fresnel collector as if they were a parabolic mirror with variable focus and directrix, thus creating a new proportional actuator. Two control techniques test the concept: split-range and PNMPC with actuators target tracking. The controllers are simple, minimize energy waste with overheating prevention and reduce safety events. **Part III** develops an exergy-based model predictive control, considered the main scientific contribution of this thesis due to the novelty and scarce publications on the subject. Exergy-based control aims to gain advantages in both solar thermal systems' dynamic and energetic performances. Hierarchical control runs a *Practical Non-linear Model Predictive Control* (PNMPC) technique in the regulatory layer and incorporates the maximization of net exergy production in the optimization layer. The exergy-based hierarchical control is compared with approaches used in the literature, such as maximizing the net energy produced and maximizing the outlet temperature. The energy balances consider the pumping energy cost, the head loss on the pipes, and the intermittent operation between day and night. According to the second law of thermodynamics, the exergy-based control performs best in terms of useful energy production and can run in any renewable energy system.

Keywords: Model Predictive Control. Concentrating solar thermal plants. Exergy.

LIST OF ABBREVIATIONS AND ACRONYMS

AR	Assessment Reports
CSP	Concentrating Solar Power
EE	Energetic Efficiency
ETSI	Escuela Tecnica Superior de Ingeniería
FLT	First Law of Thermodynamics
GHG	Greenhouse Gas
HVAC	Heat, Ventilation and Air Conditioning
IPCC	Intergovernmental Panel on Climate Change
IRENA	International Renewable Energy Agency
MPC	Model Predictive Control
NMPC	Non-linear Model Predictive Control
RE	Renewable Energy
SLT	Second Law of Thermodynamics
TFEC	Total Final Energy Consumption
UFSC	*Universidade Federal de Santa Catarina* - Federal University of Santa Catarina
UN	United Nations
UNSDG	UN Sustainable Development Goals
US	Universidad de Sevilla

CONTENTS

1 INTRODUCTION

1.1 CLIMATE CHANGE

There is a worldwide effort to reduce the impacts of greenhouse gases (GHG) on the environment. Figure 1 depicts the correlation between CO2 emissions, the main GHG, and the increase of both: temperature and sea level. The variables have been monitored since 1990 based on the best available observational reputable sources (CLIMATE CHANGE IPCC, 2013).

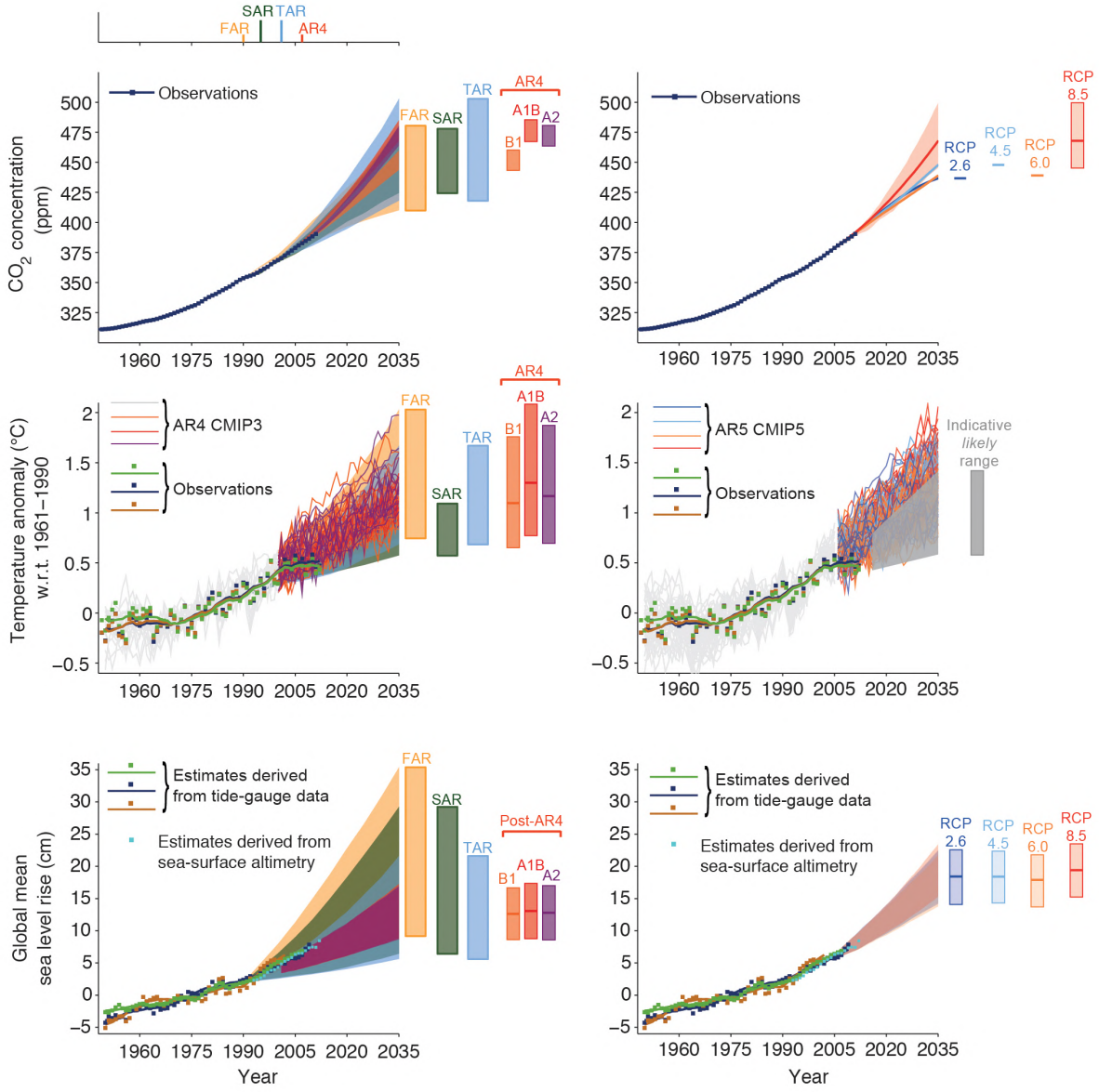

Figure 1 – (Top left) Averaged CO2 concentrations. (Middle left) Estimated changes in the averaged surface temperature anomaly. (Bottom left) Global mean sea level rise (CLIMATE CHANGE IPCC, 2013).

The reliability of the Intergovernmental Panel on Climate Change (IPCC) studies is based on the scientific methodology and continuous analysis of the past values.

Figure 1 depicts various Assessment Reports AR along the years. The left column is the four last AR measured data and projections by the time the reports were made, and the right column data is from the last AR5. A comparison between these columns shows that the AR projections foresee the CO2 and temperature trends. From the first AR to today, the United Nations Conference on Environment and Development, also known as the Rio de Janeiro Earth Summit (1992), the Kyoto Protocol (1995 -2020), the Paris Agreement (2016), and COP25 (2019), has been contributing to mitigate the climate change.

The scientific movement of IPCC influenced policies and public opinion. In this sense, UN launched the Sustainable Development Goals (UNSDG), shown in Figure 2, as a "universal call to action to end poverty, protect the planet and ensure that all people enjoy peace and prosperity by 2030" (UNDP, 2019).

Figure 2 – UNSDG (UNDP, 2019). All items are synergistic among each other. The goals 7, 9, 12 and 17 are catalyst means to reach all objectives. Goal 7 and 9 are the basis of this dissertation.

This thesis contributes to the 7th goal through the 9th goal depicted in Figure 2. The 7th goal can be reached by increasing the Renewable Energy (RE) production or the Energetic Efficiency (EE) levels. In 2018, U$D272 billion were spent on renewable energies, representing 65,4% of the total invested in new power capacity (BLOOMBERGNEF, 2019). Despite economic advances, it seems that the costs are not at an affordable level. For example, it appears that the world will not fulfill the Sustainable Development Goal 7 or the Paris Agreement, which seeks to hold the increase in global average temperature to below 2 ℃ (United Nations). In addition, the global carbon dioxide emissions grew 1.7% due to fossil fuel consumption evidencing higher costs of RE (APPAVOU et al., 2019).

Some advances have been made toward climate change through renewable energies. Although, much more technology development is necessary to match the emerging demands and even more to reach a turning point in the environmental and

energetic problems. This dissertation proposes merging exergy and MPC features as well as new models and control strategies for RE systems.

1.2 AFFORDABLE AND CLEAN ENERGY, INDUSTRY AND INOVATION

Even though the policies and economic investments are driving the global energy matrix toward a renewable network, enabling accessible and clean energy demands tackling some technical drawbacks. There are two ways to unlock this condition: (i) by increasing the RE offer, and consequently, the production (generation-side); or (ii) by increasing the energy efficiency (consumption-side).

RE is a way to generate clean energy. RE power has been steadily growing in the last four years, according to Renewables 2019 Global Status Report. In 2019, renewables grew by 18 Gigawatts in comparison to 2018. Also, when the report was made, by the end of 2018, it was expected that the generation of RE electricity share worldwide would reach 26% and maintain 18.1% of the TFEC, reaching 66% of Total Primary Energy Supply by 2050 (INTERNATIONAL RENEWABLE ENERGY AGENCY (IRENA), 2018, p. 23). By the time this dissertation was written, the TFEC value could not be evaluated. These indicators were driven by stable policies for RE which were adopted in 169 countries. Those facts have attracted policymakers, market agents, and technology-enabling companies (storage, heat pumps, automation, electric vehicles, smart grids, efficiency). However, there is still a lack of solutions, and plenty of opportunities (APPAVOU et al., 2019).

Renewable Energy generation together with consumption reduction are powerful means to counteract climate change. IPCC outlined two pathways for consumption reduction: technology-specific (energy efficiency) and behavior-specific (energy conservation). Several governmental initiatives in this sense are in pace, for example, the strategic plan from 2016 to 2020 of the Office of Energy Efficiency and Renewable Energy of USA (OFFICE OF ENERGY EFFICIENCY & RENEWABLE ENERGY, 2016). This plan sets two out of seven goals to increase the RE generation and improve energy efficiency. Also, the IRENA considers EE and RE as the main pillars of the energy transition and points to the strong synergies between them as a target area for policymakers and researchers. IRENA points that Renewable Energy and Energy Efficiency, coupled with deep electrification of end-uses, can provide over 90% of the reduction in energy-related CO_2 emissions"(INTERNATIONAL RENEWABLE ENERGY AGENCY (IRENA), 2018, p. 9, 14 and 22).

So, EE initiatives and increasing the RE generation is a trend that decreases the cost of renewables and stimulates technologies and policies on each side of the energy market. This work aims to use exergy as an efficiency index to operate in a MPC structure and develop a technology-specific solution for the operation of renewable energy processes with a selectable compromise between RE production and process

efficiency.

1.3 COMMON SCALE FOR OUR ENERGY FUTURE

The improvement of energy efficiency and the transition to renewable energy are two main climate policies to meet low carbon emission levels and to mitigate the climate change. Thereby, the choice of a variable which could properly represent a system is a key for applications using control techniques. The Second Law of Thermodynamics efficiency, or exergy efficiency, stands alone in offering a common scale for national, economy-wide energy efficiency measurement. Exergy definition rely on environment information, due to this, "the link between exergy and environment is more important than that between energy and the environment" (ROSEN, 2002). Besides, a exergy balance is a procedure generally applicable, (EUROPE, 2016, p. 12). Exergy is stated as (SCIUBBA; WALL, 2007, p. 3):

Definition 1. Exergy is the maximum theoretical useful work obtained if a system S is brought into thermodynamic equilibrium with the environment by means of processes in which the S interacts only with this environment.

Or, alternatively (MORAN; SHAPIRO, 2006, p. 278):

Definition 2. Exergy can be regarded as the magnitude of the minimum theoretical work input required to bring the system from the dead state to the given state.

The exergy approach is a tool to design useful energy systems, and account the production activity impact on the environment. Constrained exergy, or isolated available energy in a system, is the potential to drive changes. Available exergy exists when it is unconstrained and flows through its boundaries to the surroundings, or the dead state, cleverly defined as the earth environment reference. In the process, products and goods are made, irreversibilities are generated, outlets and wastes are diffused in the environment. In this way, the exergy concept can measure process usefulness for human, also the human harmfulness for environment due to production activity (DINCER; ROSEN, 2007, p. 37, 44, 50). Because of exergy features, it has been attracting the researcher's interest:

> "in 1970, about 50 articles on exergy or Available Energy were published in archival journals or presented at workshops and conferences; in 2004, this number by far exceeded 500. All major current Energy Engineering Journals publish on the average 1 or 2 articles on exergy-related concepts in each issue: since 2000 there is an International Journal of Exergy" (SCIUBBA; WALL, 2007, p. 2)."

With thermodynamic development and scientists understanding that the exergy concept can help solving the interdisciplinary problem of sustainable development, the

exergy idea is reaching policymakers, institutions and governments. Laitner (2015) study technical advantages on USA economy, stating that "if policy makers and business choose to develop those opportunities, exergy efficiency could provide as much as 60% of the needed reductions of GHG emissions by 2050 increasing U.S. economy robustness" (LAITNER, 2015, p. 248). Brockway et al. (2015) develops an exergy study in China's energy matrix and states that "useful work is a more suitable parameter for energy and economic analysis than primary energy" (BROCKWAY et al., 2015, p. 900). From the EU perspective, Kjelstrup, Dewulf, and Nordén (2015) and Hernandez and Cullen (2019) points several exergy advantages such as:

- Absolute measure: a quantity that can be used to compare technologies,
- Optimization: Minimum entropy production means maximum efficiency,
- A measure of energy and resource quality,
- A footprint index that promotes industrial efficiency,
- A measure for optimal use of limited material resources,

This dissertation seeks to contribute to exergy approach to enhance renewable energy systems control. The idea is that exergy can define process control variables setpoints such as temperature, flow, pressure, determining a intermittent process operation considering sustainable development performance indexes.

All in all, the application of exergy concepts is a way to tackle globalized economy and complex integrated energy systems. As afforested, several policy, laws and technological developments (ROMERO; LINARES, 2014) in this area are in course. However, most of the studies and techniques are applicable in steady state systems which is not the case for most of the renewable energy systems because of the intermittent nature of the sun. Besides, the few works that deals with exergy dynamics have a trade-off between using linear or non-linear MPC and the computational burden and linearisation error. Thereby, as discussed (EUROPE, 2015):

> a major challenge in striving for energy efficiency is the selection of technological systems, particularly given the need to consider multiple environmental, economic and social concerns.

Therefore, there are challenges an opportunities regarding exergy-based control of renewable energy systems. To tackle this question the author proposes a hierarchical approach using exergy-based PNMPC. The hypothesis is that embedding exergy in a hierarchical control structure separates the time scales and performance and process control indexes generating a better decision. It is worth saying that the review about the state-of-the-art of exergy-based MPC is given in Chapter 2. Next, the Objectives are set, then the text structure defined, and, lastly, the scientific contributions are given in Sections 1.4, 1.5, and 1.6, respectively.

1.4 OBJECTIVES

1.4.1 General Objective

To study and develop a hierarchical exergy-based control framework of concentrating solar systems using MPC techniques.

1.4.2 Specific Objectives

1. To develop reliable models for proof of concept of exergy-based-control.
2. To develop innovative regulatory process controllers.
3. To design hierarchical control with exergy and MPC in their formulation.
4. To analyze possible advantages of the proposals over traditional strategies through well-defined numerical comparative studies.

1.5 TEXT ORGANIZATION

During the development of this dissertation, the author made part of a PETROBRAS CSP plant design project and visited the DENiM and OCONT SOLAR projects. The latter two were in Spain through Fundación Carolina and CAPES international scholarships. These projects and scholarships had specific objectives and processes that influenced this dissertation organization.

While the PETROBRAS project aimed to design and construct Brazil's first concentrating CSP plant, the Fundación Carolina scholarship had the main objective of contributing to the 7^{th} UNSDG. The CAPES scholarship aimed to develop Control, Automation, Informatics in Industry and Services 4.0. The DENiM project aims to develop an interoperable digital intelligence platform enabling a collaborative approach to industrial energy management through IoT, digital twins, energy modeling, control, and optimization. Lastly, the OCONT SOLAR project aims to develop new MPC algorithms that use mobile solar sensor estimations and predictions to yield safer and more efficient operation of the plants allowing the effective integration of solar energy in systems. It is worth saying that the Spanish projects, and, therefore, the scholarships, focused on applying the research effort on the concentrating solar absorption cooling plant installed on the rooftop of the *Escuela Técnica Superior de Ingeniería* ETSI university building.

This work is a joint dissertation between the Santa Catarina Federal University UFSC and Seville University US due to these projects, processes and stays in Spain. The author developed a hierarchical exergy-based control and an innovative defocus concept inside the PETROBRAS CSP project. Furthermore, during his stay at Seville University, he developed a digital twin of a Fresnel Solar Collector, a digital twin of an Absorption Chiller, designed controllers using proportional defocus as manipulated variable, and designed a new whole ETSI absorption plant regulatory controller.

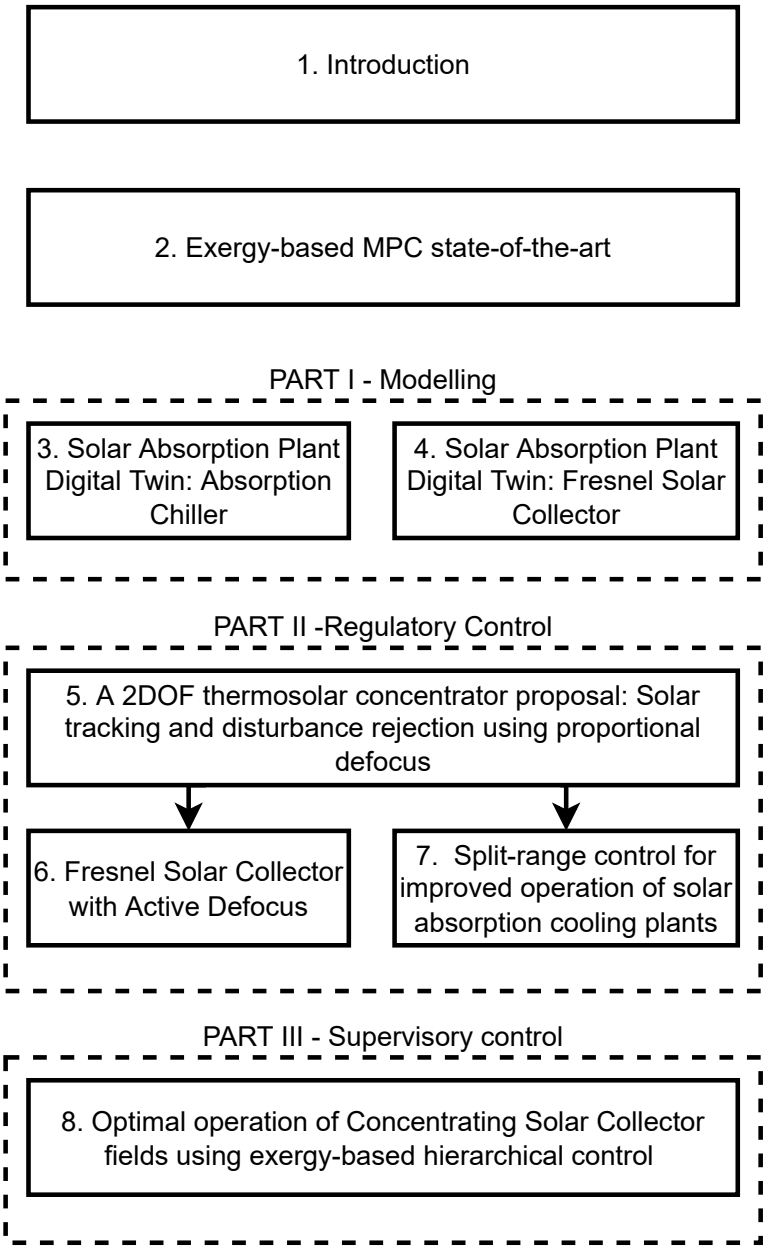

Figure 3 – Text organization where each chapter is an article detailed in Table 1

This doctoral dissertation organizes the results as a compilation of articles in chapters accordingly to Figure 3. The document is divided in initial chapters of introduction and state-of-the art of exergy-based MPC, then the document is divided in three parts. Part I consists mainly in the development of the digital twins, or adaptive models, of the absorption plant installed in the ETSI. Part II consists in regulatory controllers design considering proportional solar collectors mirrors' defocus. Lastly, Part III consists in the supervisory contribution considering the exergy-based hierarchical controls.

1.6 SCIENTIFIC CONTRIBUTIONS

Summarizing, our society faces disruptions such as the energy transition and the information and communication industrial revolution. While the first regards the relation between humankind, nature, climate change, and responsible consumption, the second relates to the human fast technological advances. Therefore, the idea of this dissertation starts with choosing a well-defined, common scale, thermodynamic value to quantify intermittent, heterogeneous renewable energy systems. In addition, to qualify, the energy flows from and to the environment. Then, incorporating this quantity into automation and control systems to drive operation. The work seeks to contribute to affordable and clean energy objectives (UNDP, 2019) using control and automation technologies.

Solar energy is clean and the most abundant renewable energy source. Concentrating solar plants can harvest solar energy by directing the solar beam into an absorber device, increasing the internal energy of a given work fluid, and using this heated fluid to generate electricity, process heat, or air-conditioning. This work focus on supervisory control of concentrating plants, considering their natural intermittency between day and night and non-linearities. To do so, accurate dynamic models and adequate regulatory control are necessary. The problem is that such systems' reliable, detailed models are unavailable due to complex phenomenological effects, non-linearities, and noisy, incomplete, or scarce data. In addition, concentrating solar plants' regulatory layer control design is challenging due to temperature gradients, dead-time, and intermittent operation. The contributions of this doctoral dissertation are (Part I) concentrating absorption plant modeling using soft computing techniques, (Part II) innovative Fresnel solar collectors regulatory control design using defocus, and, finally, (Part III) exergy-based supervisory control design using MPC techniques. The latter is the main contribution of this work.

Exergy is a general well-defined thermodynamic quantity that can work as a standard measure to integrate heterogeneous energy systems. MPC is a flexible multivariable control technique capable of embedding exergy in its formulation, delivering an optimal control solution, while handling constraints. A literature review regarding exergy-based MPC resulted in seventeen papers and three doctoral dissertations, starting in 2014, indicating that the idea is new and the theme has opportunities. Thus, this doctoral investigation seeks to answer the research statement if " it is possible to integrate exergy, MPC, and renewable energy systems in a hierarchical framework?". The hypothesis is yes, and the author proposes using a hierarchical approach to test the control philosophy.

1.6.1 Publications

The author wrote eight articles during the doctoral period. Four were published/submitted to journals, three in international conferences, and one accepted for presentation at a Brazilian congress. The articles are depicted on Table 1. Note that the articles from one to six compose this doctoral dissertation accordingly to the text organization depicted in the schematic of Figure 3. Chapters 3 and 4 have submitted status, yet they make up the document as they share the same thematic unit and give a homogeneous structure to the dissertation. Thus, only articles 4 to 8 composed the request for this doctoral dissertation by compendium.

Table 1 – Published and submitted works.

nº	Chapter. Article	Journal/ Conference	JIF Rank - Quartile[1]	Qualis CAPES[2]
1.	**Chapter 3**[3] Solar Absorption Plant Digital Twin: Absorption Chiller (Submitted)	Renewable Energy	25/119 - Q1	A1
2.	**Chapter 4**[3] Solar Absorption Plant Digital Twin: Fresnel Collector (Submitted)	Applied Energy	15/119 - Q1	A2
3.	**Chapter 5.** A 2DOF Thermosolar Concentrator Proposal: Solar Tracking and Disturbance Rejection Using Proportional Defocus (MACHADO, Diogo O.; NORMEY-RICO; ANDRADE, 2020)	Solar World Congress 2019	-	-
4.	**Chapter 6.** Fresnel Solar Collector Control With Active Defocus (MACHADO, Diogo O. et al., 2022)	European Control Conference 2022	-	-
5.	**Chapter 7.** Split-range control for improved operation of solar absorption cooling plants (MACHADO, Diogo Ortiz et al., 2022b)	Renewable Energy	25/119 - Q1	A1
6.	**Chapter 8.** Optimal operation of Concentrating Solar Collector fields using exergy-based hierarchical control (MACHADO, Diogo Ortiz et al., 2022a)	Energy	24/119 - Q1	A2
7.	Fresnel Solar Collector: distributed parameters model indentification (accepted for presentation)(translation from Portuguese)	Congresso Brasileiro de Automática 2022	-	-
8.	Neuro-Fuzzy Digital Twin of a High Temperature Generator (SALAZAR et al., 2022)	Symposium on Control of Power and Energy Systems 2022	-	-

[1] JIF - Journal Impact Factor of 2021 Journal Citation Reports. Energy and Fuels category quartile.
[2] Engenharias IV.
[3] These articles were not considered to solicit doctoral dissertation by compendium.

Next, a brief description of each chapter/article and the respective scientific contribution are given.

Chapter 3 develops a Digital Twin of the Absorption chiller using Adaptive Neuro-Fuzzy Inference Systems (ANFIS) for modelling its four subprocesses. The models

are the first to consider the whole operational range of a double-effect absorption chiller, considering day and night intermittency and using massive data for training and validation. The models have high accuracy and precision and are available for download with the measured data for validation. Note that this article is not published and did not compose the solicitation for dissertation compendium, although it is included in the document because it compose the thematic unity of the work.

Chapter 4 develops digital twins of a Fresnel solar collector using ANFIS and Partial Differential Equations models with a parameter identification. The digital entities are innovative because they are the first that considers the mirrors defocus in the dynamic model validation. Besides, there is a comparison between the models regarding the computational burden and errors. The training and validation consider a huge amount of real data, and the resulting digital entities have high accuracy and precision. Both models and data are available in a repository for reproducibility. Note that this article is not published and did not compose the solicitation for dissertation compendium, although it is included in the document because it compose the thematic unity of the work.

Chapter 5 proposes a novel Fresnel operation concept regarding the mirror's solar tracking mechanism. It proposes using the discretized Fresnel solar collector mirrors in the solar tracking mechanism to simulate a parabolic mirror capable of changing its focal point. A variable focal point can proportionally change the solar beam energy density, creating a new defocusing feature. The result is using the tracking mechanism as a proportional control actuator and not as a discrete safety mechanism, contributing to increasing controllability. The problem is that defocusing means wasting energy, question which is solved in next Chapter 6 and Chapter 7.

Chapter 6 main finding is that defocusing solar collectors mirrors is a necessary manipulated variable to avoid overheating in solar concentrating plants during regular operation. Concentrating solar plants normally have supersized solar fields concerning the power block demand. Therefore, the case where the solar field power generation is greater than the power block demand should not be seen as abnormal but as a typical event that the proportional defocus feature can tackle. The scientific contributions are a plant and control design integration, and a PNMPC capable of using the proportional defocus concept with actuator's target tracking to minimize the defocus action.

Chapter 7 describes the design of the regulatory level of the solar absorption plant, specifically, the fresnel solar collector and the high-temperature generator controllers. The work proposes the first application of a split-range advanced control technique applied in a solar collector to manipulate both flow and mirrors defocus. This technique divides the controller output, manipulating only the flow until saturation and considering full mirrors focus. If the flow saturates, it stays at the maximum, and the mirror focus becomes the actuator. In addition, the HTG controller changes from on-off

to a PI rule. The results show notable advantages in the plant stability, control error, actuators effort, and safety actions reduction.

Chapter 8 develops an optimal exergy-based hierarchical control. The structure uses a non-linear exergy optimization layer that sends the steady-state optimal temperature set-point to a non-linear Model Predictive Control layer. The problem considers process intermittency (start-up, operation, shut-down), operational constraints, and pump power. The innovative exergy-based hierarchical control gives a generalized enhanced second law of thermodynamics performance, independently of solar collector process parameters.

In summary, this doctoral dissertation's leading scientific contributions are: **Part I** - Digital twins modeling of a solar absorption cooling plant. **Part II** - An innovative proportional defocus operation of Fresnel concentrating solar collectors that results in a new manipulated variable for controlling such systems. Additionally, two controllers applications: one active defocus PNMPC and one split-range advanced control. **Part III** - A novel hierarchical exergy-based control structure with a generalized and optimal operation considering a solar parabolic concentrating solar collector.

This organization section highlights the scientific contributions, giving unity to the dissertation. Note that among the basic concepts, there is no discussion of processes and MPC in the Introduction or in the Chapter 2 because each chapter will define and discuss the processes and controller techniques. Therefore, to avoid repetition of these subjects, these matters were suppressed. Accordingly, the next chapter presents exergy fundamentals and review of exergy-based MPC, that will not be thoroughly retaken in each chapter.

2 EXERGY-BASED MODEL PREDICTIVE CONTROL: STATE-OF-THE-ART

2.1 THERMODYNAMIC FOUNDATIONS AND EXERGY DEFINITION

Current energy systems management demands modern and advanced control techniques. Among all, Model Predictive Control is widely used since it is, among the already mentioned characteristics, a model-based technique. This feature allows to use predictions of the future behavior of a system to act before a variable measurement. Various modeling techniques are available to represent mathematically a process behavior and the phenomenological approach resides on apply physics and sciences laws to determine such models. These laws have the advantages to be extrapolated once these mathematical representations are general, thus, applicable to a wide range of operation, systems and processes.

Considering Solar Power Plants, which are thermodynamic cycles and subjects of this dissertation, and that phenomenological modeling is based on application of mass and thermodynamic laws, it seems reasonable to use both the FLT and the Second Law of Thermodynamics (SLT) to control design. The first one is widely used in the form of conservative energy balances; however, the second law is not and could offer more information to the controller in order to attain better performance. Thereby, this section defines the thermodynamic basis of this dissertation and gives the SLT statements to contextualize its application on exergy-based control. This section is mainly based on the book of (MORAN; SHAPIRO, 2006).

The roots of exergy concept development reside on classical thermodynamics, probably started when Carnot stated that "the work that can be extracted of a heat engine is proportional to the temperature difference between the hot and cold reservoir" (CARNOT, 1824). After him, Clapeyron, Rankine, Thomson, contributed to developments until, finally, Clausius stated the second law of thermodynamics that "it is impossible for any system to operate in such a way that the sole result would be an energy transfer by heat from a cooler to a hotter body" . From this, Kevin-Planck stated the second law in such a way that it could be analytically expressed. The statement is that "it is impossible for any system to operate in a thermodynamic cycle and deliver a net amount of energy by work to its surroundings while receiving energy by heat transfer from a single thermal reservoir". Thermal reservoir is a special kind of system that always remains at constant temperature even though energy flow across his bounds by heat transfer. It is and ideal system which can be approximated by large systems like the environment, for example. To express the Kelvin-Planck statement analytically, two procedures are needed, first, an energy balance, described by Equation (1), and, second, a thermodynamic cycle concept (Equation (3)) (MORAN; SHAPIRO, 2006). The energy balance is expressed as

$$E_2 - E_1 = Q - W, \tag{1}$$

where E is energy, Q is heat and W is work. So, the only way that energy could change within a system is through energy flow across the system bounds in the form of heat or work, thus, the FLT states that the energy is conserved. Accordingly, another form to express an energy balance is defining the different energy natures with $\Delta E = E_2 - E_1 = (KE_2 - KE_1) + (PE_2 + PE_1) + (U_2 - U_1)$, with KE as kinetic energy, PE potential energy, U internal energy which substituting in Equation (1) gives

$$\Delta KE + \Delta PE + \Delta U = Q - W. \tag{2}$$

The sign convention is that when $Q > 0$ the heat transfer flow to the system, $Q < 0$ heat transfer flows from the system, $W > 0$ the work is done by the system and $W < 0$ the work is done on the system. Next, an energy balance is applied to a thermodynamic cycle. A cycle occurs when a given system at an initial thermodynamic state goes to a sequence of processes and returns to its initial state. Historically the FLT and SLT have roots in the study of this cycles, curiously, the first modern engineering control device which become the starting point for the theory of automatic control (MACFARLANE, 1979), the Watt's Governor (KANG, 2016), also had its development in a thermodynamic cycle, the steam engine power cycle. Resuming, the thermodynamic cycle energy balance takes the form $\Delta E_{cycle} = Q_{cycle} - W_{cycle}$. Since the system returns to the initial state $\Delta E = 0$ resulting in no net energy changes leading to

$$W_{cycle} = Q_{cycle} = Q_i - Q_o. \tag{3}$$

With this, two types of cycles will be defined. The power cycle is one which the objective is to generate W_{cycle} from two thermal bodies where $Q_i > Q_o$ with i for inputs and o for outputs. And the Refrigeration or Heat Pump cycle has the objective of temperature change of some system in comparison to its surroundings, with $Q_i < Q_o$ while applying work W_{cycle} to drive the process. Now, returning to the analytic Kelvin-Planck statement of SLT, it says that is impossible for a cycle to deliver work while receiving heat just from one thermal reservoir, resulting in

$$W_{cycle} \leq 0 \ \ (\textit{Single Reservoir}), \tag{4}$$

emphasizing that this equation is true while a system is connected to just one thermal reservoir. That is, a cycle in this condition cannot deliver a net amount of work to its surroundings, in other words, the net work of the cycle cannot be positive (MORAN; SHAPIRO, 2006). Note that the sign of Equation (4) is less or equal, this is associated to internal irreversibilities. This concept is one of the important uses of the SLT in engineering because it gives an idea of physical limits of an system and also offer insights

of systems and subsystems improvements, which in general is intimately related to profits and costs.

Thermodynamic reversibility is a characteristic that a process has when a system and its surroundings can return exactly to the initial thermodynamic state. Retaking the Clausius statement it seems that a spontaneous heat transfer process from a hotter body to a colder one is irreversible. On the contrary it would be possible to transfer heat from the hotter to the colder body without any external effect. Obviously, this is denied by both our experience and the Clausius SLT statement. In general, the irreversibilities are intrinsic to actual processes and are observable in heat transfer through finite temperature difference, expansion of gases or liquids to lower pressures, spontaneous chemical reactions, mixing, friction, electric current heat dissipation on a resistance, inelastic deformation. So, saying that a process is internally reversible is the same as saying that are no irreversibilities within the system yet it may be located in the surroundings.

Thereby the reversibility concept is useful because in a general analysis its knowledge could give more information about feasible efficiencies and its economic aspects for sustainable production conciliation. Accordingly, thermodynamic design optimization is constrained by cost factors because materials, sizes and power demand, however, for the control point of view, better algorithms could increase thermodynamic operation performance of already constructed systems with minor changes, resulting in research and application opportunities.

Now that the energy balance and thermodynamic cycle were defined, consider the thermal efficiency of a power cycle described by

$$\eta = \frac{W_{cycle}}{Q_i} = 1 - \frac{Q_o}{Q_i} = 1 - \frac{Q_C}{Q_H}. \tag{5}$$

where sub-indexes i, o, C, and H means input, output, cold and hot. It is evident that $\eta \leq 1$ because to reach 100% efficiency Q_C must be zero which would violate the Kelvin-Planck statement. Real power cycles reach efficiencies $\eta < 1$ either because a power cycle must reject heat to a cold body or because real processes are irreversible. Note that with Equation (5) is possible to evaluate any thermodynamic power cycle without a priori knowledge of characteristics of the substances, the processes or the considerations, resulting in what is known as a SLT corollary. With this and considering the Kelvin temperature scale definition on a reversible cycle basis, $(Q_C/Q_H)_{rev\ cycle} = T_C/T_H$, for instance, the heat ratio of a reversible cycle is equal to respective reservoirs temperatures ratio, the maximum efficiency expression which is known as the Carnot efficiency is given by

$$\eta_{max} = 1 - \frac{T_C}{T_H}. \tag{6}$$

The Equation (6) gives the maximum efficiency of any power cycle operating between two reservoirs. By inspection if T_C decreases η_{max} increases and/or if T_H increases η_{max} increases. Carnot efficiency gives information about feasible efficiency levels. For example, conventional power cycles have thermal efficiencies of the order of 40% which may appear a low value, although, considering an hypothetical reversible power cycle operating between 745[K] and ambient temperature of 298[K] it gives an η_{max} = 60%, resulting in a reasonable efficiency of two thirds of the maximum feasible efficiency (MORAN; SHAPIRO, 2006). This basic idea is a powerful tool for energy system analysis and this discussion was made because presents SLT concept which is embedded in the exergy concept. In the following, further thermodynamic theoretical foundations are applied using engineering balances. So, phenomenological modeling counts on science laws like the thermodynamics ones. Balances are used for analysis and design, this systematic procedure normally is based on the mass conservation principle, energy conservation principle (FLT) and the second law of thermodynamics. Thus, a rate balance is expressed as

$$\frac{dm_{cv}}{dt} = \sum_i \dot{m}_i - \sum_o \dot{m}_o, \tag{7}$$

considering the time rate of change of mass inside a control volume dm_{cv}/dt equals to the inlet mass flow $\dot{m}_i$ less the outlet mass flow $\dot{m}_o$. An energy balance is defined as

$$\frac{dE_{cv}}{dt} = \dot{Q}_{cv} - \dot{W}_{cv} + \sum_i \dot{m}_i \left(\underbrace{h_i}_{U_i} + \underbrace{\frac{v_i^2}{2}}_{KE_i} + \underbrace{gz_i}_{PE_i} \right) - \sum_o \dot{m}_o \left(h_o + \frac{v_o^2}{2} + gz_o \right), \tag{8}$$

where the time rate of change of the energy contained within the control volume dE_{cv}/dt equals the terms of heat rate, work rate, internal, kinetic and potential energy rates. Note that enthalpy is defined as $h = u + pV$ where u is internal energy and pV is known as flow work that occurs when a fluid displace a volume V against a given pressure p, for example, a piston work. The energy balance is commonly described in function of h because it is a readily available property. Next, the entropy property is defined since the exergy balance arise from this concept, to do this, the Clausius inequality must be stated

$$\oint \left(\frac{\delta Q}{T} \right)_b \leq 0, \tag{9}$$

where the contour integral is used because of the thermodynamic cycle, δQ is the heat transfer at a part of system boundary during a portion of the cycle, note that this definition counts on boundaries characteristics, T is absolute temperature and subscript b means that the evaluation considers system boundary state. Accordingly, Equation (9)

can be described with $\oint(\delta Q/T)_b = -\sigma_{cycle}$, where σ_{cycle} represents the inequality value. Thus, for $\sigma_{cycle} = 0$ the system does not have irreversibilities, for $\sigma_{cycle} > 0$ the system has irreversibilities and for $\sigma_{cycle} < 0$ is impossible according to Clausius inequality and the *SLT* statements. In summary, σ_{cycle} is a quantity that represents the level of irreversibilities of a given cycle and is identified as entropy produced or generated. Thereby, considering an internally reversible thermodynamic cycle, the definition of entropy change is given by(MORAN; SHAPIRO, 2006)

$$S_2 - S_1 = \left(\int_1^2 \frac{\delta Q}{T}\right)_{int\ rev} \quad or\ dS = \left(\frac{\delta Q}{T}\right)_{int\ rev} \tag{10}$$

where entropy $S[J/K]$ is an extensive property and could be expressed as specific entropy in a mass basis $s[J/(kgK)]$. Since entropy is a property its change in a system from a state to another is the same for all processes both internally reversible and irreversible (MORAN; SHAPIRO, 2006). With this, the entropy rate balance for control volumes is given by

$$\frac{dS}{dt} = \sum_j \frac{Q_j}{T_j} + \sum_i \dot{m}_i s_i - \sum_o \dot{m}_o s_o + \dot{\sigma}_{cv}, \tag{11}$$

where the rate of entropy change dS/dt equals the sum of rate of entropy change accompanied by heat Q/T, by inlet mass transfer $\dot{m}_i s_i$, by outlet mass transfer $\dot{m}_o s_o$, and the rate of entropy production $\dot{\sigma}_{cv}$. It is worth note that entropy balance counts on boundaries information while the energy balance does not. Accordingly, energy balance is conservative while entropy is not, as evidenced by $\dot{\sigma}_{cv}$. The latter term does not have much significance by itself but becomes an important tool to compare energy processes, this is, comparing entropy production gives information that allows to identify irreversibilities across systems and rank the components according to its inefficiency, offering means to increase overall system efficiency. However, the entropy balance requires information of both heat transfer and temperature of the boundary. This difficult direct evaluation, becoming even worst for dynamic analysis because the system is far from thermodynamic equilibrium. Also note that despite the entropy change being a property, the right-hand side terms of Equation (11) are not, thus, they depend on the nature of the process. Entropy Generation Minimization (BEJAN, 1995) is a technique based on the SLT which normally consider steady-state assumption, $dS/dt = 0$ and solves the Equation (11) seeking to minimize $T_0\sigma$ which is known as the Gouy-Stodola theorem. The theorem states that the lost available work is directly proportional to the entropy production (BEJAN, 1995). With this, Entropy Generation minimization means available work production maximization.

Next, the exergy balance is defined from the mass balance, energy balance and entropy balance. The Exergy Analysis Method (KOTAS, 1985) merge the previous

concepts for design and optimization of energy systems. SLT states that a system can produce work when two thermal reservoirs are connected and tends to the equilibrium. It seems logic that for engineering applications one of these thermal reservoirs is set as the environment. With this is defined the exergy environment reference or the dead state. For example, a thermal power cycle has basically four devices to generate power from two thermal reservoirs. A boiler, a turbine, a condenser, and a pump connected in a closed loop. Note that the hot thermal reservoir is the boiler which uses an energy source to increase the temperature and the cold reservoir is the condenser which exchange heat with the environment. See that various engineering processes and plants uses the environment as the energy sink be it an electric, thermal, gravitational, or kinetic energy process. Thus, a providential definition on exergy analysis is that one thermal reservoir is set as the environment and is called dead state. Sub-index 0 is henceforth used to identify dead state variables. In other words, if a constrained control volume at the dead state is connected to the environment reference, the potential to do work is zero, once, ultimately, the systems were at equilibrium. The exergy rate balance integrates this last dead state definition, resulting in

$$\frac{X_{cv}}{dt} = \sum_j \left(1 - \frac{T_0}{T_j}\right) \dot{Q}_j - \left(\dot{W}_c v - p_0 \frac{dV_{cv}}{dt}\right) + \sum_i \dot{m}_i x_i - \sum_o \dot{m}_o x_o - \dot{X}_d, \tag{12}$$

where dX_{cv}/dt is the rate of exergy change, $(1 - T_0/T_j)\dot{Q}_j$ is the exergy transfer accompanying heat, $\dot{W}_{cv} - p_0(dV_{cv}/dt)$ is exergy rate transfer accompanying work,$\dot{X}_d = T_0\dot{\sigma}$ is the destruction of exergy, and, lastly, x_i and x_o are specific exergy rate transfer accompanying flow given by Equation (13). Note that $\dot{X}_d = T_0\dot{\sigma}$ is the Gouy-Stodola theorem, thus, the exergy destruction minimization is equivalent to entropy generation minimization. The specific exergy is given by

$$x = h - h_0 - T_0(s - s_0) + \frac{v^2}{2} + gz, \tag{13}$$

where h and s represent specific enthalpy and entropy and h_0 and s_0 the same properties at the dead state. Now, all thermodynamic balances considered in the following works are defined through Equation (7), (8), (11) and (12).

For comparison purposes of the exergy and energy concepts lets analyze a heat example (MORAN; SHAPIRO, 2006). Imagine a hypothetical system which receive heat from a fuel source $\dot{Q}_s$ and delivers heat for a given use $\dot{Q}_u$ subject to thermal losses $\dot{Q}_l$, the energy balance and exergy balance result in

$$\dot{Q}_s = \dot{Q}_u - \dot{Q}_l, \tag{14}$$

and

$$\left(1-\frac{T_0}{T_s}\right)\dot{Q}_s=\left(1-\frac{T_0}{T_u}\right)\dot{Q}_u+\left(1-\frac{T_0}{T_l}\right)\dot{Q}_l+\dot{X}_d. \tag{15}$$

The energetic efficiency is given by

$$\eta_E=\frac{\dot{Q}_u}{\dot{Q}_s}, \tag{16}$$

and the exergetic efficiency is described by

$$\eta_X=\frac{(1-T_0/T_u)\,\dot{Q}_u}{(1-T_0/T_s)\,\dot{Q}_s}=\eta_E\frac{(1-T_0/T_u)}{(1-T_0/T_s)}, \tag{17}$$

where for the case of a perfect insulated system $\dot{Q}_l = 0$, the energetic efficiency is maximum, $\eta_E = 1$. Note that exergetic efficiency depends on the energetic efficiency and on the product/input ratio of Carnot efficiency terms related to source and use temperatures. That is the reason why exergy analysis is capable of conciliate energy source and its energy use, because for $\eta_X \rightarrow 1$ is necessary to $\eta_E \rightarrow 1$ and $Tu \rightarrow Ts$, thereby, match source and usage temperatures.

Concluding this section, "exergy is a property of the system and conceptual environment, combining the intensive and extensive properties of the system with the intensive properties of the environment" (DINCER; ROSEN, 2007). As a result, and adding the presented thermodynamics basis is concluded that (SCIUBBA, 2001)

- Exergy is an intensive property whose value is uniquely determined by the parameters of both the system and the reference environment.
- If a flow undergoes any energy interaction with other systems, the change in exergy expresses both the quantity of energetic exchanges and its quality.
- The value of a product of a process, expressed in terms of ‘resource use consumption’, may be obtained by adding to the exergy of the original inputs all the contributions due to the different streams that were used in the process.
- If a process effluent stream is required to have no impact on the environment, the stream must be brought to a state of thermodynamic equilibrium with the reference state before being discharged into the environment. The minimum amount of work required to perform this task is the exergy of the stream. For this reason, many suggest that the exergy of an effluent is a correct measure of its potential environmental cost.
- Some researchers also propose that an “invested exergy” value to be attached to a process product, defined as the sum of the cumulative exergy content of the product and the “recycling exergy” to allow the process to have zero impact on the environment.

- A proper portion of the invested exergy plus the exergy of a stream under consideration can be assigned to the stream, thereby allowing the process to be evaluated with the physical and invested exergy of its effluents.
- If a feasible formulation exists to convert the remaining “non-energetic externalities” (labor and capital) into exergetic terms, their equivalent input in any process could be added to exergy accounting for a whole system.

Note that this list considers attributing monetary values of exergetic resources, this analysis is known as Thermoeconomics or Exergoeconomics (TSATSARONIS; WINHOLD, 1985). The latter, together with Exergy Analysis and Entropy Generation Minimization are the most used SLT/exergy-based modern techniques on industrial processes and engineering. All in all, the techniques converge the four key factors of sustainable development: environmental, economic, social and resource/energy. For a historic background of exergy theory see (SCIUBBA; WALL, 2007).

2.2 STATE-OF-THE ART OF EXERGY-BASED MODEL PREDICTIVE CONTROL

Modern integrated energy systems developments demand new technologies which only have a chance if they are economically and thermodinamically feasible. The hypothesis of this dissertation is that exergy analysis and advanced control strategies integration can play a major role on CSP energy systems. Traditional thermal power plants control has the possibility to manipulate the primary energy source, e.g. fuel flow, while renewable energy plants control does not, dealing with naturally intermittent sources. CSP control must track the sun, adapt to meteorological transients, manage thermal energy storage and electric energy dispatch, resulting in a challenge for control design. As said in previous sections, exergy analysis is a powerful tool for energy assessment and most of the exergy-based solutions count on steady state techniques. Although these solutions are not capable to cope with the intermittency of solar primary energy resource. Because of that, dynamic exergy analysis has recently attracted attention of researchers but only few are really control oriented. As an example, a systematic literature review and further filtering with the following keywords on title or abstract: review, exergy-based, and control, resulted in only three articles which were published from march, 2019 to march, 2020 - (SANGI; MÜLLER, 2019), (SAYADI et al., 2019) and (JAMES; KIM; JANE, 2020). Therefore, these articles are discussed in this section and each exergy-based MPC cited paper on the reviews will be presented.

An overview about the application of the SLT to control is given by (SANGI; MÜLLER, 2019). The authors states that exergy-based control strategies are among the recently introduced control strategies which applies the SLT. Sangi et al. also comment that in almost all the time the inefficient components of a process are known, but because of economic concerns, replacing or changing plant layout is prohibitive. This

results in the idea of achieving the most efficient operation of an imperfect system. And for this task, the steady-state exergy analysis is not sufficient to solve the Renewable Energy intermittent source problems. The article points existing gaps on the application of exergy to control, especially applied on buildings. It is concluded that (i) exergy-based control strategy may led to an energy efficient operation of the system, but energy and exergy comparison must be further investigated. (ii) There is no agreement on reference environment parameters selection. (iii) It was found that since 2013 a real movement from the steady-state exergy analysis to dynamic exergy analysis has started with the objective of developing exergy-based control strategies. (iv) Only a few works of real-life applications of exergy are really control-oriented. (v) MPC is the most used control technique.

Thus, the related MPC papers are further discussed next, considering, for comparison purposes, the following classic MPC formulation

$$\begin{aligned} \min_{\Delta u} \quad & \sum_{N_1}^{N_2} \gamma_j (\tilde{y}(k+j|k) - w(k+j|k))^2 + \sum_{i=0}^{N_u-1} \lambda_i \Delta u(k+i|k)^2 \\ \text{s.t.} \quad & y_{min} \leq \tilde{y}(k+j|k) \leq y_{max} \; j = N_1,...,N_2, \\ & u_{min} \leq u(k+i|k) \leq u_{max} \; i = 0,...,N_u - 1, \\ & \Delta u_{min} \leq \Delta u(k+i|k) \leq \Delta u_{max} \; i = 0,...,N_u - 1, \end{aligned} \tag{18}$$

where the cost function considers the errors between the predicted model outputs $\tilde{y}(k+j|k)$ and reference trajectory $w(k+j|k)$ and also the incremental control actions Δu. The prediction horizons are N_1 and N_2 and the control horizon is N_u; γ and δ are respectively the error and control movement weighting factors. (SANGI; MÜLLER, 2019) states that mostly works on the area considers only regulatory control and don't care about subsystems parameters related to power and energy indexes. The authors also point that if energy savings concerns appears they are commonly dealt with control tuning. Next, each related work is discussed.

(SALAHSHOOR; ASHERI, 2014) proposed an exergy-based model predictive control design methodology to save energy in a stationary gas compressor process. The idea is to compare operation set-points from energy and exergy balances on the compressor and use the MPC to track this set-points while rejecting disturbances and respecting constraints. The results show 22% of energy savings from steady-state exergy destruction set-point definition in comparison to the energy approach. The method can provide the best operation condition and the controller output was decreased without constraints violation. However, the authors did not give control formulation details, for example, they use a state space model representation with non-linear Ordinary Differential Equations modeling without any information about the MPC optimization problem solver or model linearization.

(HADIAN; ASHERI; SALAHSHOOR, 2014) investigated an exergy-event based strategy of a large system, not only to be more energy efficient compared to energy-based MPC, but also to reduce communication and computation efforts. The authors used the same controller formulation depicted in Equation (18) in an event-based control architecture composed by two parts. One controller that computes the plant inputs, and an event-based mechanism that determines when and which outputs of the plant and the controller must be transmitted. This happens either when the maximal sampling time is achieved, or the following relative error crosses a certain level e_{max}

$$||y(k) - y(k-1)|| > e_{max}. \tag{19}$$

The authors executed a linearization of the process composed by 4 reactors and one separator. It was calculated the total destroyed exergy with steady-state assumption for tuning purposes and the Mean Squared Error of set-point tracking for comparison. The simulation results demonstrated that adequately choosing the weighting matrix led to a good compromise between control performance and number of control actions. The approach reduced energy and exergy losses, computational burden, and communication effort. All in all, was concluded that the proposed strategy saved more energy in face of the other controllers reported on literature.

(JAIN; ALLEYNE, 2015) presented what seems to be the first use of transient exergy destruction as a metric for a closed-loop decision-making algorithm. The authors applied the linear MPC formulation of Equation (18) in a Refrigeration cycle and compared a first law objective function

$$J_{FLT} = (||C_{des} - C_{ach}||_2) + \lambda \Delta t \left(\sum_{k=1}^{N_p} \dot{W}_p[k] \right), \tag{20}$$

to the second law objective function

$$J_{SLT} = \underbrace{(||C_{des} - C_{ach}||_2)}_{Performance\ Objective} + \lambda \underbrace{\Delta t \left(\sum_{k=1}^{N_p} \dot{X}_d[k] \right)}_{Efficiency\ Objective} = (||C_{des} - C_{ach}||_2) + \lambda \Delta t T_H \left(\sum_{k=1}^{N_p} \dot{\sigma}[k] \right). \tag{21}$$

Apparently, an economic-MPC was used once the cost function considers both the reference tracking, or Performance Objective, and the Efficiency objective of exergy destruction rate minimization.

The author's variables are desirable C_{des} and achievable C_{ach} cooling capacity which is given by the user or calculated with energy conservation balance. The other variables are the weighting parameter λ, prediction horizon N_p, exergy destruction rate $\dot{X}_d$ and entropy generation rate $\dot{\sigma}$. Note that for a refrigeration cycle the hot reservoir

temperature is the environment temperature, with this $\dot{X}_d = T_H\dot{\sigma} = T_0\dot{\sigma}$. Thereby, this represents the equivalence between exergy destruction rate minimization and the entropy generation minimization.

The results show that the exergy-based model predictive control accounted for irreversibilities of each component and was able to optimize the trade-off between the useful energy production and the compressor power consumption. The work demonstrates the importance of the dynamic exergy destruction rate and the optimal control on the problem.

(RAZMARA et al., 2015a, a), (RAZMARA et al., 2015b, b) applied an Exergy-based (XMPC) and an Energy-based (EMPC) NMPC on a real building HVAC testbed and compared the results to a standardized ASHRAE Rule-based Control performance. The authors state that exergy is a more appropriate metric to evaluate the performance of the system and used the exergy balance Equation (12) to minimize the exergy destruction rate $\dot{X}_d$, describing the rate of change of exergy inside a room i with an independent equation based on the change in enthalpy and entropy

$$X_i = m_i[(h-h_0)-T_0(s-s_0)] \Rightarrow \frac{dX_i}{dt} = m_i\left(\frac{dh}{dt} - T_0\frac{ds}{dt}\right) + \underbrace{\frac{dm_i}{dt}}_{0}[(h-h_0)-T_0(s-s_0)]. \quad (22)$$

Note that m_i is the mass of air inside the room which is constant since the compressibility factor of a gas at very low pressure is close to one, this assumption leads to $dm_i/dt = 0$, and only the left term of differential Equation (22) stands.

The results indicate that the MPC outperform the Rule-based control. The energy-based control led to 18% and 24% reduction on exergy destruction and energy consumption, respectively. The exergy-based control led to 22% and 36% reduction on exergy destruction and energy consumption, respectively. It was concluded that exergy-based approach offers more energy savings compared to conventional energy-based model predictive control respecting the thermal comfort constraints.

(BARANSKI et al., 2016) proposed a Buildings Exergy-based Model Predictive Control Algorithm (BExMoC) and applied it in two cases. A software in the loop approach which simulates the model on a Dymola executable program and a real HVAC system. BExMoC key feature is the process decomposition and exergy destruction minimization in each subsystem. It was concluded that the algorithm is suited to real buildings control using non-linear models, the program achieved final energy consumption reduction and the approach could improve large buildings automation systems.

(SANGI; FUETTERER; MUELLER, 2017) and (SANGI; KÜMPEL; MÜLLER, 2019) evaluated a linear exergy-based MPC using a mixed integer programming to switch between cooling and heating modes of a generic building HVAC control and compare its performance to the process default mode-based control. The authors used

a Dymola simulation model, a MATLAB data exchange management, and GAMS software as the mixed integer linear programming solver/controller in a software-in-the loop approach. The chosen cost function considered exergy destruction minimization, temperature tracking, actuation effort and permissible temperature range. The results of the first work pointed that the proposed linear exergy-based mixed integer predictive control can reduce the energy consumption up to 22,5%. The result of the second work, a real implementation, demonstrated the exergy-based control functionality. The controller made meaningful decisions maintaining the temperature with only minor deviations from the set-point. The authors point the bottleneck of modeling, saying that the team had difficulties developing dynamic simulations models and suggests that a simulation platform with all necessary components, a learning algorithm and a monitoring system would be required.

(SANGI; MÜLLER, 2018) implemented a classic agent-based control and a hybrid agent-based MPC on a modelica-based library to control a HVAC model in a hardware in the loop approach. The results were compared to the mode-based default control. Results show that the hibrid control lowered the energy consumption by 2.06% and 1.31% in comparison to the mode-based and agent-based control, respectively. The approach demonstrated that the multi-agent distributed feature enable its application on large systems and in a bigger scale, also, the proposed strategy could be further developed to integrate exergy costing and exergoeconomics analysis.

With this study the first review paper discussion ends. The second review article that will be contextualized is the work of (SAYADI et al., 2019), note that the already cited review paper of (SANGI; MÜLLER, 2019) was published in the same year. The work of Sayadi et. al addresses the merits of exergy-based control strategies in comparison to energy-based ones in terms of energetic efficiency of buildings and/or HVAC systems. The authors elect the exergy destruction as a true measure of thermodynamic inefficiencies of the system. So, exergy-based control strategies used in this work minimizes exergy destruction from the building exergy model while that satisfies the user constraints. Also, the authors claim that the results “show that the exergy-based control reduces the quality mismatch between energy supply and demand, and, therefore, increase the sustainability of building energy systems" (SAYADI et al., 2019, p.1). The authors also state a procedure for exergy-based MPC design and sets three case studies based on the same building heating system problem and varying the size and perspective of the energy supply chain. The first problem is a unit operation case while the last case is the whole system control.

A general methodology for the design of exergy-based controllers for different scale and level systems is developed. The local/regulatory control and supervisory/multivariable control cases results show that “exergy is indeed a universal practical indicator that can pave the way for designing plug & play controllers" (SAYADI et al., 2019, p.

18). Next each case is discussed. The local exergy-based control of one office building reached up to 13% of operation costs reductions. The supervisory/multi-variable control of decentralized ventilation units were capable of coordinate the system and operate near the overall optimum. Lastly, the whole system control results with the so-called Exergy-based Linear Model Predictive Control (ExLiMPC) were compared to the actual rule-based control on a software in the loop simulation. It was detected an energy demand reduction up to 23.1%.

The Sayadi et al. review paper cites the already mentioned MPC related works adding the following. (RAZMARA et al., 2016) applied a MPC on a combustion engine model for combustion phasing control seeking exergy destruction minimization. The results show that exergy-based control strategy leads to an average of 6.7% and 8.3% of fuel saving and exergy saving compared to FLT based combustion control.

The work of (JAMES; KIM; JANE, 2020) is the third and last exergy-based control literature review paper that will be discussed next. James et al. also considered exergy-based optimization scientific contributions in the review. The critical analysis evaluates efficiency improvements in energy networks. The authors found exergy-based optimization and control studies demonstrating improvements as high as 40% over traditional methods based on the FLT. The work points that a small amount of publications is available compared to other fields until the submission of the article in September 2019. The most occurring around exergy-based multi-objective optimization. The authors reported promising improvements for exergy-based control and optimization, and that there still a great opportunity to improve energy systems by exergy concept usage. In addition, is said that the research in this area will be driven by the climate change mitigation efforts, renewables increasing demand, energy systems integration needs and the increasing emphasis on efficiency. All in all, there exists an opportunity to establish whenever exergy can assist control and optimization. Next, some new paper that were not already cited from the two latter review papers are discussed.

(BARANSKI; FÜTTERER; MÜLLER, 2018) proposes an algorithm for distributed model-assisted control where the cost function is the sum of exergy destruction and loss, which is calculated using non-linear Modelica language models. The author claims that the proposed algorithms are generic and could be applied at any building energy system having a 'plug & play' feature, which allows unit operations and subsystems models optimization across levels.

(REDDY et al., 2019) developed and optimal exergy-wise predictive control and applied it on a combined micro-scale concentrated solar power and HVAC system composed by thermal energy storage, concentrating solar power unit, an Organic Rankine cycle. The authors evaluated the energy-based (EMPC) and exergy-based (XMPC) controllers' performances in face of a rule-based control (RBC). The EMPC obtained 25.7% of exergy destruction reduction and 21.6% of energy savings. The XMPC re-

duced exergy destruction by 28% resulting in 23.2% of energy saving when compared to RBC. The same authors published after the review paper a continuation of the work. (REDDY et al., 2020) presents a further developed control method with the objective of minimize the electrical energy consumption of a HVAC system. The new controller shows 45% of grid electrical energy saving compared to the RBC. In addition, a Monte-Carlo simulation probability analysis was made showing energy saving ranges from 44% to 46.5% considering the prediction uncertainties and 35% and 57.5% of energy savings considering the seasonal variations.

(JONIN et al., 2019) designed an exergy-based MPC to regulate a thermal energy storage system of a home solar heating system subject to seasons weather variations. The authors linearized the model and added in the cost function the exergy accumulation term to maximize it, instead of minimizing the exergy destruction. With this, the control system simulation maintained a reasonable stratification of the tank and kept the highest temperature the longest possible during the winter. Resuming, the exergy-based control performs closely to the optimal operation resulting in a suitable control strategy. Also, the exergy-based cost function was used to optimize the tank size for minimum operational volume, thus, for minimize comfort violations.

(TRINKLEIN; PARKER; MCCOY, 2020) implemented both traditional and exergy-based NMPC schemes on a military ship energy system driven by new emissions regulation, fuel prices and energy-intensive mission systems demands. In a ship system there are several energy transformations which occur in compartmentalized systems. The authors idea is to modeling multiple systems domains simultaneously and apply the SLT optimization to overall ship energy systems enhancement. The exergy destruction was minimized, and the simulation resulted in fuel savings of up to 0.86% when compared to fixed flowrate cooling strategy. Although, the MPC implementation is not capable of real-time operation because of model complexity and the required sampling time.

2.3 FINAL COMMENTS OF THE CHAPTER

Exergy-based MPC approach has been attracting the interest of researchers and scientific community. In general, the exergy-based control has better performances of either comparing energy-based control or the common control approaches. It was contextualized three review papers on the area: (SANGI; MÜLLER, 2019), (SAYADI et al., 2019) and (JAMES; KIM; JANE, 2020), and the Model Predictive Control related papers were discussed. The works majority deal with buildings and HVAC systems, with only one application on process control (HADIAN; ASHERI; SALAHSHOOR, 2014), one application on combustion engines (RAZMARA et al., 2016), and one on ship energy systems (TRINKLEIN; PARKER; MCCOY, 2020). From the point of view of this dissertation proposal it seems that the exergy-based MPC applied on Concentrating

Solar Power plants subject could lead to new scientific contributions. Despite literature contributions on exergy-based optimization of solar energy systems, MPC applications seem to have space for developments and publications. This is corroborated since only one of the reviewed articles considers this dissertation subjects (REDDY et al., 2019).

3 DIGITAL TWIN OF AN ABSORPTION CHILLER FOR SOLAR COOLING

Highlights

Digital Twin of an Absorption Chiller for Solar Cooling

Diogo Ortiz Machado, William David Chicaiza, Juan Manuel Escaño, Antonio J. Gallego, Gustavo A. de Andrade, Julio E. Normey-Rico, Carlos Bordons, Eduardo F. Camacho

- Four adaptive neuro-fuzzy inference systems describe a commercial absorption chiller.
- The learning considers 12 days of continuous measurement and sampling time of 20s.
- The dynamic model has generalized adaptive learning despite sun intermittency.
- The model is accurate and precise - worst error of $0.09 \pm 3.6^{o}C$ (95%).
- The model is fast - takes $8.9s$ to simulate three days of operation.

Digital Twin of an Absorption Chiller for Solar Cooling

Diogo Ortiz Machado[a,b,c], William David Chicaiza[c], Juan Manuel Escaño[c], Antonio J. Gallego[c], Gustavo A. de Andrade[b], Julio E. Normey-Rico[b], Carlos Bordons[c,d], Eduardo F. Camacho[c,d]

[a] *IFRS - Instituto Federal de Educação, Ciencia e Tecnolgia do Rio Grande do Sul Rua Alfredo Huch, 475, Rio Grande, 96201 460, Rio Grande do Sul, Brasil.*
[b] *UFSC - Universidade Federal de Santa Catarina. Departamento de Automação e Sistemas, R. Eng. Agronômico Andrei Cristian Ferreira, Florianópolis, 88040 900, Santa Catarina, Brasil.*
[c] *US - Universidad de Sevilla. Departamento de Ingeniería de Sistemas y Automática, Camino de los Descubrimientos, Sevilla, 41092, Andalucía, España.*
[d] *ENGREEN - Laboratory of Engineering for Energy and Environmental Sustainability. Universidad de Sevilla.,*

Abstract

This work develops a digital twin of a commercial absorption chiller installed in a solar plant. The objective is to use the model for further control and optimization applications. This work uses dynamic neuro-fuzzy modeling to describe the absorption chiller under transients and part-load events to overcome the problems of phenomenological complexity, solar intermittency, and non-linearities. Four sub-models divide the whole chiller where Adaptive Neuro-fuzzy Inference System (ANFIS) describe each one. Then, training, checking, and validation procedures run considering data sets of 36404, 15601, and 11911 samples, respectively, totaling 15 days of available data with a sampling time of $20s$. The ANFIS models have generalized learning and predict the measured data with a worst-case Mean Absolute Percentage Error of $MAPE = 3.30\%$. Furthermore, a comparison between the developed models and similar scientific publications shows superior precision, accuracy, and fast execution speed of the resulting digital twin. Therefore the resulting model has control and optimization applicability.

Keywords: Dynamic modeling, Fuzzy, PCA, HVAC, Fresnel Solar Collector
PACS: 0000, 1111

Email address: `Corresponding author - bordons@us.es` (Carlos Bordons)

2000 MSC: 0000, 1111

1. Introduction

Knowledge is power and time is money. In an even faster and more connected society, making the best decisions just-in-time, planning on a broader horizon with accuracy, and controlling assets give technological and economic advantages. This work develops a double-effect absorption chiller dynamic model in the framework of digital twins using adaptive neuro-fuzzy networks. The intention is to use the resulting smart energy system to plan, integrate, and control the ETSI absorption plant installed in Seville, Spain.

The building energy sector is responsible for 40% of the world's energy use [1]. In this context, solar heating and cooling systems have the potential to reduce fossil fuel use and alleviate CO2 emissions [2]. Solar absorption chilling produces cold from a solar-heated source through an absorption thermodynamic cycle [3]. An advantageous feature of the solar absorption system is that the chilling demand follows the primary energy availability - solar irradiance. Absorption chillers are considered the most desirable method to harness solar thermal energy for cooling due to their relative maturity, reliability, and higher efficiency. However, Shirazi et al. [4] show that currently available absorption chillers cannot economically compete with conventional cooling. Therefore, improving the economic performance of these systems with control and optimization through digitalization tools [5] and artificial intelligence is highly desirable [6].

A Digital Twin is a "virtual representation of a physical asset enabled through data and simulators for real-time prediction, optimization, monitoring, controlling, and improved decision making" [7]. The first DT started in 2015 to be used in the entire life cycle of an asset, from concept to operation [8]. Since then, the concept has gained popularity and applications in energy area due to key enabler development and DT advantages, such as remote monitoring and control in real time, greater efficiency and safety [9], accurate prediction [10], what-if analysis [11], integration of disparate systems, among others [7, 12].

This paper develops a Digital Twin of the solar absorption chiller of *Escuela Técnica Superior de Ingeniería de Seville* (ETSI), Spain, for control and optimization. The plant is located on the roof of the ETSI building and has the objective of supplementing the air conditioning system with chilled

water to reduce electric consumption, CO2 emissions and operating costs [13]. The plant is a multi-energy system once it transforms solar irradiance into thermal internal energy, hot water into chilled water (thermal to thermal), and gas chemical energy into thermal internal energy. This system is also evident as highly non-linear and dynamic, switching between electric, gas, and solar resources according to meteorology and demand profiles.

The dynamic simulation of absorption chillers is critical to describe the system performance and aid control during activation or part-load operation [14]. Thus, dynamic simulation is even more essential if it is driven by an intermittent solar resource. This paper focuses on the dynamic modeling of the absorption chiller of the ETSI solar plant to compose the whole DT. The plant exists as a physical entity, has computers and servers that work as the virtual space, and is equipped with an industrial network capable of connecting the physical and virtual spaces [15]. Therefore, the only asset missing for the absorption chiller DT consolidation is its adaptive virtual entity representation - its adaptive dynamic model. Based on previous contributions to the ETSI plant absorption chiller modeling and control [13, 16, 17, 18], the following model specifications for this paper are set:

1. To have sufficient accuracy and precision accordingly to the last scientific publications.
2. To run fast enough to be used in Model Predictive Control (MPC) techniques.
3. To describe the chiller operation under transients, part-load, during the day and night for further operation decisions.
4. To describe the gas boiler for forthcoming economic analysis.
5. To cope with the aging of the plant for long-term and life-cycle assessment.
6. To incorporate the embedded, inaccessible, proprietary chillers‘ controls that regulate the process, avoiding dangerous operation and the crystallization of the Lithium Bromide (Li-Br) solution.

The problem is that dynamic modeling of absorption chillers is not trivial, nor is the creation of its DT. Research on energy integration and dynamic control of absorption chillers has been mainly overlooked in favor of performance studies. Most modeling and simulations works consider steady-state thermodynamic models, and just a few are dynamic and control-oriented [19]. The few dynamic models, in their turn, are phenomenological or object-oriented, complex, and computationally expensive [4]. In addition, for the

specific case of this work, the authors have an incomplete and noisy set of variables. Therefore, soft computing modeling techniques are preferred because they use incomplete available data, describe a system with imperfect information, and are capable of updating the model online [20].

Adaptive neural networks (ANN) are successfully applied to solve complex, non-linear, dynamic, and multivariable problems because they also tolerate errors, imprecision, and missing data [21]. However, the application of ANN for dynamic modeling of absorption chillers is scarce [22], and the main contributions refer to steady-state performance prediction [14]. The authors found the following scientific contribution to the dynamic modeling of absorption chillers:

Lazrak et al. [14] obtain an ANN dynamic model of a single-effect absorption chiller of $15kW$ operating with H2O–LiBr considering two days of experimental data with no information on sampling time. Three ANNs describe the outlet temperatures of the absorption chiller subsystems: the generator with relative mean errors (RME) of 4.4 and 9.3%, the evaporator with RME of 4.9 and 5.0%, and the absorber+condenser with RME of 1.2 and 1.6% for two separated evaluation data sets,

The results show good performance of the dynamic models, although the final ANN model is a black-box representation of the system because the mathematical equations are not explicit. In addition, the work did not inform the sampling times.

Adaptive Neuro-Fuzzy Inference Systems (ANFIS) is a hybrid concept that implements a fuzzy inference system using ANN. The ANFIS constructs a set of *if-then* rules with adequate membership functions to find the desired input-output pairs. The advantage of ANFIS is that it can model non-linear functions and identify non-linear components online in a control system with good performance [23]. Furthermore, unlike neural networks, ANFIS allows the subsequent inclusion of rules or phenomenological modeling, and the resulting model has explicit functions that can be used in a wide range of optimization solvers that require the evaluation of model equations [24]. Because of this gray-box feature, this work employs ANFIS modeling. Further scientific research on the topic of dynamic absorption chiller modeling using ANFIS finds the following works.

Tamiru et al. [25] develop an ANFIS to dynamically model a double effect LiBr/H2O steam absorption chiller for fault detection purposes. The work uses a day of experimental data with a sampling time of 20 s. The model output is the absorber + condenser and evaporator outlet tempera-

tures with good performance with respect to model vs. actual temperature plots, although, without any error analysis.

Abdalla et al. [26] develop a dynamic subtractive clustering SC-ANFIS model of two steam absorption chillers with $4400kW$ of cooling load. The model predicts energy consumption, cooling load, coefficient of performance (COP) and cooling water return temperature (absorber+ condenser), the latter with a mean standard error and standard deviation of 1.724^oC and 0.132, respectively. The work considers 20 days of experimental data with a sampling time of $T_s = 1\ h$.

Considering the scarce works on the theme, this paper proposes dynamic modeling using Adaptive Neuro-Fuzzy Inference Systems (ANFIS) [23] to generate a transparent model with explicit equations, using 15 days of operation data with a sampling time of $T_s = 20\ s$. This work contributes to:

1. Developing a dynamic neuro-fuzzy model of all outlet temperatures of a commercial absorption chiller. Note that simulating these temperatures enables further study of performance indexes.
2. Training, checking, and validating the ANFIS with 15 days of measured data sampled every 20 seconds. This massive amount of data results in a generalized dynamic model capable of representing the behavior of the absorption chiller across a broad operational range.
3. The model is helpful for describing operations between day and night, during part-load operations, or in standby loosing heat, whether or not its boiler is used.
4. The resulting dynamic model is computationally fast with explicit equations and therefore suitable for use with MPC and dynamic optimization techniques.

The organization of the rest of paper is as follows. Section 2 defines the absorption chiller process and presents the data preparation. Section 3 describes input dimension reduction techniques to increase the model's computational speed, such as correlation coefficient analysis and Principal Component Analysis (PCA). Section 4 describes the architecture of the dynamic ETSI absorption chiller model and defines training and checking parameters. Section 5.2 presents the validation results and Section 6 closes this work with the conclusions.

2. Absorption Chiller Process

Figure 1 shows the schematic of the ETSI plant that started its operation in 2008. The objective of the plant is to complement the energy for the air conditioning system of the ETSI building. The building has an automatic heat, ventilation and air conditioning (HVAC) system that manages electric chillers and the use of the absorption plant. The absorption chiller has three primary external hydraulic connections. One connects the chiller to the Fresnel solar collector that receives heat Q_{solar}, the other connects the chiller to the ETSI building that delivers the chilled stream Q_{evap}, and another connects the chiller to the Guadalquivir River to reject heat $Q_{abs+cond}$. The Fresnel Solar collector has a mirror's aperture surface of 354 m^2 operating with nominal pressurized water at 13 bar, outlet nominal temperature of 180^oC. Furthermore, the absorption chiller is a multi-energy BROAD BZH15 model with $174kWh$ cooling capacity, 1.34 nominal Coefficient of Performance (COP), using Fresnel heated water or direct-fire gas heat [27]. Table 1 compiles the nominal operation points of the BROAD BZH15 absorption chiller, where Rated A refers to the manufacturer's recommended operation and Rated B refers to the available operation range without affecting cooling capacity or COP.

Table 1: Rated operation points of BROAD BZH15 absorption chiller [27, p.42-43]

	Var.	**Rated A**	**Rated B**
Chilled water flow[a] (m^3/h)	$V1$	30	21.4
Chilled water inlet temperature (^oC)	$T1$	12	14
Chilled water outlet temperature (^oC)	$T2$	7	7
Cooling water flow[b] (m^3/h)	$V2$	36.6	46.6
Cooling water inlet temperature (^oC)	$T3$	30	32
Cooling water outlet temperature (^oC)	$T4$	37	37.5
Heat source water flow (m^3/h)	$V6$	7.6	7.6
Heat source water inlet temperature (^oC)	$T6A$	180	180
Heat source water outlet temperature (^oC)	$T6B$	165	165

[a] Rated A adjustable chiller water flow rate: $50 \sim 120\%$ $(15 \sim 36\ m^3/h)$
[b] Rated A adjustable cooling water flow rate: $30 \sim 140\%$ $(11 \sim 51\ m^3/h)$

The ETSI plant is a unique process pairing a double-effect absorption chiller, with a direct-fire gas boiler and concentrating solar collectors. Bermejo et al. analyze the operation of the plant showing that it has a solar heat frac-

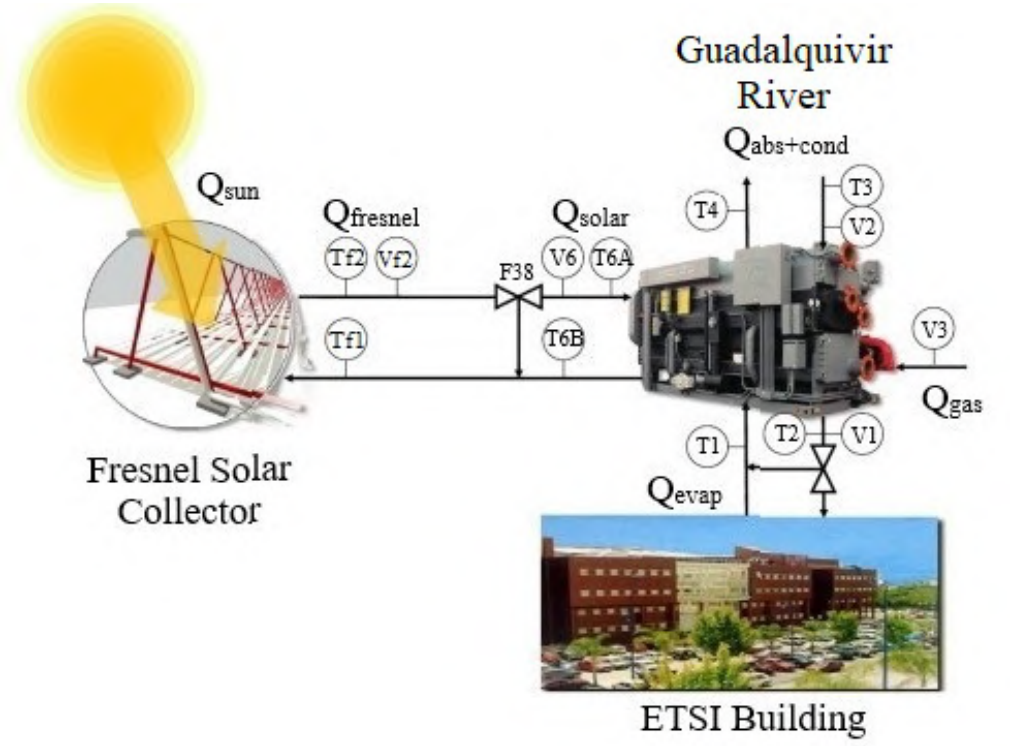

Figure 1: General schematic of the absorption plant in the *Escuela Técnica Superior de Ingeniería (ETSI)* in Seville University. Modified from [13].

tion of 0.75, a cooling ratio of 0.44, a COP of 1.1-1.4, and an average cooling power of $135kwh$ (77% nominal). The performance of the ETSI solar absorption plant is a step forward in solar absorption technology [13]. Still, it offers improvement possibilities [16].

The BROAD BZH15 operates with internal solutions of water + lithium bromide (LiBr), where water is the refrigerant and the bromide is the absorbent. Double-effect means using LiBr streams with different concentrations by employing cascade heat exchangers to increase the overall COP of the system through higher inlet temperatures thresholds. For further information about absorption chillers multi-effects refers to [28].

The manufacturer's design manual [27, pg.40] depicts in detail the BROAD BZH process flow diagram (PFD) and the nomenclature used in this work. For simplicity and because the measurements of the internal variables are not available for model validation, this work considers the Figure 2 PFD. See that internal streams of LiBr (gray arrows in Figure 2) only exchange heat with external solutions (black arrows in Figure 2), not exchange mass or mixing. Besides, there is no available data from these internal streams; hence, they are suppressed. The main difference between the manufacturer's and this work PFD is that the latter embeds the HTG, the LTG, the LTHE, and the HTHE processes, shown in [27, pg.40], in one process called High-Temperature Generator (HTG) in Figure 2.

Note in Figure 2 that HTG (red color in Figure 2) can receive heat from two heat sources: the solar Fresnel collector (Q_{solar}) or the gas boiler (Q_{gas}). If the plant is operating with solar heat, valve F38 opens and water from the Fresnel collector enters the High Temperature Generator (HTG) at temperature T6A and flow V6. The flow of heat source water, V6, with a given temperature T6A, exchanges Q_{solar} with a concentrated LiBr solution within the HTG at temperature T5. After exchanging heat, affecting T5, the solar collector stream exits HTG and goes to the Fresnel collector again; therefore, the solar hydraulic system is a closed loop. Note that the temperature T6B is an important variable for the operation of the whole plant. If the HTG operates with gas, the process receives Q_{gas} from direct gas burning, increasing T5, according to the gas flow V3, affecting the temperature of the exhaust gas T6. Temperature T5 is a critical variable for the absorption chiller and the entire plant because it connects the Fresnel solar collector and the chiller, affecting the plant dynamics, cooling capacity, and COP.

The absorption cycle must reject heat to the environment to operate. This heat rejection occurs in the condenser and absorber (blue in Figure 2). The

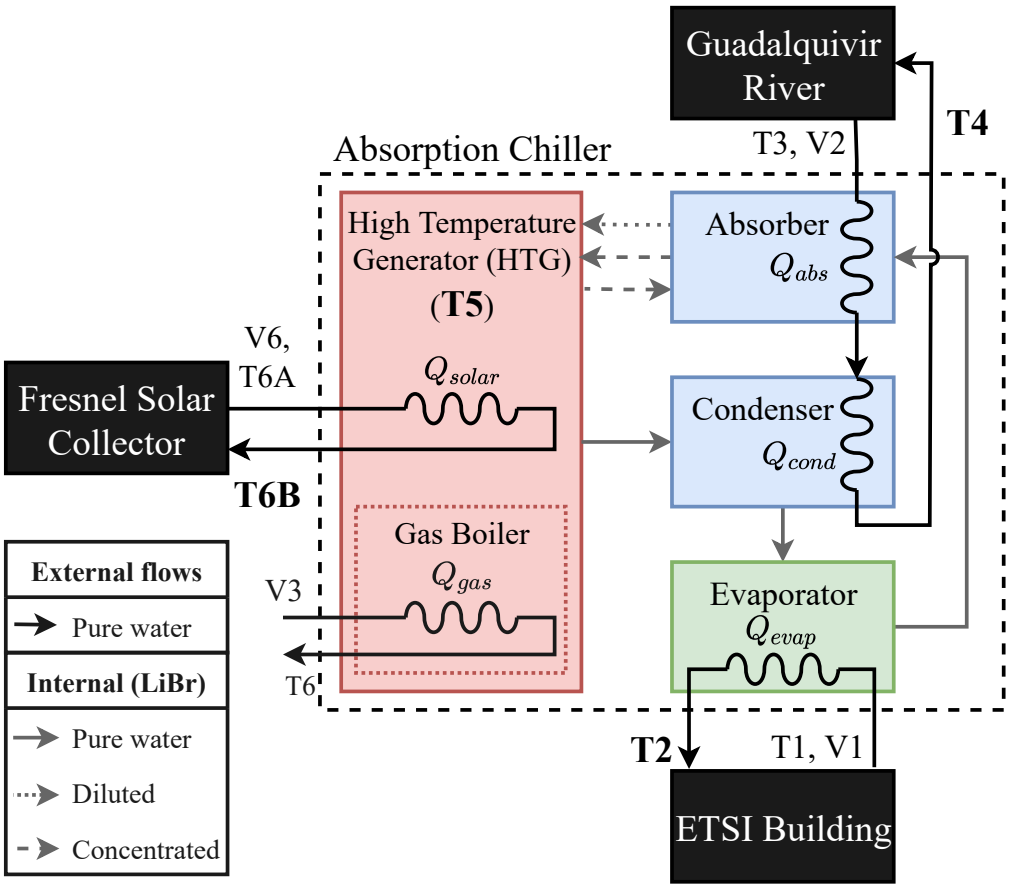

Figure 2: Simplified schematic of the absorption chiller. Model 1 - HTG internal LiBr temperature T5. Model 2 - HTG (red color) outlet temperature T5. Model 3 - Absorber + condenser (blue color) outlet temperature T3. Model 4 - Evaporator (green color) outlet temperature T2. Bold variables are the chosen model outputs.

condenser turns the LiBr vapor from the HTG into liquid, and the absorber cools the LiBr concentrated solution from the HTG. The ETSI plant uses a heat exchanger connected to an open-loop pumping system that uses water from the Guadalquivir River. The inlet temperature is given by T3, the outlet temperature is T4, and the flow is V2. The difference between T3 and T4 is essential for the operation of the chiller.

The cooling effect of air conditioning occurs in the evaporator (green in Figure 2) due to LiBr concentrations and pressure differences. The inlet evaporator temperature is T1, the outlet temperature is T2, and the flow is V1. Temperature T2 is the essential variable of the absorption chiller once. T2 represents the objective of the whole process of chilling water to supplement the HVAC system of the ETSI building. Accordingly, this work uses the following output variables of the chiller model: internal HTG LiBr solution temperature T5, solar heat source - water outlet temperature T6B, absorber + condenser cooling - water outlet temperature T4, and evaporator chilled water outlet temperature T2, all variables are in bold in Figure 2.

It is worth noting in the manufacturer's design manual [27, pg.40] that the absorption chiller has Programmable Logic Controllers, instrumentation, and a control network that connects the plant to the Internet. Besides, not all the variables depicted in the appendix's scheme are available or are reliable. The measurement data from the Supervisory Control and Data Acquisition (SCADA) system presents outliers, zeros, physically impossible negative values, heterogeneous sampling times, and other inconsistent entries that must be corrected. The following section presents this raw data preparation for further ANFIS training once data-driven modeling is highly sensitive to the input data.

2.1. Data Preparation

This work uses SCADA system operation data. The raw data was stored in sheets where each day of operation generated one file with 41 variables (columns). The sheets were imported into Matlab as timetables, with 42 column names (headers) organized in the same fixed sequence for all imported sheets to avoid combining different variables. Then each timetable was concatenated by time, considering consecutive days. The problem is that there were missing, repeated, and irregular variable samples between different days. The irregular sampled data were re-sampled and aggregated using linear interpolation with sampling times of $T_s = 20\ s$. The result is five regular concatenated timetables from August 11 to 12, 14 to 17; September

02 to 03, 22 to 25; and October 14 to 16, totaling 15 days of operational data.

Next, a moving mean filter with 6 *min* window removed outliers from data sets. Furthermore, a one-by-one evaluation substituted negative pressures, flows, and inconsistent variables sets by the minimum or maximum absorption chiller operation range considering Table 1. The variable-by-variable inspection also led to the discovery of empty columns further deleted. Also, Gaussian interpolation is used to smooth pressure and flow variables, respectively, with a 15 sampling times window. As a result, 25 variables compose the final data set with 63916 samples.

3. Inputs Dimensionality Reduction

Four models make up the absorption chiller representation. Each model has one output; therefore, there are 24 input variables available for each output. The problem is that the computational complexity of data-driven models is directly proportional to the number of inputs. Input reduction techniques are essential enablers for the Digital Twins application [29]. Data reduction techniques preserve information while decreasing the number of variables, enabling fast processing for real-time control and optimization. This work applies two techniques: correlation coefficient matrix clustering and Principal Component Analysis (PCA). The first quantifies the variables correlated with each output of the model, discards uncorrelated variables, and groups correlated variables. The second reduces the dimensionality of each correlated data group by decomposing the whole group into only uncorrelated variables in a lower-dimensional space. The following section describes the theoretical background of these techniques.

3.1. Correlation Coefficients Matrix

The correlation coefficient of two random variables measures their linear dependence. The Pearson correlation coefficient for n scalar observations between variables $x_1 = [x_{1,1},\ x_{2,1},\ ...,\ x_{n,1}]$ and $x_2 = [x_{1,2},\ x_{2,2},\ ...,\ x_{n,2}]$ is:

$$\rho(x_1, x_2) = \frac{1}{n-1} \sum_{i=1}^{n} \left(\frac{x_{i,1} - \bar{x}_1}{\sigma_{x_1}} \right) \left(\frac{x_{i,2} - \bar{x}_2}{\sigma_{x_2}} \right), \tag{1}$$

where $\bar{x}$ is the mean and σ is the standard deviation. By definition, $\rho = 1$ indicates a strong positive relationship, $\rho = -1$ a strong negative relationship, and $\rho = 0$ no relationship at all. The correlation coefficient matrix of L

random variables is a $L \times L$ matrix of correlation coefficients for each combination of pairwise variables that, for only x_1 and x_2, results in the following 2×2 matrix:

$$C = \begin{pmatrix} \rho(x_1, x_1) & \rho(x_1, x_2) \\ \rho(x_2, x_1) & \rho(x_2, x_2) \end{pmatrix} = \begin{pmatrix} 1 & \rho(x_1, x_2) \\ \rho(x_2, x_1) & 1 \end{pmatrix}. \tag{2}$$

Figure 3 shows the correlation coefficient matrix of the data from the ETSI plant. In order to evaluate the degree of correlation for each input regarding each output, the next step is sorting the input variables in a degree of relationship to analyze which variables impact the model outputs concerning a threshold to compose further PCA.

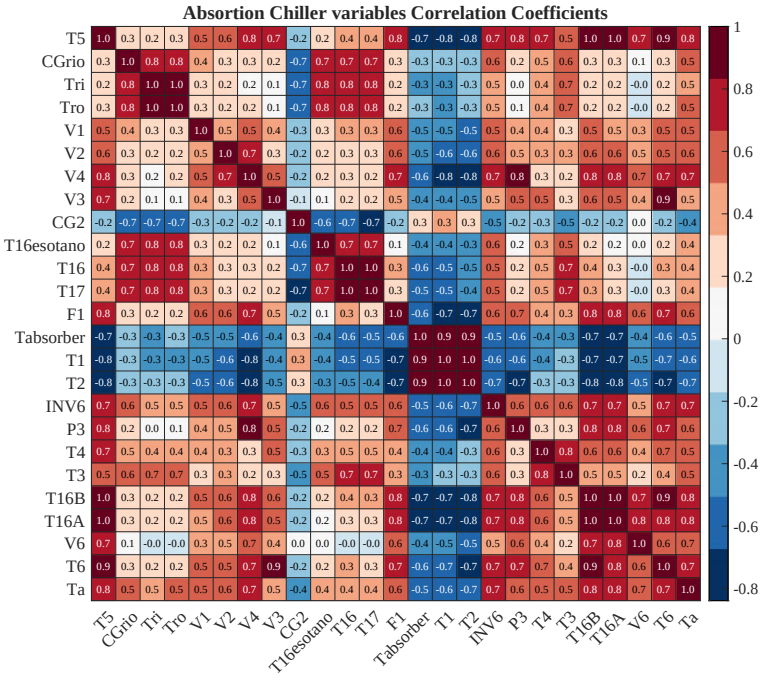

Figure 3: Correlation coefficients matrix of the prepared ETSI plant data.

3.2. Principal Component Analysis - PCA

PCA is a multivariate statistical technique that allows optimal representation in a reduced-dimensional space observations of an n-dimensional

space. It transforms the original generally correlated variables into new uncorrelated orthogonal variables in a new coordinate system (subspace of the principal components).

The observations made by the SCADA system of the ETSI absorption plant form the data matrix $\mathbf{X}$:

$$\mathbf{X} = \begin{pmatrix} x_{1,1} & x_{1,2} & x_{1,j} & \cdots & x_{1,m} \\ x_{2,1} & x_{2,2} & x_{2,j} & \cdots & x_{2,m} \\ x_{i,1} & x_{i,2} & x_{i,j} & \cdots & x_{i,m} \\ \vdots & \vdots & \vdots & \ddots & \vdots \\ x_{n,1} & x_{n,2} & x_{n,j} & \cdots & x_{n,m} \end{pmatrix},$$

where, $\mathbf{X} \in \Re^{N \times M}$, n is the instantaneous measurement taken from each sensor m, matrix $\mathbf{X}$ consists of several samples N of the various sensors M contained in the system. Each variable m in the data matrix $\mathbf{X}$ must be normalized to zero mean and unit variance (Eq.(3)) to give them equal weight. As PCA is defined by the variance criterion that depends on the units of measurement, it implies that the principal components in the covariance matrix $\mathbf{R}$ change if the units of measurement of each variable have a different scale [30, 31].

$$\mathbf{z}_{i,j} = \frac{x_{i,j} - \overline{x}_j}{\sigma_j}. \tag{3}$$

The PCA of a standardized data set $\mathbf{Z} \in \Re^{n \times m}$, with rank r ($r \leq min\{n, m\}$) is obtained from its covariance matrix $\mathbf{R}$ and its singular value decomposition (SVD).

$$\mathbf{R} = \frac{1}{N-1}\mathbf{Z}^T\mathbf{Z}, \tag{4}$$

where N is the total number of samples in the matrix $\mathbf{Z}$. The singular value decomposition (SVD) of the matrix $\mathbf{Z}$ is related to the eigen decomposition of the covariance matrix $\mathbf{R}$.

$$\mathbf{Z} = \mathbf{U}\mathbf{S}\mathbf{V}^T, \tag{5}$$

where, $\mathbf{U} \in \Re^{n \times r}$, $\mathbf{V} \in \Re^{m \times r}$ are matrices with orthogonal columns[1], and $\mathbf{S} \in \Re^{r \times r}$ is a diagonal matrix $diag\{\sigma_1, \sigma_2, \cdots, \sigma_r\}$ whose elements are the

[1]Therefore $\mathbf{U}^T\mathbf{U} = \mathbf{I} = \mathbf{V}^T\mathbf{V}$ with the identity matrix $\mathbf{I} \in \Re^{r \times r}$. The colums of $\mathbf{V}$ are

square root of the eigenvalues of $\mathbf{Z}\mathbf{Z}^T$ in decreasing order $\big(\sigma_1 \geq \sigma_2 \geq \cdots \geq \sigma_r\big)$. Therefore, the eigen decomposition of $\mathbf{R}$ is obtained as:

$$\big(N-1\big)\mathbf{R} = \big(\mathbf{U}\mathbf{S}\mathbf{V}^T\big)^T\big(\mathbf{U}\mathbf{S}\mathbf{V}^T\big), \tag{6a}$$

$$\big(N-1\big)\mathbf{R} = \mathbf{V}\mathbf{S}\mathbf{U}^T\mathbf{U}\mathbf{S}\mathbf{V}^T, \tag{6b}$$

$$\big(N-1\big)\mathbf{R} = \mathbf{V}\mathbf{S}^2\mathbf{V}^T, \tag{6c}$$

$$\big(N-1\big)\mathbf{R} = \mathbf{V}\mathbf{\Lambda}\mathbf{V}^T, \tag{6d}$$

where, $\mathbf{\Lambda} \in \Re^{r\times r}$ is a diagonal matrix $diag\big\{\lambda_1, \lambda_2, \cdots, \lambda_r\big\}$ with the eigenvalues of $\big(N-1\big)\mathbf{R}$ in decreasing order $\big(\lambda_1 \geq \lambda_2 \geq \cdots \geq \lambda_r\big)$ with $\lambda_r = \sigma_r^2$. The columns of $\mathbf{V}$ are the eigenvectors $\mathbf{v_r}$ of the eigenvalues λ_r.

3.3. Obtaining projected data in the main components

The observations of an n-dimensional space can be optimally represented in a reduced-dimensional space employing the PCA. The eigenvectors of $\mathbf{V}$ mark the direction of the new principal component (PC) space and are stored in a new matrix $\mathbf{P} \in \Re^{m\times m}$ called the loading matrix. The matrix $\mathbf{P}$ contains the coefficients of the principal components of each variable m and is used to project the data into a new reduced dimension space.

$$\mathbf{T} = \mathbf{Z}\mathbf{P}, \tag{7a}$$

$$\big[\mathbf{t}_1 \cdots \mathbf{t}_m\big] = \big[\mathbf{z}_1 \cdots \mathbf{z}_m\big]\big[\mathbf{p}_1 \cdots \mathbf{p}_m\big], \tag{7b}$$

where, $\mathbf{T} \in \Re^{n\times m}$, is the score matrix that contains a new component $\mathbf{t_m}$ projected in its respective principal component $\mathbf{p_m}$. Usually, the data matrix is projected onto the component containing the highest variability[2]. Moreover, there is no correlation between the new projected variables.

The variability associated with the principal components set which was retained can measure the quality of any n-dimensional approximation. Therefore, it is a standard way that can measure the quality of a principal component as a percentage proportion of the total variance [31]:

---

the eigenvectors of $\mathbf{Z}\mathbf{Z}^T \in \Re^{m\times m}$ associated with their nonzero eigenvalues. Similarly, the columns of $\mathbf{U}$ are the eigenvectors of $\mathbf{Z}\mathbf{Z}^T \in \Re^{n\times n}$.

[2]The first principal component is a linear combination of the original variables. It defines the direction of the greatest variability in the data set, so it has the greatest sum of variance in the matrix $\mathbf{\Lambda}$ [32].

$$\pi_j = \frac{\lambda_j}{\sum_{j=1}^{p} \lambda_j} \times 100\%. \tag{8}$$

4. Neuro-fuzzy Modeling

The following section presents the background of the ANFIS architecture, its parameterization, the training and checking procedures, and, lastly, the validation concept of the ANFIS model.

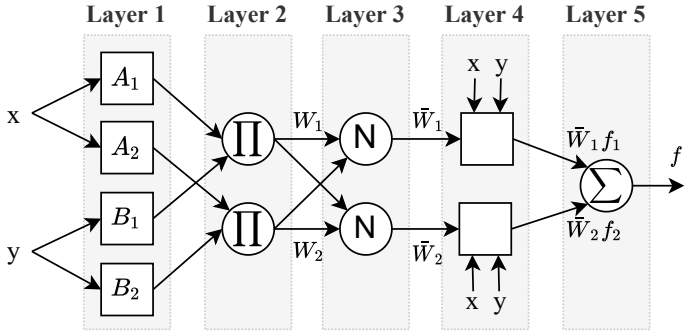

Figure 4: Adaptive Neuro-fuzzy Inference System (ANFIS) architecture [23].

The nodes and directional links compose the ANFIS as depicted in Figure 4, where the nodes have fixed (circle) or adaptive (square) parameters, and the links represent the direction of the signal flow. Thus, the node output depends on the input and its parameters. The ANFIS architecture has five layers. In the first layer, fuzzification occurs, which transforms the inputs x, y into linguistic labels with a degree of membership. The second layer is a product stratum composed of nodes that multiply each input. The output represents the firing strength of the node rule that flows to the next layer. The third layer normalizes each node output considering the total number of nodes. In the fourth layer, there occurs the defuzzification with a weighted output of the *if-then* rules. The mathematical representation of each fuzzy set (Fij) is a Gaussian membership function (MF) with $\{a_i, b_i, c_i\}$ as the parameter set that defines the mean, height, and width of the Gaussian. As the values of the parameters change, the MFs also change, representing various forms and combinations of membership functions. Lastly, the fifth layer has a unique node that sums up all the heightened rules outputs.

This work uses type-3 fuzzy reasoning. Thus, the ANFIS uses Takagi-Sugeno type rules [33]. The output of each rule is a linear combination of input variables summed to a constant term, and the final output of the inference system is the weighted average of each output of the rule. For a detailed description of ANFIS, refer to [23, 24]. After defining the ANFIS architecture, the problem becomes deciding the number of rules and MF in the nodes. This work uses the subtractive clustering method to estimate the number and initial centers of the premises of the fuzzy rule, avoiding the necessity of previous knowledge or the designer's experience [34, 24]. Once the rules and MF are defined, the ANFIS is ready for training.

The ANFIS training objective is to choose the MF parameters, minimizing the error between the training data and the ANFIS output by varying these parameters. The training procedure runs epochs or sweeps, where one epoch is both the direct information pass and the backward pass along the ANFIS layers. ANFIS uses a hybrid technique. First, a gradient descent to optimize the antecedent parameters, then a least-squares estimate to select the consequent linear parameters at each epoch or sweep. Therefore, the ANFIS learning procedure combines the gradient method and least squares to update the MF parameters, reducing the training time. The next question is, how many epochs are sufficient for training? The ideal number of epochs is the one that produces the stable and minimum error. The practice is to select a given supersized number of epochs and infer when the error does not decrease and stabilizes in error versus epoch graphic.

The checking procedure evaluates the error between the checking data set; a new data set not used in training. The checking runs after each epoch during the training, and it has the objective of evaluating if the ANFIS training results in generalized learning. If the ANFIS output has low errors with unknown inputs, then it is said that the ANFIS model had general learning. Typically, the checking considers the root mean squared error (RMSE) given by Equation (9)

$$RMSE = \sqrt{\frac{\sum_{i=1}^{N}(x_{i,j} - \hat{x}_{i,j})^2}{N}}, \tag{9}$$

where $x_{i,j}$ is a given actual variable j with N samples, and $\hat{x}_{i,j}$ is the output of the predicted variable. This work considers normalized outputs for training and checking. Therefore, the normalized RMSE, given by Equation (10), is used.

$$nRMSE = \sqrt{\frac{\sum_{i=1}^{N}(z_{i,j} - \hat{z}_{i,j})}{N}}. \tag{10}$$

Lastly, the model validation compares the ANFIS outputs with the validation data set, a new, unused data set. The validation objective is to evaluate the final model's ability to predict outputs. Validation tests the accuracy of the model with respect to different actual data that are not used in training or checking. Two indexes evaluate the accuracy and precision of the models based on their errors. The arithmetic error means to evaluate the accuracy, or the distance between the error points and their true center value; it is given by Equation (11).

$$\bar{E} = \frac{\sum_{i=1}^{N}(x_{i,j} - \hat{x}_{i,j})}{N} \tag{11}$$

and standard deviation, given by Equation (12), provide information about precision, therefore, how much the error is dispersed,

$$\sigma_E = \sqrt{\frac{\sum_{i=1}^{N}(E_{i,j} - \bar{E})^2}{N}}. \tag{12}$$

In addition to mean and standard deviation, this work calculates the validation metrics of each scientific publication cited in the Introduction for comparison purposes. Abdalla et al. [26] employ Equation (12) and standard mean error (SE), another measure of precision, given by Equation (13),

$$SE = \frac{\sigma_E}{\sqrt{N}}, \tag{13}$$

where SE measures how the number of samples N affects the dispersion of different datasets, as the size of the data increases, the SE decreases; hence, the SE estimates the true mean of the population with greater precision. Lazrak et al.[14] do not explicitly defines its validation index, called the relative mean error (RME). It happens to be the Mean Absolute Percentage Error (MAPE), which Equation (14) describes,

$$MAPE = \frac{\sum_{i=1}^{N} \frac{|(x_{i,j} - \hat{x}_{i,j})|}{x_{i,j}}}{N} \times 100\%. \tag{14}$$

where it is a measure of the precision of a predictive system considering absolute prediction errors, $|(x_{i,j} - \hat{x}_{i,j})|$, relative to the actual measured data, $x_{i,j}$.

5. Absorption Chiller Digital Twin

The Absorption chiller modeling considers four models: (1) internal HTG LiBr temperature, (2) outlet HTG temperature, (3) absorber + condenser, and (4) evaporator. The modeling consists of training, checking, and validation procedures using the total input data from the model. Each model input choice considers only prepared data variables sorted using the correlation coefficient $|\rho| \geq 0.5$ and decomposed using PCA analysis. The result is the total inputs from Model 1, G_1, given by (15):

$$G_1 = [G_{11}\ G_{12}\ G_{13}\ G_{14}], \tag{15a}$$
$$G_{11} = [T_{6B}\ T_{6A}\ T_6\ T_5(k-2)\ T_5(k-1)\ T_5], \tag{15b}$$
$$G_{12} = [V_4\ P_3\ F_1\ T_{amb}\ INV_6\ V_6\ T_4\ V_3], \tag{15c}$$
$$G_{13} = [V_2\ V_1\ T_3], \tag{15d}$$
$$G_{14} = [T_{abs}\ T_1\ T_2], \tag{15e}$$

where G_1 is the total prepared inputs for model 1, G_{11} is the group input 1 of model 1, etc., and each total vector has 63916 samples representing the measured data for 15 days of operation. Note that Model 1 uses three previous samples of T_5; therefore, it is of the third order.

The modeling procedure divides the total prepared inputs, G_1, into three subsets. Equation (16) defines the training inputs,

$$G_1^{train} = [G_{11}^{train}\ G_{12}^{train}\ G_{13}^{train}\ G_{14}^{train}], \tag{16}$$

which uses 56% (8.5 days - 36404 samples) of the total prepared data G_1. Equation (17) defines the checking inputs,

$$G_1^{check} = [G_{11}^{check}\ G_{12}^{check}\ G_{13}^{check}\ G_{14}^{check}], \tag{17}$$

which uses 24% (3.5 days - 15601 samples) of total prepared data G_1. Equation (18) defines the validation input, using 20% (3 days - 11911) of the total prepared data,

$$G_1^{valid} = [G_{11}^{valid}\ G_{12}^{valid}\ G_{13}^{valid}\ G_{14}^{valid}]. \tag{18}$$

Equation (19) describes the training score matrix using the training data set;

the same idea extends to the checking and validation data sets.

$$\mathbf{T}_{11}^{train} = \mathbf{G}_{11}^{train} \times \mathbf{P}_{G_{11}}, \tag{19a}$$

$$\mathbf{T}_{12}^{train} = \mathbf{G}_{12}^{train} \times \mathbf{P}_{G_{12}}, \tag{19b}$$

$$\mathbf{T}_{13}^{train} = \mathbf{G}_{13}^{train} \times \mathbf{P}_{G_{13}}, \tag{19c}$$

$$\mathbf{T}_{14}^{train} = \mathbf{G}_{14}^{train} \times \mathbf{P}_{G_{14}}, \tag{19d}$$

where the loading matrix $\mathbf{P}_{G_{1,g}}$ contains the coefficients of the first principal components of each input group (g = 1,2,...,4) that have a variability greater than 80%.

The ANFIS learning process uses consolidated training, check, and validation data sets. These sets are composed of projections of the grouped inputs and the actual output to be modeled, Equations (20) to (22) describe these sets.

$$\mathbf{Trn}^{G_1} = [\mathbf{T}_{11}^{train}\ \mathbf{T}_{12}^{train}\ \mathbf{T}_{13}^{train}\ \mathbf{T}_{14}^{train}\ \mathbf{T}_{5}^{train}(k+1)], \tag{20}$$

$$\mathbf{Chk}^{G_1} = [\mathbf{T}_{11}^{check}\ \mathbf{T}_{12}^{check}\ \mathbf{T}_{13}^{check}\ \mathbf{T}_{14}^{check}\ \mathbf{T}_{5}^{check}(k+1)], \tag{21}$$

$$\mathbf{Val}^{G_1} = [\mathbf{T}_{11}^{valid}\ \mathbf{T}_{12}^{valid}\ \mathbf{T}_{13}^{valid}\ \mathbf{T}_{14}^{valid}\ \mathbf{T}_{5}^{valid}(k+1)]. \tag{22}$$

Once the learning process is completed, it results in a third-order recursive NF model of the absorption machine. Figure 5 depicts model 1. Note that the respective inputs are multiplied by a constant loading matrix $\mathbf{P}_{G_{1g}}$, truncated in the first two columns, and then fed into the FIS. For example, let us take the training procedure of Model 1, the FIS input results in $G_{11}^{train}(1 \times 6) \times P_{11}(6 \times 2) = T_{11}^{train}(1 \times 2)$, where T^{train} is the score matrix that feeds the FIS for training. Figure 5 depicts the model 1 schematic that predicts the internal temperature of the HTG LiBr, $T_5(k+1)$.

Note that several loading matrices, $\mathbf{P}$, make up the model, reducing the FIS inputs from 20 to 8. The blue lines in Figure 5 are the previous samples of the outlet variable that are fed back and form G_{11}. The same methodology applies to the other models, from 2 to 4, in which the schematics are suppressed to avoid repetition, but are available in Appendix B.

The final ANFIS uses Gaussian MF functions with a hybrid learning method, having a linear MF function output. Table 2 presents the resume of each ANFIS parameter for each chiller subsystem. The number of MFs and rules was chosen based on the subtractive clustering method that empirically varied the influence range. The following subsection describes the selection of epoch numbers.

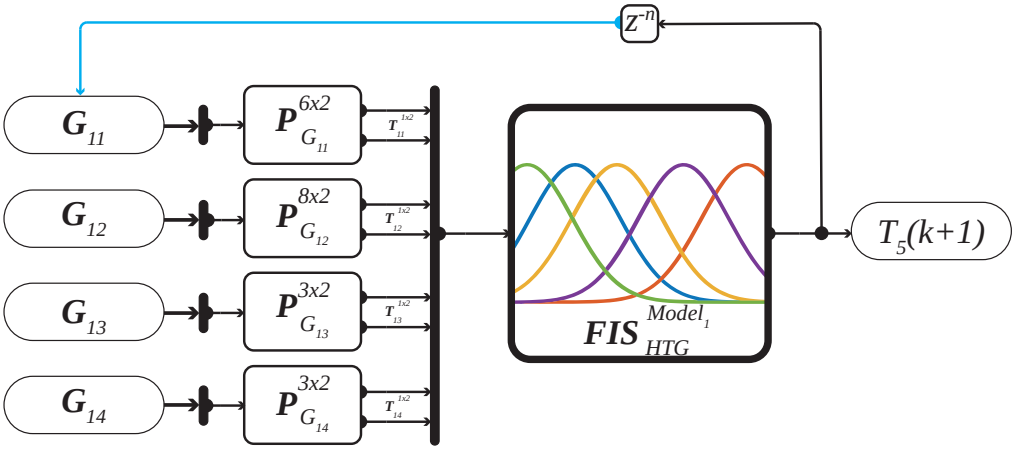

Figure 5: Model 1 - HTG internal LiBr temperature ANFIS model.

Table 2: ANFIS parameters for each Absorption Chiller subsystem.

Subsystem	1	2	3	4
FIS output	T5	T6B	T4	T2
Number MFs:	3	2	3	3
Number rules:	3	2	3	3
Influence range	0.7	0.8	0.7	0.7
Epoch number:	1250	1250	1250	200

5.1. Twinning - Training and Checking

Twinning is "the act of synchronisation between the two entities" [8], or the model update. For the ANFIS model, the twinning occurs when the network is trained and checked. Figure 6 shows the training errors (gray) and check errors (red) of each absorption chiller model versus the epoch number considering the training G^{train}, and checking G^{check}, data set. The number of epochs for Models 1 to 3 was chosen based on the decrease and stabilization of normalized RMSE (nRMSE) at epoch 1250. The learning and checking of model 4 are faster and more stable than the others. Thus, model 4 has 200 epochs. After selecting epochs, each model ran its training and check, varying its influence range, which affects the number of MF and fuzzy rules. Table 3 compiles the minimum normalized root mean square error of the best training and checking tests.

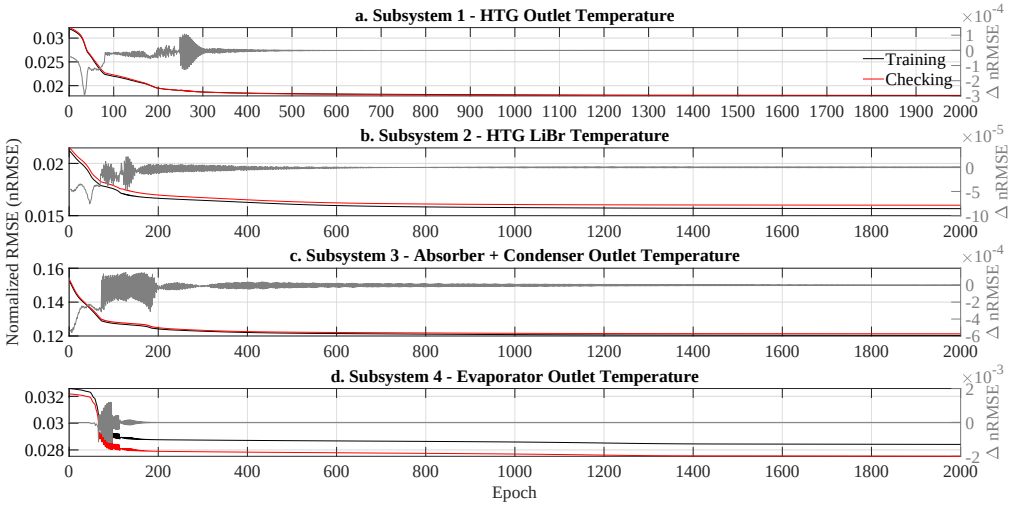

Figure 6: Normalized Root Mean Squared Error (nRMSE) vs. epoch.

Table 3: nRMSE index obtained of learning process (training and checking) for each ANFIS, and twinning/model updating time.

Subsystem	1	2	3	4
FIS output	T5	T6B	T4	T2
$nRMSE_{train}(\times 10^{-3})$	18.08	18.35	120.32	26.24
$nRMSE_{check}(\times 10^{-3})$	17.85	19.14	120.23	26.59
$t_{tw}/sample(ms)$	17.85	19.14	120.23	26.59
$t_{tw}/day(min)$	17.85	19.14	120.23	26.59

5.2. Validation and Discussion

Figure 7 depicts the validation procedure, which consists of comparing the output of the models (black) and the actual validation data set G^{valid} (red).

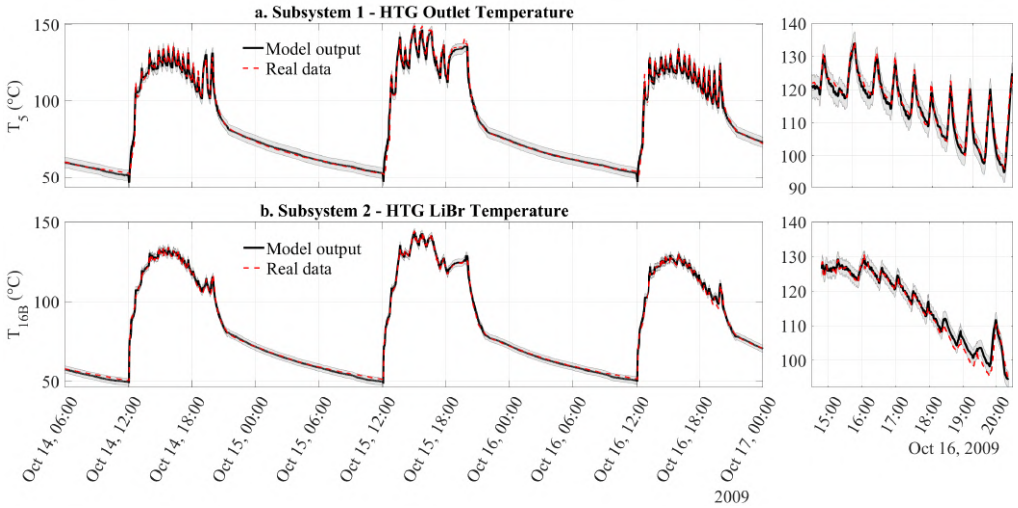

Figure 7: Validation results of model 1 (a) and model 2 (b). The gray shaded area depicts the standard deviation with 95% confidence interval ($T(t) \pm 2\sigma$). The right figure depicts a detailed comparison between model output and actual data during operation.

It can be seen in Figure 7 that the temperatures are intermittent, where the peaks indicate the operation of the chiller and the valleys represent the decrease in overnight temperature due to heat losses with the plant off. The chiller's start-up typically occurs at noon. The delay between sunrise (07:00) and start-up occurs because the Fresnel solar collector takes all morning to heat tubes and water masses to reach the minimum temperature of operation of the chiller heat source of $T6A_{min} = 140^oC$. After reaching the minimum temperature, the F38 inlet valve opens and the chiller runs from 12:00 to 20:00 in a hybrid way, using the solar resource and the gas boiler when solar power is not sufficient.

Figure 7.a describes the internal temperature of LiBr $T5$ during operation. It oscillates between 110 and 140 ^oC due to the controller's action on the F38 inlet chiller valve. Figure 7.a has a zoomed region on the right that depicts this oscillatory behavior from 15:00 to 20:00 on October 16th. Finally, the chiller shutdown occurs at 20:00 with the valve F38 closed, and T_5 decreasing

due to ambient heat losses. The shut-down happens at 20:00 because, with low solar irradiance, the Fresnel cannot feed the chiller. Due to economic disadvantages, the chiller does not run only with the gas boiler.

Figure 7.b shows heat source outlet temperature, $T6B$, which has a profile similar to the internal temperature of LiBr $T5$. This similar profile makes sense since $T6B$ is the outlet temperature of the HTG heat exchanger tube. Thus, $T6B$ results from heat transfer between the inlet temperature of the chiller, $T6A$ and the internal temperature of LiBr, $T5$, along the length of the heat exchanger. The figure on the right 7.b shows the details of $T6B$ during operation. Note that the $T6B$ model follows the trend of peaks and valleys generated by the control and source valve $F38$ operation.

By inference, it can be said that the right-hand-zoom section of Figure 7 indicates that model 1 and model 2 describe the HTG temperatures $T5$ and $T6B$ within the rated operation range. Both models maintain the measured data (red dashed) within two standard deviation intervals (gray area in Figure 7). Therefore, the resulting models describe the chiller at night, when the plant is idle and losing thermal energy to the ambient, and during the day, when the control system modulates the inlet water valves or gas valves while the chiller is operating. These models can describe the plant in its operating range, considering daily events and practical limitations that strongly affect or constrain plant performance. Therefore, the neuro-fuzzy approach embeds the control laws of each model. It is worth saying that the chiller control laws are proprietary and inaccessible. Considering the manufacturer's internal control laws is an essential feature of the model once it is ready to optimize start-up and shut-down times, temperatures, gas boiler use, and prompts to evaluate new control approaches while considering the internal controls.

Figure 8. a shows the absorber + condenser, Model 3, outlet temperature. Note, on the y-axis of Figure 8.a, that $T4$ has a narrow operating range oscillating between 27 and 38^oC. In inspection, it can be seen that the standard deviation (gray) of $T4$ is proportionally higher because the temperature amplitude is approximately 10^oC. The temperature amplitude is narrow because Model 3 is responsible for rejecting the absorption chiller heat from the Guadalquivir river. Therefore, the river temperature drops $T4$, fluctuating around the river temperature. Absorber + condenser has a strong oscillatory behavior during operation that seems to be caused by the HTG on-off temperature control and the $T4$ control that modulates the Guadalquivir river flow. Despite the standard deviation and oscillations, ANFIS model 3 is capable of following the actual $T4$ at night and during operation, as can

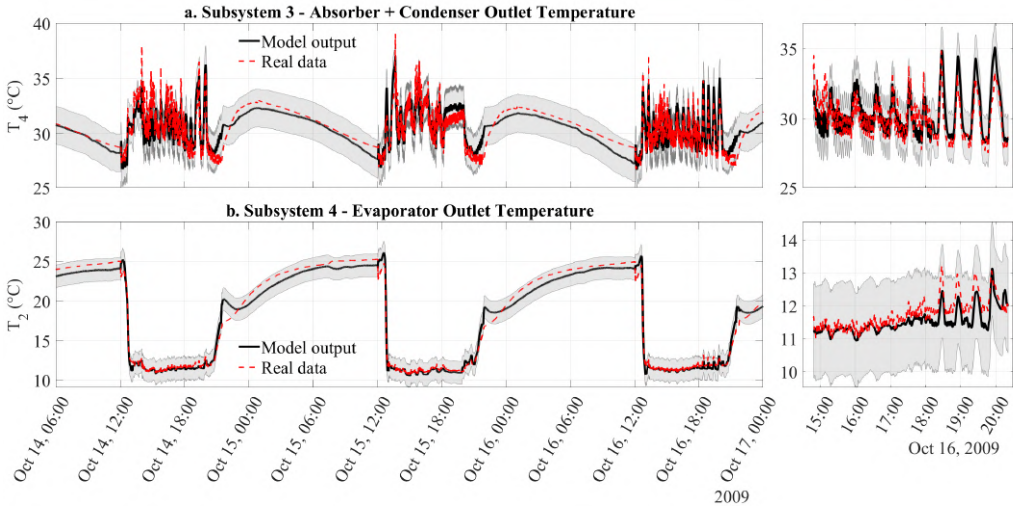

Figure 8: Validation results of model 3 (a) and model 4(b). The gray shaded area depicts the standard deviation with 95% confidence interval ($T(t) \pm 2\sigma$). The right figure depicts a detailed comparison between model output and real data during operation.

be seen in the zoomed right graph of Figure 8.a.

Figure 8.b presents the evaporator, model 4, outlet temperature. The temperature $T2$ represents the temperature of the chilled water. Note that $T2$ in Figure 8.b oscillates between 10 and 27^oC and has an inverse correlation with $T5$ and $T6B$ in Figure 8.a and Figure 8.b. This inverse correlation connects the performance of the Fresnel solar collector in supplying the HTG heat source to the absorption chiller production that the ETSI building HVAC system will ultimately use.

Table 4 compiles the validation metrics. The greater mean error ($\bar{E}$) is 0.27^oC of model 4 - evaporator, followed by 0.20^oC, of the absorber + condenser model 3. Therefore, models 3 and 4 have their output mean slightly super-estimated, while models 1 and 2 have practically centered output mean errors. Furthermore, the greater standard deviation, with 95% of the confidence interval ($2\sigma_E$), is 3.58^oC of model 1, followed in sequence by models 2, 3, and 4, the latter having $2\sigma_E = 1.44$.

The absorber plus condenser ANFIS and SC-ANFIS models in the literature [26] present $\sigma_E = 1.72$. Table 4 shows that the proposed model 3 has $\sigma_E = 0.88$, almost half of the error dispersion that was presented early. The same paper validated the absorber + condenser models considering SE, with

Table 4: Validation indexes.

Model	1	2	3	4
Output	T5	T6B	T4	T2
$\bar{E}$ (^oC)	0.09	0.07	0.20	0.27
σ_E (^oC)	1.79	1.18	0.88	0.72
$2\sigma_E$ (^oC)	3.58	2.36	1.77	1.44
SE	0.02	0.01	0.01	0.01
$MAPE$ (%)	1.24	1.12	2.21	3.24

0.13252 for the ANFIS model and 0.13300 for the SC-ANFIS model [26]. Table 4 presents the ANFIS model 3, with $SE = 0.01$, which is one order of magnitude lower SE. This precision gain in SE is related to the number of samples used. This work validates the results with 11911 samples, while the early published work with 260 [26]. Accordingly, the largest validation set results in fewer SE and a more precise model.

Another previous work develops ANN models considering the MAPE of models 2 to 4. The HTG, absorber + condenser, and evaporator outlet temperatures have MAPEs of 4.4%, 1.6%, and 4.9%, respectively [14]. Table 4 presents this work MAPE, with 1.12%, 2.21%, and 3.24%. Therefore, having lower MAPE for models 2 and 4 and a higher MAPE for model 3, compared to [14]. This should not be a problem once Model 3 cooling water output varies in a narrow ambient temperature range according to the Guadalquivir temperature. In contrast, Model 2 represents the internal temperature of LiBr HTG, and Model 4 represents the temperature of the evaporator's chilled water. Note that this two variables are critical and wide-range variables for plant control and performance. Lastly, no scientific publication of the dynamic ANN modeling of the internal LiBr temperature of the HTG (model 1) was found for comparison.

Table 5: Computational execution time.

Model	1	2	3	4	sum
Average step (ms)	0.18	0.18	0.16	0.16	0.68
Total validation (s)	2.32	2.38	2.07	2.14	8.90

Table 5 shows the computational execution time of the average simulation step, considering 11911 samples, and the total simulation time of the validation data set, or three days of operation. The model runs on MATLAB on

Windows 11 Enterprise 64 bits, with an Intel Core i7-10870H central processing unit, running at 2.20 GHz, having 16GB of RAM. The execution time of the model is a powerful feature. Note that the total time to simulates three days of operation is 8.9s. Considering that the SCADA of the absorption plant runs with sampling times of 20s, and all models execute a simulation step in less than 0.20 ms according to Table 5, the entire chiller computation time of one step results in 0.68 ms, on average, that is, almost 30000 times faster than a sampling time. The model computational speed indicates that it is suitable for Model Predictive Control applications and, together with its gray-box representation, is also an enabling asset for fast what-if analysis and optimization.

6. Conclusions

This work has developed the digital twin of a commercial absorption chiller installed on the roof of the ETSI building in Seville, Spain. The objective was to develop a dynamic model to run what-if analysis, model predictive control improvements, and optimizations. This paper has developed four generalized dynamic models using adaptive neuro-fuzzy inference systems, ANFIS. They describe the internal temperature of HTG from the chiller, the outlet temperatures of the HTG hot source water, the condenser + absorber cooling water, and the evaporator chilled water. The total available data consists of 15 days of operation with a sampling time of $T_s = 20s$, resulting in 63916 samples divided into training, checking, and validation data sets of 36404, 15601, and 11911 samples, respectively. The developed models have shown the following features:

1. Sufficient accuracy and precision accordingly to error mean, standard deviation, standard error, and mean absolute percentage error validation metrics when compared to scientific publications of ANN dynamic models of absorption chillers.
2. Run three days of operation in 8.9s with a simulation time step of 0.68ms while the sampling time is 20s; therefore, fast enough to be used in Model Predictive Control (MPC) techniques.
3. Properly follow actual measurement trends during the day and night with a worst-case mean error of 0.27^oC, and worst-case standard deviation of 3.58^oC (95% confidence interval);
4. Consider boiler gas flow as model inputs; therefore, the HTG models can evaluate the boiler's dynamic operation.

5. Can be re-trained, coping with the plant aging or process modifications because the neuro-fuzzy ANFIS is an adaptive technique.
6. Embed the inaccessible proprietary chillers‘ controls. Therefore, any further investigation on control or optimization of the whole plant would have the actual chiller constraints and controllers' dynamic behavior information.

Before all the above, this work contributes to the ANFIS dynamic modeling of absorption chillers considering its further use in a digital twin framework. Specifically, for the absorption plant modeled in this study, future works will develop further modeling of the Fresnel solar collector to consolidate the whole plant digital twin. Furthermore, its digital twin will unlock control and optimization investigations, which, with the ANFIS feature of gray-box models, will offer a multitude of options.

Acknoledgement

The authors would like to acknowledge the Coordenação de Aperfeiçoamento de Pessoal de Nível Superior (CAPES), Finance Code 001, the Conselho Nacional de Desenvolvimento Científico e Tecnológico (CNPq), under grant 304032/2019–0, the Agencia Estatal de Investigación (AEI) of the Spanish Ministry of Science and Innovation, under grant PID2019-104149RB-I00/10.13039/501100011033 (project SAFEMPC), to the European Commission for funding this work under Project DENiM, this project has received funding from the European Union's Horizon 2020 research and innovation programme under grant agreement No 958339, and the European Research Council under Advanced Research Grant OCONTSOLAR (789051), for funding this work. Diogo O. Machado thanks to IFRS- campus Rio Grande for capacity support, *Fundación Carolina*, SEGIB and PrInt-UFSC programms for mobility scholarships.

Appendix A. Validation data

Supplementary data associated with the validation of this article can be found in `https://data.mendeley.com/datasets/c9jzbmwxsz/1` [35].

Appendix B. Absorption chiller subsystem ANFIS models

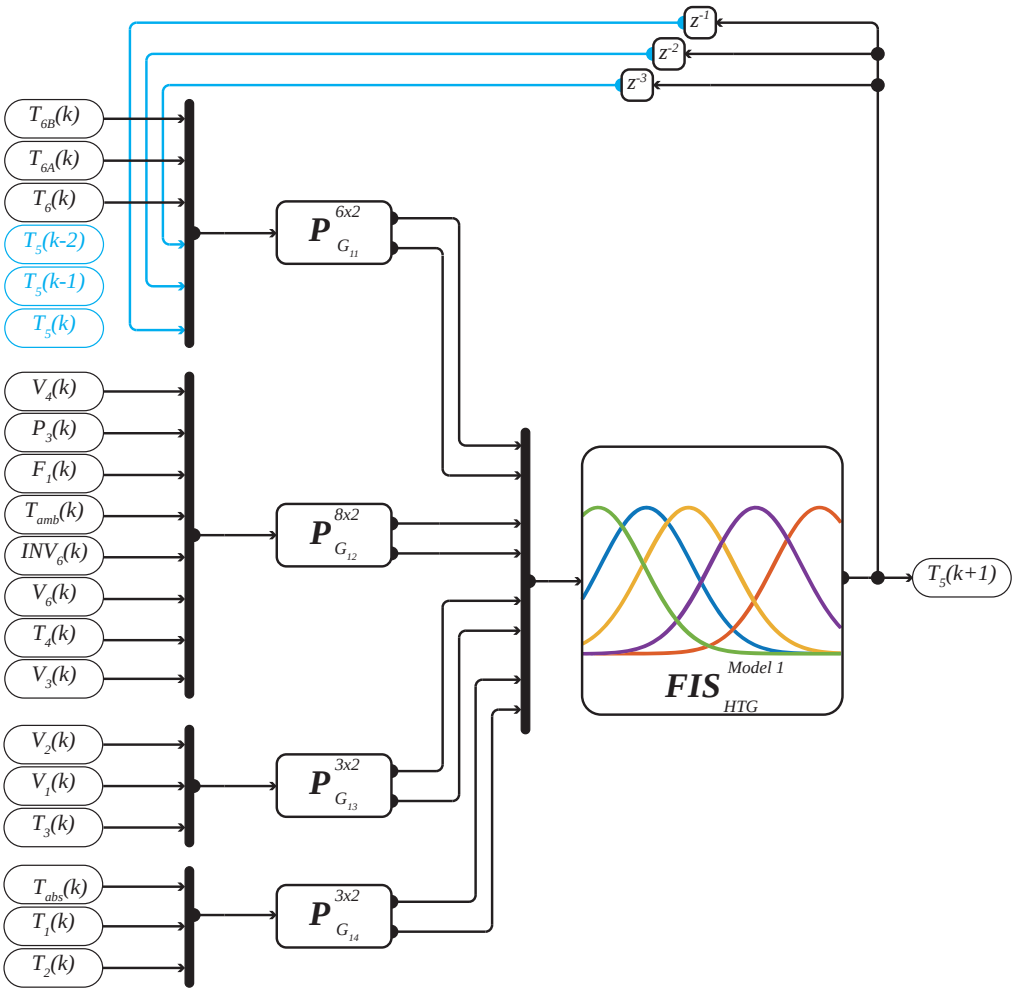

Figure B.9: NF model 1 of HTG internal LiBr temperature T5.

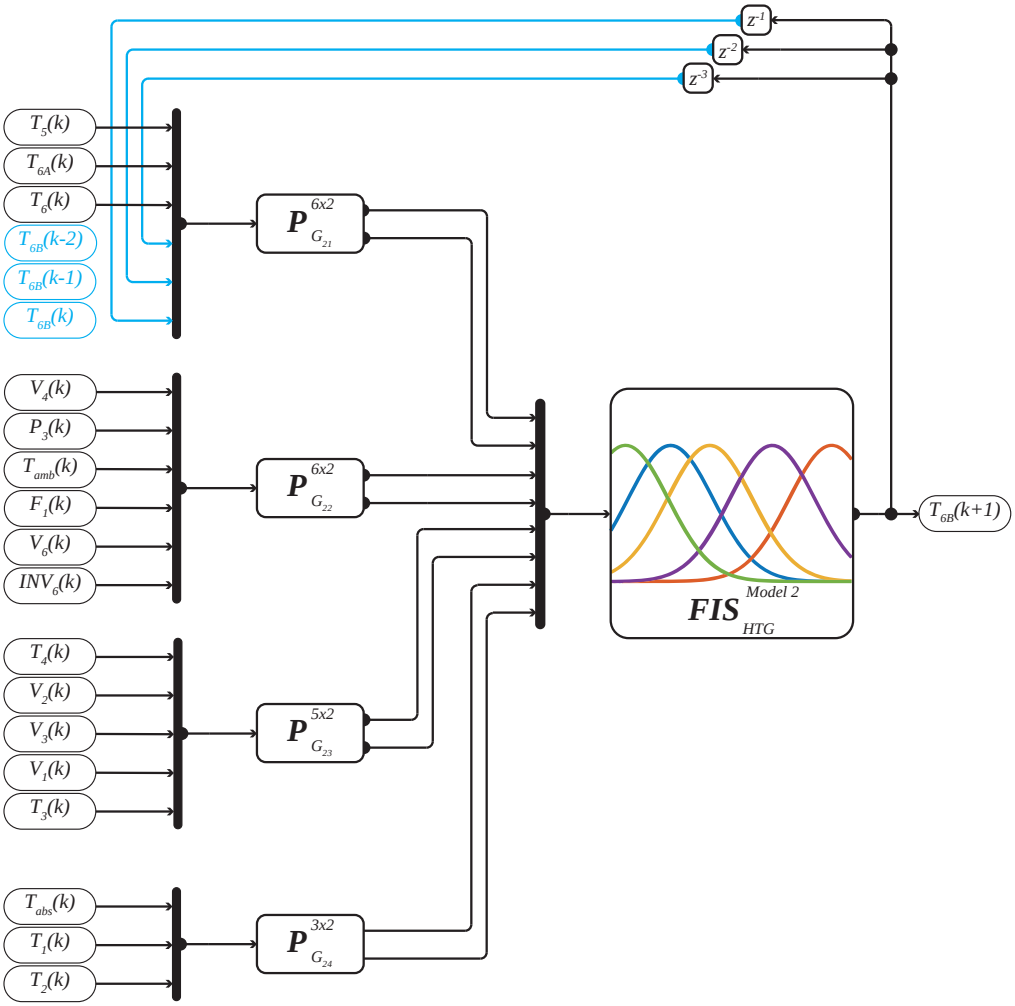

Figure B.10: NF model 2 of HTG outlet temperature T6B.

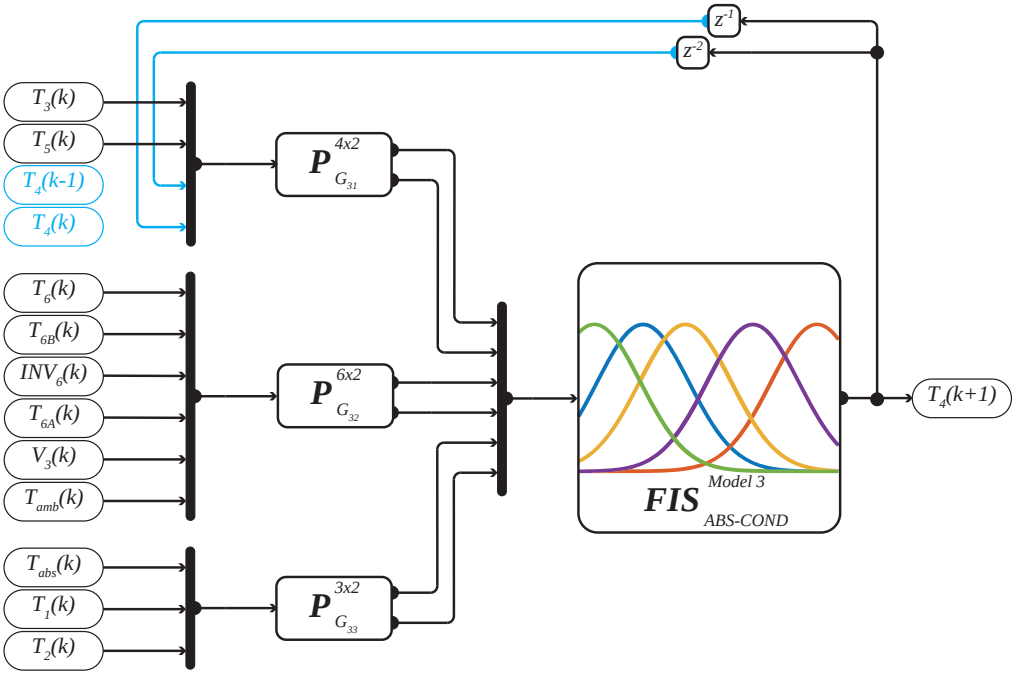

Figure B.11: NF model 3 of absorber + condenser outlet temperature T4.

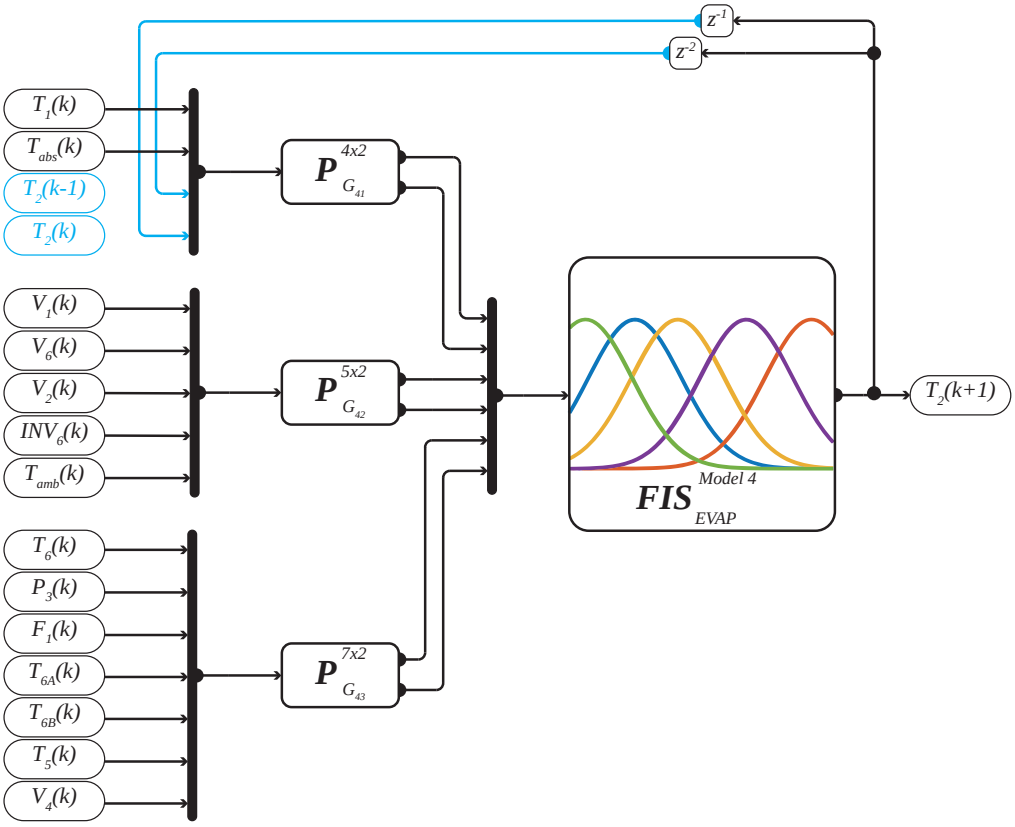

Figure B.12: NF model 4 of evaporator outlet temperature T2.

References

[1] International Energy Agency, Net zero by 2050 - a roadmap for the global energy sector, IEA (2021).
URL https://www.iea.org/reports/net-zero-by-2050

[2] S. Lindmark, The role of absorption cooling for reaching sustainable energy systems, Master's thesis, KTH, Stockolm (2005).

[3] M. Moran, H. Shapiro, D. Boettner, M. Bailey, Fundamentals of Engineering Thermodynamics, 8th Edition, Wiley, 2014.
URL https://books.google.com.br/books?id=uxObAwAAQBAJ

[4] A. Shirazi, R. A. Taylor, G. L. Morrison, S. D. White, Solar-powered absorption chillers: A comprehensive and critical review, Energy Conversion and Management 171 (2018) 59–81. doi:https://doi.org/10.1016/j.enconman.2018.05.091.
URL https://www.sciencedirect.com/science/article/pii/S0196890418305752

[5] M. E. Mondejar, R. Avtar, H. L. B. Diaz, R. K. Dubey, J. Esteban, A. Gómez-Morales, B. Hallam, N. T. Mbungu, C. C. Okolo, K. A. Prasad, Q. She, S. Garcia-Segura, Digitalization to achieve sustainable development goals: Steps towards a smart green planet, Science of The Total Environment 794 (2021) 148539. doi:10.1016/J.SCITOTENV.2021.148539.

[6] M. W. Ahmad, M. Mourshed, B. Yuce, Y. Rezgui, Computational intelligence techniques for hvac systems: A review article history, Building Simulation (2016). doi:10.1007/s12273-016-0285-4.

[7] A. Rasheed, O. San, T. Kvamsdal, Digital twin: Values, challenges and enablers from a modeling perspective, IEEE Access 8 (2020) 21980–22012. doi:10.1109/ACCESS.2020.2970143.

[8] D. Jones, C. Snider, A. Nassehi, J. Yon, B. Hicks, Characterising the digital twin: A systematic literature review, CIRP Journal of Manufacturing Science and Technology 29 (2020) 36–52. doi:https://doi.org/10.1016/j.cirpj.2020.02.002.
URL https://www.sciencedirect.com/science/article/pii/S1755581720300110

[9] M. Yan, W. Gan, Y. Zhou, J. Wen, W. Yao, Projection method for blockchain-enabled non-iterative decentralized management in integrated natural gas-electric systems and its application in digital twin modelling, Applied Energy 311 (2022) 118645. doi:https://doi.org/10.1016/j.apenergy.2022.118645.
URL https://www.sciencedirect.com/science/article/pii/S0306261922001131

[10] M. You, Q. Wang, H. Sun, I. Castro, J. Jiang, Digital twins based day-ahead integrated energy system scheduling under load and renewable energy uncertainties, Applied Energy 305 (2022) 117899. doi:https://doi.org/10.1016/j.apenergy.2021.117899.
URL https://www.sciencedirect.com/science/article/pii/S0306261921012125

[11] J. Granacher, T.-V. Nguyen, R. Castro-Amoedo, F. Maréchal, Overcoming decision paralysis—a digital twin for decision making in energy system design, Applied Energy 306 (2022) 117954. doi:https://doi.org/10.1016/j.apenergy.2021.117954.
URL https://www.sciencedirect.com/science/article/pii/S0306261921012629

[12] Oracle, About the iot digital twin framework (2022).
URL https://docs.oracle.com/en/cloud/paas/iot-cloud/iotgs/iot-digital-twin-framework.html

[13] P. Bermejo, F. J. Pino, F. Rosa, Solar absorption cooling plant in Seville, Solar Energy 84 (8) (2010) 1503–1512. doi:10.1016/j.solener.2010.05.012.

[14] A. Lazrak, F. Boudehenn, S. Bonnot, G. Fraisse, A. Leconte, P. Papillon, B. Souyri, Development of a dynamic artificial neural network model of an absorption chiller and its experimental validation, Renewable Energy 86 (2016) 1009–1022. doi:https://doi.org/10.1016/j.renene.2015.09.023.
URL https://www.sciencedirect.com/science/article/pii/S0960148115303025

[15] A. E. Navas, Refrigeration solar plant with fresnel solar collector (in spanish), Master's thesis, Seville University, Spain (2018).

[16] M. Guerrero Delgado, J. Sánchez Ramos, D. Castro Medina, T. R. Palomo Amores, A. Cerezo-Narváez, S. Álvarez Domínguez, Fresnel solar cooling plant for buildings: Optimal operation of an absorption chiller through inverse modelling, Energy Reports 8 (2022) 3189–3212. doi:https://doi.org/10.1016/j.egyr.2022.02.128.
URL https://www.sciencedirect.com/science/article/pii/S2352484722003742

[17] A. J. G. Len, A. J. S. del Pozo Fernández, J. M. E. González, E. F. Camacho, Model Predictive Control of Solar Cooling Plants: Review and Applications, IFSA Publishing, 2018, Ch. 3, pp. 119–150.
URL https://idus.us.es/handle/11441/108799#.Ym2hcWjCjNM.mendeley

[18] E. F. Camacho, A. J. Gallego, J. M. Escaño, A. J. Sánchez, Hybrid nonlinear mpc of a solar cooling plant, Energies 12 (14) (2019). doi:10.3390/en12142723.
URL https://www.mdpi.com/1996-1073/12/14/2723

[19] P. Li, H. Qiao, Y. Li, J. E. Seem, J. Winkler, X. Li, Recent advances in dynamic modeling of hvac equipment. part 1: Equipment modeling, HVAC&R Research 20 (1) (2014) 136–149. arXiv:https://doi.org/10.1080/10789669.2013.836877, doi:10.1080/10789669.2013.836877.
URL https://doi.org/10.1080/10789669.2013.836877

[20] D. S. Naidu, C. G. Rieger, Advanced control strategies for hvac&r systems—an overview: Part ii: Soft and fusion control, HVAC&R Research 17 (2) (2011) 144–158. arXiv:https://doi.org/10.1080/10789669.2011.555650, doi:10.1080/10789669.2011.555650.
URL https://doi.org/10.1080/10789669.2011.555650

[21] S. A. Kalogirou, Artificial neural networks in renewable energy systems applications: a review, Renewable and Sustainable Energy Reviews 5 (4) (2001) 373–401. doi:https://doi.org/10.1016/S1364-0321(01)00006-5.
URL https://www.sciencedirect.com/science/article/pii/S1364032101000065

[22] K. Gopalakrishnan, S. K. Khaitan, S. Kalogirou, Soft Computing in Green and Renewable Energy Systems, Springer, 2011.

[23] J.-S. Jang, Anfis: adaptive-network-based fuzzy inference system, IEEE Transactions on Systems, Man, and Cybernetics 23 (3) (1993) 665–685. doi:10.1109/21.256541.

[24] J. Jang, C. Sun, E. Mizutani, Neuro-fuzzy and Soft Computing: A Computational Approach to Learning and Machine Intelligence, MATLAB curriculum series, Prentice Hall, 1997.
URL https://books.google.com.br/books?id=vN5QAAAAMAAJ

[25] A. Tamiru, C. Rangkuti, F. M. Hashim, Neuro-fuzzy and pso based model for the steam and cooling sections of a cogeneration and cooling plant (ccp), in: 2009 3rd International Conference on Energy and Environment (ICEE), 2009, pp. 27–33. doi:10.1109/ICEENVIRON.2009.5398677.

[26] E. A. H. Abdalla, P. Nallagownden, N. M. Nor, M. F. Romlie, M. Nayan, Model behavior of cooling plant using subtractive clustering, Journal of Fundamental and Applied Sciences (2018). doi:10.4314/jfas.v10i3s.57.

[27] BROAD Air Conditioning, BROAD IX absorption chiller: model selection and design manual, IFA JISA ARI (2004).

[28] B. H. Gebreslassie, M. Medrano, D. Boer, Exergy analysis of multi-effect water–libr absorption systems: From half to triple effect, Renewable Energy 35 (8) (2010) 1773–1782. doi:https://doi.org/10.1016/j.renene.2010.01.009.
URL https://www.sciencedirect.com/science/article/pii/S0960148110000133

[29] D. Hartmann, M. Herz, U. Wever, Model order reduction a key technology for digital twins, Springer International Publishing, 2018. doi:10.1007/978-3-319-75319-5_8.

[30] S. Joe Qin, Statistical process monitoring: basics and beyond, Journal of Chemometrics 17 (8-9) (2003) 480–502. arXiv:https://analyticalsciencejournals.onlinelibrary.wiley.com/doi/

pdf/10.1002/cem.800, doi:https://doi.org/10.1002/cem.800.
URL https://analyticalsciencejournals.onlinelibrary.wiley.com/doi/abs/10.1002/cem.800

[31] I. T. Jollife, J. Cadima, Principal component analysis: a review and recent developments, Philosophical Transactions of the Royal Society A: Mathematical, Physical and Engineering Sciences 374 (4 2016). doi:10.1098/RSTA.2015.0202.
URL https://royalsocietypublishing.org/doi/abs/10.1098/rsta.2015.0202

[32] S. Wold, K. Esbensen, P. Geladi, Principal component analysis, Chemometrics and Intelligent Laboratory Systems 2 (1) (1987) 37–52, proceedings of the Multivariate Statistical Workshop for Geologists and Geochemists. doi:https://doi.org/10.1016/0169-7439(87)80084-9.
URL https://www.sciencedirect.com/science/article/pii/0169743987800849

[33] T. Takagi, M. Sugeno, Derivation of fuzzy control rules from human operator's control actions, IFAC Proceedings Volumes 16 (13) (1983) 55–60, iFAC Symposium on Fuzzy Information, Knowledge Representation and Decision Analysis, Marseille, France, 19-21 July, 1983. doi:https://doi.org/10.1016/S1474-6670(17)62005-6.
URL https://www.sciencedirect.com/science/article/pii/S1474667017620056

[34] S. L. Chiu, Fuzzy model identification based on cluster estimation, J. Intell. Fuzzy Syst. 2 (3) (1994) 267–278.

[35] D. Machado, W. Chicaiza, J. M. Escaño, A. Gallego, G. de Andrade, J. Normey-Rico, C. Bordons, E. Camacho, Digital twin of an absorption chiller for solar cooling - validation data, Mendeley Data 1 (2022). doi:10.17632/C9JZBMWXSZ.1.

4 DIGITAL TWIN OF A FRESNEL SOLAR COLLECTOR FOR SOLAR COOLING

Highlights

Digital Twin of a Fresnel Solar Collector for Solar Cooling

Diogo Ortiz Machado, William David Chicaiza, Juan Manuel Escaño, Antonio J. Gallego, Gustavo A. de Andrade, Julio E. Normey-Rico, Carlos Bordons, Eduardo F. Camacho

- This work validates neuro-fuzzy (NF) and differential (PDE) models with massive data.
- The models generally represent the process day and night.
- The models are fairly accurate and precise - worst-case MAPE of 2.49%.
- The NF model has ten times faster simulation time than the PDE model.
- The validated dynamic models are the first accounting with mirror's focus action.

Digital Twin of a Fresnel Solar Collector for Solar Cooling

Diogo Ortiz Machado[a,b,c], William David Chicaiza[c], Juan Manuel Escaño[c], Antonio J. Gallego[c], Gustavo A. de Andrade[b], Julio E. Normey-Rico[b], Carlos Bordons[c,d], Eduardo F. Camacho[c,d]

[a] *IFRS - Instituto Federal de Educação, Ciencia e Tecnolgia do Rio Grande do Sul Rua Alfredo Huch, 475, Rio Grande, 96201 460, Rio Grande do Sul, Brasil.*
[b] *UFSC - Universidade Federal de Santa Catarina. Departamento de Automação e Sistemas, R. Eng. Agronômico Andrei Cristian Ferreira, Florianópolis, 88040 900, Santa Catarina, Brasil.*
[c] *US - Universidad de Sevilla. Departamento de Ingeniería de Sistemas y Automática, Camino de los Descubrimientos, Sevilla, 41092, Andalucía, España.*
[d] *ENGREEN - Laboratory of Engineering for Energy and Environmental Sustainability. Universidad de Sevilla.,*

Abstract

This work develops digital entities of a commercial Fresnel Solar Collector (FSC) installed in an absorption cooling plant. The objective is to create and validate models that describe the FSC dynamics across its whole operation range during the day and the night. Thus, the temperatures range between operation temperature of 180 °C and almost ambient temperature due to overnight heat losses. In the same sense, the flow range between zero to $13m^3/h$. The idea is that the digital twin will aid start-up and shut-down optimization and control design reliability. The paper employs two modelling approaches, then evaluates their twinning/adaptation time and performance validation. One model uses phenomenological modeling through Partial Differential Equations (PDE) and parameters identification, and another uses a data-driven technique with Adaptive Neuro-Fuzzy Inference Systems (ANFIS). The available measurement data sets comprise 25 days of operation with a sampling time of 20 s which, after outlier removal, filtering and treatment resulted in 108416 samples. For the validation procedure, six separate operating days have been considered. Results show that both models can

Email address: Corresponding author - bordons@us.es (Carlos Bordons)

twinning/adapt considering measured data. The models present pretty good results and are suitable for control and optimization. Besides, this is the first paper considering the FSC mirror defocus action on the dynamic modelling and validation.

Keywords: Adaptive Neuro Fuzzy Inference System, Distributed parameter dynamic model, dynamic modelling, validation, absorption plant
PACS: 0000, 1111
2000 MSC: 0000, 1111

---

1. Introduction

The solar power that daily strikes planet earth is the driving energy that sustains all life that evolved to an intricate and delicate equilibrium. Therefore, knowing how to harness this power source in a practical and versatile manner will pave the way for a sustainable future. This work contributes to developing two adaptive models of a Fresnel Solar Collector (FSC) in the framework of digital twins. One uses data-driven neuro-fuzzy (NF) networks, and the other uses phenomenological Partial Differential Equations (PDE) with parameters identification. The main idea is to employ both digital entities, considering their particularity, to plan, integrate, and control the absorption plant installed at the *Escuela Tecnica Superior de Ingenieria* - ETSI, Seville, Spain, to increase the renewable energy use.

Policies have been increasing investments and knowledge development to solve the energy problem, considering fossil fuel burning continues to worsen the climate crisis. The reason is that CO_2 emissions from the energy and industry sectors have increased by 60% despite the United Nations Framework Convention on Climate Change in 1992 [1]. The energy sector is the primary source of global emissions, accounting for approximately 60% of global greenhouse gas emissions [2], and the building sector uses 40% of the world's energy production, which 5% is for cooling. Furthermore, the cooling demand tends to grow due to a hotter climate [3]. In this line, investments of 7.4 trillion euros are estimated, in the next 25 years, for the deployment of technologies that eliminate net CO_2 emissions [3]. Therefore, solar cooling technologies development is a clever way to reduce the CO_2 emissions while enhancing cooling plants' technological maturity and economic viability [4]. Thus, solar cooling technology has received much attention [5].

Solar absorption plants produce cold from a solar-heated source through

an absorption thermodynamic cycle [6]. It has the feature of having solar energy availability following the cooling demand. The problem is that using solar energy as the primary source adds the complexity of having a process that is intermittent during the day, night, and year seasons. Besides, sun irradiance that strikes the absorber is subject to clouds that strongly affect the plant's dynamic behavior. Thus, it is critical to generate a stable heat source for the absorption chiller.

Several concentrating solar collector types harvest thermal solar energy. Parabolic Trough Collectors (PTC) and Fresnel Solar Collectors (FSC) are among the line focus systems. Despite PTC technological maturity and higher efficiency, the FSC has advantages compared to PTC [7], mainly, cheaper production resulting in equivalent Levelized Cost of Electricity. Besides, FSC has room for further technological development [7, 5]. In this way, improving the technological/economic performance of these systems [8] is highly desirable [9]. This work seeks to improve FSC operation through its Digital Twin formulation for control and optimization.

A Digital Twin (DT) has many definitions. In a review study, Rasheed et al. [10] state that a Digital Twin is a "virtual representation of a physical asset enabled through data and simulators for real-time prediction, optimization, monitoring, controlling and improved decision making". Although the concept, its definition, and the related studies, continue to evolve in many areas [11]. Digital Twin is one of the most promising enabling technologies for Industry 4.0 viability, already having applications in the industry through publications, patents, and best practices of leading companies. The applications cover product lifecycle, product design, reliable/flexible production, prognostics, and health management [12]. The application of DT in the energy sector is relatively scarce. Rasheed et al. [10] compiles DT contributions to the energy sector, having studies on asset maintenance, energy saving, improving efficiency in smart factories aiming to reduce both production costs and greenhouse gas emissions, design, construction, and performance of residential buildings. Although, only one study was published with a full-scale DT of a district heating and cooling network. As can be seen, a core DT enabling technology is the modelling, simulation, verification, and validation.

This paper develops both physical and data-driven models of the Fresnel Solar Collector (FSC) of *Escuela Técnica Superior de Ingeniería de Seville* (ETSI), Spain, to compose its DT, and validates their performances considering the computational execution time and statistical indexes. The plant location is on the roof of the ETSI building. It aims to supplement the air

conditioning system with chilled water to reduce electric consumption, CO_2 emissions, and operating costs [13]. The plant is a multi-energy system once it transforms solar irradiance into thermal internal energy, hot water into chilled water (thermal to thermal), and gas chemical energy into thermal internal energy. This system is also complex, highly non-linear, and dynamic, switching between electric, gas, and solar resources according to meteorology and demand profiles. The objective is to integrate and enhance the energy system with control [14] and optimization techniques [15].

It is worth noting that the ETSI plant is a physical entity. It has computers, servers, and industrial communication structures able to connect the virtual and physical spaces. Thus, the only asset not available for the ETSI absorption plant DT is its adaptive virtual entity or its adaptive dynamic model. This work seeks to expand the ETSI FSC model with the following specifications:

1. To consider the transitory regime, the continuous focus/defocus of the mirrors, and the cleanliness factor.
2. To have defined accuracy and precision indexes through validation with a representative amount of data.
3. To run fast enough to be used in Model Predictive Control (MPC) techniques.
4. To describe transients, and part-load, during the day and night for control, optimization, and what-if decisions.
5. To adapt and cope with the aging of the FSC for updated plant operation, long-term and life-cycle assessment.

These specifications have the following justification. Describing the solar collector considering day and night is especially important because solar plants are intrinsically intermittent and have appreciable heat losses during the night. Thus, this model feature can aid start-up/shut-down decision-making, contributing to optimal thermal storage strategy formulation [13]. The focus/defocus action is critical for the safety [16] and control [17] of FSC. However, to the best of authors' knowledge, there is no FSC validated model published considering the defocus feature. The cleanliness factor is related to thermal efficiency and varies over time. Thus, a model that can adapt such parameter is necessary to predict when it is necessary to stop the FSC for maintenance, and cleaning [16]. Stating the model's accuracy and precision with mean error and standard deviation, among other statistical indexes,

gives information about the models' confidence and the fidelity level of DT's simulations and what-if analysis [10, 18, 19, 20]. The updating/adapting procedure of the virtual entities/models is called twinning. The twining is synchronizing the virtual and physical entities [18], measuring the physical entity state, and updating the virtual entity to reduce the difference between them. This process can occur either from physical-to-virtual or virtual-to-physical spaces, in a closed loop, with a twinning rate. To the authors' best knowledge, there is no published FSC dynamic model to consider such features. A specific literature review for the modelling of FSC on the ETSI absorption plant leads to the following works:

Robledo et al. [21] develop a phenomenological lumped parameter dynamic model considering the optical and thermal models and an ordinary differential equation. The authors used least-squares methods to identify the model's parameters. The validation considered four operation days data, with a 7.5h duration each. The validation outlet temperature range is from 85 to 165°C, the results are qualitatively presented, contrasting the actual data and model output plots.

Spoladore et al. [22] develop a phenomenological, distributed parameters, dynamic model, considering the optical and thermal models and Partial Differential Equations (PDE). The authors used least squared methods to identify the global heat loss and the metal-fluid heat transmission coefficients considering second-degree polynomial functions. The validation considered two operation days data from 11:00 to 18:00, on May 27, 2010, and November 17, 2009. The validated outlet temperature range is from 100 to 180°C, with a maximum error of 8°C. The authors present qualitative comparison plots between model prediction and actual data.

Pino et al. [16] develop phenomenological, steady-state, thermal, and optical models using algebraic equations that account for the focus of the mirrors. The validation considers the mirror's rows inclinations, absorbed heat, and outlet temperature during operation between 13:00 and 15:30 of May 27, 2009. The validated outlet temperature range is from 147 to 168.5°C, with relative errors of less than 1%.

Chicaiza et al. [23] develop data-driven dynamic models based on Adaptive Neuro-Fuzzy Inference System (ANFIS) to compose a DT. The ANFIS training considers two days of actual data and artificial data from PDE models. The validated outlet temperature range is from 40 to 180°C in three days of actual data. The authors present qualitative plots between measured and model outlet temperatures and calculate the Root Mean Squared

Error (RMSE) and the Mean Absolute Percentage Error (MAPE) for each day. The worst-case RMSE=12.96 ℃ and MAPE=8.54%, while the best-case RMSE=3.67 ℃ and MAPE=2.27%.

Considering the previous works on the ETSI FSC modelling, this paper has the following contributions.

1. It develops dynamic models using both ANFIS [24] and PDE [25] to generate a transparent model with explicit equations and expand FSC models capabilities. This work uses 25 days of operation data with a sampling time of $t_s = 20\ s$, with continuous data between day and night.
2. The ANFIS twinning (training and checking), and validation consider 19 days of measured data. On the other hand, the identification of PDE model parameters uses 4 days of measurement data re-sampled every 5s to avoid numerical integration instability. The massive amount of data in twinning results in generalized dynamic models of both ANFIS and PDE.
3. The validation procedure considers six days of actual operation data, three in June, and three in October. The validation results indicate that the models can adequately represent the behavior of the FSC outlet in a wide temperature range, from 40 to 180℃.
4. The models describe operations continuously during day and night, part-load operations, or overnight, with heat losses.
5. To the best authors' knowledge, this work presents the first FSC-validated dynamic models that describe the mirror's focus/defocus action.
6. Lastly, this work contributes to testing the computational speed of resulting dynamic models during twinning and simulation, setting the execution time limits of the models regarding MPC and dynamic optimization techniques.

The organization of the rest of the paper is as follows. Section 2 defines the FSC process and presents the real data preparation and its correlation analysis, closing with the FSC operation description. Section 3 presents the FSC phenomenological distributed parameters modelling and its identification. Section 4 states the ANFIS architecture and defines its training procedure. Section 5 defines the simulation planning with the model structure definition and data sets preparation. Section 6 states the results divided in

two parts, the first is the twinning time of both models (training and identification), and the second part is devoted to validation results and indexes considering actual data. Lastly, Section 7 shows the findings of this work and closes the paper.

2. Fresnel Solar Collector Process

The Fresnel solar collector (FSC) installed at ETSI was constructed by PSE AG, which activities have passed to Mirrox Gmbh, and today is Industrial Solar [26]. Figure 1 depicts the referred Fresnel concentrating solar collector that generates heat for an absorption chiller that, in its turn, supplements the building air conditioning system with a renewable primary energy source. The solar field has an 18° orientation in the east-west direction, a total area of 352 m^2, where 11 mirror rows and 16 modules compose the optical system, summing 64 m of length, which focus the solar irradiance to the receiver as depicted in Figure 2. The receiver, in its turn, is composed of a secondary reflector and an absorber tube, where glass thermal insulation equips both. Steel DNI 1.4541 (AISI321) composes the SCHOTT PTR70 [27] absorber tube, installed 4 meters above the mirror's plane.

Water is the heat transfer fluid and flows inside the absorber tube, with 13 *bar* and 180 ℃ of nominal pressure and temperature, respectively. Table 1 presents the main characteristics of the Fresnel solar collector.

The FSC objective is to generate a hot outlet temperature flow. The incident irradiance and the inlet temperature are the critical disturbances of the solar collector process because they fastly and widely affect the outlet temperature. The plant start-up occurs when the solar irradiance reaches a minimum, starting the pump and generating flow inside the absorber tube. After this beginning, the controller manipulates the flow to regulate the outlet temperature of the collector with the objectives of reference tracking and disturbance rejection. The plant's shut-down occurs when irradiance reaches a given minimum value.

2.1. Data Preparation

Neuro-fuzzy (NF) and Partial Differential Equations (PDE) models are updated and validated using actual data. Therefore, it is necessary to filter instrumentation noise and carefully choose variables that affect the process.

This work employs raw data from the solar absorption plant's SCADA system that stores measurements in Excel data sheets daily. Each file has

Table 1: ETSI Fresnel solar collector characteristics [13, 27].

Parameter (symbol)	Value	Unit
Total area	512	m^2
Total mirror area (A_t)	352	m^2
Absorber length	64	m
Absorber height	4	m
Mirror unitary length	4	m
Mirror unitary width	0.5	m
Total Mirror aperture (G)	5.5	m
Mirrors rows	11	-
Number of mirrors	176	-
Absorber tube specific mass (ρ_m)	8027	kg/m^3
Absorber tube external diameter	0.07	m
Absorber internal diameter	0.066	m
Absorber tube specific heat (c_m)	500	$J/(kg$ ℃)
Receiver cavity aperture	0.3	m
Heat transfer fluid	Água	-
Nominal temperature	180	℃
Nominal pressure	13	bar
Nominal thermal power	120	kW

18 variables (columns) imported to Matlab as timetables with the respective headers or variable names. An algorithm tests each Excel sheet header to maintain the same variables' order names to avoid mixing different variables in one array. Then each available day of operation was concatenated by time, considering consecutive days. Data inspection indicates incomplete data, missing measurement values, and irregularly sampled data. The data preparation consists of re-sampling the initial timetables using linear interpolation using the new sample as the mode of raw data heterogeneous sampling times, which is t_s=20s. After the data import and re-sample procedure, it passes through a concatenation, resulting in eight regular timetables: from June 9 to 12, 23 to 26; 29 to 30, August 11 to 12, 14 to 17; September 2 to 3, 22 to 25; and October 14 to 16, totaling 25 days of operational data.

Next, a moving mean filter with a 6min window was applied to remove outliers from data sets. Furthermore, a one-by-one evaluation substituted

Figure 1: Fresnel solar collector installed at ETSI absorption solar plant [23].

negative pressures, flows, and inconsistent variables by the minimum or maximum absorption solar collector operation range considering manufacturer's data-sheet [26]. The variable-by-variable inspection also led to the discovery of empty columns further deleted. Furthermore, pressure and flow variables were smoothed using Gaussian interpolation, with a 15 sampling window. As a result, 14 variables compose the final data set with 108416 samples. The following section presents the data selection based on correlation maps.

2.2. Correlation analysis of FSC field I/O variables

The correlation coefficient measures of association between variables, the most widely used is the linear correlation coefficient. Pearson's correlation coefficient (ρ) for pairs of variables $(\mathbf{x}, \mathbf{y})$ with n samples $\mathbf{x} = [x_{1,1}, \cdots, x_{n,1}]$ and $\mathbf{y} = [y_{1,1}, \cdots, y_{n,1}]$ is given by

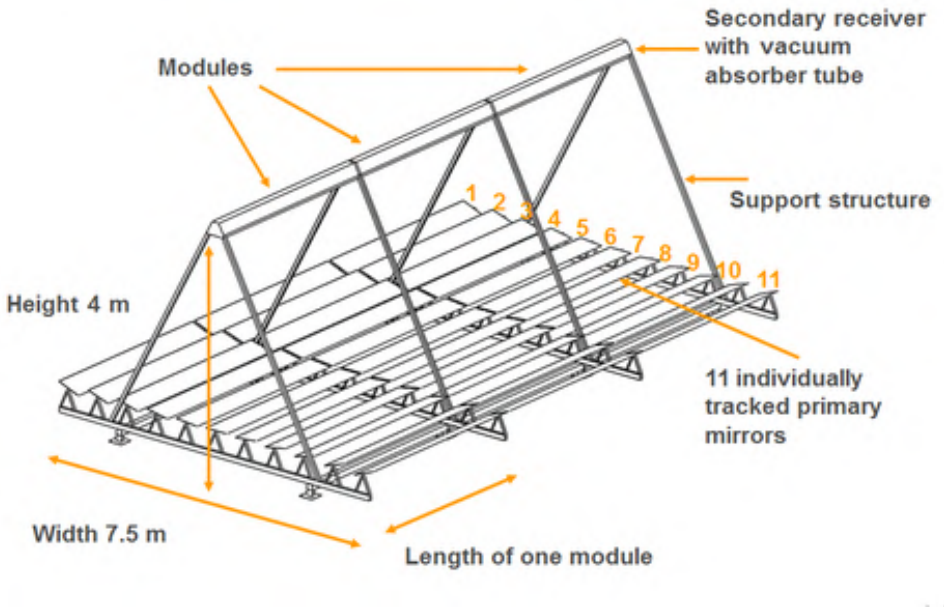

Figure 2: Fresnel solar collector model installed at ETSI absorption solar plant [26].

$$\rho(x,y) = \frac{1}{n-1}\sum_{i=1}^{n}\left(\frac{x_{i,1}-\mu_x}{\sigma_x}\right)\left(\frac{y_{i,2}-\mu_y}{\sigma_y}\right), \tag{1a}$$

$$\mu_x = \frac{1}{n}\sum_{i=1}^{n} x_{1,i}, \tag{1b}$$

$$\sigma_x = \sqrt{\frac{1}{n-1}\sum_{i=1}^{n}(x_{1,i}-\mu_x)^2}, \tag{1c}$$

where μ_x and σ_x are the mean and standard deviation of the samples of $\mathbf{x}$, respectively, and μ_y and σ_y are the mean and standard deviation of $\mathbf{y}$. The values that ρ can take are between $[-1, 1]$, where $\rho = -1$ represents a complete negative correlation, $\rho = 1$ represents a complete positive correlation, and a value of $\rho = 0$ indicates that the variables $(\mathbf{x}, \mathbf{y})$ are uncorrelated.

The correlation coefficient matrix ($\mathbf{R}$) of the random variables M is $\mathbf{R} \in \Re^{M\times M}$ for each combination of pairwise variables. Only for x and y, result in the following matrix $\mathbf{R} \in \Re^{2\times 2}$:

$$\mathbf{R} = \begin{pmatrix} \rho(x,x) & \rho(x,y) \\ \rho(y,x) & \rho(y,y) \end{pmatrix} = \begin{pmatrix} 1 & \rho(x,y) \\ \rho(y,x) & 1 \end{pmatrix}. \tag{2}$$

The next step is sorting the input variables in a degree of relationship. The sort evaluates the degree of correlation for each input regarding the desired output to analyze which variables impact the model output concerning a threshold. In the case of FSC, the desired output is the outlet temperature $Tf2$. Figure 3 shows the correlation coefficient matrix of the actual Fresnel solar field data. Where f is the mirrors' focus, varying between 0 for full defocus to 1 for complete focus; q is the volumetric flow, P is the hydraulic pressure, $Tf1$ and $Tf2$ are the inlet and outlet temperatures, respectively; ws is the wind speed, I is the solar irradiance, H is the humidity, $Tamb$ is the environment temperature. $EffOpt$ is the optical efficiency accordingly to Brandão et al. [28], and $Tf1$ *delay* is the delayed inlet temperature calculated accordingly to Normey-Rico et al. [29].

2.3. FSC operation

Figure 4 depicts the main operation variables from the prepared data considering two operation days: from June 24, 06:00; to June 26, 00:00,

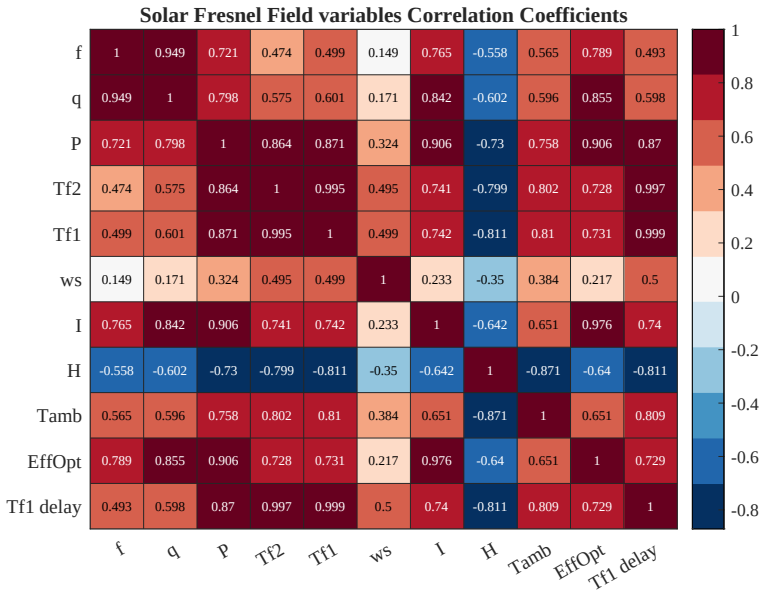

Figure 3: Correlation coefficients matrix of the prepared ETSI FSC field data.

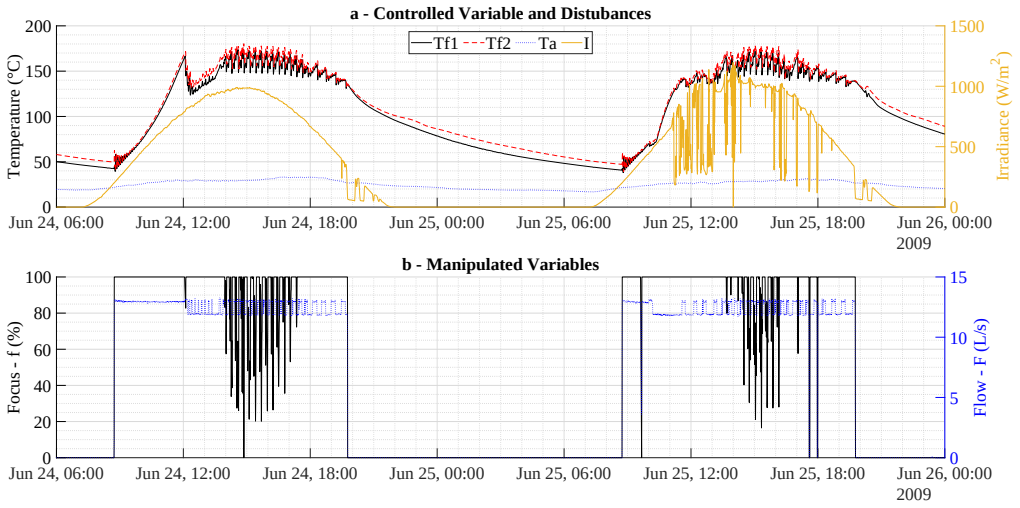

Figure 4: FSC consecutive days operation actual data. a. The FSC outlet temperature $Tf2$ is the controlled variable, while the inlet temperature $Tf1$ and Irradiance I are the prominent disturbances. b. The FSC installed at ETSI has two manipulated variables, the typical flow F, and the mirror's focus f.

2009. It is worth saying that the validation section uses the exact actual data.

By inspecting Figure 4.a, one can see two days of irradiance profile. The irradiance profile (continuous yellow line) of June, 24, is smooth, with the sunrise at about 06:00, a peak at 15:00, and the sunset at 22:00. The operation stages follow the irradiance profile, where the start-up occurs when there is enough irradiance, $I \geq 200$ (W/m^2), at almost 09:00 turning on the pump, see Figure 4.b. Note that the flow goes from 0 to 13 m^3/h together with the mirror's focus from 0 to 100%. Next, the heating phase occurs with the FSC increasing its temperature from 09:00 to 12:00. Then, the absorption chiller consumes the FSC thermal power. It generates a sudden temperature drop followed by a temperature increase return between 12:00 and 14:00. The temperature drop results from the absorption chiller's lower internal temperature injection in the FSC hydraulic loop. After a recovery period, the temperature increases again due to the gas boiler operation.

After the absorption chiller start-up, aided by the backup gas boiler from 12:00 to 14:00, the boiler is shut-down. The plant operates roughly at the nominal point with solar irradiance only, producing chilled water for the ESTI air conditioning system. Note that the temperatures are highly oscillatory from 14:00 to 20:00 due to the absorption chiller on-off controller operation. The two-position valve effect is evident in the hydraulic loop flow (blue dotted line) in Figure 4.b, where F varies between two levels during operation. This bi-stable event happens because when the controller feeds the chiller High Temperature Generator, a heat exchanger with long tubes generates a pressure drop reflecting the flow changes in Figure 4.b. For further information on the whole plant control logic, refer to [17].

When the irradiance is too low, that is I$\leq$200 (W/m^2), the flow and focus go to zero, and the plant shuts down at 20:00. Then, from 24 June, 22:00, to 25, 09:00, the FSC temperatures decrease overnight- see Figure 4.a. After these heat losses, the operation is re-started on June 25, at 09:00. The sequence of the same events as the previous day happens. It is worth noting that the irradiance profile of June 25, unlike the previous day, is very oscillatory.

Considering Figure 4, where the actual operation of the ETSI absorption plant is depicted, it is evident that the process is complex, highly non-linear, and intermittent with a wide operational range of the variables, such as temperatures, flows, and solar irradiance. Thus, developing the FSC digital twin is not trivial, and the respective models must cope with and describe such

a wide range of operations and phenomena to reflect the dynamic behavior of the FSC. After the FSC digital twin creation, it allows for optimizing the start-up, operation, and shut-down, considering changing meteorological and plant conditions while offering accurate predictions for model-based predictive control techniques. The following sections present the two model structures used in this work.

3. Phenomenological - PDE Modeling

The mathematical description of the Fresnel's temperature distributed in time and space is given by the partial differential equations (3) and (4) [25].

$$\rho_m c_m A_m \frac{\partial T_m}{\partial t}(t,x) = \dot{Q}_{sun}(t) - \dot{Q}_a(t,x) - \dot{Q}_f(t,x), \tag{3}$$

$$\rho_f c_f A_f \frac{\partial T_f}{\partial t}(t,x) + \rho_f c_f q(t) \frac{\partial T_f}{\partial x}(t,x) = \dot{Q}_f(t,x), \tag{4}$$

where the sub-indexes m, f, sun and a refers to the metal absorber tube, fluid, the sun, and the environment, respectively. The variable ρ is the specific mass (kg/m^3), c is the specific heat (J/(kg °C)), q is the mass flow (kg/s), such that the volumetric flow is $F(t) = \rho_f q(t)$, T, is the temperature (°C), t is the time (s), $x \in [0, L]$, with $L > 0$, is the space (m), $\dot{Q}_{sun}$ is the sun heat rate (W) that flows from the sun to the solar collector, $\dot{Q}_a$ represents the thermal losses (W) to the ambient, and $\dot{Q}_f$ is the heat rate (W) that relates to the mass flow. Eq. (5) gives the boundary condition of Eq. (3),

$$T(t,0) = Tf1(t), \tag{5}$$

where $Tf1$ is the Fresnel inlet temperature. Finally the initial conditions of the system are given by Eq. (6)

$$T_m(0,x) = T_m^0(x), \qquad T_f(0,x) = T_f^0(x), \tag{6}$$

where T_m^0 and T_f^0 are functions that satisfy the steady state condition of eqs. (3) and (4).

Papers found in literature use the system of equations (3)-(6) for both parabolic through and Fresnel collectors. The difference among the different solar collector's equations is mainly in calculating the optical efficiency η_{opt} once each type of solar collector has a specific primary and secondary mirrors

scheme [30]. The optical efficiency is in the inlet solar heat term, $\dot{Q}_{sun}$, which Eq. (7) describes,

$$\dot{Q}_{sun} = \eta_T \eta_{opt} A_t I(t), \tag{7}$$

where η_T and η_{opt} are the thermal and optical efficiency, respectively, $A_t(\mathrm{m}^2)$ is the total area of collector's mirrors, and I is the solar irradiance per mirror length in $\mathrm{W/m}^2$.

A Fresnel efficiency has both variable and constant parameters in time. For example, having a given collectors' orientation and solar time is possible to calculate the solar beam's incidence angles and the respective reflection cosine losses. Although the reflexivity and other characteristics of the mirrors vary with plant aging, dirt accumulation, and water condensations in the mirrors. Thus, this work considers that the variable η_{opt} contains the deterministic and constant parameters, which are calculated accordingly to Brandão et al. [28], considering the geometrical relation between the mirrors and absorber. With η_{opt} is possible to calculate the equivalent irradiance that arrives in the absorber tube $I_{eq} = I(t)\eta_{opt}$. The time-varying and, a priori, unknown efficiency-related parameters are embedded in one unique parameter called thermal efficiency η_T, which this work estimates using an identification technique.

This work applies Euler's finite differences discrete approximation, according to Figure 5 schematic, to solve equations (3) and (4), that are continuous in time and space. The spatial derivative in a given time instant is given by

$$\frac{\partial T_f}{\partial x}(t,x) \approx \frac{T_f(t,n) - T_f(t,n-1)}{\Delta x},$$

where $\Delta x = L/S$ is the length of the spatial discretization, S is the number

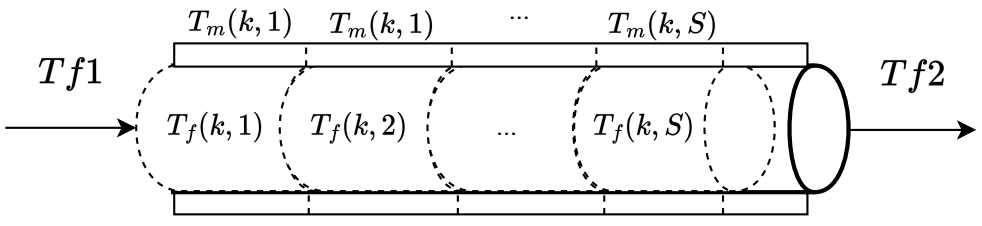

Figure 5: Absorber tube discretization considering S=16.

of points, and $n \in \{1, \ldots, S\}$ is the respective given volume. Note that $T_{t,0} = Tf1(t)$, as equation (5) presents.

Considering the time derivatives, M constant time intervals composes the whole time horizon $t \in [0, t_f]$, where t_f is the final time, such that $\tau_k \in [0, t_f]$, $k = \{1, \ldots, M\}$, are points in the discretization mesh with respect to the time, with

$$0 = \tau_1 < \cdots < \tau_{M-1} < \tau_M = t_f.$$

This discretization is considered equidistant for simplicity. Thus,

$$\Delta t = \frac{t_f}{M-1}, \qquad \tau_k = (k-1)\Delta t, \qquad k \in \{1, \ldots, M\}.$$

and the time derivatives approximations are

$$\frac{\partial T_m}{\partial t}(t,x) \approx \frac{T_m(k+1,x) - T_m(k,x)}{\Delta t},$$
$$\frac{\partial T_f}{\partial t}(t,x) \approx \frac{T_f(k+1,x) - T_f(k,x)}{\Delta t}.$$

The derivative approximations in time and space above transform equations (3)-(4) in algebraic discrete equations (8) and (9)

$$\begin{aligned} T_m(k+1,n) &= T_m(k,n) \\ &\quad + \Delta t \left(\frac{\dot{Q}_{sol}(k)}{\rho_m c_m A_m} - \frac{\dot{Q}_a(k,n)}{\rho_m c_m A_m} - \frac{\dot{Q}_f(k,n)}{\rho_m c_m A_m} \right), \end{aligned} \tag{8}$$

$$\begin{aligned} T_f(k+1,n) &= T_f(k,n) \\ &\quad + \Delta t \left(\frac{q(k)}{A_f} \frac{T_f(k,n) - T_f(k,n-1)}{\Delta x} + \frac{\dot{Q}_f(k,n)}{\rho_f c_f A_f} \right), \end{aligned} \tag{9}$$

where

$$\dot{Q}_a = D_m \pi [a(T_m(k,n) - T_a(k))^3 + b(T_m(k,n) - T_a(k))], \tag{10}$$

$$\dot{Q}_f = D_f \pi H t (T_m(k,n) - T_f(k,n)), \tag{11}$$

$D_m(m)$ is the equivalent diameter of the tube walls, $D_f(m)$ the internal tube diameter, a and b are the coefficients of heat losses of the absorber polynomial

function, and $H_t(W/(m\ ^\circ C))$ the coefficient of heat transfer between the tube walls and the fluid.

It is worth noting that this paper proposes a third-order heat loss polynomial function to describe the heat losses coefficient, equation (10), instead of fourth and second-order polynomials that are typically used [22, 21]. The third-order polynomial is employed because it becomes possible to change the sign of $\dot{Q}_a$ of equation (10), and consequently, the heat losses term of equation (8). That is, by using a third-order polynomial, the tube can also represent the case where the heat enters the tube instead of exiting. The case where the tube receives heat occurs if the plant does not operate for days. Therefore, the tube's temperature tends to ambient temperature. In this case is possible that $T_m < T_a$. Thus, the model can reproduce the plant's dynamic behavior in real-time, becoming a tool for what-if analysis of the start-up and shut-down of the plant independently of the state of the process after day and night of operation.

To integrate equations (8) and (9), it is necessary to iterate $T_m(k+1, n)$ and $T_f(k+1, n)$ from the initial and boundary conditions given in $T(0, n)$ and $T(k, 0)$, respectively, from n=1 to n=S, and from k=1 until k=M. This work employs the *ode45* package of MATLAB [31] for the integration of the phenomenological model.

3.1. Identification

The previous section has presented the FSC's model considering phenomenological concepts and, therefore, the main dynamics that occur in the plant. The model has thermodynamical characteristics such as specific mass, specific heat, and heat transfer coefficients between the heat transfer fluid, the metallic tube, and the environment. Despite knowing these parameters for pure substances and materials references, the values can vary sensibly due to the plant aging, corrosion, mirror soiling, and internal pipe walls crusting. Thus, these parameters are time-varying; thus, it is necessary to identify their values to plug in the model for representing the process in a given time regarding the data used for identification.

One advantage of eqs. (8) and (9) is the possibility to estimate the parameters' values by comparing the model output with experimental data. To do so, a quadratic non-linear minimization algorithm through Eq. (12) is employed to adjust the proposed model parameters. The cost function is the sum of the normalized quadratic error between the Fresnel model predicted outlet temperature, $T_f(k, 64)$, and the measured outlet temperature,

$T_f^*(k)$. The model's parameters are the decision variables of the optimization problem, with the initial points and maximum bounds set considering experimental and manufacturer data.

For $n \in \{1, \ldots, S\}$, Eq. (12) defines the optimization problem:

$$
\begin{aligned}
&\min_{\eta_T, \rho_f, c_f, a, b, Ht} \quad \sum_{k=1}^{M} \frac{(T_f(k, 64) - T_f^*(k))^2}{T_f^*(k)^2} \\
&\text{subject to,} \\
&\text{equation (8)}, \\
&\text{equation (9)}, \\
&T_m(0, j) = T_m^0(j), \\
&T_f(0, j) = T_f^0(j), \\
&T_f(k, 0) = Tf1(k), \\
&0 \leq \eta_T \leq 1, \\
&800 \leq \rho_f \leq 1000, \\
&4200 \leq c_f \leq 4500, \\
&0 \leq a \leq \infty, \\
&0 \leq b \leq \infty, \\
&353 \leq Ht \leq 2500,
\end{aligned}
\tag{12}
$$

where $M = 207605$ is the number of measurements, and the lower and upper bounds were chosen based on the materials' physical parameters and properties tables. Each Eq. (12) iteration integrates equations (8) and (9) along the tube, from 1 to S, and the time, from 1 to M. The code execution continues until the stopping criteria condition. Such conditions are the maximum number of iterations and the objective function derivative convergence to a minimum constant value.

The *fmincon* [32] Matlab's algorithm solves the model parameter identification problem. The decision variables are the thermal efficiency η_T, the specific mass of the fluid ρ_f, the polynomial coefficients a and b of thermal losses regarding Eq. (10), lastly, Ht is the heat transfer coefficient between the metal and water. The identification procedure considers that all parameters are equal along the tube length. Besides, the simulation considers steps of 5 seconds to avoid numerical instability; therefore, it is necessary to interpolate the input data accordingly. Section 6.1 discusses the identification results of the FSC parameters.

4. Neuro-fuzzy Modeling

The modeling of a system to faithfully represent its behavior has a certain level of complexity due to the random dynamics of the unknown nature of the process, making it a challenge to describe its behavior utilizing mathematical equations. Often an accurate model will be represented by several mathematical equations. However, a model supported by mathematical tools (e.g., differential equations) is sometimes not always adequate to deal with uncertain systems. In addition, developing control and optimization strategies using nonlinear models to obtain the system prediction implies a high computational burden. It is the principal hindrance if the problem must be solved in a given constrained time, considering the sampling time, so a fast model is indispensable.

Fuzzy models have proven to be an effective technique for modeling and controlling nonlinear systems, successfully expressing the original nonlinear model as a set of local linear models interpolated by a membership function containing the nonlinearities of the original model. In addition, fuzzy inference systems (FIS) describe the behavior of a process based on rules with linguistic labels from human language. Thus, FIS represents the qualitative aspects of human knowledge and reasoning processes, avoiding precise quantitative analyses.

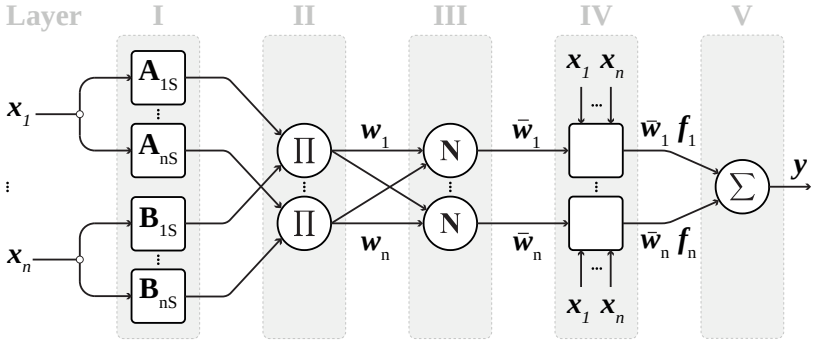

Figure 6: Adaptive Neuro-fuzzy Inference System (ANFIS) architecture [24].

The ANFIS architecture [24], also called the Neuro-Fuzzy (NF) system, is an artificial intelligence (AI) technique. One ANFIS has five layers, as depicted in Figure 6, where the nodes of the first (I) and fourth layers (IV) have adaptive (square blocks) parameters, and the remaining layers have fixed parameters (circle blocks). The first layer contains the fuzzification

interface, which transforms a crisp input into linguistic labels with a certain degree of membership, forming the fuzzy sets [33, 34] characterized by the membership functions (MF). The parameters are adaptive and are called *antecedent parameters*. The second layer outputs the product of the incoming signals from each fixed node and represents the firing strength of each node rule. The third layer normalizes the output of each node, calculated as the ratio of the firing strength of the node's rule to the sum of all the firing strengths of each node rule. In the fourth layer is the defuzzification interface, and each node function provides the weighting of a first-order polynomial crisp function, whose parameters are called *consequent parameters*. Lastly, the fifth layer contains a single node aggregating all rule outputs. For a detailed description of the ANFIS architecture network, refer to [24, 35].

4.1. Training of ANFIS.

The resulting FIS, after training, contains a set of rules of Takagi-Sugeno [36] type as the following:

$$\texttt{IF } x_1 \texttt{ is } F_{1j} \texttt{ and } x_2 \texttt{ is } F_{2j} \texttt{ and } x_i \texttt{ is } F_{ij} \ ,$$
$$\texttt{THEN} : f_j(x) = g_{0j} + g_{1j}x_1 + \cdots + g_{ij}x_i.$$

Each rule has an antecedent and consequent parameter. The fuzzy sets F_{ij} of each crisp entry x_i consist of Gaussian membership functions of the type:

$$\mu_{F_{ij}}(x_i) = \frac{1}{1 + \left[\left(\dfrac{x_i - c_{ij}}{a_{ij}}\right)^2\right]^{b_{ij}}} \tag{13}$$

where $\{a_{ij}, b_{ij}, c_{ij}\}$ are the *antecedents parameters* that define the mean, height and width of the Gaussian used to vary the MFs[1], and the terms $g_{ij} \in \Re$ of each first-order polynomial function are the *consequent parameters*. The learning process of the ANFIS neuronal architecture adapts both parameters. The output of each rule f_j is a linear combination of input variables added to a constant term. The final output of the fuzzy inference system is the weighted average of each rule's output.

[1]The value that the function $\mu_{F_{ij}}$ takes for a given x_i is known as the degree of membership of x_i for the fuzzy set F_{ij}.

The learning process of the ANFIS network architecture uses the training and checking sets to capture better the system's dynamics, which allows for an acceptable model that predicts its behavior. The ANFIS uses as inputs the variables $\{I, EffOpt, f, T_{amb}, q, Tf_1, ws, H, P, Tf_{1\ delay}\}$ and as output Tf_2, thus constructing a mapping of the input-output variables that represent the behaviour of the solar field. Initially, the subtractive clustering (SC) method [37] is used to estimate the number and initialization centers of the Gaussian MF of the fuzzy rules. In addition, learning employs a hybrid learning method. The method runs a back-propagation algorithm [38] to obtain the parameters defining the MF of each fuzzy set (*antecedents parameters*).Next, the learning also executes a least-squares to estimate the terms of the first-order polynomial function (*consequent parameters*) of the output of each rule at each epoch. An epoch, or sweep, is one forward and backward parameter update.

It is worth noting that the checking procedure evaluates the error between the ANFIS output and the actual output of the checking data set (a new data set not used in training). The checking runs after each epoch during the training and has the objective of evaluating if the ANFIS training results in generalized learning. If the ANFIS output has low errors with unknown inputs, then it is said that the ANFIS model had general learning. Typically, the checking considers the root mean squared error (RMSE) given by Eq. (14)

$$RMSE = \sqrt{\frac{\sum_{i=1}^{N}(x_{i,j} - \hat{x}_{i,j})^2}{N}}, \tag{14}$$

where $x_{i,j}$ is a given actual variable j with N samples, and $\hat{x}_{i,j}$ is the output of the predicted variable. This work considers normalized outputs ($z_{i,j}$) for training and checking. Therefore, the normalized RMSE, given by Eq. (15), is used.

$$nRMSE = \sqrt{\frac{\sum_{i=1}^{N}(z_{i,j} - \hat{z}_{i,j})}{N}}. \tag{15}$$

The Table 2 presents the parameters of the ANFIS that captures the behaviour of the heat transfer fluid outlet temperature.

Table 2: ANFIS parameters.

Description	ANFIS
MF type:	Gaussian
Number MFs:	4
Number rules:	4
Influence range	0.8
Epoch number:	1500

5. Simulations planning

This section describes the FSC PDE and NF models structure with inputs/outputs, their twinning/updating characteristics, and validation specifications. The input selection considers the prepared data sorted accordingly to the outlet temperature $Tf2$ correlation coefficients, described in the Correlation Matrix on Figure 3. Thus, the PDE and NF models have the structure, inputs and characteristics summarized in 7.a and Figure 7.b, respectively.

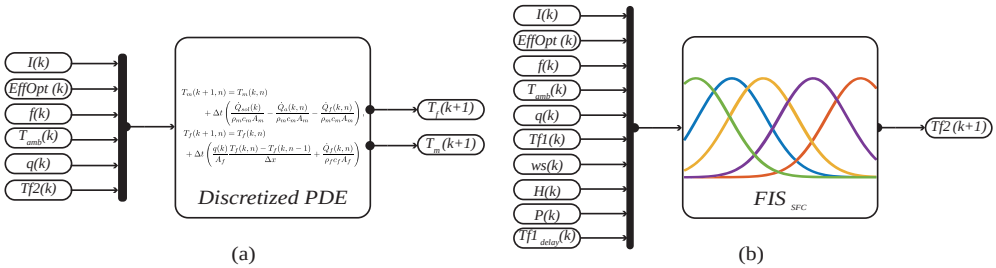

Figure 7: a - SFC outlet heat-trasfer fluid temperature PDE model. b - SFC outlet heat-trasfer fluid temperature ANFIS model.

Table 3 compares Figure 7.a PDE model and Figure 7.b model with two different integrations steps of 5s and 20s. The PDE model has six inputs, while the NF model has ten inputs. This difference happens because, on the one hand, the PDE model does not describe meteorological variables such as wind speed ws, humidity H, and hydraulic circuit pressure P. On the other hand, it is easy to add these input variables to the NF model. The wind speed and air humidity affect the heating process of the Heat Transfer Fluid, changing the convective heat coefficient between the absorber tube and the environment, refer to Figure 3. In addition, the PDE model

Table 3: Simulation planning.

Schematic	Figure 7.a	Figure 7.b	Figure 7.b
Structure	PDE(dt=5)	ANFIS(dt=5)	ANFIS(dt=20)
nº Inputs variables	6	10	10
nº outputs variables	T_f and T_m	$Tf2$	$Tf2$
Twinning	Par. Identification	Learning	Learning
Method	LS[1]	LS and GD[2]	LS and GD
Data-set	$G_{PDE}^{Twinning}$	$G_{NF}^{Twinning}$	$G_{NF}^{Twinning}$
Data-set size	4 days	19 days	19 days
Data-set samples	14188	311666	78032
Sampling Time (s)	5	5	20
Stopping criteria	Eq.(12)	nRMSE[3]	nRMSE
Simulation	ODE45	1° polynomial	1° polynomial
Data-set	G^{Val1}, G^{Val2}	G^{Val1}, G^{Val2}	G^{Val1}, G^{Val2}
Data-set size	6 days of 2009	6 days of 2009	6 days of 2009
Data-set samples	95282	95282	23822
Integration step (dt)	5	5	20
Validation	Table 5	Table 5	Table 5

[1]LS - Least-squares. [2]GD - Gradient Descent. [3]nRMSE - Normalized Root Mean Squared Error.

intrinsically describes the FSC inlet temperature dead time; thus, the delayed inlet temperature $Tf1$ *delay* is employed only in the NF model. Besides, the model outputs are different. While the PDE model has two outputs vectors $T_f(k)$ and $T_m(k)$ that describe the temperature gradient along the absorber tube length, the NF model has a scalar outlet temperature output $Tf2$. It is worth noting that the PDE outputs are arrays with 16 values, where the last value represents the outlet temperature $Tf2 = T_f(16, k)$;

After defining the models' structure, the next step is twinning the models to adjust their parameters to follow the plant's actual data. The PDE model is updated using least squares (LS), while the NF model uses LS and Gradient Descent (GD). The PDE model employs $G_{PDE}^{Twinning}$ as twinning data set with four days of measurement, totaling 14188 samples. While the NF model twinning data set is $G_{NF}^{Twinning}$ which uses 19 days of data, totaling 311666 and 78032 samples, for sampling times of 5s and 20s, respectively. Refer to the middle section of Table 3 for details.

The twinning rate of a given digital twin is the updating rate of a model. Thus, knowing the twinning time of a given model is essential to defining the twinning rate of the virtual entity once the twinning rate must be lower

than the models' twinning time. The twinning time is the processing time the model's twinning takes to converge the model error to a given minimum stopping criteria tolerance.

The twining data reduction for the PDE model is because the computational burden of the PDE parameter identification is high. In preliminary tests, the identification leads to more than one week of processing using the whole available twinning data set, which results in impractical twining rates of the FSC. In addition, the sampling time was reduced to five seconds to avoid numerical instability of the PDE integration, increasing the total number of samples - see Table 3.

The re-sampling of $G_{PDE}^{Twinning}$, further PDE model updating and simulation would lead to unfair execution times compared to the NF model. Note that the latter model was initially updated and simulated, considering the prepared data with a sampling time of 20 seconds. Therefore, to compare the PDE and NF models updating performance, the NF model twinning is run with sampling times of 5 seconds, which is the same re-sampled data of the PDE model. Each column of Table 3 describes each situation, with the first column representing the PDE model with integration steps of dt=5s in four days of actual data, while the second and third columns have the NF model with dt=5s and the NF model with dt=20s, specifications, respectively. Both NF models use the same 19 days of actual data operation. The performance indexes for twinning are the total twinning time t_{tw}, which is the total time that takes for updating the model, the twining time per sample, $t_{tw}/sample$, and twinning time per day of operation, t_{tw}/day, given by equations (16) and (17), respectively

$$t_{tw}/_{sample} = \frac{t_{tw}}{t_s}, \tag{16}$$

$$t_{tw}/_{day} = \frac{t_{tw}}{86400 t_s}, \tag{17}$$

where 86400 is one-day duration in seconds. Section 6.1 presents the models' performance on twinning.

After the twinning is necessary to validate the models to evaluate their performances. Table 3 summarizes the validation procedure. The NF model simulation considers the MATLAB's ODE package and G^{Val1} and G^{Val2} data set that comprise almost six days of actual data. The simulations with integration steps of dt=5s have 95282 samples, while the NF model simulation

with dt=20s has 23822 samples. It is worth noting that the NF model that uses the twinning data set with t_s=5s is not run in validation. Only the training procedure is done with t_s=5s to give a fair twinning time comparison between the models.

The validation procedure compares the model's outputs with a new validation data set of actual data, neither used for the ANFIS training nor the PDE parameter identification. The objective is to evaluate the model's ability to predict outputs, and the results are the accuracy and precision indexes of the final model. The arithmetic error mean is an index that evaluates the accuracy, or the distance between the error points and their true center value; it is given by Eq. (18)

$$\bar{E} = \frac{\sum_{i=1}^{N}(x_{i,j} - \hat{x}_{i,j})}{N}, \tag{18}$$

and standard deviation is quantifies precision, therefore, how much the error is dispersed, it is given by Eq. (19),

$$\sigma_E = \sqrt{\frac{\sum_{i=1}^{N}(E_{i,j} - \bar{E})^2}{N}}. \tag{19}$$

This study considers other statistical validation indexes as standard mean error (SE), which is another measure of precision, given by Eq. (20),

$$SE = \frac{\sigma_E}{\sqrt{N}}, \tag{20}$$

where SE measures how the number of samples N affects the dispersion of different datasets, as the size of the data increases, the SE decreases. Mean Absolute Percentage Error (MAPE), accordingly to Eq. (21),

$$MAPE = \frac{\sum_{i=1}^{N} \frac{|(x_{i,j} - \hat{x}_{i,j})|}{x_{i,j}}}{N} \times 100\%, \tag{21}$$

where it is a measure of the precision of a predictive system considering absolute prediction errors, $|(x_{i,j} - \hat{x}_{i,j})|$, relative to the actual measured data, $x_{i,j}$. And the coefficient of determination R^2, given by Eq. (22)

$$R^2 = 1 - \sum_{i=1}^{N} \frac{(x_{i,j} - \hat{x}_{i,j})^2}{(x_{i,j} - \bar{x}_{i,j})^2}. \tag{22}$$

where $\bar{x}$ is the mean value of the data. R^2 is a number between 0 and 1, that measures how well a statistical model predicts an outcome. If $R^2 = 0$, the model does not describe the outputs, if $0 < R^2 < 1$, the model partially predicts the outputs, and if $R^2 = 1$ the model perfectly predicts the outputs.

It is worth pointing out that the NF model validation with integration steps of dt=5s considers the trained model using the dataset sampled with t_s=20s. As will be seen in Section 6.2, this difference in sampling time of NF model twinning does not affect its simulation and validation.

6. Fresnel Solar Collector Digital Twins

This section presents the models' twinning results, mainly the twinning time. Then, the validation section discusses the models' performance through qualitative comparison between the models' outputs and actual data of six days of operation. Then, the performances are summarized and described using the statistical indexes presented in the previous section.

6.1. Twinning

Table 4 presents the twinning results of the models.

Table 4: Twinning times.

	PDE(dt=5s)	NF(dt=5s)	NF(dt=20s)
t_{tw}(h)	52.34	6.88	2.36
$t_{tw}/sample$ (s)	2.73	0.08	0.11
t_{tw}/day(min)	785.01	22.53	7.71

The NF model updated with input data sampled each 20s has the short twinning, taking 2.36h to update, followed by the NF model with re-sampled input data of 5s, and finally the PDE model - see Table 4. The PDE model parameter identification is the slower among the models, despite having fewer input data and a lower number of samples than both NF models. The PDE model's twinning time per input sample is 2.73s, more than 20 times greater than the NF models. Updating the models with one day of operational data results in 7.71 minutes for the NF model with dt=20s, 22.53 minutes for the NF model with dt=5, and 785.01 minutes for the PDE model. The NF model has appreciable advantages concerning mirroring the models with actual plant data. For example, updating the NF model daily at night is

possible because it takes less than 7 hours to do the procedure. The same does not occur for the PDE model that needs more than two days for twinning. Thus, the PDE model can be updated weekly, starting on Friday, after the operation, and having the updated model early on Monday.

6.2. Validation and Discussion

Figure 8.a depicts the validation results for data set 1. It consists of comparing the actual measured data set G^{Val1} (continuous black line) to the PDE model (dashed red line) and to the NF model (dotted blue line).

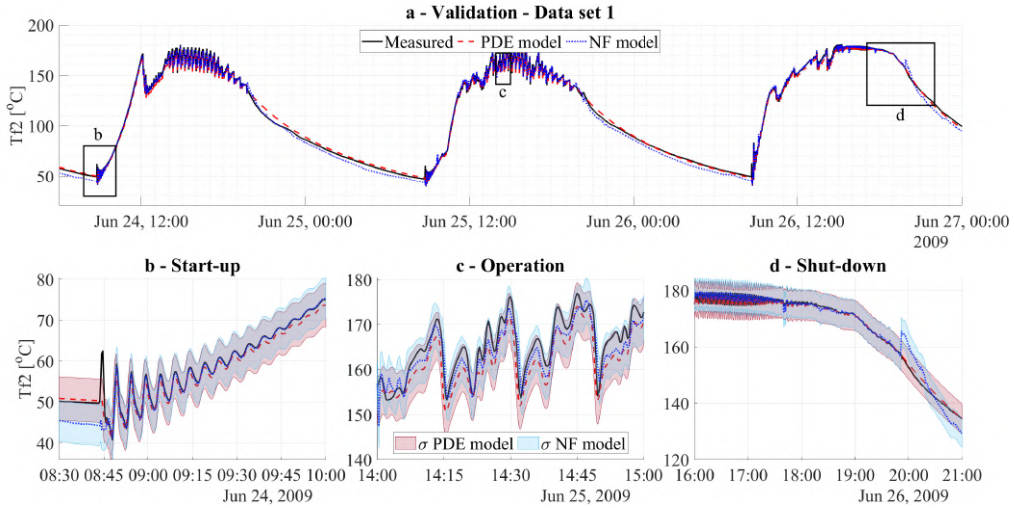

Figure 8: a. Validation results considering data set 1 measured data (black continuous line), PDE model (red dashed line), and NF model (blue dotted line), outputs. The bottom figures b, c, and d refer to zooming the boxes at plot a. Red and blue shaded areas depict the standard deviation with 95% confidence interval ($Tf2(\mathrm{t}) \pm 2\sigma$) of each model.

Note on Figure 8.a that the ETSI absorption plant has an intermittent operation day and night. The maximum values refer to operation with sun irradiance absorption and temperature increase, while the minimum values refer to overnight heat loss and temperature decrease. By inspecting Figure 8.a, the PDE and NF models can follow the measured data profile during three days of operation.

Figure 8.b presents in detail the June, 24, start-up box shown on Figure 8.a. The plant starts when $I > 200[W/m^2]$, which typically occurs between 08:00 and 09:00 for all validation days, starting the pump that generates flow

inside the absorber tube. The reason for strong oscillations in Figure 8.b, and other day start-ups, is that the water inside the tube has a temperature gradient along the tube length that flows towards the outlet temperature sensor. This temperature distribution is affected by the day before shut-down condition and overnight heat losses. Figure 8.b shows that the PDE model presents less error just before the start-up than the NF model, and both models fail to represent the first start-up peak. Although after the first oscillation, the two models can successfully cope with measured data with lower error for the NF model and practically the same standard deviation among the models.

After the start-up oscillations, the outlet temperature $Tf2$ increases with the solar irradiance in the morning. When $Tf2$ reaches the thermal load preset temperature, the absorption chiller starts. Feeding the chiller causes a sudden drop in the temperature ramp. See $Tf2$ profile in Figure 8.a, before noon. The plant thermal gradient along the tubes oscillates due to the closed hydraulic loop and the absorption chiller on-off control [17]. Figure 8.c presents the Fresnel outlet temperature profile during nominal plant operation. By inspection, the NF model has a slightly lower error, and both models have similar standard deviation ranges.

Figure 8.d presents the plant shut-down that occurs at sunset when I<200 [W/m^2]. The outlet temperature presents an atypical oscillation during operation on June 26 due to an absorption chiller's gas boiler use along this day. Note that at 19:00, the $Tf2$ slope changes, and the temperature decreases more rapidly because the pump is off and the flow goes to zero. Both models can follow the measured data, but, differently from the previous figures, the NF model has a more significant error, presenting an unusual peak oscillation at 20:00.

Figure 9.a presents the results of validation data set 2. In comparison to validation 1, validation 2 has bigger maximum $Tf2$ values and also higher oscillations amplitudes, contrast Figure 8.a and Figure 9.b. This difference occurs because the irradiance power is greater in June than in October. Despite different days, irradiance and meteorological values, both models follow the measured variables on validation 2, see Figure 9.a. A proper dynamic representation of both models in different year periods indicates that they can represent the plant dynamics in a wide operational range, from 40 to 180 ℃.

Figure 9.b presents the October, 14, start-up with the same oscillatory behaviour than in Figure 8.b. The NF model is the only one capable of

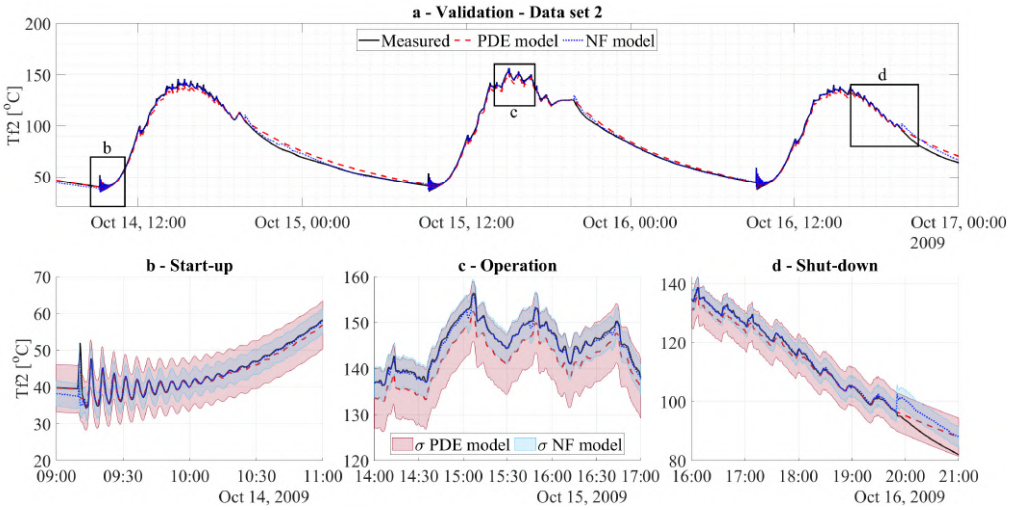

Figure 9: a. Validation results considering data set 2 measured data (black continuous line), PDE model output (red dashed line), and NF model (blue dotted line), outputs. The bottom figures b, c, and d refer to the zoom boxes in plot a. Red and blue shaded areas depict the model's standard deviation with 95% confidence interval ($Tf2(\mathrm{t}) \pm 2\sigma$) of each model.

describing the first peak oscillation on October 14, 09:15. The NF model has lower errors than the PDE model during the start-up, operation, and shut-down. See Figure 9.b, Figure 9.c, and Figure 9.d, respectively. Also, the NF model has an appreciably narrow standard deviation than the PDE model. Compare the red and blue bands, and note that the σ NF model is less than the σ PDE model.

Table 5 compile the overall Validation 1 and Validation 2 model's index results. Note that the NF model was subject to two validation considering different input data sampling times, one with 20 and another with 5 seconds. These two analyses of the NF model give a fair comparison between the simulation times regarding the PDE model that must run with integration steps of 5 seconds to avoid numerical problems. Note that the NF model has the same error performance despite using different integration steps, which indicates that t_s does not affect the results. The next section discusses the PDE and NF modelling error indexes.

Based on the mean error, $\bar{E}$, it is possible to infer that while the PDE model sub-estimates the outlet temperature for validation 1, the NF model super-estimates the $Tf2$ value, once $\bar{E}$ is positive and negative, respectively.

Table 5: Validation index results.

	PDE(dt=5)	NF(dt=5)	NF(dt=20)
$\bar{E}$ (°C)	-0.36	0.51	0.51
σ (°C)	2.18	2.55	2.55
2σ (°C)	4.37	5.09	5.09
SE (°C)	0.01	0.02	0.02
MAPE (%)	1.92	2.49	2.49
RMSE (°C)	2.18	2.54	2.54
R^2	0.997	0.996	0.996
t/dt (s)	0,0197	0.0034	0.0013
t/day (s)	340.28	59.14	5.79

The models do not present a sensible difference in the standard deviation σ, assuming a normal error distribution. The differences are almost 0.30 ℃ and 0.60 ℃, considering 68% and 95% confidence intervals, respectively. The massive amount of samples results in low SE values, showing that the validation has an adequate number of analysis points. Lastly, the Root Mean Squared Error of PDE is 2.18 ℃ and for the NF is 2.49 ℃, which are low values considering that the Fresnel collector has a nominal operating temperature of 180 ℃. This fact is reflected in low values of Mean Absolute Percent Error of 1.92% and 2.30% for the PDE and NF, respectively. Now, closing the validation indexes discussion, the linear regression between predicted and actual FSC outlet temperatures gives coefficients of determination $R^2 \geq 0.996$ for both models. All in all, both PDE and NF models have similar error values.

Note on Table 5 that the execution time per integration step, t/dt, and execution time to simulate one day of samples t/day, show appreciable differences among the models. The PDE model takes 0.0197s seconds to integrate one step, while the NF model, with the same integration time of dt =5, takes 0.0034s. Thus, the NF model shows almost six times faster integration step time than the PDE. These integration step times result in 61.92 seconds for the PDE model to simulate one day of operation, while the NF model takes 20.50. Thus, the NF model is three times faster. An interesting feature of the NF model is that it presents the same error levels when using integration steps of 5 or 20 seconds. Table 5 indicates that the NF model with simulation step of 20s is the faster model, simulating one day of operation more than

ten times faster than the NF model using dt=5s and almost 60 times faster than the PDE model.

7. Conclusion

This work has developed the digital twin of a commercial Fresnel Solar Collector (FSC) installed on the roof of the ETSI building in Seville, Spain. The authors seek to create models to simulate what-if analysis, model predictive control improvements, and optimizations through virtual and physical entities exchange. This paper has developed two generalized dynamic models, one using ANFIS systems and another using phenomenological modelling using Partial Differential Equations (PDE) and parameter identification tools. The models describe the FSC outlet temperature day and night during plant start-up, operation, and shut-down. The total available data consists of 25 days of measurement data with a sampling time of $t_s = 20s$, resulting in 101854 total samples. The twinning process for the ANFIS is its training and checking, while for the PDE model is the identification procedure. The PDE model identification procedure has a higher computational burden than the ANFIS. Thus, it was necessary to reduce the PDE model twinning input data, resulting in four days for identification, while the ANFIS model utilizes 19 days for training and checking. The developed models have shown the following features:

1. The models are validated and have defined accuracy and precision indexes accordingly to error mean, standard deviation, standard error, and mean absolute percentage error considering six days of operation data and 23822 samples.
2. All models follow actual measurement trends during the day and night with a worst-case mean error of 0.51 ℃, a worst-case standard deviation of 5.09 ℃ (95% confidence interval), and a worst-case mean absolute percentage error of 2.49%
3. The models consider the primary mirrors variable focus as model inputs; therefore, this work states and validate the first FSC dynamic model with the focus/defocus effect on the outlet temperature.
4. PDE model and NF model with integration steps 0f 5s run one day of operation in 340.28s and 59.14s, with a simulation time step of 19.7 ms and 3.4ms, respectively; therefore, fast enough to be used in Model Predictive Control (MPC) techniques.

5. The NF model with integration steps of 20s runs one day of operation in 5.79s and one simulation step in 1.3ms. Therefore, almost three times faster than the NF with dt=5s and more than fifteen times faster than the PDE.
6. The models run a twinning, coping with plant aging or process modifications because the neuro-fuzzy ANFIS is an adaptive technique, and the identification procedure can update the PDE model parameters.
7. The PDE model takes 785.01min to twinning one day of operation data, while the NF model takes 22.53min, considering ts=5s. The NF model twinning with ts=20s takes 7.71min. Thus, the ETSI solar absorption plant twinning can occur at night or on the weekend when the plant is off.

In conclusion, this work contributes to the dynamic modeling of an FSC, considering its further use as a digital entity on a digital twin framework. Future works will further model the long pipes that connect the absorption chiller and the FSC to consolidate the whole plant's digital twin. Furthermore, the plant DT will unlock control and optimization investigations, offering several possibilities for the operation of the plant enhancements and scientific contributions.

Acknoledgement

The authors would like to acknowledge the Coordenação de Aperfeiçoamento de Pessoal de Nível Superior (CAPES), Finance Code 001, the Conselho Nacional de Desenvolvimento Científico e Tecnológico (CNPq), under grant 304032/2019–0, the Agencia Estatal de Investigación (AEI) of the Spanish Ministry of Science and Innovation, under grant PID2019-104149RB-I00/10.13039/501100011033 (project SAFEMPC), to the European Commission for funding this work under Project DENiM, this project has received funding from the European Union's Horizon 2020 research and innovation programme under grant agreement No 958339, and the European Research Council under Advanced Research Grant OCONTSOLAR (789051), for funding this work. Diogo O. Machado thanks to IFRS- campus Rio Grande for capacity support, *Fundación Carolina*, SEGIB and PrInt-UFSC programms for mobility scholarships.

Appendix A. Validation data

Supplementary data associated with the validation of this article can be found in https://data.mendeley.com/datasets/rzggrvczf6/1 [39].

References

[1] United Nations, United Nations Framework Convention on Climate Change United Nations, United Nations Frameork Convention on Climate Change (1992) 1–33.
URL https://treaties.un.org/pages/ViewDetailsIII.aspx?src=TREATY&mtdsg_no=XXVII-7&chapter=27&Temp=mtdsg3&clang=_en

[2] United Nations Organization, 7th sustainable development goal (2019).
URL https://www.un.org/sustainabledevelopment/energy/

[3] International Energy Agency, Net zero by 2050 - a roadmap for the global energy sector, IEA (2021).
URL https://www.iea.org/reports/net-zero-by-2050

[4] S. Lindmark, The role of absorption cooling for reaching sustainable energy systems, Master's thesis, KTH, Stockolm (2005).

[5] P. Esfanjani, S. Jahangiri, A. Heidarian, M. S. Valipour, S. Rashidi, A review on solar-powered cooling systems coupled with parabolic dish collector and linear fresnel reflector, Environmental Science and Pollution Research 29 (2022) 42616–42646. doi:10.1007/S11356-022-19993-3/FIGURES/9.
URL https://link.springer.com/article/10.1007/s11356-022-19993-3

[6] M. Moran, H. Shapiro, D. Boettner, M. Bailey, Fundamentals of Engineering Thermodynamics, 8th Edition, Wiley, 2014.
URL https://books.google.com.br/books?id=uxObAwAAQBAJ

[7] S. Jie, Z. Zhang, L. Wang, Z. Zhenwen, W. Jinjia, Comprehensive review of line-focus concentrating solar thermal technologies: Parabolic trough collector (PTC) vs linear fresnel reflector (LFR), Journal of Thermal Science 29 (2020). doi:10.1007/s11630-020-1365-4.

[8] M. W. Ahmad, M. Mourshed, B. Yuce, Y. Rezgui, Computational intelligence techniques for hvac systems: A review article history, Building Simulation (2016). doi:10.1007/s12273-016-0285-4.

[9] M. E. Mondejar, R. Avtar, H. L. B. Diaz, R. K. Dubey, J. Esteban, A. Gómez-Morales, B. Hallam, N. T. Mbungu, C. C. Okolo, K. A. Prasad, Q. She, S. Garcia-Segura, Digitalization to achieve sustainable development goals: Steps towards a smart green planet, Science of The Total Environment 794 (2021) 148539. doi:10.1016/J.SCITOTENV.2021.148539.

[10] A. Rasheed, O. San, T. Kvamsdal, Digital twin: Values, challenges and enablers from a modeling perspective, IEEE Access 8 (2020) 21980–22012. doi:10.1109/ACCESS.2020.2970143.

[11] M. Liu, S. Fang, H. Dong, C. Xu, Review of digital twin about concepts, technologies, and industrial applications, Journal of Manufacturing Systems 58 (2021) 346–361, special issue: Digital Twin towards Smart Manufacturing and Industry 4.0. doi:https://doi.org/10.1016/j.jmsy.2020.06.017.
URL https://www.sciencedirect.com/science/article/pii/S0278612520301072

[12] F. Tao, H. Zhang, A. Liu, A. Y. Nee, Digital twin in industry: State-of-the-art, IEEE Transactions on Industrial Informatics 15 (2019) 2405–2415. doi:10.1109/TII.2018.2873186.

[13] P. Bermejo, F. J. Pino, F. Rosa, Solar absorption cooling plant in seville, Solar Energy 84 (2010) 1503–1512. doi:10.1016/j.solener.2010.05.012.

[14] G. Ceusters, R. C. Rodríguez, A. B. García, R. Franke, G. Deconinck, L. Helsen, A. Nowé, M. Messagie, L. R. Camargo, Model-predictive control and reinforcement learning in multi-energy system case studies, Applied Energy 303 (2021) 117634. doi:https://doi.org/10.1016/j.apenergy.2021.117634.
URL https://www.sciencedirect.com/science/article/pii/S0306261921010011

[15] L. M. P. Ghilardi, A. F. Castelli, L. Moretti, M. Morini, E. Martelli, Co-optimization of multi-energy system operation, district heating/cooling network and thermal comfort management for buildings, Applied Energy 302 (2021) 117480. doi:https://doi.org/10.1016/j.apenergy.2021.117480.
URL https://www.sciencedirect.com/science/article/pii/S0306261921008680

[16] F. Pino, R. Caro, F. Rosa, J. Guerra, Experimental validation of an optical and thermal model of a linear fresnel collector system, Applied Thermal Engineering 50 (2) (2013) 1463–1471, combined Special Issues: ECP 2011 and IMPRES 2010. doi:https://doi.org/10.1016/j.applthermaleng.2011.12.020.
URL https://www.sciencedirect.com/science/article/pii/S1359431111007174

[17] D. O. Machado, A. J. Sánchez, A. J. Gallego, G. A. de Andrade, J. E. Normey-Rico, C. Bordons, E. F. Camacho, Split-range control for improved operation of solar absorption cooling plants, Renewable Energy 192 (2022) 361–372. doi:https://doi.org/10.1016/j.renene.2022.04.064.
URL https://www.sciencedirect.com/science/article/pii/S0960148122005249

[18] D. Jones, C. Snider, A. Nassehi, J. Yon, B. Hicks, Characterising the digital twin: A systematic literature review, CIRP Journal of Manufacturing Science and Technology 29 (2020) 36–52. doi:10.1016/J.CIRPJ.2020.02.002.

[19] F. Tao, Q. Qi, L. Wang, A. Y. Nee, Digital twins and cyber–physical systems toward smart manufacturing and industry 4.0: Correlation and comparison, Engineering (2019). doi:10.1016/j.eng.2019.01.014.

[20] J. Granacher, T.-V. Nguyen, R. Castro-Amoedo, F. Maréchal, Overcoming decision paralysis—a digital twin for decision making in energy system design, Applied Energy 306 (2022) 117954. doi:https://doi.org/10.1016/j.apenergy.2021.117954.
URL https://www.sciencedirect.com/science/article/pii/S0306261921012629

[21] M. Robledo, J. M. Escaño, A. Núñez, C. Bordons, E. F. Camacho, Development and experimental validation of a dynamic model for a fresnel solar collector, IFAC Proceedings Volumes 44 (2011). doi:10.2514/6.2015-1563.
URL https://www.sciencedirect.com/journal/ifac-proceedings-volumes/vol/44/issue/1

[22] M. Spoladore, E. F. Camacho, M. E. Valcher, Distributed parameters dynamic model of a solar fresnel collector field, in: IFAC Proceedings Volumes (IFAC-PapersOnline), Vol. 44, IFAC Secretariat, 2011, pp. 14784–14789. doi:10.3182/20110828-6-IT-1002.02992.

[23] W. D. Chicaiza, A. J. Sánchez, A. J. Gallego, J. M. Escaño, Neuro-fuzzy modelling of a linear fresnel-type solar collector system as a digital twin, in: Joint Proceedings of the 19th World Congress of the International Fuzzy Systems Association (IFSA), the 12th Conference of the European Society for Fuzzy Logic and Technology (EUSFLAT), and the 11th International Summer School on Aggregation Operators (AGOP), Atlantis Press, 2021, pp. 242–249. doi:https://doi.org/10.2991/asum.k.210827.033.
URL https://doi.org/10.2991/asum.k.210827.033

[24] J.-S. Jang, Anfis: adaptive-network-based fuzzy inference system, IEEE Transactions on Systems, Man, and Cybernetics 23 (3) (1993) 665–685. doi:10.1109/21.256541.

[25] E. Camacho, M. Berenguel, F. R. Rubio, D. Martínez, Control of Solar Energy Systems, Springer London Dordrecht Heidelberg New York, 2006. doi:10.1007/978-0-85729-916-1.

[26] Industrial Solar, Fresnel Collector LF-11 datasheet (2007).
URL https://www.google.com/search?q=Industrial+solar+LF-11&source=lmns&bih=625&biw=1366&hl=pt-BR&ved=2ahUKEwibir29u8DoAhUzCbkGHetXBnwQ_AUoAHoECAEQAA

[27] Schott Solar, SCHOTT PTR70 Receiver The 4 th Generation (2013).
URL https://d3pcsg2wjq9izr.cloudfront.net/files/31497/download/461508/1-schott_ptr70_4th_generation_brochure.pdf

[28] A. S. M. Brandão, P. R. da Costa Mendes, J. E. Normey-Rico, Simplified optical model, aiming strategy and partial defocusing strategy for solar Fresnel collectors, Renewable Energy 188 (2022) 11–36. doi:10.1016/J.RENENE.2022.02.019.

[29] J. E. Normey-Rico, C. Bordons, M. Berenguel, E. F. Camacho, A robust adaptive dead-time compensator with application to a solar collector field1, IFAC Proceedings Volumes 31 (19) (1998) 93–98, iFAC Workshop on Linear Time Delay Systems (LTDS '98), Grenoble, France, 6-7 July. doi:https://doi.org/10.1016/S1474-6670(17)41134-7.
URL https://www.sciencedirect.com/science/article/pii/S1474667017411347

[30] N. Kincaid, G. Mungas, N. Kramer, M. Wagner, G. Zhu, An optical performance comparison of three concentrating solar power collector designs in linear fresnel, parabolic trough, and central receiver, Applied Energy 231 (2018) 1109–1121. doi:https://doi.org/10.1016/j.apenergy.2018.09.153.
URL https://www.sciencedirect.com/science/article/pii/S0306261918314648

[31] L. F. Shampine, M. W. Reichelt, S. J. S. Comput, The matlab ode suite *, Society for Industrial and Applied Mathematics 18 (1997) 1–22.
URL http://www.siam.org/journals/sisc/18-1/27642.html

[32] R. H. Byrd, J. C. Gilbert, J. Nocedal, A trust region method based on interior point techniques for nonlinear programming, Mathematical Programming, Series B 89 (2000) 149–185. doi:10.1007/PL00011391.

[33] L. Zadeh, Fuzzy sets, Information and Control 8 (3) (1965) 338–353. doi:https://doi.org/10.1016/S0019-9958(65)90241-X.

[34] L. A. Zadeh, Outline of a new approach to the analysis of complex systems and decision processes, IEEE Transactions on Systems, Man, and Cybernetics SMC-3 (1) (1973) 28–44. doi:10.1109/TSMC.1973.5408575.

[35] J. Jang, C. Sun, E. Mizutani, Neuro-fuzzy and Soft Computing: A Computational Approach to Learning and Machine Intelligence, MATLAB

curriculum series, Prentice Hall, 1997.
URL https://books.google.com.br/books?id=vN5QAAAAMAAJ

[36] T. Takagi, M. Sugeno, Derivation of fuzzy control rules from human operator's control actions, IFAC Proceedings Volumes 16 (13) (1983) 55–60, iFAC Symposium on Fuzzy Information, Knowledge Representation and Decision Analysis, Marseille, France, 19-21 July, 1983. doi:https://doi.org/10.1016/S1474-6670(17)62005-6.

[37] S. L. Chiu, Fuzzy model identification based on cluster estimation, J. Intell. Fuzzy Syst. 2 (3) (1994) 267–278.

[38] P. J. Werbos, Beyond regression : new tools for prediction and analysis in the behavioral sciences, Ph.D. thesis, Harvard University, Cambridge, Massachusetts (Aug 1974).

[39] D. Machado, W. Chicaiza, J. M. Escaño, A. Gallego, G. de Andrade, J. Normey-Rico, C. Bordons, E. Camacho, Digital twin of a fresnel solar collector for solar cooling - validation data, Mendeley Data 1 (2022). doi:10.17632/RZGGRVCZF6.1.

5 A 2DOF THERMOSOLAR CONCENTRATOR PROPOSAL: SOLAR TRACKING AND DISTURBANCE REJECTION USING PROPORTIONAL DEFOCUS

A 2DOF THERMOSOLAR CONCENTRATOR PROPOSAL: SOLAR TRACKING AND DISTURBANCE REJECTION USING PROPORTIONAL DEFOCUS.

Diogo O. Machado[1,2], Julio Normey-Rico[1] and Gustavo A. de Andrade[1]

[1] Universidade Federal de Santa Catarina - UFSC, Florianópolis (Brazil)

[2] Instituto Federal de Educação, Ciência e Tecnologia do RS - IFRS, Rio Grande (Brazil)

Abstract

In this work, a novel two-degree-of-freedom linear Fresnel solar collector is proposed. The equipment can vary the power density in the receiver using a proportional geometric defocus besides the conventional solar tracking. This concept was designed to benefit the dynamics and control operations of solar power plants using variable distributed concentration ratio in the concentrating solar collector. For conceptual validation, a numeric scenario of a solar distillation plant with a modified Forristal concentrator operating in a closed-loop fashion with a Filtered Dynamic Matrix Control strategy is presented. Henceforth, is shown the impact of adding this new manipulated variable on the dynamics and control operations. The idea results in a faster actuator which provides both, better performance and operation under constraints.

Keywords: Defocus, 2 DOF solar concentrator, control, MPC, modified Forristal.

1. Introduction

Concentrating Solar Power (CSP) systems are used to transform sun energy to a wide number of applications, such as hydrogen production, heating water systems, electricity generation, liquid waste recycling and desalination. In these applications, the concentrators are used to direct and increase the solar irradiation in the receptor spot and convert it to thermal and electrical energy with the use of a power cycle. The main commercial solar concentrators configurations are shown in Figure 1, where each one of these structures have specifications (Shantia, 2013), advantages and disadvantages (EDF, 2012; Orioli and Orioli, 2011; Kumar, 2015).

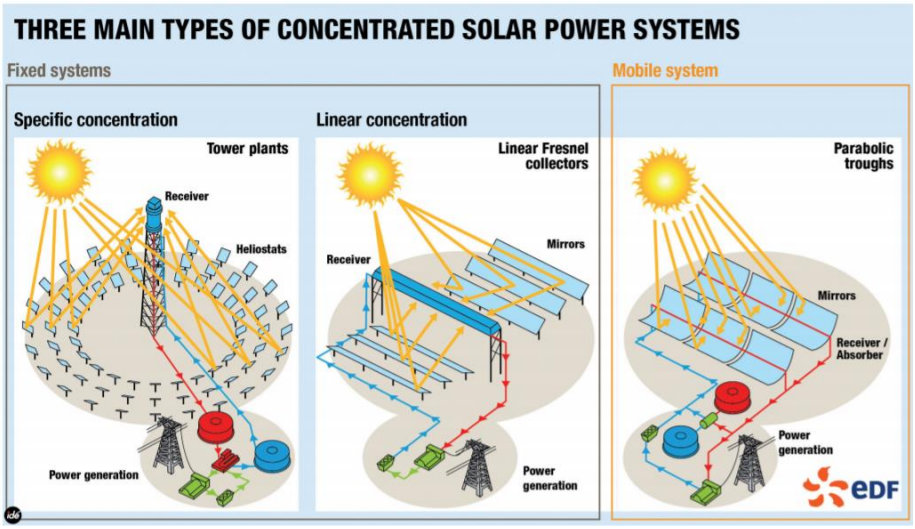

Figure 1 – Common solar concentrators for power generation. Central Tower (left), Linear Fresnel (middle) and parabolic through (right) (EDF, 2012).

Although there are several applications of CSPs, at the present, most systems focus on electricity generation. Solar thermal power plants use the solar energy to heat a thermal fluid by a system of collectors to produce steam in order to feed steam-turbines coupled with generators (Duffie and Beckman 1991). Several disturbances could overheat the system resulting in fluid degradation, premature component failures and performance reduction. Electric power limitations can also be received from the transmission system operator. In this case, the power is decreased by reducing the flow rate leading to an increase in the temperature (Sanches et al 2018). Live steam

doi:10.18086/swc.2019.01.05 Available at http://proceedings.ises.org

parameters have a strong influence on the life span of the steam turbines, an expensive asset, and unlike in plants supplied by fossil sources, the steam supplied from solar thermal power plants varies depending on the irradiation (Willwerth et al., 2018). In this sense, mechanisms to deal with these conflicting issues are the interest topic of this research.

Regardless of the CSP application and technology, there are situations where it is necessary to defocus the solar concentrator for safety, operation, optimization or maintenance of the system. The most classic examples of such scenarios are in the occurrence of storms, strong wind and high solar radiations. Thus, the concentrator defocus is an important operational alternative for safe and cost-effective plant operations. Nowadays the industrial concentration systems only have total or partial defocus options, and the latter is made using the solar tracking in parabolic troughs mechanism to change the optimum relative angular sun incidence.

From the industrial process control perspective, the work fluid flow (control variable) inside the absorber tubes of the solar concentrator is manipulated, by means of a radial pump, in order to maintain the outlet temperature (controlled variable) around the desired set point. The most common disturbances for the control system are the solar irradiation, pressure fluctuations, ambient temperature, optical efficiency and inlet temperature of the working fluid. Another interesting aspect is the transport lag, once the temperature sensor is located at the collector outlet and the pump is installed at the inlet. This implies that the temperature will be affected by the flow of previous time instants, due to the residence time of the fluid inside the collector.

In this topic of research, Araujo (2018) proposed a modification in the solar concentrator control system. Basically, a new binary variable was included in the computation of the control law by means of a non-linear model predictive control formulation. This variable was used to deal with total or partial mirror defocus considering the actual solar tracking mechanism technology, thereby, the partial defocus operates advancing or lagging the relative angular focal point to the irradiance angle. Although, the focal angular change can generate thermal and mechanical stress due to irregular temperature gradient in the absorber (Steinman and Eck, 2000). However, these authors did not consider a detailed study of the collector optical aspects (Zheng et al., 2014). The system used for conceptual evaluation is the thermal absorption model presented in the works of Torrico et al. (2010) and Lima et. al (2016). These articles applied control techniques in a solar system of a desalting plant.

This work proposes the addition of one more degree-of-freedom (DOF) in solar concentrators control systems permitting the focal manipulation and consequently, the energy absorbed in the receiver tube. This can be performed varying the aperture area/absorber ratio or the energy density in the absorber area related to the direct normal irradiation (DNI). The system is a two-degree-of-freedom control actuator linear Fresnel solar collector which is capable of proportional defocus and solar tracking simultaneously. Because of the mechanical nature of Fresnel modules and the distributed construction of a solar field, is expected that adding this manipulated variable to the control system could enhance performance maintaining safety. Although, in this approach only the defocus is evaluated. The Filtered Dynamic Matrix Controller (FDMC) multi-input multi-output (MIMO) was chosen to validation because it is a modification of DMC, widely used in industry (Normey-Rico and Camacho 2007) dealing with variable dead-time, multiple variables and considering constraints at project phase. So, a mathematical model of this new Fresnel module is made in section 2, while in section 3 the solar field model is defined, in section 4 the control specification and logic are stated. In the section 5, the response results are described with this novel concentrator to validate the concept, and, finally the conclusions are stated in section 6.

2. Fresnel 2DOF

This section is based on the work of Ozturk (2011) and presents the basic geometric concepts of parabolic through and linear Fresnel concentrators.

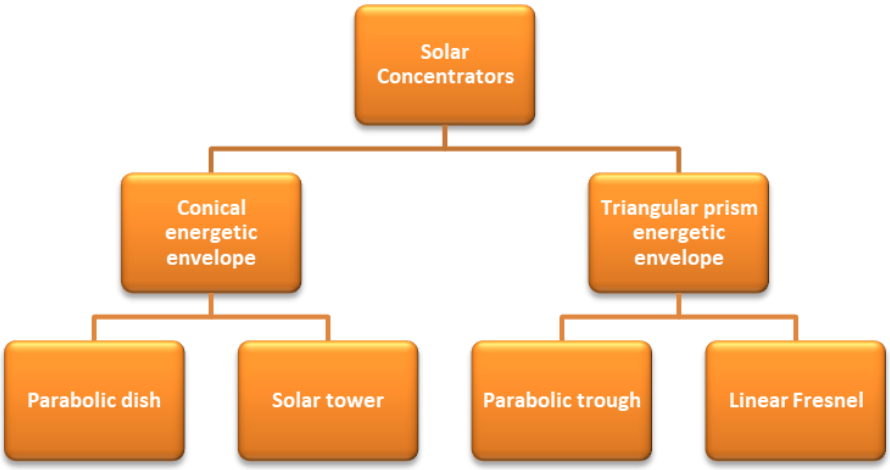

Figure 2- Solar collector classification to the energetic volume. Modified from Ozturk (2011)

Figure 2 shows a classification of solar collectors based on the created energy volume because of the geometric nature of collectors. This definition was modified once, in one hand, the disc collectors directs the incident irradiation to a focal point and, in the other hand, the parabolic through forms a focal line. Therefore, it happens that the commercial collectors are designed to coincide the absorber in the same point of the optical focal point, thereby, all the incident irradiation in the mirror area is directed to the collector. Although, if the mirror could in some way change its format it would be possible to change its focal point, or line, and, therefore, change the power density in receptor or vary the aperture/receptor areas ratio. This idea is presented in the graphics of Figure 3.

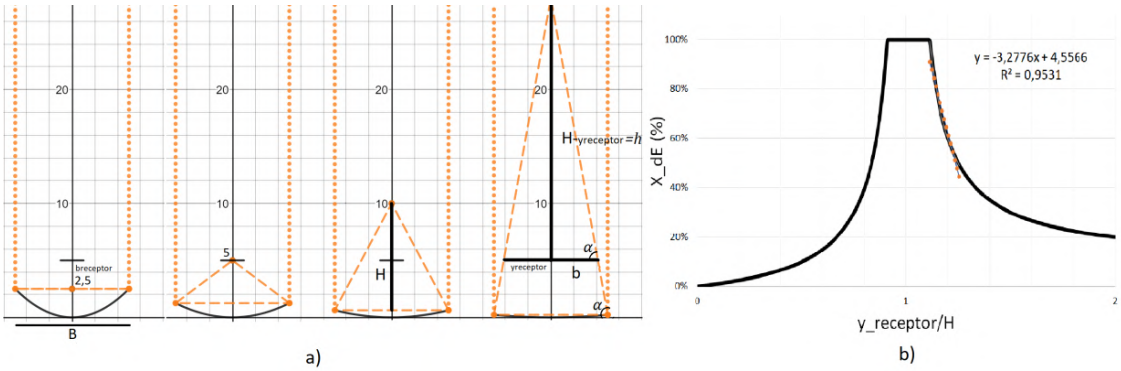

Figure 3 – Transversal cut in a parabolic through collector with constant area and different focal points. (a) First case is a focal point below the receptor height. Second case is a coincident receptor height and focal point (100% concentration). Third and fourth case are different concentration ratio, or energy density in the triangle prism cut in the receptor height due to focal point position variation. (b) is the sensitivity analysis of the variation depicted in (a) with respect of the normalized power density. Full concentration case is in the $y_{receptor}/H = 1$. The left side represents the focal point variation below the receptor height while the right side represents the focal point above the receptor height. The saturated wide section depends on the receiver wide.

Thereby, if the receptor is not in the same distance of the focal point a ratio between collector aperture area and receptor area governs the energy transfer to the work fluid, or, an area of a pyramid energy trunk coincides with the receptor height. The incident energy on the receptor, if the focal point is coincident with the receptor height, is given by Forristal (2003) *apud* Shantia (2013) equation:

$$\dot{q_{Sol}}_{abs} = \dot{q}_{\iota}\eta_{abs}\alpha_{abs} \qquad \text{(eq.1)}$$

where $\dot{q_{Solar}}_{abs}[W/m^2]$ is the solar heat incident in the receptor, $\dot{q}_{\iota}[W/m^2]$ is the solar irradiation, η_{abs} is the optical efficiency and α_{abs} is the mirror absorption factor.

For the case in which the focal point does not coincide with the receptor, there is an aperture/absorber area ratio, and for simplification and model usage, for now on it will be considered prism energy envelopes relationships, thereby, parabolic through and linear Fresnel collectors are defined. Considering the schematic of Figure 3, and

hypotheticals A mirror width of 10 m and receptor B of 2 m, in first case (a) is possible infer that all incident irradiation is concentrated in the receptor, or absorber, and, therefore, the concentration is of 100%. In the sequence cases of (a) the energy density plane that cut the triangular prism on absorber height is diminished with the increase of the triangle height and is approximated considering the relations of eqs. 2, 3, and 5, of the rectangles triangles that compose the isosceles triangle of the last case on Figure 3a.

$$tg(\alpha) = \frac{2H}{B} = \frac{2h}{b} \quad \text{(eq. 2)}$$

$$h = H - y_{receptor} \quad \text{(eq. 3)}$$

$$b = \frac{B(H - y_{receptor})}{H} \quad \text{(eq. 4)}$$

$$X_{dE} = \frac{b_{receptor}}{b} = \frac{b_{receptor}}{B} \frac{H}{(H - y_{receptor})} \quad \text{(eq. 5)}$$

$$\dot{q}_{Solabs} = \dot{q}_{\iota} X_{dE} \eta_{abs} \alpha_{abs} \quad \text{(eq. 6)}$$

So, for a variable energetic density and constant absorber width the total absorbed energy will vary. Thereby, it would be possible to use the defocus system not just for safety cases but also for disturbance rejection. The collector aperture area and the triangle prism cut area at absorber height could be related to the irradiation fraction which is effectively concentrated by the mirrors to the absorber. Thereby, is possible to change the Forristal eq. 1 to a modified one, eq. 6, that considers the proportional defocus or aperture / absorber areas ratio.

From the Forristal modified equation and the hypothetical configurations is plotted the graph which considers $\dot{q_{Solabs}} = f(H/y_{receptor})$, thereby, the absorbed heat in receptor is a function of the ratio between the focal point height and the absorber height, this sensitivity analysis indicate agreement between the simulated results with a more detailed model of Ozturk (2011). Also, in the position which is installed the receptor occurs a dead band with full absorption, this happens because the absorber width, once the focal plane must be greater than the absorber area to the ratio begins to change. For a negative displacement, considering the absorber in the origin, if the focal point is below the absorber height there is a decrease in the energy density until it reaches zero, this point has an analogous behavior with the positive displacement. In the case which the focal point is above the absorber height the energy density values drop to the absorber area/aperture area ratio which is 2/10 meters or 20%.

Although, the practical problem to vary the focal point of rigid mirrors that composes commercial solar concentrators could restrict it construction. Is technically challenging to dynamically vary the shape of a whole solar concentrator mirror because of the mirror material nature and the actuation system. Considering these restrictions is proposed the utilization of Fresnel collectors. Fresnel collectors are composed by various mirror stripes disposed in a flat linear composition, in which each mirror could be independently positioned. In solar tracking systems the mirrors could one by one adapt its angles depending on the solar irradiation angle to enhance the concentration on the absorber for a given solar angle. Therefore, the defocus usually is to flatten only the mirrors, in other hand, parabolic throughs uses on-off mode or leading and lagging the whole structure for solar tracking position. The last option could generate non-uniform heat distribution and mechanical stress (Steinman and Eck, 2000). Also, commercial flat Fresnel mirrors are mechanically coupled to reduce costs and increase design simplicity. In these conditions, just one motor is needed for the coupled mirror mechanism to be able to adjust the mirrors angles due to solar tracking. Once the Fresnel concentrator utilizes plane mirrors and each one could operate independently is possible to extrapolate its common or commercial operation to vary its focal point in the logic of the presented logic. Considering the differences of the two concepts, the first step is to correlate the Fresnel operation to the parabolic troughs in a way that connects the variable focal point collector concept and the Fresnel collector construction flexibility.

In Figure 5a is demonstrated the discretization of a parabolic concentrator. This is done in small parabolic mirror intervals on the parabolic surface. In 5b the trimmed mirrors are grouped over a plane surface in $y = 0$. Although, the angles direct the irradiation in different focal points once the global surface of mirror are not positioned along a parable anymore, but in a horizontal line at the origin. Therefore, is necessary an adjustment in the relative mirrors angles for the system to have a coincident focal point. So, if is possible to correlate the angles between the mirrors on the Fresnel module to have a common focal point, therefore, is possible to add one more mechanical actuator and propose a 2 degrees of freedom (DOF) Fresnel collector which operates varying the focal point,

thereby, governed by the modified Forristal eq. 6.

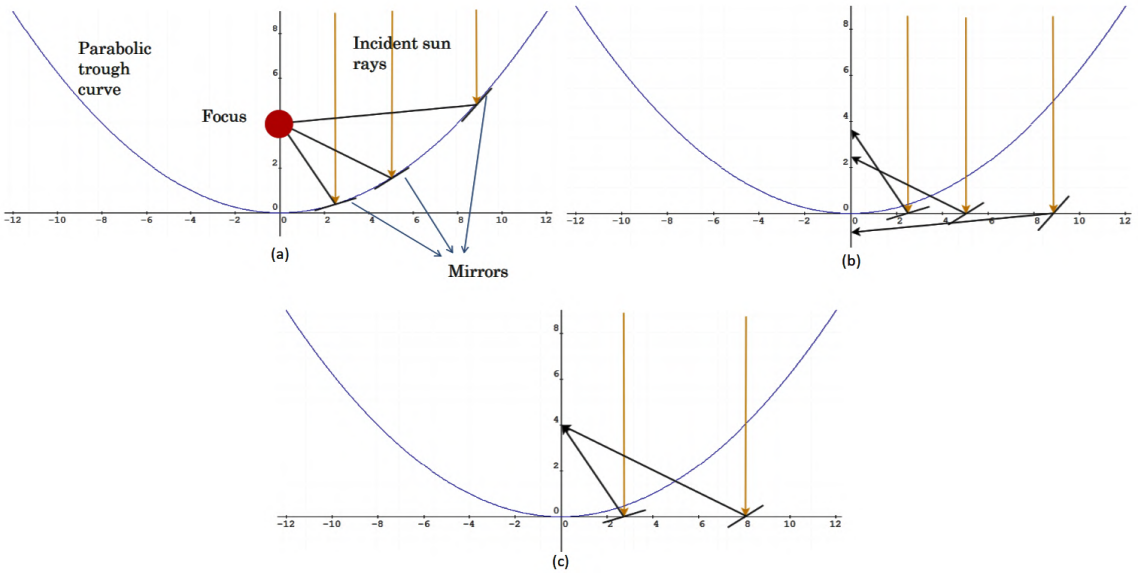

Figure 4 – Geometric transformation of parabolic through to linear Fresnel (Ozturk,2011). (a) cut the parabolic mirror in small plane sections. (b) Translation of the plane mirrors a plane in origin. (c) relative angle correction to coincide the focal point of the discretized mirror.

In this sense, is stated the logic of the a 2DOF Fresnel solar collector concept and viability. The equipment that is not just dynamic capable to actuate during transients for control purposes but also to operate in safety and process limits. To reach this synergic objective is necessary a control technique which considers the constraints in design phase and the dead time nature of the solar thermo fluid dynamic process. For this motive, in this conceptual proof is used a filtered predictive controller. The shading and block effects on the collectors that impacts the plant operation are not considered (Zheng et al., 2014).

3. Solar field definition

The system used for conceptual analysis of the 2DOF Fresnel collector proposed in this work is the desalting plant AQUASOL (Roca et. al, 2008a, 2008b). This plant is located at the Plataforma Solar de Almería, Spain, and it is used to desalt water with solar thermal energy. It is composed by a compound parabolic concentrator solar field, storage tanks, multi-effect distiller with 14 stages and an absorption heat pump. The plant optimal operation point is at 66.5 ºC in the first cell, and it can operate in 3 modes: solar, fossil or hybrid heating. The solar field work fluid is water, and the field is made up of 252 collectors with an area of roughly 500 m² in 4 loops of 63 collectors. There are collectors connected in parallel in seven groups three by three, as can be seen in Figure 5.

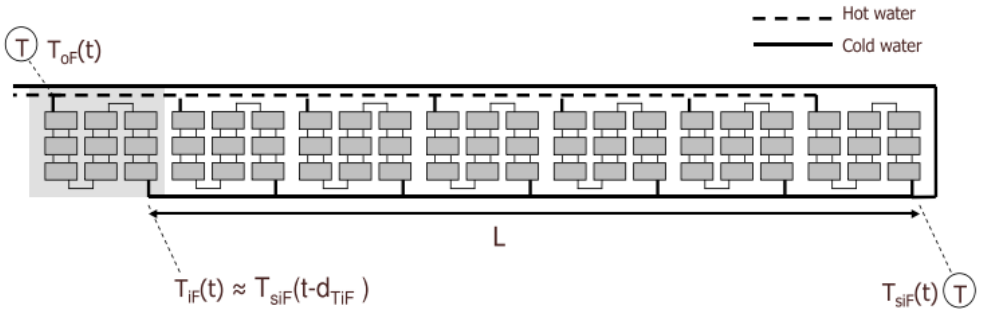

Figure 5 – AQUASOL desalting plant solar field structure. One loop is composed by 7 groups with 3 parallel connections and 7 collectors each (Torrico et al.,2010).

The system detailed description, modelling and validation is available in Roca et. al (2008a, 2008b). The dynamic model of the water temperature at the output of the solar collector field is given by the following equation:

$$\rho C_p A_a \frac{\partial T_{OF}(t)}{\partial t} = \beta_I I(t) - \frac{H}{Leq}(\bar{T}(t) - T_a) - C_p \dot{m_{eq}}(t - d_c)\frac{T_{OF}(t) - T_{iF}(t)}{Leq} \quad \text{(eq. 7)}$$

For the computation of $\dot{m_{eq}}$ it has to be taken into account the number of operational loops in the solar field (n_l), number of colectors in each loop (n_c), number of parallel conections (n_{cp}) and the number of absorbers in each collector (n_a):

$$\dot{m}_{eq} = \frac{\dot{m_F}}{n_l n_c n_{cp} n_a}$$

Table 1 - Models parameters and operations points (OP).

Symbol – Name	Value	Symbol - Name	Value [limits]
ρ- Water especific mass	975 (kgm^{-3})	n_{eq}- Collectors parameters	5.88
C_p- Specific thermal capacity	4190 ($Jkg^{-1}ºC^{-1}$)	L_{eq}- Absorber tube length	5.67 (m)
A_a- Cross-section area	1.745e-4 (m^2)	$\bar{T}_{OF}$- Out temperature OP	
β_I- Irradiance parameter	0.1024 (m)	$\bar{T} = \frac{T_{OF}(t) - T_{iF}(t)}{2}$	20.42 [5-25] (ºC)
H- Termal losses coefficient	4 ($Jkg^{-1}K^{-1}$)	$\bar{\dot{m}}_F$- Mass flow OP	2.55 [1.2,4.4] (L/s)
L_{eq}- Absorber tube length	5.67 (m)	$\bar{I}$- Irradiance OP	800 (W/m^2)
d_c- Mass flow I/O dead time	40 [30,50] (s)	$\bar{X}$- Focus energy OP	100 [50,100] (%)

In this context is proposed a modification on the eq. (7) which represents the mathematical description of the 2DOF Fresnel collector idea. This modification adds the proportional variation of the energetic density in a hypothetical Fresnel collector as depicted by the eq. (6) and Figure 3a. Is important to say that the AQUASOL utilizes parabolic trough. In this sense, the collector parameters are well known and were used in this conceptual analysis, even knowing that the collector proposal is possible considering a Fresnel structure. So, the resulting model equation presents a new $X(t)$ variable related to the new working logic, so eq. (7) was modified in this work to count on the proportional defocus:

$$\rho C_p A_a \frac{\partial T_{OF}(t)}{\partial t} = \beta_I I(t) X(t) - \frac{H}{L_{eq}}(\bar{T}(t) - T_a) - C_p \dot{m}_F(t - dc)\frac{T_{OF}(t) - T_{iF}(t)}{n_{eq} L_{eq}} \quad \text{(eq. 8)}$$

were the percentual defocus, $X(\%)$, was added with mass flow $\dot{m}_F(L/s)$ as manipulated variables. The controlled variable is the outlet temperature of solar field $T_{OF}(°C)$, and disturbances are irradiation, $I(W/m^2)$, ambient temperature $T_a(°C)$, and inlet temperature of the field T_{iF} $(°C)$, other parameters are available in Table 1. The energy density is operated in the range of 50-100% because of the nonlinear behavior showed in Figure1 b.

The next steps to execute the simulation of the eq. (8) and to run the controller tests are the linearization and discretization. The linearization method is the forward approximation of the derivative and the operational points, therefore, linearization point, are defined in Table 1. The linearized equation resulted in:

$$\Delta T_{OF}(t) = \Delta T_{OF}(t-1) + a[\Delta I(t-1) + \bar{I}\Delta X(t-1)] - b[\Delta T_{OF}(t-1) + \Delta T_{iF}(t-1) - 2\Delta T_a(t-1)] + c[-\bar{m}_F \Delta T_{OF}(t-1) + \bar{m}_F \Delta T_{iF}(t-1) + (\bar{T}_{iF} - \bar{T}_{OF})\Delta m_F(t-1-d_c) \quad \text{(eq. 9)}$$

With this, applying the z transform, the final numeric discrete transfer function is described in eq. (10):

$$\Delta T_{OF}(z) = \frac{-0.18\, z^{-8}}{z-0.98}\Delta \dot{m}_F(z) + \frac{0.57}{z-0.98}\Delta X(z) + \frac{0.72e-3}{z-0.98}\Delta I(z) + \frac{0.02}{z-0.98}\Delta T_{iF}(z) + \frac{0.49e-2}{z-0.98}\Delta T_a(z) \quad \text{(eq. 10)}$$

All in all, the system is a multiple-input single-output MISO process. Where T_{OF} is the controlled variable, $\dot{m}_F$ and X are the manipulated variables and I, T_{iF}, T_a are the disturbances. Considering this structure, a Filtered Dynamic Matrix controller is discussed next.

4. Control Definitions

In this work, the authors propose the use of the FDMC strategy with two manipulated variables: the standard one, the inlet fluid flow, and a novel one, the proportional defocus, possible through the 2DOF Fresnel collector

described in Section 2. The work of Lima et al. (2015) describe details of the application of the FDMC in the context of solar plants. The dynamic behavior of the AQUASOL plant presents some challenges for the control design due to the location of the temperature sensor and the pump, leading to delays for different input or output variables. In Normey-Rico and Camacho (2007), the authors showed that the Dynamic Matrix Controller (DMC), a model predictive control strategy, implicitly uses a Smith predictor (SP) structure, a famous dead time compensator (DTC) structure. Also, these authors propose the inclusion of a first order filter in the SP structure, in order to improve the poor disturbance rejection capabilities and lack of robustness properties of the original SP.

This technique has become well-known in literature as the filtered Smith predictor (FSP). In this context, Lima et al. (2014) suggested a modification of the standard DMC to merge the Filtered Smith Predictor and the Dynamic Matric Controller advantages. With this, the resulting FDMC tuning procedure have one more degree of freedom to adjust disturbance rejection and robustness. More proofs and example about robustness and rejection are available in the base article (Lima et al. 2016) as well as the recursive implementation used in this work. Some additional advantages of FDMC are the parameter tuning simplicity and practical implementation, since the algorithm needs minor changes of the industry standard DMC.

Basically, the FDMC technique seeks to minimize the following cost function J:

$$J = \left(\hat{\Upsilon} - W\right)^T Q_y \left(\hat{Y} - W\right) + \Delta u^T Q_u \Delta u \qquad \text{(eq. 11)}$$

where Q_y and Q_u are diagonal matrices that represents the weights of future errors and future control increments. And W is the future reference vector while $\hat{Y}$ is the predictions process variable vector in a chosen horizon. For the calculation of $\hat{Y}$ is defined eq. 12:

$$\hat{Y} = G\Delta u + H\Delta u(t-1) + H_n \Delta n(t) + 1\hat{y}(t + d_n|t) \qquad \text{(eq. 12)}$$

where G, H and H_n are matrices $N_y \times N_u$, $N_y \times M$ and $N_y \times M + 1$, N_y and N_u are the prediction and control horizons and M is the number of step coefficients of the input-output and disturbances-output responses. So, $\hat{\Upsilon} = \left[\hat{y}(t + d_n + 1|k), \dots, \hat{y}\left(t + d_n + N_y\middle|k\right)\right]^T$, the future increment vector $\Delta u = [\Delta u(t), \dots, \Delta u(t + N_u - 1)]^T$, the past control increments $\Delta u(t-1) = [\Delta u(t-1), \dots, \Delta u(t + N_u - 1]^T$, and finally the measurable disturbance $\Delta n = [\Delta n(t), \dots, \Delta n(t - M)]^T$. For a compact description of the predictions, the eq. 12 can be separated in free and forced response:

$$\hat{Y} = G\Delta u + f \qquad \text{(eq. 13)}$$

where f contains all the terms which are not affected by the control actions, therefore, the free response is the process response if no control action is made. The term $G\Delta u$ is the forced response and represents the process response due to future control actions. The Δu is calculated through eq. 11 and in a case which all future references are constant, $W = 1r(t)$, and with no constraints, an algebraic equation solution emerges for $\Delta u = K(W - f)$. Further mathematical manipulation can be done to show that the control signal $u(t)$ could be obtained by the equation:

$$U(z) = C(z)\left(R(z) - \hat{Y}(z)\right) + C_{ff}(z)N(z) \qquad \text{(eq. 14)}$$

Concluding, this means that the DMC controller can be represented by a classical control scheme. It has a primary feedback controller that considers the reference and prediction error in a control horizon, also, a feed-forward controller like depicted in Figure 6.

All in all, the predictor structure is used to obtain the expected value of the outputs after the dead time. So, some modifications are made to count on the transport lag of the process. Considering $G_{DMC}(z)$ and $G_{pDMC}(z)$ as the nominals models shifted for a dead-time number of samples for a step response of the system.

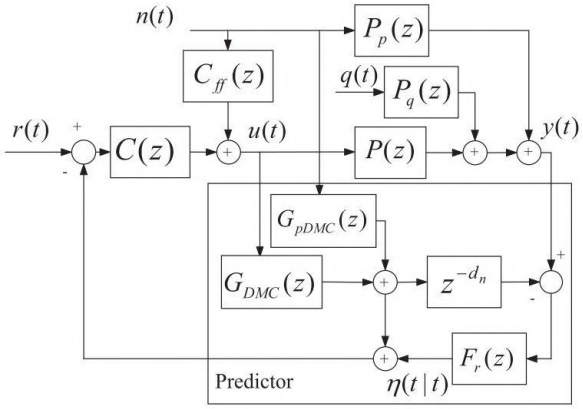

Figure 6 - Block diagram of the DMC interpreted as a DTC structure with feed-forward (Lima et al., 2016). This predictor structure merges the advantages of FSP and DMC.

The structure of Figure 6 is characterized by an FSP structure, where $n(t)$ is the measurable disturbance, $q(t)$ is an unmeasured disturbance that affects the process through $P_q(z)$. Defined the structure some behaviors are highlighted:

- Measurable disturbance rejection in the nominal case, $G_{pDMC}(z) \cong z^{d_n} P_{pn}(z)$, where P_{pn} is the nominal disturbance-output transfer function. The rejection will be only dependent of $C_{ff}(z)$ and $C(z)$, this happens because the filter $F_r(z)$ do not have effect on the response for the perfect prediction.
- Measurable disturbance rejection in the dead-time error case, $G_{pDMC}(z) \neq z^{d_n} P_{pn}(z)$. The prediction on $t + d_n$ will be an approximation.
- No available disturbance measurement case. Considering the filter $F_r(z) = 1$, the original DMC algorithm is equivalent to the SP. Therefore, the issues about disturbance rejection will be sustained, or, if the tuning is made to improve set-point tracking the robustness could be compromised.

5. Results

In this section, two days data are simulated and compared to the published results of Lima et al. (2014) using the FDMC controller with and without the proposed 2DOF Fresnel collector. The tuning guidelines were the same for the two cases. $N_y = 50$,$N_u = 10$ and $Q_u = \lambda_n K_p^2$, where K_p is the gain of the nominal model and $\lambda_n = 1$. Where the Q_u was normalized because the selection of the λ_n does not depend on the process gain (Normey-Rico and Camacho, 2007). The nominal values of the linearization and for the simulation are described in Table 1. Also, a low-pass filter was used for attenuation of noise effects:

$F_r(z) = \frac{0.15}{z-0.85}$

The main purpose of the control system is to maintain the difference of the inlet and outlet temperatures within the range of 5-20ºC to optimal collector efficiency and less material stress due to the temperature gradient. The process delay was set in 40 s, thereby, 8 sample times, with variation of ± 10 s depending on the mass flow. In the simulation time there was changes in the temperature setpoints as can be seen in upper plot of Figure 7 and 8.

So, the two simulation scenarios are depicted in Figure 7 and 8. The upper plot shows the setpoint, the 1DOF and the 2DOF responses outlet temperature profiles, or the controlled variable. The middle plot has two y axis, were the left axis is the manipulated variable field flow, the black continuous and dashed lines are the flow profiles for the 2DOF and 1DOF structure respectively. Right y axis is the second manipulated variable that is the normalized energy density in orange continuous line. So, the middle plot depicts the manipulated variables. Finally, the bottom plot presents the disturbances profiles that are from real data of the AQUASOL plant. It is composed by the ambient temperature, inlet water field temperature and by the Direct Normal Irradiation.

In Figure 7 the irradiation follows the day normal distribution until almost the 2500 sample, were it gets perturbed. The ambient temperature shows a ramp from 250 to 750 and suddenly drop its value. The inlet water field

temperature stays stable along the simulation. Is evidenced the fast actuation of the mechanical system of the proportional defocus varying the energy density in comparison of the pump actuation to change the field inlet flow on the middle plot. Also, the collector actuation varies the irradiation of the whole field while the mass flow has a greater dead time depending on the temperature sensor location and velocity. In top plot the dashed black line is related to the 1DOF collector and it is farthest from the set point orange dashed line in comparison of the black continuous line of the 2DOF concept collector. An interesting behavior is that the inlet field flow for 1DOF collector is lower than the 2DOF this results in a greater gain for the proportional defocus, although, the total energy converted decreases once the outlet mass flow is lower for a given temperature.

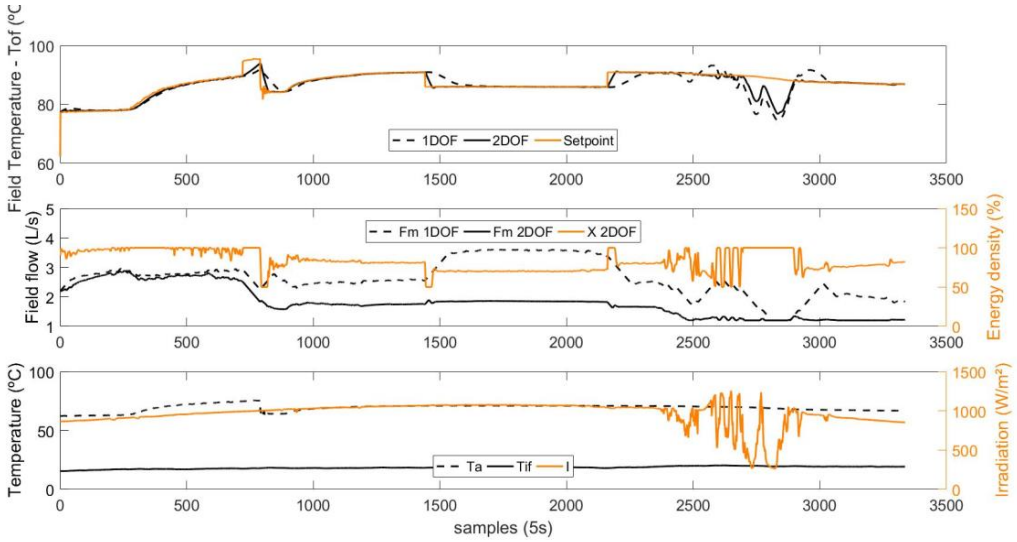

Figure 7 – Data set 1 – Top plot is controlled variable. Middle plot are the manipulated variables. Bottom plot are the disturbances.

In Figure 8 is possible to see a normal irradiation until sample 1500. Between 1500 and 2000 there was an irradiation disturbance and after 2000 the irradiation become very low and noisy. The ambient temperature had a negative step between 500 and 1000 and is steady in the rest of the data set, also the inlet temperature stayed stable in all simulation. The manipulated variables can be evaluated with the middle plot. It is possible to compare the field flow with the 2DOF Fresnel collector and with the 1DOF. Also, the impact of the proportional defocus varying from 50-100%. The operation can be discussed based on the upper plot, which represents the 1 DOF performance with the dashed line and the 2DOF with a continuous line. By inspection of the plot is evident that the 2DOF actuator can maintain the temperature at the setpoint better than in the 1DOF case. Also, for an increase

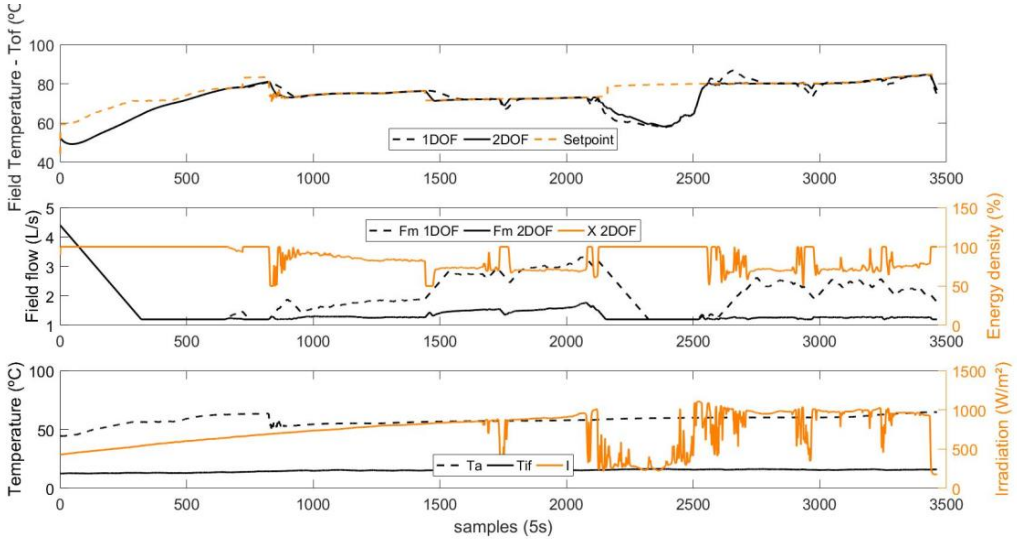

Figure 8 - Data set 2 – Top plot is controlled variable. Middle plot are the manipulated variables. Bottom plot are the disturbances.

in temperature the two concepts have the same behavior, although, in the cases of decreasing irradiation the 2DOF have a better response to track the setpoint because the field flow is lower, leading to a greater gain for the focus/defocus operation considering less mass in the absorber. In 2500 to 3500 is possible to evaluate that the defocus mechanism can deal with the fast irradiation disturbances, also, in the 1DOF case, the field mass flow has slower dynamics resulting in more variation in the Field Temperature. Other interesting behavior is from 2000 to 2500 samples, were the energy density stayed saturated at 100% because of the low irradiation, even with the temperature decrease. To sum up, Table 2 depict the IAE index:

Table 2 - Integral of Absolut Error (IAE) index for the two data sets depicted in Figure 7 and 8.

	1DOF Fresnel	**2DOF Fresnel**
Data set 1	7.9545e+03	5.3968e+03
Data set 2	16.105e+03	13.460e+03

6. Conclusions

This work is an effort to connect different advantages of different areas to reach a simple, yet powerful, idea of 2DOF collector. Firstly, is stated the basic functioning of parabolic trough collectors and the geometric nature of a parable mirror. After, is defined a hypothesis of a variable focal point collector and, them, is used the Fresnel linear collector construction characteristics to connects the idea of a variable parable to a feasibility collector that is described by a modified Forristal equation. After, the AQUASOL desalting plant is presented and its models are modified to embed the idea of a collector for disturbance rejection. Then, is stated the control algorithm and the basic idea behind FDMC. Two real data sets are used to run the simulation. The two compared control structures can reject the disturbances, and results section generated some relevant advantages:

- The IAE index of the 2DOF collector is less than the same index o 1DOF, which implies in a faster setpoint tracking of the proposed collector.
- The proposed 2DOF collector have smaller constant times than the inlet field flow, therefore, the collector has better dynamic responses operating in higher frequencies. So, the control system has capacity of reject a wider range of disturbances.
- Due to the tuning and weighting of the DMC is possible to change the response behavior of the 2DOF case. Although, to the comparison purpose the tuning were equivalent.

The main disadvantage of the 2DOF collector operation with the inlet field flow is that the flow could operate in lower levels respecting the desired temperature set-point. In this sense, the total energy output of the solar field is lower once the calculation of the total energy is made multiplying the mass, temperature and specific heat of the work fluid. So, in many cases of Figure 7 and 8 in which the both actuators are not saturated at maximum, is possible to optimize the outlet energy.

For future works this relation should be evaluated and a solution to maximize the energy output with the temperature constraints should be developed.

7. Acknowledgments

This work has been developed within the context of all activities related to the R&D project registered with ANEEL under the code PD-00553-0042/2016 and sponsored by Petroleo Brasileiro (PETROBRAS).

The authors are thankful for the financial support from Petrobras/ANEEL and for the capacitation support of Instituto Federal de Educação, Ciência e Tecnologia – IFRS – Campus Rio Grande.

J. E. Normey-Rico thanks CNPq for financial support, project 305785/2015-0

8. References

Willwerth, L., Feldhoff, J.F., Krüger, D., Keller, L., Eickhoff, M., Krüger, J., Pandian, Y., Tiedemann, J., Succo, M., Khenissi, A., 2018. Experience of operating a solar parabolic trough direct steam generation power plant with superheating. Sol. Energy 171, 310–319. https://doi.org/10.1016/j.solener.2018.06.089

Araujo, T. D. Costa, P. R. C. Noremy-Rico, J. E. and Bordons, C. Optimal Solar Collectors Defocusing Based on Maximum Temperature. 9th International Renewable Energy Congress (IREC). DOI: 10.1109/IREC.2018.8362488. Isbn: 9781538609989. Hammamet, Tunisia. March, 2018.

EDF. Technolgy unveiled - concentrated solar power. n. June, 2012.

Kumar, R. Solar Thermal Technologies for Power Generation in India. v. 2, n. 6, p. 41–44, 2015.

Forristall, R. Heat Transfer Analysis and Modeling of a Parabolic Trough Solar Receiver Implemented in Engineering Equation Solver. n. October, 2003

Orioli, F. S.; Orioli, V. S. Parabolic or Fresnel ? 2011. Disponível em: <www.soltigua.com/wp-content/uploads/2009/09/Soltigua{\\ _}Energetica{_}ind>.

Özturk, A. Sensitivity of Energy Yield of CSP Systems with Fresnel Mirrors to Structural Parameters. 2011.

Shantia, A. Low cost / high performance Linear Fresnel Receiver design for Concentrated Solar Power applications. Master thesis, KTH. Stockolm. 2013.

Torrico, B. C. et al. Robust nonlinear predictive control applied to a solar collector field in a solar desalination plant. IEEE Transactions on Control Systems Technology, v. 18, n. 6, p. 1430–1439, 2010. ISSN 10636536.

Lima DM, Normey-Rico JE, Plucênio A, Maia TL. Improving robustness and disturbance rejection performance with industrial mpc. In: XX Congresso Brasileiro de Automática (CBA); 2014. p. 3229–3236. ⟨http://www.swge.inf.br/CBA2014/anais/PDF/1569926319.pdf⟩

Lima DM, Normey-Rico JE, Maia Santos TL. Filtered dynamic matrix control applied to a solar collector field. In: 2015 6th International Renewable Energy Congress (IREC). Sousse, Tunisia: IEEE; 2015. p. 1–6.

Lima, D. M.; Normey-Rico, J. E.; Santos, T. L. M. Temperature control in a solar collector field using Filtered Dynamic Matrix Control. ISA Transactions, v. 62, p. 39–49, 2016. ISSN 00190578. Disponível em: <http://dx.doi.org/10.1016/j.isatra.2015.09.016>.

Normey-Rico, J. E.; Camacho, E. F. Control of Dead-time Processes. 2. ed. [S.l.]: Springer Science & Business Media, 2007.

Roca L, Berenguel M, Yebra L, Alarcón DC. Preliminary modeling and control studies in AQUASOL project. Desalination 2008;222(1–3):466–73.

Roca L, Berenguel M, Yebra L, Alarcón-Padilla DC. Solar field control for desalination plants. Solar Energy 2008;82(9):772–86.

Zheng, J. et al. Solar tracking error analysis of fresnel reflector. Scientific World Journal, Hindawi Publishing Corporation, v. 2014, n. December, 2014. ISSN 1537744X.

Duffie, J. A., Beckman, W. A., 1991. Solar engineering of thermal processes, second ed., John Wiley & Sons, New York

Sánchez A.J., Gallego A.J., Escaño J.M., Camacho E.F., 2018. Event-based MPC for defocusing and power production of a parabolic trough plant under power limitation. Solar Energy, vol. 174, 570-581.

Steinmann, W.-D., Eck, M., 2000. Direct solar steam generation in parabolic troughs: thermal stress due to variations in irradiation. In: Proceedings of the 10th SolarPACES Symposium.

6 FRESNEL SOLAR COLLECTOR CONTROL WITH ACTIVE DEFOCUS

2022 European Control Conference (ECC)
July 12-15, 2022. London, United Kingdom

Fresnel Solar Collector Control With Active Defocus

Diogo O. Machado[1,2,3], Adolfo J. Sanchez[4], Gustavo A. de Andrade[2],
Julio Normey-Rico[2], Carlos Bordons[3], Eduardo F. Camacho[3]

Abstract— **Line focus concentrating solar collectors control operates by manipulating the flow for tracking the desired outlet temperature under normal conditions. This solar collector can also use the solar tracking device to manipulate the mirror's angle for defocusing under abnormal events. Defocusing mirrors is the last control measure to avoid overheating because defocusing means wasting energy. This work proposes changing the defocus use as the last control resort for safety, to a standard manipulated variable combined with the flow for outlet temperature tracking. The proposal uses a multi-variable non-linear MPC technique with a modified objective function and simulates three scenarios on a Fresnel solar collector. Besides, this paper indicates that the defocus action is necessary for regular operation; thus, it is also essential to consider the defocus as a manipulated variable for controller design. The proposed controller tracks reference and rejects disturbances while having defocus minimization, overheating prevention, and thermal power reference tracking features.**

I. INTRODUCTION

A solar collector is a heater that produces thermal energy for electricity generation, process heating, or district heating. Fresnel solar concentrating collectors use sections of plane mirrors mounted on a tracking device capable of following the sun, reflecting its solar beam, and focusing the irradiance into a receiver. Inside the receiver there is a tube where a fluid flows, this fluid gains internal energy and exits the system with a higher temperature. The solar collector is highly non-linear, and a distributed system that presents transport delay, resulting in a challenge to control systems design.

The typical control objective in the solar collector is to reject disturbances of irradiance and inlet temperature while tracking outlet temperature reference by manipulating the fluid flow [1]. The problem is that a concentrating solar collector is susceptible to overheating. Overheating could damage the piping system, degrade the heat transfer fluid, or generate undesirable steam [2]. Three main events could lead to overheating: failures, thermal power demand changes, and disturbances. Note that all problems are related to flow saturation. Solar collectors avoid critical overheating using passive safety heat dissipation devices. The problem of safety devices actuation is that it leads to undesired shut-downs or high oscillations [2]. Another safety option is to change mirror focus incidence angles using the tracking control, and avoiding solar heating. Thus, despite not being a passive device, mirror's angles can contribute to safety and operation [2] in another safety layer. The problem is that defocus also leads to oscillations if implemented with an on-off control strategy. Besides, if the mirror's angles manipulation is proportional, a trade-off between overheating prevention and solar energy rejection appears [3]. The following section presents literature investigations of this trade-off.

Emergency and safety events usually count on defocus [1]. Study [4] contributes to integrating safety defocus on the controller design. The same authors propose a hybrid predictive controller for operating in the overheating case [5]. A non-linear Model Predictive Control (MPC) with a discrete defocus variable on a unique objective function regulates a non-linear plant model. The problem is solved using mixed-integer non-linear programming. Next, the authors compare the on-off and partial defocus results, where total on-off strategy leads to better overheating prevention. The technique is further evaluated in [6], presenting a solution for safety defocus under pump failure scenario.

Some works investigate the use of defocus not just for safety but also for power limitation events. In [7] the authors propose an event-based Generalized Predictive Controller (GPC) for defocus specific loops based on temperature thresholds. The same authors develop an adaptive incremental state-space GPC to deal with both flow saturation and power limitations events [8].

Due to the safety approach and defocus energy waste disadvantage, the control design practice does not consider defocus as a manipulated variable for regular operation. Although summing up the scientific contributions, it is noticed that the defocus is essential for regular plant operation. Further investigation shows that defocus is necessary because of the plants' Solar Multiple (SM), which is a plant design variable defined as the quotient between nominal solar field power and the nominal consumer power. Even solar plants without thermal storage have a solar multiple greater than one. The solar multiple is chosen to operate the power block during a longer period than the one obtained if SM=1 [9] under nominal conditions. Thus, it is expected that, throughout the year, the plant will regularly overheat and

*The authors would like to acknowledge the Coordenação de Aperfeiçoamento de Pessoal de Nível Superior (CAPES), Finance Code 001, the Conselho Nacional de Desenvolvimento Científico e Tecnológico (CNPq), under grant 304032/2019–0, the Agencia Estatal de Investigación (AEI) of the Spanish Ministry of Science and Innovation, under grant PID2019-104149RB-I00/10.13039/501100011033 (project SAFEMPC), and the European Research Council under Advanced Research Grant OCONTSOLAR (789051), for funding this work.

[1] Instituto Federal de Educação, Ciência e Tecnologia do Rio Grande do Sul - IFRS - Campus Rio Grande, RS, Brasil.

[2]Universidade Federal de Santa Catarina - UFSC. Departamento de Automação e Sistemas. Florianópolis, SC, Brasil.

[3] Systems Engineering and Automatic Control Department and also from ENGREEN, Laboratory of Engineering for Energy and Environmental Sustainability, Universidad de Sevilla, 41092, Seville, Spain.

[4] Department of Mechanical, Biomedical and Manufacturing Engineering, Munster Technological University, Cork T12 P928, Ireland.

saturate the pump, mainly on sunny days. Therefore, solar concentrating plants will trigger the safety defocus regularly. Thus, this paper proposes to integrate both flow and defocus as manipulated variables for concentrating solar collectors' temperature control using a multivariable controller (single input multiple output (SIMO)) to improve plant operation.

The main idea is that using both actuators can enhance dynamic performances because the defocus has faster dynamics than the flow. Besides, the defocus and flow have different controllability ranges. While flow dissipates already absorbed energy, defocus avoids energy input. Another feature is the possibility to tune the actuators' target weights, thus, choose a pump desired response concerning electricity consumption, pressure surges, and harmonics. Furthermore, if the proposed controller can satisfy set-point tracking and disturbance rejection conditions, it will indirectly provide overheat prevention.

The proposed approach uses active defocus together with flow manipulation to enhance the dynamic response of the collector. The main contributions of this work are: (i) to design a multivariable non-linear MPC that manipulates both flow and focus to control collector's temperature; (ii) the resulting controller has defocus minimization, overheat prevention, and thermal power tracking features, (iii) the controller does not count on event-based or mixed-integer programming; (iv) the conceptual proof considers a validated Fresnel solar collector model.

II. METHODOLOGY

The main idea of this paper is to bring the defocus concept, conventionally used at the safety layer, to the normal operation layer. To implement and test this idea, first, the solar collector model is defined in section II-A, second, the non-linear MPC controller is stated in section II-B, then, the simulation scenarios are set in section II-C, finally, the results are discussed in section III.

A. Fresnel Solar Collector Modelling

The Fresnel solar collector installed at Seville's School of Engineering (EIS) was chosen for simulation. The plant has a total field aperture of $352[m^2]$, absorber tubes model Schott PTR 70 with a length of $64[m]$. The heat transfer fluid is saturated liquid water, the operating temperature and pressure are $180[^\circ C]$ and $13[bar]$, respectively [10].

The EIS collector model is described by the partial differential equations (1) and (2)

$$\rho_m c_m A_m \frac{\partial T_m}{\partial t} = I\eta G d - H_l G(T_m - T_a) - LH_t(T_m - T_f), \quad (1)$$

$$\rho_f c_f A_f \frac{\partial T_f}{\partial t} + \rho_f c_f q \frac{\partial T_f}{\partial x} = LH_t(T_m - T_f), \quad (2)$$

where m and f sub-indexes refer to tube metal and fluid, respectively, $\rho[kg/m^3]$ is the specific mass, $c[J/(kg^\circ C)]$ is the specific heat, $A[m^2]$ is the cross section area, $T[^\circ C]$ is the temperature, $t[s]$ is the time. The first term in the Right Hand Side (RHS) of equation (1) is the solar energy input, where $I[W/m^2]$ is the solar irradiance, η is the overall efficiency, $G[m^2]$ is the mirrors aperture area, and $d[adim.]$ is the fresnel mirrors proportional defocus varying from 0 (null defocus or full focus) to 1 (full defocus or null focus) [3]. A null defocus means that the mirrors perfectly aim the solar beam in the absorber tube, and vice-versa. One objective is to maximize solar energy absorption, therefore, $d \to 0$. The second term of RHS of equation (1) describes the ambient heat losses where $H_l[W/(m^2\ ^\circ C)]$ is the global coefficient of thermal losses and $T_a[^\circ C]$ is the ambient temperature. The third term of RHS of equation (1) describes the heat exchange between the pipes metal walls and the fluid flow, where $L[m]$ is the length of the absorber pipe, and $H_t[W/(m^2\ ^\circ C)]$ is the coefficient of heat transmission metal–fluid. Besides, equation (2) has the flow $q[m^3/s]$, and pipe length $x[m]$. For heat transfer coefficients, material properties, and further details refer to [11]. The partial differential equations (1) and (2) are solved discretizing the collector in 64 segments of $1[m]$ and integrating the system in time steps of $0.5[s]$.

B. Practical Non-linear MPC - PNMPC

This work proposes an MPC strategy, which is widely used in the process industry [12]. PNMPC technique [13] is specifically used to cope with solar collector non-linearities. This strategy uses a computational procedure to linearize the non-linear model of the plant in each iteration step to solve a Quadratic Programming (QP) problem at each sample time. Equation (3) is the cost function of the proposed PNMPC. Note in the latter equation that apart from the terms on the temperature tracking error and control effort, it has two new terms to force the manipulated variables to track their targets. The idea is to force the defocus to go to null defocus, avoiding energy waste, and to force the flow to a given target sent by the power block system, for example.

$$\begin{aligned}\min_{\Delta u} \quad & \sum_{j=N_1}^{N_2} \gamma(\tilde{T}(k+j|k) - T_{sp}(k+j|k))^2 \\ & + \sum_{i=0}^{N_u-1} \lambda_1 \Delta q(k+i)^2 \\ & + \sum_{i=0}^{N_u-1} \lambda_2 \Delta d(k+i)^2 \\ & + \sum_{i=0}^{N_u-1} \sigma_1 (q(k+j|k) - q_{sp}(k+j|k))^2 \\ & + \sum_{i=0}^{N_u-1} \sigma_2 d(d(k+j|k) - d_{sp}(k+j|k))^2,\end{aligned} \quad (3)$$

$$\begin{aligned}\text{s.t.} \quad & 2.7 \le q(k+i|k) \le 10 \ i = 0, ..., N_u - 1, \\ & 0 \le d(k+i|k) \le 1 \ i = 0, ..., N_u - 1, \\ & 0 \le \Delta q(k+i) \le 0.6 \ i = 0, ..., N_u - 1. \\ & 0 \le \Delta d(k+i) \le 0.5 \ i = 0, ..., N_u - 1.\end{aligned}$$

In equation (3), N_1 and N_2 are the prediction horizons, γ, λ, σ are the control weights for reference tracking, control effort and manipulated variables target, respectively. $\tilde{T}$ is the predicted outlet temperature, where subscript sp is the set-point, k is the actual sample time, N_u is the control horizon, Δq is the flow increment, Δd is the defocus increment.

The model used for the prediction calculation is the same described by equations (2) and (1) with length discretization of $8[m]$ leading to 8 tube segments. This discretization reduces the PNMPC computation time. The horizons are $N_1 = 1$, $N_2 = 12$ and $N_u = 6$ samples with simulation sample times of $t_s = 20[s]$. Defocus, d, is considered to vary simultaneously in all fresnel collector segments to enhance controllability [14] and produce a even solar tracking system wear for maintenance purposes. Next, the simulation scenarios are set.

C. Simulations Scenarios

Simulation plan seeks to evaluate the contribution of the active defocus concept on the solar collector control. The weights $\gamma,\ \lambda_1,\ \lambda_2,\ \sigma_1,\ \sigma_2$, are chosen in order to combine the different terms of equation (3). Three scenarios emerge from the weights combinations, see Table I.

TABLE I
PNMPC TUNNING PARAMETERS USED IN THE DIFFERENT SIMULATION SCENARIOS.

Scenario	Controller	γ	λ_1	λ_2	σ_1	σ_2
1. Flow	PNMPC1	10	1	0	0	0
2. Flow+Defocus	PNMPC2	10	1	100	0	0
3. Flow +Defocus +actuator reference tracking	PNMPC3	10	1	100	10	100

Note that Scenario 1 uses the typical MPC objective function. It considers the reference tracking and the control effort of the manipulated flow. Scenario 2 considers reference temperature tracking and both flow and defocus manipulated variables with respective control effort terms. Finally, Scenario 3 assesses this paper's control solution, where, besides the above-defined terms, two more manipulated variable targets terms were added.

Next, disturbances profiles are defined to evaluate the controllers' performances. The test is a combination of changes based on a practical control application of this plant [11]. Figure 1 is divided into 4 sections benchmarks. Section A refers to outlet temperature reference changes from 12:00 to 13:00. Section B is related to inlet temperature disturbances, a degree at 13:15 and two ramps from 13:30 to 14:00. The inlet temperature degree at 13:15 simulates a sudden power block consumption decrease, and the ramps simulate a power block transient event. The inlet temperature increase and decrease events can be caused by coupling the solar collector and the power block. Section C presents solar irradiance disturbances, first strong clouds passing at 14:15 and 14:45, then an exceeding irradiance profile from 15:15 to 15:45 that simulates an SM greater than one. Section D starts at 16:00 and depicts the case where the power block decreases its power demand from the solar collector, forcing the Fresnel to operate in a given flow.

Finally, two performance indexes are defined. The first one is the Integral of Squared Error (ISE)

$$ISE = \int_0^{t_f} e^2(t)dt, \tag{4}$$

where t_f is the final simulation time, and $e = T - T_{sp}$ is the outlet temperature error. The second is the normalized total energy production E_n

$$E_n = \frac{\int_0^{t_f} q(t)\rho(T)c(T)T(t)dt.}{\int_0^{t_f} q_{max}\rho(T_{sp})c(T_{sp})T_{sp}(t)dt,} \tag{5}$$

where $q_{max} = 10[m^3/h]$ is the maximum flow. E_n is calculated considering the total energy produced divided by a total energy produced with a perfect reference tracking. The perfect control energy produced is calculated accordingly to T_{sp} profile and q_{max}, see denominator of equation (5).

III. RESULTS AND DISCUSSION

Figure 1 shows the simulation results of the proposed PNMPC1 strategy considering scenario 1. The upper graphic depicts solar collector outlet temperature, inlet temperature, and reference temperature. Besides, the right y-axis shows solar irradiance. The bottom graphic represents the manipulated variables, flow and defocus. Despite its maximum flow, the PNMPC1 cannot track reference from 12:00 to 12:30. After this first hour, it is capable of following the set-point. The controller can reject the inlet temperature disturbances of section B at 13:15, although it fails to track outlet temperature set-point in the case of the re-circulation mode of the plant at 13:30. The solar collector increases more than $10[^\circ C]$ in this event, which could lead to a safety action or plant failure.

The controller has an adequate irradiance disturbance rejection at 14:15 and 14:45 caused by clouds. Note that the temperature decreases until the clouds unblock the solar irradiation. Cloud shading is a severe event because the controller reduces flow to avoid temperature drop. Suddenly, the irradiance increases, causing a sharp pump actuation and overshoot to reestablish the outlet temperature reference tracking. However, the controller is insufficient to control the plant under surplus irradiance power from 15:15 to 15:45. Note that the ramps simulate a solar plant with SM greater than one.

Lastly, section D of Scenario 1 assesses power block generation reduction. Thus, flow is reduced to a given value at 16:00 to simulate this case. After setting the flow, the outlet temperature stays $3[^\circ C]$ above the set-point until the end of the simulation. Therefore, PNMPC1 is not capable of coping with generation reduction events.

Scenario 2 is depicted in Figure 2, note the defocus effort (dashed line) in the bottom figure. In section A the controller can track all references because of the active defocus action. For example, from 12:00 to 12:15 the flow is maximum and

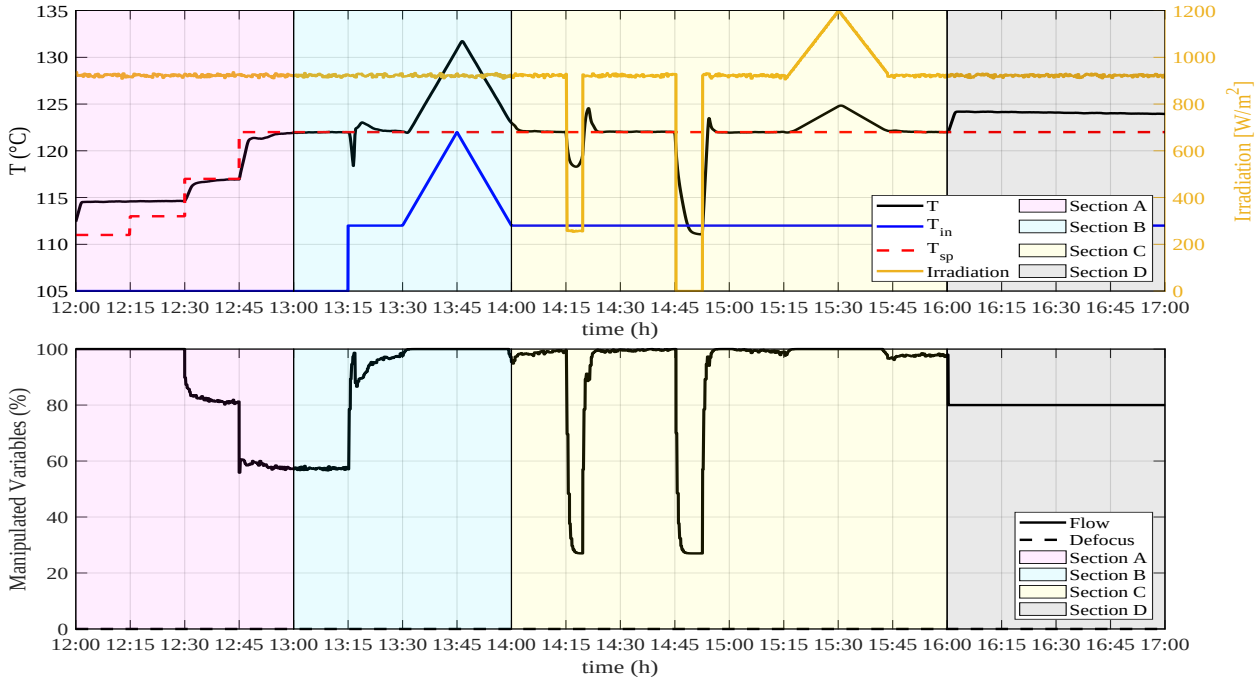

Fig. 1. Scenario 1 - Control results manipulating only the flow.

the defocus is at almost 40%, from 12:15 to 12:45 both flow and defocus are not saturated. Note that PNMPC2 wastes energy because it is possible to increase flow and reduce defocus.

Section B of Scenario 2 shows inlet temperature disturbance rejection at 13:15. Besides, now the controller succeeds in maintaining the outlet temperature in the re-circulation case at 13:30, having a small error than in Scenario1, and preventing possible overheating events.

Note at the bottom graphic of figure 2, that the defocus has an action (dashed line). In section A the controller can track all references because of the active defocus action. For example, from 12:00 to 12:15, flow saturates and defocus is at 40%. Then the defocus decreases as the set-point increases.

Section B of Scenario 2 shows appropriate inlet temperature disturbance rejection at 13:15. Besides, now the controller succeeds in maintaining the outlet temperature in the case of a re-circulation mode of the plant at 13:30, having a small error, and preventing possible overheating events.

Figure 2, section C, shows that the active defocus can reject clouds disturbances with smaller overshoot values than the simulation of scenario 1. Furthermore, the controller can control the plant under surplus irradiance power due to solar multiple, from 15:15 to 15:45, with almost no reference tracking error.

Section D of figure 2 depicts the reduction of heat demand. Note that the manipulated variables target are not considered on the PNMPC2, see Table I. Like PNMPC1, the PNMPC2 cannot receive a signal from the power block to change its generation under energy reduction scenarios. Even so, as in Scenario 1, the flow is forced to the same value at 16:00. Note that in the case of Scenario 2, setting the flow to 80% at 16:00 means increasing the flow. This flow rise happened because multiple combinations of flow and defocus solve the outlet temperature reference tracking. Thus, from 15:45 to 16:00, the controller found a steady-state equilibrium point with the flow at 60% and defocus at 40%. After the flow stabilization, the controller was able to track the reference with a minor error. Therefore, active defocus results in reference tracking capabilities together with generation demand events solution.

The main drawback of the Scenario 2 controller is that it produces less thermal power due to stabilization in steady-state points where the flow does not saturate. Note in Figure 2 that the defocus maintains a value even if the flow does not reach its maximum. Thus, the defocus system is rejecting valuable solar energy. Therefore, the controller can operate safely without possible overheating events, although there is a conflict between reference tracking and energy optimization. A possible solution is to add targets to manipulated variables in cost function as depicted on PNMPC3 weights, see table I.

Figure 3 shows Scenario 3. Note at the bottom figure that the defocus (dashed line) actuates to track reference and reject disturbances, then the defocus tends to zero to increase energy production.

Section A of figure 3 shows that the controller is capable of tracking the temperature reference. Note that from 12:00 to 12:30, the controller maintains the flow saturated and manipulates only the defocus. Then, from 12:30 to 13:15,

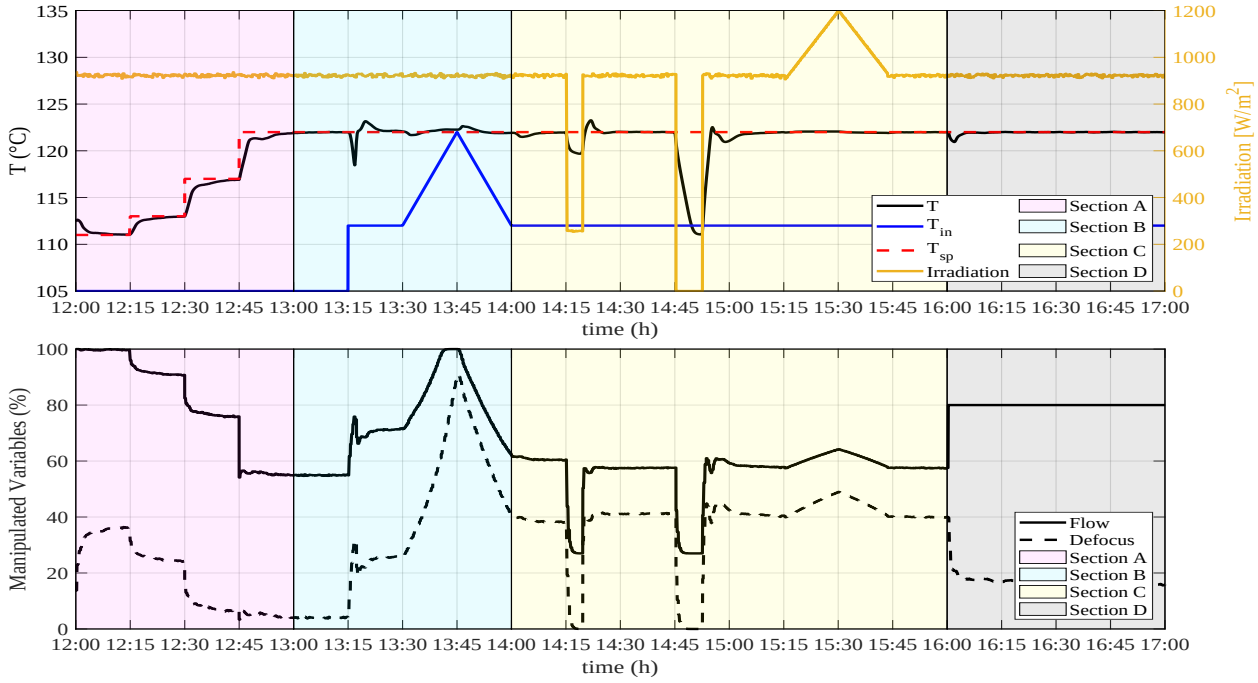

Fig. 2. Scenario 3 - Control manipulating the flow and focus without manipulated variables targets.

both manipulated variables operate to follow their target. The defocus tends to zero after the transient, thus, meaning that the solar collector operation absorbs more solar energy than in scenario 2. This result shows that the proposed controller with the active defocus can enhance reference tracking while maintaining optimal production.

Figure 3, section B, shows that the controller has a suitable inlet temperature disturbance rejection at 13:15. The PNMPC can also cope with re-circulation mode and respective inlet temperature increase from 13:30 to 14:00. However, the outlet temperature error increases in comparison to Scenario 2. The increase happens because the solution proposed in Scenario 3 tends to saturate the flow, absorbing more solar energy. Therefore, the defocus is the only manipulated variable available to reject the inlet temperature profile; compare the manipulated variables profiles of bottom figure 2 and figure 3 from 13:30 to 14:00. Summing up, the proposed solution has a suitable inlet temperature rejection with energy optimization and overheat prevention capabilities.

Figure 3, section C, shows that PNMPC3 is capable of irradiance disturbance rejection at 14:15, and 14:45. A comparison between Scenario 3 and Scenario 2 shows that both controllers have small overshoots at 14:20 and 14:50, with the better dynamic response from Scenario 2. However, the controller in Scenario 3 tends to saturate the flow, thus optimizing energy production, with pump smoother operation that can avoid quick pump action with respective pressure fluctuations and hydraulic strokes. Besides, the controller can operate under surplus solar power events from 15:15 to 15:45. Again PNMPC3 and PNMPC2 have similar dynamic performance, with PNMPC3 with slightly dynamic disadvantages, while having great energy production advantages. Note, from 15:15 to 15:45, that the pump operates at full flow, and the active defocus rejects only the necessary surplus solar energy to track reference.

Section D of Figure 3 depicts a flow target definition at 16:00, respective defocus actuation and almost no temperature disturbance. The PNMPC3 is the only controller capable of receiving a explicit thermal power $\dot{Q} = qc(T)T$ reference, both T_{sp} and q_{sp}, in its formulation, see Table I and Equation (3). Controlling thermal power is an important controller feature that gives response capabilities to the solar field in the case of power block production changes.

TABLE II
PERFORMANCE INDEX

	PNMPC1	PNMPC2	PNMPC3
ISE	38.125	11.773	14.772
E_n	1.0097	0.9983	0.9995

Table II summarizes the performance indexes between scenarios and controllers for comparison. The proposed PNMPC3 produces 99.95% of a perfect production, having an $ISE = 14.772[°C]$. Therefore it has the best energy production with enhanced control performance. Note that an $E_n > 1$ is not desirable because the plant would operate above the reference temperature for some time. The latter means that the plant is subject to overheating, and safety stoppage. Further research could evaluate the energy and economic impacts of the active defocus concept in a more

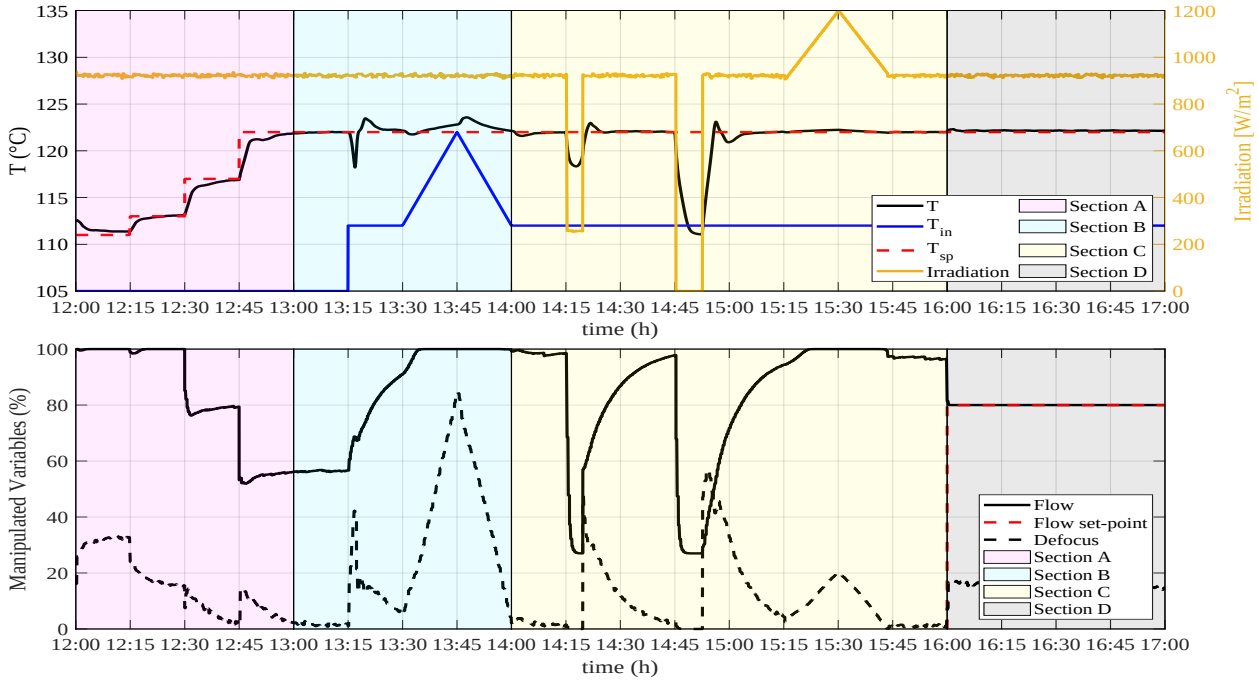

Fig. 3. Scenario 2 - Control manipulating the flow and focus with manipulated variables targets.

realistic solar irradiation profile and power block conditions.

IV. CONCLUSIONS

Solar concentrating plants have a solar multiple greater than one. Therefore, a control with active defocus action is necessary for reference tracking and disturbance rejection under regular operation. This paper implements and tests a multivariable PNMPC considering both flow and defocus in its objective function. The formulation avoids the need for mixed-integer programming or event-based algorithms. Results show that the proposed controller can track reference and reject disturbances, having the features of defocus minimization, overheat prevention, and power block demand reduction. Future works should test the controller in a real plant, evaluating the economic and energetic advantages.

ACKNOWLEDGMENT

Diogo O. Machado thanks to IFRS- campus Rio Grande for capacity support, *Fundación Carolina*, SEGIB and PrInt-UFSC programms for mobility scholarships.

REFERENCES

[1] E. F. Camacho, M. Berenguel, F. R. Rubio, and D. Martínez, *Control of solar energy systems*. Springer Verlag, 2012.

[2] E. Frank, F. Mauthner, S. Fischer, P. Frey, F. Giovannetti, K. Jakob, Z. Klier, P. Kratz, and C. Zahler, "Overheating prevention and stagnation handling in solar process heat applications," IEA SHC Task 49, Tech. Rep., 2015.

[3] D. Machado, J. E. N. Rico, and G. A. de Andrade, "A 2dof thermosolar concentrator proposal: Solar tracking and disturbance rejection using proportional defocus." in *ISES Solar World Congress SWC 2019*. International Solar Energy Society, 2019. [Online]. Available: https://doi.org/10.18086%2Fswc.2019.01.05

[4] T. de Araújo Elias, P. R. C. Mendes, J. E. Normey-rico, and C. Bordons, "Optimal solar collectors defocusing based on maximum temperature," in *2018 9th International Renewable Energy Congress (IREC)*, 2018, pp. 1–5.

[5] T. de Araújo Elias, P. R. C. Mendes, and J. E. Normey-Rico, "Hybrid predictive controller for overheating prevention of solar collectors," *Renewable Energy*, vol. 136, pp. 535–547, jun 2019.

[6] A. Brandão, P. R. C. Mendes, T. de Araújo Elias, and J. E. Normey-Rico, "Overheating prevention in solar collectors using a hybrid predictive controller," in *ISES Solar World Congress SWC 2019*. International Solar Energy Society, 2019. [Online]. Available: https://doi.org/10.18086%2Fswc.2019.18.02

[7] A. J. Sánchez, A. J. Gallego, J. M. Escaño, and E. F. Camacho, "Event-based MPC for defocusing and power production of a parabolic trough plant under power limitation," *Solar Energy*, vol. 174, pp. 570–581, nov 2018.

[8] A. J. Sánchez, A. J. Gallego, J. M. Escaño, and E. F. Camacho, "Adaptive incremental state space MPC for collector defocusing of a parabolic trough plant," *Solar Energy*, vol. 184, pp. 105–114, may 2019.

[9] M. J. Montes, A. Abánades, J. M. Martínez-Val, and M. Valdés, "Solar multiple optimization for a solar-only thermal power plant, using oil as heat transfer fluid in the parabolic trough collectors," *Solar Energy*, vol. 83, no. 12, pp. 2165–2176, 2009.

[10] P. Bermejo, F. J. Pino, and F. Rosa, "Solar absorption cooling plant in Seville," *Solar Energy*, vol. 84, no. 8, pp. 1503–1512, aug 2010.

[11] A. J. Gallego, G. M. Merello, M. Berenguel, and E. F. Camacho, "Gain-scheduling model predictive control of a Fresnel collector field," *Control Engineering Practice*, vol. 82, pp. 1–13, jan 2019. [Online]. Available: https://doi.org/10.1016/j.conengprac.2018.09.022

[12] E. Camacho and C. Bordons, *Model Predictive Control*. Springer, 2007.

[13] A. Plucenio, D. Pagano, A. Bruciapaglia, and J. Normey-Rico, "A practical approach to predictive control for nonlinear processes," *IFAC Proceedings Volumes*, vol. 40, no. 12, pp. 210–215, 2007, 7th IFAC Symposium on Nonlinear Control Systems. [Online]. Available: https://www.sciencedirect.com/science/article/pii/S1474667016355288

[14] A. J. Sánchez, A. J. Gallego, J. M. Escaño, and E. F. Camacho, "Parabolic Trough Collector Defocusing Analysis: Two control stages vs four control stages," *Solar Energy*, vol. 209, pp. 30–41, oct 2020.

7 SPLIT-RANGE CONTROL FOR IMPROVED OPERATION OF SOLAR ABSORPTION COOLING PLANTS

Renewable Energy 192 (2022) 361–372

Contents lists available at ScienceDirect

Renewable Energy

journal homepage: www.elsevier.com/locate/renene

Split-range control for improved operation of solar absorption cooling plants

Diogo Ortiz Machado [a, b, c], Adolfo J. Sánchez [d], Antonio J. Gallego [c], Gustavo A. de Andrade [b], Julio E. Normey-Rico [b], Carlos Bordons [c, e, *], Eduardo F. Camacho [c, e]

[a] IFRS - Instituto Federal de Educação, Ciencia e Tecnolgia do Rio Grande do Sul, Rua Alfredo Huch, 475, Rio Grande, 96201 460, Rio Grande do Sul, Brazil
[b] UFSC - Universidade Federal de Santa Catarina, Departamento de Automação e Sistemas, R. Eng. Agronômico Andrei Cristian Ferreira, Florianópolis, 88040 900, Santa Catarina, Brazil
[c] US - Universidad de Sevilla, Departamento de Ingeniería de Sistemas y Automática, Camino de los Descubrimientos, Sevilla, 41092, Spain
[d] MTU - Munster Technological University, Department of Mechanical, Biomedical and Manufacturing Engineering, Cork, T12 P928, Ireland
[e] ENGREEN - Laboratory of Engineering for Energy and Environmental Sustainability, Universidad de Sevilla, Spain

ARTICLE INFO

Article history:
Received 2 February 2022
Received in revised form
16 February 2022
Accepted 10 April 2022
Available online 29 April 2022

Keywords:
Renewable energy
Fresnel solar collector
Defocus
Absorption chiller
Solar cooling
Split-range control

ABSTRACT

This paper proposes the first application of a split-range control technique on a concentrating solar collector to improve an absorption plant production. Solar absorption plants have solar power availability in phase with cooling demand under design conditions. Thus, it is a powerful cooling technology in the context of renewable energy and energy efficiency. These plants need control systems to cope with solar irradiance intermittency, reject irradiation disturbances, manage fossil fuels backup systems and dump closed-loop thermal-hydraulic oscillations. In this work, control techniques are proposed and simulated in an absorption plant in Spain. The plant consists of a concentrating Fresnel solar collector connected to an absorption chiller. The objectives are to operate with 100% renewable solar energy and avoid safety defocus events while reducing temperature oscillations and control actuators effort. Firstly, the current available plant controllers are defined, then two modifications are proposed. The first modification is a split-range controller capable of manipulating both flow and defocus of the Fresnel collector, the second modification is a PI controller to substitute the original chiller on-off controller. The results compare, through validated models, the different control systems and indicate that using both proposed controllers reduces 94% of the sum of actuators effort and 43% of the integral of absolute set-point tracking error compared to the plant's factory pre-set controllers. The suggested controllers increase 66% of energy production and 63% of exergy production. Besides, the split-range technique can be extended to any concentrating solar collector control.

1. Introduction

Currently, electrical energy continues to be produced to a large extent by fossil fuel power plants, nuclear and other energy sources that are not renewable [1]. The use of renewable sources is essential to reduce the environmental impact caused by the use of fossil fuels [2,3]. It should be noted that of all renewable energy sources solar energy is undoubtedly the most abundant. Due to the current situation regarding global warming, governments are trying to boost electricity generation using renewable or sustainable energy sources, through agreements, in order to reduce global warming to well below 2 °C, although the objective is to limit it to 1.5 °C [4].

Solar energy faces different challenges when entering the market. The main and most important of all is to make it economical and competitive [3,5]. In order to overcome these challenges, it is necessary to improve the operation of the plant and optimize its production. However, these are improvements are increasingly complex to achieve due to the large size of current plants. Among the different solar concentrating technologies it can be found parabolic trough solar plants, concentrating tower solar plants or concentrating linear Fresnel solar plants. This article

* Corresponding author. US - Universidad de Sevilla, Departamento de Ingeniería de Sistemas y Automática, Camino de los Descubrimientos, Sevilla, 41092, Spain.
E-mail address: bordons@us.es (C. Bordons).

https://doi.org/10.1016/j.renene.2022.04.064

focuses on the development of control algorithms for linear Fresnel solar technology plants.

The operation of concentrating solar plants is based on the concentration of solar energy in a receiving pipe through which a heat transfer fluid circulates. The fluid will be heated by the solar radiation concentrated in the receiving pipe. Later this fluid, at high temperature, will be transported to use the heat and convert it into electrical energy, for example. However, linear Fresnel plants also have the capability to be installed in buildings for solar use, as is the case of the solar Fresnel plant of the Escuela Superior de Ingeniería de Sevilla (ETSI), University of Seville. A solar Fresnel plant installed on its roof takes advantage of solar energy to generate cold through the use of an absorption machine. This cold is used for the air conditioning of the building during hot seasons.

The main objective of the control systems in solar plants is to track a reference temperature at the outlet of the solar field. That is, to follow an optimal nominal temperature set by the operators to maximize the plant's performance. This optimization is not an easy task because solar plants are, in general, highly nonlinear and distributed processes that present significant transport delays and depend on the size of the plant. The plant complexity is a challenge to design advanced controllers to optimize production and operation.

The studies carried out on the control of the outlet temperature of solar fields are numerous such as [6] where an adaptative Model Predictive Control (MPC) strategy is designed for the Fresnel solar plant located at the ETSI, Seville. An unscented Kalman filter is used as a state estimator of the metal-fluid temperature profiles and effective solar radiation. Results are compared with a PID + feedforward control and a Generalized Predictive Control (GPC). Results showed that the proposed adaptative MPC outperformed these two strategies in temperature tracking and disturbance rejection.

The development of fuzzy incremental controller on a small-scale linear Fresnel reflector solar plant is presented in Ref. [7]. Authors used an ant colony algorithm for an optimal tuning of a PID + feedforward controller parameters to compare the proposed PI-like fuzzy incremental algorithm. Results of the Fresnel plant shows that the proposed PI-fuzzy like algorithm outperforms the conventional PI algorithm in terms of the time response metrics. The work presented in Ref. [8] presents a two layer control strategy for temperature tracking and disturbance rejection of a solar Fresnel plant. The first layer is a nonlinear MPC for regulating the outlet temperature of the solar field, while the second layer is a fuzzy algorithm for the adequate operation mode considering the operation conditions.

Other works analyzed the optimization of the solar fields, as in Ref. [9] where authors present a study on the optimization of the solar multiple[1] when designing linear Fresnel solar fields of direct generation. This work is a case study of a 50 MW Fresnel plant to find the optimum of the solar multiple. An economic optimization is used to determine the lowest Levelized Cost of Electricity (LCOE). Authors come to the conclusion that a Fresnel plant without Thermal Energy Storage (TES) should have a solar multiple of 1.7 while if it has a TES system the field should be greater with a solar multiple of 2, for 2 h energy storage. In this sense it is logical to assume that solar concentrating solar plants will need to defocus the solar field mirrors under normal operation. Therefore, control techniques as the proposed split-range that considers a proportional focus in the process control layer [11], instead of on-off defocus on the safety layer, would provide operation advantages.

[1] Solar multiple is defined as the ratio between the thermal power produced by the solar field (generator) at the design point and the thermal power required by the power block (consumer) at nominal conditions [10].

In general, concentrating solar plants must start and stop every day. The start-up is done during sunrise. Plants can use a gas burner to start-up the plant, since they must start the turbine that has been cooling overnight. In the same way, the ETSI solar Fresnel plant has a natural gas burner to pre-heat the entire circuit as well as the absorption machine to start working. However, the use of gas is not the most convenient strategy when operating renewable plants and even more if we are talking about solar renewable energy.

The previous heating of the solar field as well as the absorption machine is crucial for the operation of the plant, since the operation of the absorption machine must be carried out in a very narrow temperature range [12], around 160[$^{\circ}C$]. This article shows how the plant begins to work thanks to the use of the gas burner. However, if the heating of the circuit is carried out in an uncontrolled way, it can cause oscillations in the outlet temperature that will be maintained over time, since initially the entire system is cold and by increasing the flow-rate through the pipes, the cold flow will be moving towards the solar field. It will take a while for the entire circuit to be homogeneous at nominal temperatures. As long as this does not happen, there will be temperature fluctuations caused by the mass transport of water. These temperature oscillations are fed back as it is a closed circuit and will cause the system to continuously activate and deactivate the absorption machine several times since it would be leaving the nominal operating temperature of the absorption machine and the operating mode must be changed [8]. In addition to changing the operating mode of the absorption machine, it would also be consuming gas again to try to raise the internal Lithium-Bromide temperature. However, the use of gas is a resource that could be eliminated if a controlled start-up to heat the pipes and the absorption machine were made. This would not only reduce the cost of the bill caused by the use of gas but also in the installation of the plant itself, since it would not be necessary to invest in the installation of a gas burner. Starting the plant with gas becomes a difficult decision, if later it may turn out that the day turns cloudy and it would not be possible to operate anymore, in which case gas and money would have been wasted, something that will not happen if only the solar resource is used.

In this paper, a split-range controller on the Fresnel and a PI controller on the High Temperature Generator (HTG) of the absorption machine are proposed on the ETSI absorption plant. The objective is to avoid the use of natural gas in the start-up as well as to avoid possible safety defocusing actions. The HTG controller will be in charge of reducing the oscillations of the plant as well as the control effort, while the strategy based on the split-range controller will be in charge of accelerating the start-up of the plant without using natural gas. The split-range controller will be able to accelerate the process avoiding overheating, which translates into an improvement in the stability of the plant and consequently an increase in production. In addition, the split-range controller will take into account that the flow rate is the main manipulated variable, at least until it reaches saturation, at which point the flow rate will be at its maximum and the split-range controller must begin to manipulate the defocus to control the outlet temperature.

The rest of the paper is organized as follows: Section 2 describes the process and the operation of the ETSI Fresnel absorption plant. In Section 3 the inherited factory pre-set and revamp control schemes are presented and simulated to motivate this paper controllers proposals of Section 4. Plant models details, simulations plans, and the results are presented in Section 4. Section 5 draws the paper to an end with some conclusions.

2. ETSI solar absorption plant and control premise

The purpose of solar plant studied in this work is to reduce non-renewable energy consumption and avoid carbon dioxide (CO_2)

emissions. Its objective is to generate chilled water through an absorption chiller using hot water from a concentrating solar collector. The chilled water is fed to the ETSI building in order to supplement the heat ventilation and air conditioning (HVAC) system [12].

Table 1 organizes the main characteristics of the plant. The absorption chiller worked with a daily average cooling power of 135 kW, with a worst-case of 70 kW, and a Coefficient of Performance (COP) between 1.1 and 1.25 in a campaign of five days of operation during the cold demand season [12]. Equation (1) calculates the Solar Heat Fraction (SHF) where Q_{solar} is the energy generated in the solar collector and Q_{gen} is the energy used in the absorption machine

$$SHF = \frac{Q_{solar}}{Q_{gen}}, \tag{1}$$

that results in 0.75 from operational data. This means that 75% of injected heat in the chiller was from the solar resource and the other 25% came from gas burning [12].

The problem is that the purpose of the solar cooling plant is to reduce non-renewable energy consumption and avoid carbon dioxide emissions. The authors in Ref. [12] investigate the ETSI absorption plant trade-off between burning gas, CO_2 generation, and costs, performing an economic and CO_2 emission analysis and comparing the hybrid gas/solar chiller to an electric one. Table 2 updates and summarizes the analysis considering actual gas [13] and electricity [14] costs in Spain.

Table 2 compares the performance of chillers considering a fixed output cooling generation of 1000 kWh. ETSI absorption plant hybrid operation reduces 75% of the associated cost and CO_2 emissions compared to the gas chiller. However, Table 2 shows that the electric compression chiller has lower cost and emissions than the gas absorption chiller. Therefore, it is more profitable and less pollutant to compose solar cooling with electricity instead of gas.

The ETSI building has a HVAC system equipped with electric compression chillers which is an option to avoid using the backup boiler equipped in the absorption chiller, see Fig. 1. Therefore, this paper's premise is to operate the solar absorption cooling plant only with solar energy, thus, a SHF = 1, as it seems a better strategy. Thereby, the gas boiler is not modeled or simulated in this work. The next section presents the legacy controls simulations and the motivation of this work considering the above mentioned premise.

Table 2
Comparison between electric compression, thermal absorption, a hybrid solar/gas absorption performances.

Chiller	Compression	Absorption	ETSI Hybrid Absorption	
Primary energy	electric	gas	solar	gas
COP	3,50	1,10	1,10	
Energy output [*kWh*]	1000,00	1000,00	1000,00	
Energy input [*kWh*]	285,71	909,09	681,82	227,27
Input cost [*euro*/*kWh*]	0,17	0,07	0,00	0,07
Associated cost [*euro*]	49,59	66,55	0,00	16,64
CO_2 emissions [*kg*/*kWh*]	0,26	0,19	0,00	0,19
Associated CO_2[*kg*]	74,29	176,36	0,00	44,09

3. Motivation

This paper proposes new control techniques to enhance the ETSI solar absorption plant operation. Fig. 1 depicts the plant schematic where each fluid stream has a label from 1 to 12. The plant comprises the Fresnel collector as the solar heat source, the absorption machine as the heat sink, long pipes that connects both processes, and a valve that can route the water streams. Note that the absorption machine's evaporator generates the cooling effect, which is delivered to the HVAC system by streams 9 and 10.

The objective of Controller C1 is to supply the HTG with water at appropriate temperature by regulating the solar collector outlet temperature T_2 through manipulating the mirror focus f, or the pump flow q. The objective of Controller C2 is to regulate HTG lithium-bromide solution temperature T_8 of the absorption machine by manipulating valve aperture v. The Fresnel collector inlet stream 1 is the stream 7 after flowing through the pipe. And the stream 7 is a mixture of the HTG outlet stream 6 and the valve bypass stream 4. Therefore, the process is a hydraulic closed loop. This thermo-hydraulic system has complex dynamics such recycle [15] that could arise integrating snow-ball effect [16,17], dead-times, because mass transfer across long pipes [18], and resonance modes [19], that leads to strong non-linearities and oscillations reported in Ref. [12], and in measurement data. Next, plant simulations illustrate the oscillations considering the legacy controller of the plant, and discusse the operation issues and

Table 1
ETSI Solar Absorption plant characteristics.

Fresnel collectors	
Solar field aperture	352 m^2
Absorber tube length	64 m
Absorber tube model	SCHOTT PTR 70
Heat transfer fluid	Saturated liquid water
Operation temperature (max)	180 °C
Operating pressure	13 bar
Mirror reflectivity	0.92
Pipelines	
Inner diameter of pipeline	0.052 m
Total solar circuit length	365 m
Absorption chiller BROAD-BZH15	
Cooling capacity	174 kW
COP	1.34
Temperature evaporator inlet	12 °C
Temperature evaporator outlet	7 °C
Evaporator flow rate	30 m^3/h
Temperature condenser inlet	30 °C
Temperature condenser outlet	37 °C
Condenser flowrate	37 m^3/h
Fuel	Natural gas
HTG Temperature	145 °C

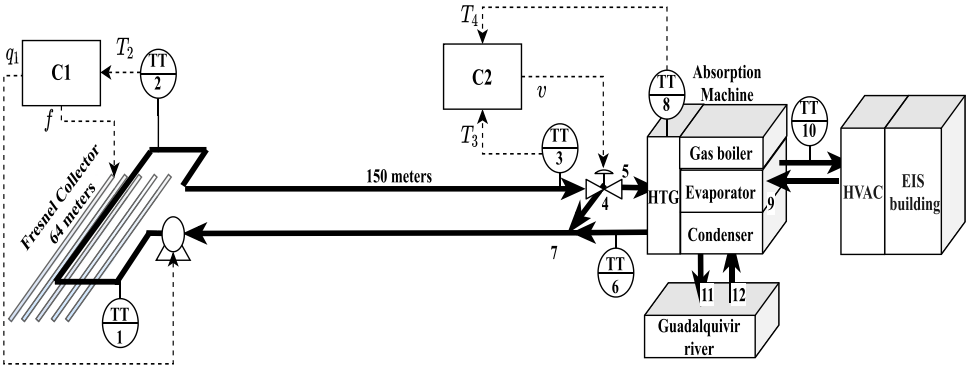

Fig. 1. General schematic of the absorption plant in the *Escuela Tecnica Superior de Ingenieria (ETSI)* in Seville University.

opportunities. This work considers the absorption chiller model and the Fresnel solar collector model described and validated in Ref. [8], and [20], respectively.

There are two inherited control strategies implemented in the Fresnel's hardware and one implemented on the chiller hardware. The original Fresnel control rules running on controller C1 are described in Equation (2).

$$\begin{cases} q_1 = 0, & \text{if } I \leq 250, \\ q_1 = 12, & \text{if } I > 250, \\ f = 0, & \text{if } q_1 = 0, \\ f = k_{p1}\left(e_1(t) + \int \frac{1}{t_{i1}} e_1(t)dt\right), & \text{if } q_1 = 12, \end{cases} \tag{2}$$

where $q[m^3/h]$ is the flow, $I[W/m^3]$ is sun irradiance, f is the mirror 's focus with a range from 0 to 1, k_{p1} is the proportional gain of controller C1, t_{i1} is the integral time of controller C1, $e_1(t) = T_{sp2} - T_2(t)$ is the error between the desired set-point, $T_{sp2} = 170[^\circ C]$, and the outlet temperature, T_2 of controller C1. The first Fresnel controller has an on-off flow manipulation with $q_1 = 0$ when the irradiance is below a minimum value, and $q_1 = 12[m^3/h]$ when the irradiance is sufficient to start the plant, the latter condition allows manipulating the focus with a proportional plus integral (PI) law. The original Fresnel controller (C1) performance is depicted on Fig. 2.a and 2.c. C1 starts the pump at 9:00 considering a clear sky irradiance profile (yellow line) of Fig. 2.b. Then, the PI controller starts regulating the outlet temperature T_2 by manipulating the mirrors focus when the flow is at maximum and $I > 250$, accordingly to Equation (4). This phase is called preheating and recirculates water between the collector and chiller valve with full focus until T_3 reaches a predefined temperature starting the chiller.

$$v = \begin{cases} 1, & \text{if } T_3 > 160 \text{ and } T_8 < 135, \\ 0, & \text{if } T_3 \leq 160 \text{ or } T_8 \geq 145. \end{cases} \tag{3}$$

Controller C2 is responsible for starting the absorption chiller, the original control rules are described in Equation (3). Where $v = [0, 1]$ is the three-way valve opening, when $v = 1$ it is feeding the chiller, when $v = 0$ it is by-passing the chiller, T_3 is the valve inlet temperature, and T_8 is the HTG temperature. Note that the chiller factory pre-set C2 is an on-off controller with hysteresis that seeks to maintain the HTG temperature inside a band between the lower temperature set-point $\underline{T}_{sp8} = 135$ and the upper temperature set-point $\bar{T}_{sp8} = 145[^\circ C]$, see Fig. 2.b.

The plant simulation considering the factory pre-set C2 is depicted in Fig. 2.b and 2.d. When the HTG inlet temperature T_3 reaches a predefined temperature $T_{sp3} = 160[^\circ C]$ and the internal HTG temperature T_8 is below $\underline{T}_{sp8} = 135[^\circ C]$ the controller opens the valve aperture v and feeds the HTG, both events happen at 13:00 on Fig. 2.b and Fig. 2.d, respectively. Then, T_8 reaches $\bar{T}_{sp8}$ and the valve closes, decreasing the HTG temperature. The problem is that when T_8 drops below $\underline{T}_{sp8}$ again, the valve does not open owing to $T_3 < 160$, because the first valve aperture itself decreases the water temperature inside the pipes and, ultimately, T3. If T_8 stays below $\underline{T}_{sp8}$ for more than 30 min after the start-up, the boiler start burning gas. Fig. 2 shows that the boiler would burn gas between 13:00 and 14:00. The gas backup heat effect is not seen because the premise of this work of not using the boiler and, therefore, the boiler is not simulated.

Note that just before the valve opens at 13:30, T_3 and T_8 are at temperature of 160 and 75$[^\circ C]$, respectively. Thus, when the valve opens, the internal water, that was inside the HTG at 75$[^\circ C]$, enters in the pipes with water at 160$[^\circ C]$, generating a temperature gradient of 85$[^\circ C]$. Then, both low and high temperature water plug flows travel inside the pipes concomitantly which reflects the oscillatory temperatures depicted on Fig. 2.a. Note on Fig. 2.a that the C1 cannot stabilize T_2 even with strong focus actuation effort depicted on Fig. 2.c. It is also worth noting on Fig. 2.a that the temperature oscillations have a minimum of T_8, and a maximum of T_3 at 13:00, just before start feeding the HTG. Note that the oscillations periods are coincident with the pipes hydraulic residence time, $\tau = (V_{fresnel} + V_{piping})/q_1$. In other words, the period of temperature oscillations on Fig. 2.a is the time that the cold plug flow takes to make one lap on the hydraulic circuit concerning the temperature transmitter TT2 position. Resuming, the factory pre-set control strategy leads to temperature gradients, strong focus actuation and boiler gas burning.

These results show that even though the factory pre-set control does not trigger safety total defocus, a security control to prevent overheating, the factory pre-set control leads to bad reference tracking of both Fresnel and HTG temperatures, and a strenuous effort of the solar tracking device, which results in premature wear of the focus mechanism. In practice, a second controller was implemented in the plant's hardware to reduce the focus mechanism wear, and also to reduce solar energy rejection [21].

The second Fresnel controller C1, henceforth called revamp control, exchange the focus proportional manipulation to flow proportional manipulation, and it is described by Equation (4). Focus manipulation is on-off with $f = 0$ when the irradiance is below a minimum value, and $f = 1$ when the irradiance is sufficient

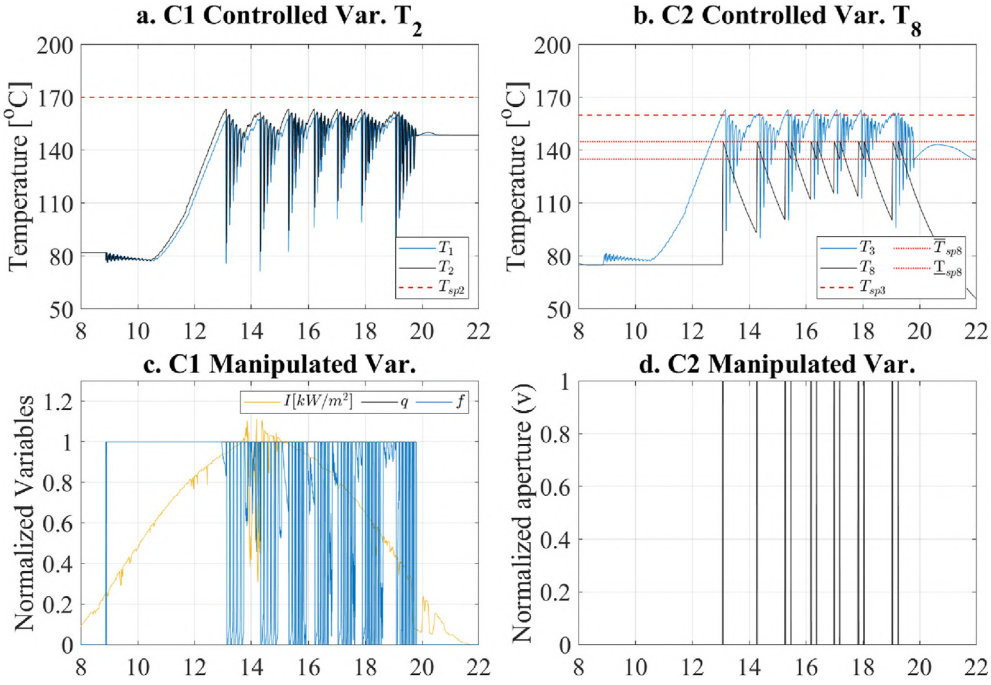

Fig. 2. Original factory pre-set control performance on Scenario 1 (S1).

to start the plant. The latter condition allows using a PI law with proportional flow q_1 range from 2 to 12$[m^3/h]$. The revamp Fresnel's controller performance is depicted on Fig. 3.a and 3.c.

$$\begin{cases} f = 0, & \text{if } I \leq 250, \\ f = 1, & \text{if } I > 250, \\ q_1 = 0, & \text{if } f = 0, \\ q_1 = k_{p1}\left(e_1(t) + \int \frac{1}{t_{i1}} e_1(t)dt\right), & \text{if } f = 1. \end{cases} \tag{4}$$

The revamp controller performance depicted on Fig. 3 has faster

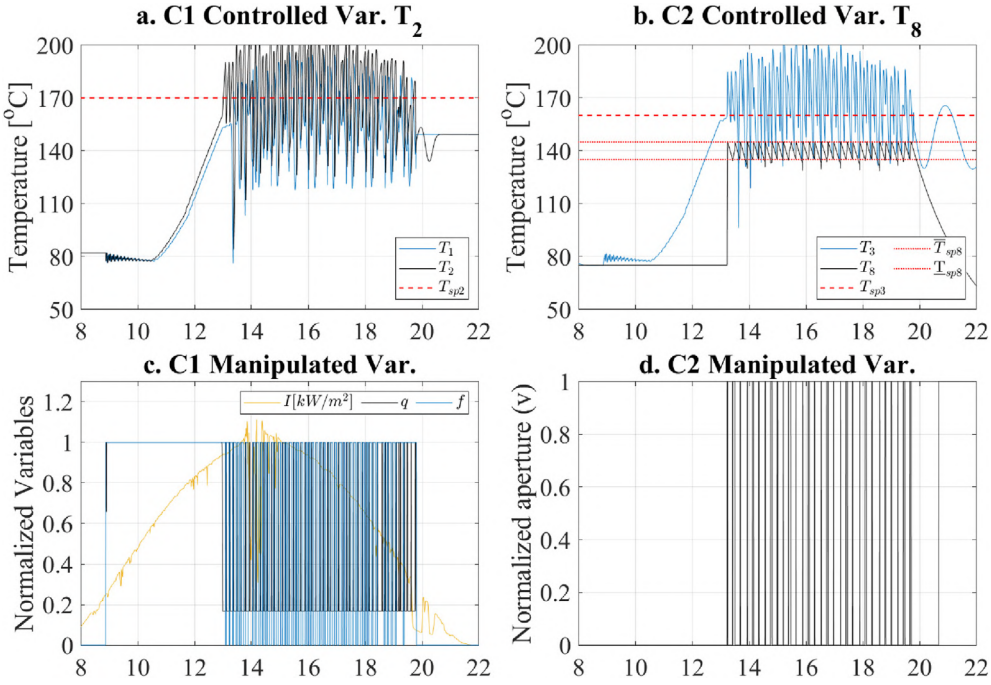

Fig. 3. Revamp control performance on Scenario 2 (S2).

start-up than the factory pre-set control due flow manipulation capability. The revamp controller regulates the HTG temperature T_8 avoiding burning gas. Although it has qualitatively worst gradient temperature and oscillations than the factory pre-set controller. Note that the focus has actuation on 3.c despite not having low irradiance. This is because the Fresnel's safety defocus device described by Equation (5).

$$f_s = \begin{cases} 1 & \text{if } T_2 \leq 160[^\circ C], \\ 0 & \text{if } T_2 \geq 190[^\circ C]. \end{cases} \tag{5}$$

Thus, the Fresnel solar collector has a safety full defocus system which overrides the process controller. The safety action cools the outlet temperature from an abnormal outlet temperature of 190[°C] to 160[°C]. Fig. 3.b depicts the revamp controller safety full defocus events (blue line).

Resuming, both simulations of inherited factory pre-set control and revamp control of the ETSI absorption plant show strong oscillatory behaviour and poor set-point tracking disregarding the gas boiler operation. On the one hand the factory pre-set control advantage is that it does not have safety defocus events, although, it has disadvantages as it does not track the HTG temperature set-point properly, would start the gas boiler, has a slower start-up ramp, and cause solar energy rejection. On the other hand the revamp control advantages is that it tracks the HTG temperature setpoint, would not burn gas, have a faster start-up, although, it presents safety defocus actuation as draw-back. Therefore, the controllers have complementary advantages. The following section proposes combining the advantages and suppressing the disadvantages of inherited controllers in a new control proposal to enhance the plant performance.

4. Proposed controls

Firstly, this work proposes using a proportional plus integral (PI) law on the chiller controller C2 on Section 4.1. It is expected that the PI controller would lead to both reduction of oscillations and Fresnel's actuators effort. Secondly, this work proposes using a split-range advanced control technique on the Fresnel controller C1 on Section 4.2. It is expected that using both flow and focus in the same PI controller scheme would combine the fast start-up performance of manipulating the flow with the extended controllability of using the focus proportionally. The latter ultimately will avoid unnecessary solar energy rejection and safety full defocus events. The results of the two solutions together would avoid gas burn and safety defocus events while stabilizing operation, and increasing energy production.

4.1. High Temperature Generator controller

The HTG inlet temperature T_3 comes from the Fresnel solar collector outlet temperature T_2 through the pipes and vice versa. The problem is that the factory controller has an on-off law that generates strong oscillations a temperature gradients in the plant. Therefore, it is proposed the proportional plus integral control (PI) law described in Equation (6).

$$v = k_{p2}\left[e_2(t) + \frac{1}{t_{i2}}\int e_2(t)dt\right]. \tag{6}$$

where k_{p2}, t_{i2}, and $e_2(t)$ are the proportional gain, integral time, and error of controller C2. The error is calculated as $e_2(t) = T_{sp8} - T_8(t)$, it is the difference between the desired set-point, $T_{sp8} = 145[^\circ C]$, and the outlet temperature, T_8 of controller C2. The control law was discretized using a backward Euler technique, and its was tuned using trial an error, the same tuning is used in all controllers and simulations.

4.2. Split-range controller on concentrating solar collectors

A split-range controller is functional when there are two or more manipulated variables associated with a controlled variable. It is typically applied to extend the controller's steady-state range by switching the primary actuator when it becomes saturated [22]. Therefore, concentrating Fresnel solar collectors are typical processes where the split-range advanced control can improve operation. Specifically, the ETSI Fresnel automated system is capable of manipulating the flow and the mirror's focus, therefore, implementing a split-range controller. Selecting the flow as the primary manipulated variable seems logical because it actuates in absorbing the solar heat that has already entered the receiver. The focus is the secondary manipulated variable because it operates rejecting the solar irradiance and wasting energy. In other words, the flow will absorb the maximum solar incident energy on the solar field until saturation; then, the defocus will act because it is the only manipulated variable capable of affecting the outlet temperature. Fig. 4 depicts the split-range schematic on the Fresnel solar collector.

Equations (7) and (8) describe this controller. It is worth noting that the control law is the well known PI with an internal output signal u_1 chosen to vary from 0 to 100. The splitter divides signal u_1 between both actuators as depicted on Fig. 5. The problem here is that the flow and focus must have inverse proportional gain signal because increasing the focus will increase T_2, while increasing the flow will decrease T_2. A positive and a negative slope of the linear equations depicted on Equation (8) solve this question, which Fig. 5 exemplifies geometrically. Note that the manipulated variables ranges used in simulations are from 2 to 12[m^3/h] for the flow and from 0 to 1 for the focus.

$$u_1 = k_{p1}\left[e_1(t) + \int \frac{1}{t_{i1}} e_1(t)dt\right]. \tag{7}$$

$$\begin{cases} q_1 = 2 + 0.2u_1, & 0 \leq u_1 \leq 50; \\ f = 1 - 0.02(u_1 - 50), & 50 < u_1 \leq 100. \end{cases} \tag{8}$$

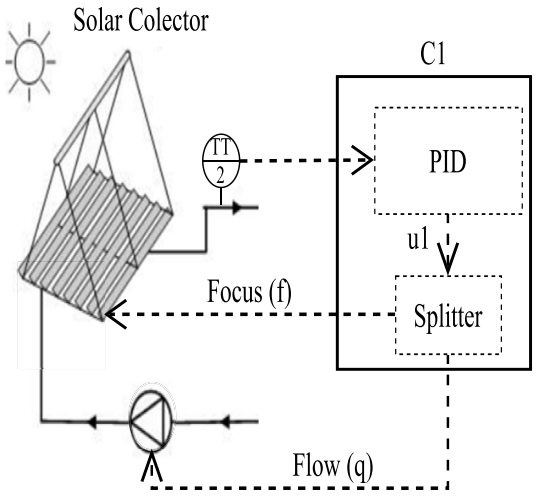

Fig. 4. Split-range block diagram on the Fresnel solar collector.

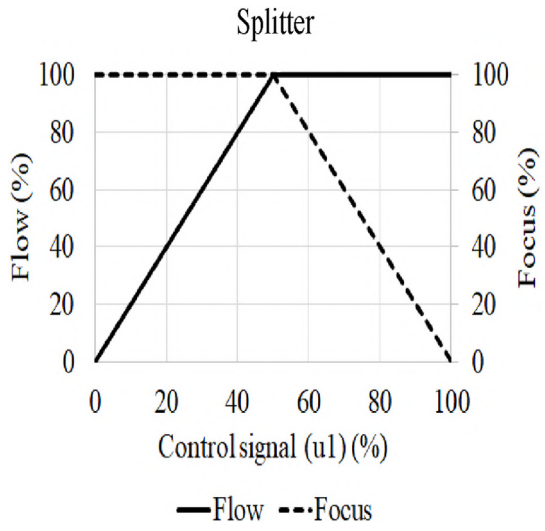

Fig. 5. Split range signal scheme.

The mirror focus will reduce from its maximum only when the pump saturates, that is, when it becomes impossible to increase sun heat absorption through the flow. Therefore, this solution increases thermal energy production since the focus reduction is sufficient to follow the temperature reference with minimum solar energy rejection. In practice, the split-range technique merges the factory pre-set and revamp controllers ideas of the IES plant. It has the advantage of using the flow to maximize energy production and focus on maintaining the controllability of the outlet temperature.

To summarize, the split-range is the most straightforward and advanced control technique capable of manipulating the flow and defocus together. It has an active defocus already in the process control automation layer contributing to avoiding safety total defocus action of the safety automation layer.

5. Simulation studies

This section is divided in four subsections approaching the mathematical model of the solar cooling plant, the simulation cases, the performance indexes and the results.

5.1. Mathematical model of the solar cooling plant

This work uses the absorption machine model described in Ref. [8], which was validated with real data and demonstrated that it is a good representation of the real process. The model consists of three parts: the high-temperature generator (HTG) connected to the solar collector, the condenser connected to the Guadalquivir river, and the evaporator connected to the ETSI building through the HVAC system. Each sub-model is a lumped parameter model.

The Fresnel solar collector subsystem is composed by two parts where a phenomenological distributed parameters model describes each. Equation (9) describes the metal tube, and Equation (10) describes the water flow.

$$\rho_m c_m A_m \frac{\partial T_m}{\partial t} = If\eta_{opt}\eta_{geo}Gf_s - H_l G(T_m - T_a) - LH_t(T_m - T_f), \tag{9}$$

$$\rho_f c_f A_f \frac{\partial T_f}{\partial t} + \rho_f c_f q \frac{\partial T_f}{\partial x} = LH_t(T_m - T_f), \tag{10}$$

where m and f sub-indexes refer to metal and fluid, respectively. The variable $A_m[m^2]$ is the cross-section area of metal absorber pipe, $I[W/m^2]$ refers to direct solar irradiance, η_{opt} is the optical efficiency, η_{geo} is the geometric efficiency, $G[m]$ is the mirrors' total aperture, $H_l[W/(m^2\ ^\circ C]$ is the global coefficient of thermal loss, L $[m]$ is the absorber pipe length, and $H_t[W/(m^2\ ^\circ C]$ is the coefficient of heat transmission between metal and fluid. The proportional mirrors focus f, and the safety full defocus f_s were added to the model to evaluate the effect of this actuator. While the first can vary the concentrated solar energy density on the receiver with values between 0 and 1, the latter has a discrete state of 0 or 1. For heat transfer coefficients, material properties, validation, and further model details, refer to Ref. [20]. Equations (9) and (10) were discretized in space and in time to be solved in integration steps of 15 $[s]$.

The piping system is an essential part of the IES plant. The tubes connect the systems and have an appreciable length. Note that the total solar circuit length is 365$[m]$ where only 64$[m]$ is composed by the Fresnel absorber length. Therefore, the piping is not negligible in the dynamics of this plant because of hydraulic recycle, snowball effect, dead-times, resonance modes, and tube-water mass thermal accumulation between the chiller and the solar collector. The thermal capacitance of the piping system is 82% of the total circuit. Thus, the tubes' accumulated energy affects the plant operation. The piping models are the same as the ones in Equation (9), and (10), but with different ambient losses and null solar input terms.

The valve is a three-way, electrically actuated, with proportional regulation capacities. This valve can change the plant operation from recirculating to feeding the HTG and vice-versa. The valve is modeled as a flow splitter and mixer system based on the energy and mass conservation laws. The valve itself is a splitter that has one mass input and two outputs modeled by Equation (11) and Equation (12), respectively,

$$q_5 = \nu q_3, \tag{11}$$

$$q_4 = (1-\nu)q_3. \tag{12}$$

The Fresnel inlet flow comes from the mixer point, calculated as $q_7 = q_4 + q_6$. The dynamics of the thermal processes are appreciably slower than the actuators. Thus the modeling considers that the pump and the valve actuators are instantaneous.

5.2. Simulation cases

Two different irradiation profiles, depicted in Fig. 6, are considered to contrast the controllers' performance.

For the study, twelve scenarios were considered, as depicted in Table 3. They are obtained combining the three different control strategies in C1 and two different controllers in C2, and the two irradiation profiles.

Simulations S1 to S3 use the C2 on-off controller. Simulation S1 considers C1 controller with fixed flow and variable focus. Simulation S2 uses C1 controller with proportional flow and fixed focus, while simulation S3 depicts the split-range controller C1, proportionally manipulating both flow and focus. Simulations S4 to S6 consider the respective C1 control laws of S1, S2, and S3 but with the PI control law on C2. Simulations S1 to S6 consider the clear day irradiation profile of Fig. 6.A, were simulations S7 to S12 have the same combinations of controllers C1 and C2 as mentioned in S1, S2 and S3, but considering the cloudy sky irradiation profile of Fig. 6.B. The initial conditions are based on the normal conditions of the plant after the night considering that the plant worked the day before. The initial pipes temperature is 80$[^\circ C]$ because ambient heat losses of the processes and pipes during the night drops the

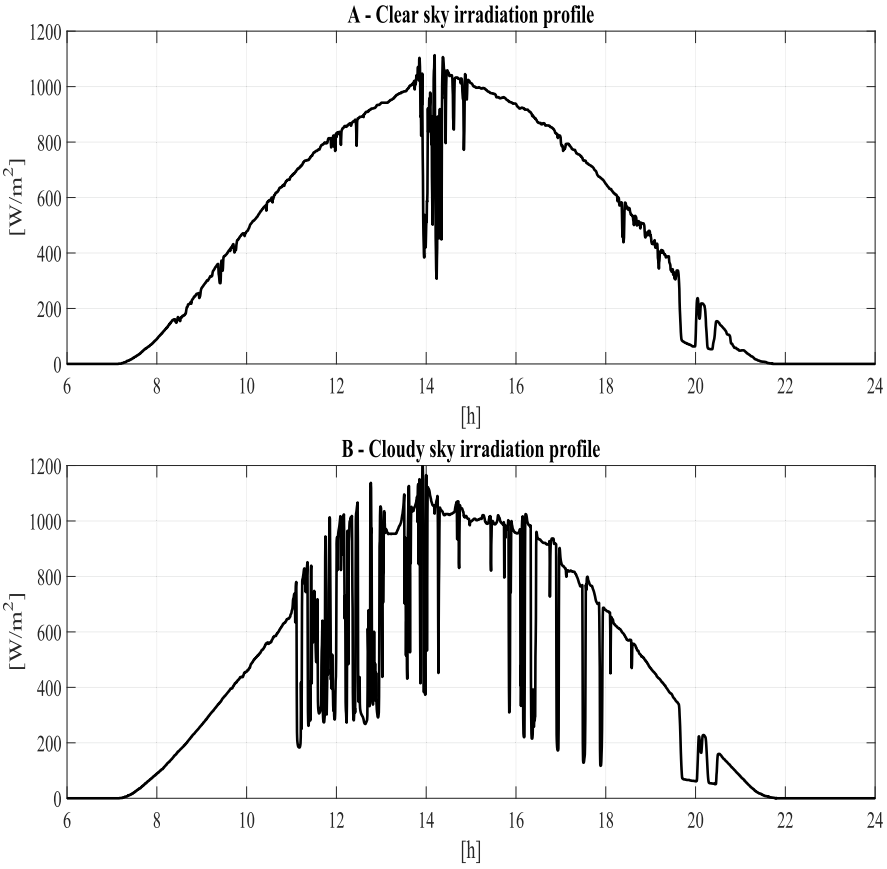

Fig. 6. Local solar irradiation measurements. A - Clear sky irradiation profile of June 09, 2009. B - Cloudy sky irradiation profile of June 26, 2009.

Table 3
Simulations scenarios. C1: PI-Focus (Equation (2)), PI-Flow (Equation (4)), PI-Split-Range (Equation (8)). C2: on-off (Equation (3)), PI (Equation (6)).

Simulation		I	C1	C2
S1	Factory	90A - clear sky	PI - Focus	on-off
S2	Revamp		PI - Flow	on-off
S3	Improved1		PI - Split-range	on-off
S4	Improved2		PI - Focus	PI
S5	Improved3		PI - Flow	PI
S6	Proposal		PI - Split-range	PI
S7	Factory	90B- cloudy sky	PI - Focus	on-off
S8	Revamp		PI - Flow	on-off
S9	Improved1		PI - Split-range	on-off
S10	Improved2		PI - Focus	PI
S11	Improved3		PI - Flow	PI
S12	Proposal		PI - Split-range	PI

temperature 80[$^{\circ}C$] during 12:00[h] [12].

5.2.1. Performance indexes

This section defines indexes used to compare the control strategies of each simulation case depicted in Table 3. The indexes quantifies safety full defocus events, gas boiler trigger use, operation time, and production performances. Note that this work premise is not using gas. Therefore, the gas boiler trigger is a detection of the condition where the absorption chiller would start burning gas, and not the boiler simulation. The boiler trigger BT is a boolean variable. In other words, it gives a measure if a given control system fulfills, or not, the condition of not burning gas.

The control performance indexes are the Normalized Cumulative Actuator Effort (NCAE) [23], the Integral of Absolute Error (IAE) of temperature control, and gas boiler trigger ($BT = 0, 1$), which is 1 if the controller is not capable of maintaining the HTG temperature in the set-point 30 min after HTG start-up.

Equation (13) describes the actuator effort for a generic manipulated variable u

$$NCAE = \frac{1}{\delta u} \sum_{k=1}^{N} |\Delta u|, \tag{13}$$

where $\delta u = u_{\max} - u_{\min}$ is the manipulated variable range, N is the total number of samples in the simulation time considering $I \geq 250$

$[W/m^2]$, thus, sufficient irradiance power for plant operation, $\Delta u = u(k) - u(k-1)$ is the control increment, and $u[k]$ is the manipulated variable value in sample time k.

Equation (14) is the Integral of Absolut Error (IAE) used here to measure the tracking and disturbance rejection responses of the closed-loop control system considering the error as $e = y_{sp} - y$ of a generic controlled variable y

$$IAE = \sum_{k=1}^{N} |e(k)|. \tag{14}$$

The safety performance index is the number of full defocus events N_{fs} that occur according to the conditions of Equation (5). The operation time t_{op} is defined to evaluate the start-up effect on plant production. It is the time of the chiller operation during the simulation. Note that the lower the start-up time, the greater the chiller operation time considering the same sundown time.

The production performance indexes are the total energy production E and total exergy production X. The energy production is given by Equation (15)

$$E = t_s \sum_{k=1}^{N} q_{10}(h_{10}(k) - h_9(k)), \tag{15}$$

where t_s is the sampling time, $h = cT[J/kg]$ is the specific enthalpy, which is the product of the specific heat capacity $c[J/(kg^{\circ}C)]$ and the stream temperature $T[^{\circ}C]$.

Exergy is the measure of the departure of the state of the system from that of environment, therefore, it is attributed to both, the system and the environment [24]. Exergy is a concept that indicates the energy quality considering its transformations and different natures. Despite exergy having more than one hundred years of existence just in the later years it has been applied to heat and cooling policies with focus in increasing efficiency [25,26]. The total exergy production is given by Equation (16) [24].

$$X = t_s \sum_{k=1}^{N} q_{10}(x_{10}(k) - x_9(k)), \tag{16}$$

where $x = c(T - T_0 - T_0 \ln(T/T_0))$ is the specific exergy, and $T_0[^{\circ}C]$ is the ambient temperature.

5.3. Results - clear sky scenario

Fig. 7 depicts Scenario S6 results considering the proposed controllers. It is evident that the proposed solution leads to an expressive plant stability enhancement if compared to the inherited controls shown in Figs. 2 and 3. In addition, both C1 and C2 track T_{sp2} and T_{sp8}, C1 does not have any total safety defocus event, and C2 would not burn gas. Fig. 7.c shows that the Fresnel controller imposes a low flow and high focus from 9:00 to 13:00, resulting in a fast start-up of the plant presented in Fig. 7.a. At 13:00, the Fresnel inlet temperature T_1 has a fall disturbance rejected by the flow, according to Fig. 7.c (black line). Fig. 7.d shows that the chiller valve opening at almost 13:00, together with the T_8 and T_3 difference, propagates in the pipes and causes T_1 disturbances. It is worth noting in Fig. 7.b that the valve opens because of $T_3 \geq T_{sp3}$. The PI law implemented on C2 has a critical impact on smoothing v, T_8, and T_1, resulting in a whole plant stable operation. The split-range law implemented on C1 has pivotal importance on controlling T_2 and avoiding overheating the solar collector. It is worth noting in Fig. 7.a that $T_1 > T_{sp2}$ just before 14:00. The inlet temperature above the outlet set-point temperature means that the flow loses its controllability, since increasing the flow will not decrease the outlet temperature. Regardless of the flow limitation, Fig. 7.c shows that the split-range controller switches from the saturated flow to the focus as manipulated variable, rejecting irradiance disturbances at 14:00, and decreasing T_2 to the set-point.

Table 4 resumes the performance of scenarios S1 to S6 regarding a clear sky irradiation case. Simulation S1 to S3 uses the original on-off control on C2. Note that Fig. 2, and Fig. 3 show S1 and S2 performances. Table S1, columns N_{fs} and BT, show that the split-range implementation on C1 (S3) does not trigger the boiler as S1 while reducing the defocus events compared to S2. However, scenario S3 shows that C1's split-range control in combination with the on-off control on C2 is insufficient to operate the plant without safety defocus events. In this sense, S1 to S3 controls are unsuitable because neither fulfill the premise of not burning gas and operating without triggering the safety defocus.

Note in Table 4 that scenarios S4 to S6 have $BT = 0$. Thus, implementing the PI on C2 avoids triggering the boiler in all scenarios. Although, Scenario S5 presents safety defocus events indicating that modifying exclusively the PI on C2 is also not sufficient to operate the plant without full defocus events. Furthermore, S5 has the most intensive $NCAE$ and the worst performance of IAE, E_{evap} and X_{evap}. This performance occurs because manipulating only the flow is insufficient to decrease Fresnel's outlet temperature. Therefore, T_2 reaches the high safety threshold, triggering safety total defocus, generating oscillations, and poor plant performance.

The two scenarios that do not trigger the boiler and do not have safety defocus events in Table 4 are S4 and S6. A further comparison between S6 and S4 shows that S6 has a IAE_T of 9.54×10^4 while S4 of 1.08×10^5, thus S6 has a total IAE_T reduction of 11%. Where IAE_T is the sum of IAE, $IAE_T = IAE_{C1} + IAE_{C2}$. Scenario S6 presents a total $NCAE_T$ of 10.11 while Scenario S4 of 17.48, a reduction of 42%. Where $NCAE_T$ is the sum of $NCAE$, $NCAE_T = NCAE_q + NCAE_f + NCAE_v$. Furthermore, Scenario S6 presents an energy and exergy production increase of 9% compared to S4. Such enhancements are due to the split-range controller used on the Fresnel, since S4 and S6 use the same PI controller in the chiller. The split-range controller impose a low flow in the Fresnel at the dawn and sundown, resulting in faster start-up and a delayed shut-down, increasing chiller time of operation t_{op}, see Fig. 7.c. The factory pre-set controller, in its turn, is not capable of proportionally manipulating the flow. Therefore it takes more time to reach T_{sp2}, having a lower t_{op}. Thus this work finds a trade-off between preheating time and initial accumulated energy in the hydraulic loop with energy production and plant stability. The more preheating phase accumulates, the more stable the start-up and the following operation of the absorption machine will be. The problem is that prolonged thermal accumulation in the hydraulic loop leads to a delayed chiller start-up, shortening its operation time and reducing production.

Comparing the proposed control evaluated on scenario S6 with the factory pre-set control simulated on scenario S1 indicates that the proposed controller has 43% IAE_T reduction, 94% $NCAE_T$ reduction, and 66% and 63% of energy and exergy production increase. Therefore, the Fresnel collector split-range control with the HTG PI control does not burn gas or has safety defocus, resulting in the best overall control performance of Table 4.

5.4. Results - cloudy sky scenarios

Fig. 8 depicts scenario S12 which describes the proposed controller results. Note that the proposed controllers can reject disturbances and track set-points of the plant in the case of a cloudy sky irradiance. The proposed controllers have the same overall performance as presented in Fig. 7. The difference is that Fig. 8.c highlights the split-range controller disturbance rejection capabilities. Note that C1 manipulates the flow (black line) to reject the strong irradiance disturbances (yellow line) from 11:00 to 14:00, while the focus (blue line) is at maximum. Then, from 14:00 to

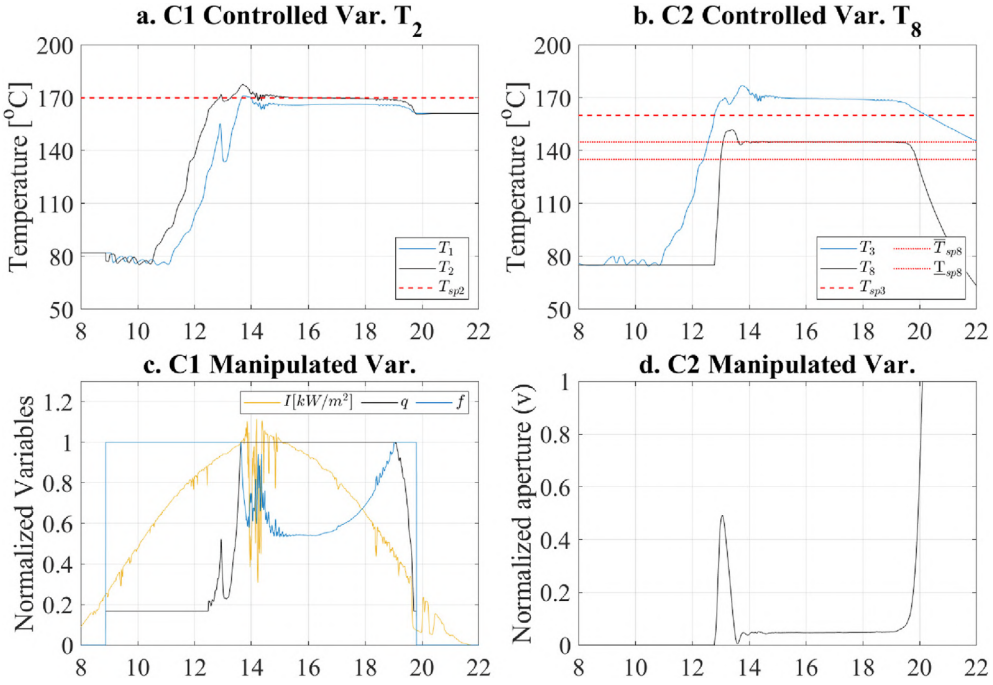

Fig. 7. Proposed Controller performance on Scenario 6 (S6).

Table 4
Scenarios performance indexes in a clear sky day.

Scenario	IAE_{C1} [°Ch]	$NCAE_f$	$NCAE_q$	N_{fs}	BT	IAE_{C2} [°Ch]	$NCAE_v$	t_{op} [h]	E_{evap} [MJ]	X_{evap} [MJ]
S1	1.47×10^5	130.09	2.40	0	1	2.53×10^4	24.00	6.58	−495.07	25.97
S2	1.51×10^5	0.00	107.34	45	0	4.43×10^2	58.00	6.41	−653.46	33.06
S3	1.16×10^5	165.86	105.41	3	0	4.32×10^2	72.00	6.86	−771.07	38.85
S4	1.08×10^5	13.55	2.40	0	0	1.12×10^3	1.53	6.58	−752.02	38.82
S5	1.38×10^5	0.00	103.22	41	0	8.45×10^3	7.82	6.41	−707.53	36.64
S6	9.54×10^4	4.82	3.25	0	0	2.20×10^3	2.04	6.86	−822.33	42.33

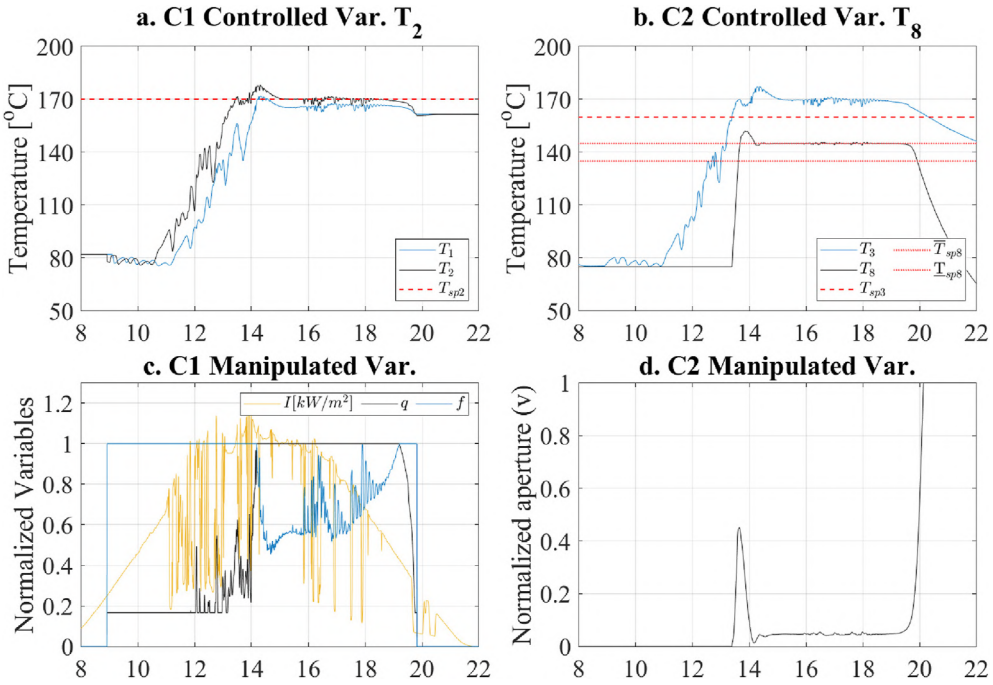

Fig. 8. Proposed Control performance on Scenario 12 (S12).

Table 5
Scenarios performance indexes in a cloudy sky day.

Scenario	IAE_{C1} [°Ch]	$NCAE_f$	$NCAE_q$	N_{fs}	BT	IAE_{C2} [°Ch]	$NCAE_v$	t_{op} [h]	E_{evap} [MJ]	X_{evap} [MJ]
S7	1.51×10^5	132.16	2.40	0	1	1.16×10^4	24.00	4.36	−315.89	16.79
S8	1.49×10^5	0.00	120.78	40	0	1.46×10^3	58.00	5.73	−605.86	30.93
S9	1.24×10^5	134.80	101.36	3	0	3.09×10^2	62.00	5.94	−564.86	28.79
S10	1.21×10^5	35.17	2.40	0	0	1.30×10^3	1.63	5.68	−523.01	27.44
S11	1.42×10^5	0.00	107.17	39	0	1.38×10^4	9.54	6.13	−663.25	34.58
S12	1.07×10^5	11.84	10.13	0	0	2.09×10^3	2.06	6.05	−608.53	31.69

19:00, the flow saturates at maximum, and C1 manipulates the focus, reducing it to reject the irradiance disturbances. Note in Fig. 8.a that the T_2 steadily follows the set-point despite the strong irradiance disturbances of irradiance (yellow lin) in Fig. 8.c.

Table 5 depicts scenarios S7 to S12 regarding cloudy sky irradiation cases. In this case, columns N_{fs} and BT of Table 5 show that no controller evaluated in scenarios S7, S8, and S9 is suitable to operate the absorption plant without burning gas and avoiding safety complete defocus events. All simulations from S10 to S12 do not start the gas boiler, although Scenario S11 presents safety full defocus events. The defocus action shows that the PI law in C2 alone cannot avoid overheating for a cloudy sky scenario. Interestingly, the revamp controller simulated on scenario S11 presents the best energy and exergy production of Table 5. This production occurs because the plant operates at a higher temperature for an extended period. Since Equation (15) and Equation (16) describe the energy and exergy production, the higher temperature, the higher the production. This operation is undesirable once the energy production enhancement results from an abnormal dangerous overheating condition that degrades the equipment.

Again the controllers of scenarios S10 and S12 are the only ones capable of operating the plant without triggering the gas burner and avoiding safety full defocus events. Compare the S10 and S12 performance indexes compiled in Table 5. The controller performance on simulation S10 leads to $-523.01[MJ]$ and $27.44[MJ]$ of energy and exergy production, while the proposed controllers on simulation S12 produce $-608.53[MJ]$ and $31.69[MJ]$ of cooling energy and exergy, respectively. Therefore, the proposed controllers increase 16% of cooling energy production and 15% of exergy production compared to S10. The production increase follows an IAE_T reduction of 12% and an $NCAE_T$ reduction of 39%.

6. Conclusion

The proposed Fresnel split-range and HTG PI controllers enable operating the EITS solar absorption plant avoiding gas burning, and safety defocus events. While the absorption chiller PI controller drastically reduces plant oscillations and actuators' effort, the split-range controller accelerates plant start-up with overheat prevention, enhanced stability, and increased production. The split-range control sums the advantages of manipulating the flow and focus in a simple, well-known, yet powerful control technique. As far as the authors know, this is the first application of a split-range advanced control technique in a line focus solar collector. For future works, it would be interesting to apply this control in the actual plant to evaluate its performance, and to develop a systematic split-range controller design approach to generalize its use in concentrating solar collectors.

CRediT authorship contribution statement

Diogo Ortiz Machado: Conceptualization, Investigation, Writing – original draft. **Adolfo J. Sánchez:** Conceptualization, Investigation, Writing – original draft. **Antonio J. Gallego:** Conceptualization, Software, Resources. **Gustavo A. de Andrade:** Software, Writing – review & editing, Supervision, Writing – review & editing. **Julio E. Normey-Rico:** Project administration, Resources, Supervision, Writing – review & editing. **Carlos Bordons:** Project administration, Resources, Supervision, Writing – review & editing. **Eduardo F. Camacho:** Writing – review & editing.

Declaration of competing interest

The authors declare that they have no known competing financial interests or personal relationships that could have appeared to influence the work reported in this paper.

Acknowledgement

The authors would like to acknowledge the Coordenação de Aperfeiçoamento de Pessoal de Nível Superior (CAPES), Finance Code 001, the Conselho Nacional de Desenvolvimento Científico e Tecnológico (CNPq), under grant 304032/2019–0, the Agencia Estatal de Investigación (AEI) of the Spanish Ministry of Science and Innovation, under grant PID2019-104149RB-I00/10.13039/501100011033 (project SAFEMPC), and the European Research Council under Advanced Research Grant OCONTSOLAR (789051), for funding this work. Diogo O. Machado thanks to IFRS- campus Rio Grande for capacity support, *Fundación Carolina*, SEGIB and PrInt-UFSC programms for mobility scholarships.

References

[1] C. Heeckt, S. Kolaric, Urban Sustainability in Europe: what Is Driving Cities' Environmental Changes?, Tech. rep., European Environment Agency. URL https://www.eea.europa.eu/publications/urban-sustainability-in-europe-what.
[2] M.J. Blanco, L.R. Santigosa, Advances in Concentrating Solar Thermal Research and Technology, first ed., Woodhead Publishing, 2017.
[3] European Commission, Communication of the commission to the european parliament and the council concerning the paris protocol- a blueprint for tackling global climate change beyond 2020, URL, https://ec.europa.eu/info/publications/paris-protocol-blueprint-tackling-global-climate-change-beyond-2020, 2015.
[4] E. Commission, Climate action. paris agreement, URL, https://ec.europa.eu/clima/eu-action/international-action-climate-change/climate-negotiations/paris-agreement_en, 2015.
[5] N. Engineering, National academy of engineering. grand challenges for engineering, URL, www.engineeringchallenges.org, 2008.
[6] A.J. Gallego, A.J. Sánchez, M. Berenguel, E.F. Camacho, Adaptive ukf-based model predictive control of a fresnel collector field, J. Process Control 85 (2020) 76–90.
[7] R. Meligy, M. Rady, A.E. Samahy, W. Mohamed, Proportional–integral-like fuzzy controller of a small-scale linear fresnel reflector solar plant, IET Renew. Power Gener. 14 (8) (2020) 2620–2628.
[8] E. F. Camacho, A. J. Gallego, J. M. Escaño, A. J. Sánchez, Hybrid nonlinear MPC of a solar cooling plant, Energies 12 (14). doi:10.3390/en12142723.
[9] C. Marugán-Cruz, D. Serrano, J. Gómez-Hernández, S. Sánchez-Delgado, Solar multiple optimization of a dsg linear fresnel power plant, Energy Convers. Manag. 184 (2019) 571–580.
[10] M.J. Montes, A. Abánades, J.M. Martínez-Val, M. Valdés, Solar multiple optimization for a solar-only thermal power plant, using oil as heat transfer fluid in the parabolic trough collectors, Sol. Energy 83 (12) (2009) 2165–2176, https://doi.org/10.1016/j.solener.2009.08.010.
[11] D. Machado, J.E. Normey-Rico, G.A. de Andrade, A 2dof thermosolar concentrator proposal: solar tracking and disturbance rejection using proportional

defocus, in: ISES Solar World Congress SWC 2019, International Solar Energy Society, 2019, pp. 34–41, https://doi.org/10.18086/swc.2019.01.05. URL.
[12] P. Bermejo, F.J. Pino, F. Rosa, Solar absorption cooling plant in Seville, Sol. Energy 84 (8) (2010) 1503–1512, https://doi.org/10.1016/j.solener.2010.05.012.
[13] Mercado Iberico Del Gas, Natural gas prices, URL, https://www.mibgas.es/en, 2021.
[14] Red Electrica España, Electric energy cost, URL, https://www.ree.es/es/accionistas-e-inversores/la-accion/red-electrica-en-bolsa, 2021.
[15] J. Morud, S. Skogestad, Effects of recycle on dynamics and control of chemical processing plants, Comput. Chem. Eng. 18 (1994) S529–S534, https://doi.org/10.1016/0098-1354(94)80086-3. URL.
[16] W.L. Luyben, Dynamics and control of recycle systems. 1. Simple open-loop and closed-loop systems, Ind. Eng. Chem. Res. 32 (3) (1993) 466–475, https://doi.org/10.1021/ie00015a010.
[17] W.L. Luyben, Dynamics and control of recycle systems. 3. Alternative process designs in a ternary system, Ind. Eng. Chem. Res. 32 (6) (1993) 1142–1153, https://doi.org/10.1021/ie00018a020.
[18] J.E. Normey-Rico, E.F. Camacho, Control of Dead-Time Processes, Springer, 2007.
[19] E. Camacho, M. Berenguel, F.R. Rubio, D. Martínez, Control of Solar Energy Systems, Springer London, Dordrecht Heidelberg New York, 2006, https://doi.org/10.1007/978-0-85729-916-1.
[20] A.J. Gallego, G.M. Merello, M. Berenguel, E.F. Camacho, Gain-scheduling model predictive control of a Fresnel collector field, Control Eng. Pract. 82 (2019) 1–13, https://doi.org/10.1016/j.conengprac.2018.09.022. URL.
[21] M.V. Robledo, Description and Commissioning of a Solar Absorption Refrigeration Plant. Modeling and Control of the Fresnel Solar Collector (in spanish), Ph.D. thesis, Universidad de Sevilla, 2012. URL, http://bibing.us.es/proyectos/abreproy/12074.
[22] A. Reyes-Lúa, C. Zotică, K. Forsman, S. Skogestad, Systematic design of split range controllers, IFAC-PapersOnLine 52 (1) (2019) 898–903, https://doi.org/10.1016/J.IFACOL.2019.06.176.
[23] M. Bartyś, B. Hryniewicki, The trade-off between the controller effort and control quality on example of an electro-pneumatic final control element, 2019, Actuators 8 (1) (2019) 23, https://doi.org/10.3390/ACT8010023. URL, https://www.mdpi.com/2076-0825/8/1/23/htmhttps://www.mdpi.com/2076-0825/8/1/23.
[24] M.J. Moran, H.N. Shapiro, Fundamentals of Engineering Thermodynamics, fifth ed., John Wiley & Sons, 2006 https://doi.org/10.1038/1811028b0. http://www.nature.com/doifinder/10.1038/1811028b0.
[25] IEA ECBCS, "Annex 49: low exergy system for high-performance building and communities" Stuttgart, Germany, Fraunhofer Verlag, 2011. Available online: www.annex49.com. (Accessed 22 March 2020).
[26] M. Virtanen, J. Palmer, Heating and Cooling with a Focus on Increased Energy Efficiency and Improved Comfort ECBCS Annex 37 Project Summary Report, AECOM Ltd on behalf of the International Energy Agency, 2010. URL, www.ecbcs.org.

8 OPTIMAL OPERATION OF CONCENTRATING SOLAR COLLECTOR FIELDS USING EXERGY-BASED HIERARCHICAL CONTROL

Energy 239 (2022) 122462

Contents lists available at ScienceDirect

Energy

journal homepage: www.elsevier.com/locate/energy

Optimal operation of Concentrating Solar Collector fields using exergy-based hierarchical control

Diogo Ortiz Machado [a, b, c, *], Gustavo Artur Andrade [b], Julio Elias Normey-Rico [b], Carlos Bordons [c]

[a] Instituto Federal de Educação do Rio Grande do Sul - IFRS, Rio Grande, RS, 96201-460, Brazil
[b] Departamento de Automação e Sistemas, Universidade Federal de Santa Catarina - UFSC, Florianópolis, SC, 88040-900, Brazil
[c] Systems Engineering and Automatic Control Department and ENGREEN, Laboratory of Engineeringfor Energy and Environmental Sustainability, Universidad de Sevilla, 41092, Seville, Spain

ARTICLE INFO

Article history:
Received 16 April 2021
Received in revised form
27 September 2021
Accepted 26 October 2021
Available online 28 October 2021

Keywords:
Hierarchical control
Exergy
Model predictive control
Concentrating solar collector

ABSTRACT

This work develops an exergy-based hierarchical control for the ACUREX solar collector field. The objective is to simulate and to determine the optimal control operation based on exergy. The control structure uses a nonlinear exergy optimization layer that sends the steady-state optimal temperature set-point to a nonlinear Model Predictive Control layer. The simulations show that the control can track references, reject disturbances, and optimize the production considering process intermittency (start-up, operation, shut-down), operational constraints, and pump power. The study compares the proposed control to common literature approaches such as energy-based and maximum outlet temperature reference generation. The main findings are: (i) the proposed exergy-based controller design gives an enhanced second law of thermodynamics performance independently of solar collector process parameters; (ii) despite modest energy production and efficiency advantages (1%) on ACUREX solar field, the real application of the control law does not imply any new investments or hardware changes; (iii) seeking the maximum temperature is a simple, quasi-optimal strategy for the ACUREX solar field; and (iv) energy-based optimization is not a suitable strategy for ACUREX solar field from the second law of thermodynamics (exergy) perspective.

1. Introduction

A Concentrating Solar Collector (CSC) is a heat exchanger that uses mirrors to concentrate and transform the renewable and clean sun irradiation to internal energy of a Heat Thermal Fluid (HTF). The thermal energy can be used for a wide range of applications, from district heating and cooling [1] to process heat [2] and power generation (solar power, cogeneration, hybrid) [3].

As the CSC uses the intermittent solar resource, its control system must consider, every day, a start-up and a shut down procedures, and weather dynamics, once clouds and weather conditions fastly impact the operation. A concentrating solar field can be composed by connecting collectors in series and parallel, reaching several meters in length. It uses pumps to maintain a desired outlet HTF temperature despite disturbances in inlet temperature, ambient temperature, and solar irradiance. Also, these systems usually have defocus devices to avoid overheating.

The operation of a solar field (SF) needs control techniques. And its control is a challenge because the solar input is broad, intermittent, and weather dependent; the process has temperature, pressure, power, and other operational constraints; lastly, a solar field has long pipes. Thus, the pump energy consumption, head loss in tubes, and flow delays are quantities that impact production.

SF control objectives are [4] (i) secure outlet temperature operation using the flow, (ii) track outlet temperature set-point and reject disturbances from irradiance, ambient temperature, and inlet temperature; lastly, (iii) maximize production. The SF operates safely maintaining the flow and temperature inside a secure range. A well-chosen and tuned controller normally attains objectives (i-ii). Since the controller can deliver previous objectives, optimal

* Corresponding author. Instituto Federal de Educação do Rio Grande do Sul - IFRS, Rio Grande, RS, 96201-460, Brazil.
E-mail addresses: diogo.machado@riogrande.ifrs.edu.br (D.O. Machado), gustavo.artur@ufsc.br (G.A. Andrade), julio.normey@ufsc.br (J.E. Normey-Rico), bordons@us.es (C. Bordons).

https://doi.org/10.1016/j.energy.2021.122462
0360-5442/

Nomenclature

Abbreviations

CSC	Concentrating solar colector
HTF	Heat thermal fluid
IAE	Integral of absolute error
MPC	Model predictive control
PNMPC	Practical non-linear MPC
SF	Solar field

Subindices

amb	Ambient
C	Collector
E	Energy
f	Flow
in	Inlet
k	Kinectic
out	Outlet
P	Pump
PD	Pressure drop
ref	Reference, set-point
X	Exergy

Variables

α	Collector efficiency [*adim.*]
$\dot{E}$	Net energy rate [W]
$\dot{Q}$	Heat transfer rate [W]
$\dot{S}$	Entropy rate [$W/^\circ C$]
$\dot{V}$	Volumetric flow [m^3/s]
$\dot{W}$	Power/Work rate [W]
$\dot{X}$	Net exergy rate [W]
ε	Roughness [m]
η	Efficiency [*adim.*]
γ	Error weigth [*adim.*]
λ	Control weigth [*adim.*]
μ	Dynamic viscosity [$Pa\ s$]
ρ	Specific mass [kg/m^3]
σ	Auxiliary variable [*adim.*]
A	Cross-sec. absorber area [m^2]
c	Specific heat [$J/(kg^\circ C)$]
D	Internal diameter [m]
f	Friction factor [*adim.*]
G	Collector aperture [m]
g	Acceleration of gravity [m/s^2]
I	Irradiance [W/m^2]
L	Loop length [m]
l	Specific energy flow loss [W]
L_t	Total length [m]
n_{loop}	Number of active loops
P	Pressure [Pa]
Re	Reynold's number [*adim.*]
T	Temperature [$^\circ C$]
t	Time [s]
t_d	Time delay [s]
t_s	Sampling time [s]
v	Velocity [m/s]

energy production is economically advantageous. Scientific contributions have been published to tackle these complex problems. It was found that the works on SF control and thermodynamic optimization areas are complementary.

On the one hand, control-oriented publications solve the dynamic constrained temperature set-point tracking and disturbance rejection issues seeking practical application. The reviewed works in this area consider hierarchical controls with fuzzy and empiric economic optimizations plus feedforward and I + PD controllers showing experimental results [5,6], outlet temperature maximization with model predictive controllers [7], maximizing outlet temperature and optimizing Rankine cycle power using an adaptative PI controller [8]. Other works develop a high order linear time-invariant model estimation to map nominal operation points, and a gain scheduling MPC to track maximum achievable temperature [9]. Lastly, contributions develop a unique MPC layer to regulate and optimize three objective functions: thermal power, minimizing and maximizing outlet temperature [10]. Therefore, the literature mainly considers maximizing the outlet temperature or optimizing energy production for reference generation.

On the other hand, thermodynamic-oriented publications define physical limits and prove that considering the second law of thermodynamics, entropy and exergy concepts, lead to better objective functions for optimization from a theoretical perspective. The reviewed works in this area consider variational calculus to analytically optimize the exergy of solar collector and deliver the maximum useful energy, which is not coincident with maximum temperature. Another result is that outlet temperature must follow the irradiance profile throughout the day [11,12]. There are contributions to exergy and control simulations on solar collectors. However, the techniques count with a priori knowledge of future values of irradiances [13,14] or just steady-state cases [15,16]. These works conclude that energy-based techniques could be misleading and that an exergy-based controller is highly desirable, showing maximum exergy production advantages. A practical implementation of exergy optimization techniques on solar collectors is found in Ref. [17]. Therefore, these studies are mainly theoretical, lack dynamics and constraints considerations, or count on future variable knowledge in their formulations.

These scientific papers evidence complementary characteristics of control and thermodynamic optimization. Control has powerful dynamic techniques for set-point tracking, disturbance rejection, and constraints consideration. However, it uses or energy or empiric temperature maximization solutions to define the reference values, which the second law of thermodynamics concepts can enhance. Thermodynamic optimization, in its turn, uses systematic physics theoretical foundations to unambiguously model, analyze and define steady-state optimal exergy operating points. However, the works lack dynamic attention and control techniques to deal with essential SF transient behaviors (disturbances) and operational limits.

Exergy is stated as “the maximum theoretical useful work obtained if a system is brought to thermodynamic equilibrium with the environment through processes in which the system interacts only with the environment”. Exergy and energy sources comparison leads to the same kinetic, potential gravitational, mechanical, and electrical values since these sources are entirely available and can, ideally, be changed from one kind to another. Although the

exergy is a fraction of the energy content of chemical, heat, and irradiance sources, indicating that it is physically impossible to transform these resources completely.

In fact, from 1950 to 1970, authors showed that any process in which energy is converted from one form into another cannot be adequately measured by the first law of thermodynamics and therefore is better expressed in exergy terms [18]. Energy balance is the industry approach and has been driving technology development. In this context, the exergy concepts are complementary and not opposite. An energy balance analysis is essential for all energy systems evaluation, but it can be enhanced by exergy analysis, whose advantages grow as complexity and efficiency standards grow.

In this sense exergy approach has been benefiting theoretical areas such as efficient resource use, energy conservation, efficiency improvement, with engineering applications on power cycles, components, and heat exchangers. The last contributions can be found in process conversion efficiency, process structure optimization, and exergy life-cycle assessment [18].

Exergy combined with control is relatively new in the literature and under-populated with articles. For example, only two review papers and one thesis that compiles contributions integrating exergy and control areas were found. The second law and exergy concepts have been used on steady-state energy systems analysis and optimization, although very few are dynamic and control-oriented.

James et al. compiles exergy-based control and optimization works [19]. Among 35 papers selected, ten use MPC techniques, and from these, only one is related to concentrating solar energy systems. The unique work obtains 23% of energy savings on a micro-scale concentrated solar power (MicroCSP) with a building Heat, Ventilation, and Air Conditioning (HVAC) integrated system [20]. The other review paper [21] and the thesis [22] do not present any exergy-based MPC application on SF systems with the majority of contributions on low exergy systems such as HVAC and district heating.

This work seeks to combine the exergy thermodynamic concept with practical and operational control capabilities in one structure. Hierarchy Control [23] approach is used since it is a suitable way to decompose solar collector optimization and control complex problems, and solve them separately in a functional structure [24]. To assess whether this proposal is advantageous for SF operation, we implemented it and compared it to the performance of common literature control approaches considering process intermittency, constraints, and pump power.

This paper uses an exergy non-linear optimization layer to maximize steady-state exergy production and a MPC layer capable of constrained operation, temperature set-point tracking, and disturbance rejection [4] along a whole day. The following questions are investigated: is the exergy-based hierarchical control capable of controlling the SF process? Why entropy and exergy-based reference generation were not used in any SF real control application until today? How much the pump power impacts SF optimization? and how is the performance of practical approaches compared to the exergy optimization considering the same operational constraints? And how is the performance of approaches compared to the exergy optimization considering the same operational constraints?

Thus, this paper develops an exergy-based hierarchical control on the SF process and clarifies the differences between this proposal and the literature control approaches. It is worth noting that no previous cited paper simultaneously considered the SF intermittency, operational constraints, pump power with control reference tracking, disturbance rejection, and production optimization. Moreover, as far as the authors know, the obtained results are the first exergy hierarchical control simulation to consider a whole day simulation on a solar collector field. Thus, these aspects are evaluated together and the main contributions are:

1. Developing an integrated exergy-based hierarchical control for SF;
2. Pointing the advantages and disadvantages between the exergy and practical literature approaches;
3. Evidencing the pump power effect on the optimization results;
4. Calculating the exergy constrained optimal performance;

The text organization is the following. Section 2 exposes the basic concepts of solar collectors operation, modeling, and presents the Practical Nonlinear Model Predictive Control (PNMPC). Section 3 defines the Hierarchical Control methodology and simulation scenarios which are discussed in Section 4, Results. The latter comprises three parts, one considering only the optimization layer analysis, another with the whole hierarchical control solution applied in two days, one clear and another cloudy, and the third analyzes start-up and shut down phases. Lastly, the conclusions in Section 5 sum up the contributions of this work.

2. Preliminaries

The Concentrating Solar Collector's hierarchical control structure has two layers: Exergy Optimization and Temperature Control. This section contextualizes the exergy-based control, presents the Practical Nonlinear Model Predictive Control technique (PNMPC), and describes solar collectors' operation, defining its model. This work considers that the controller and optimizer models match the process model, which is the nominal case; this implies that do not exist error between the model and the process.

2.1. Process Definition

This study is limited on the ACUREX solar field system. The study also does not consider a priori knowledge of thermal energy use. Despite the many uses of thermal energy, this work's scope is to investigate an exergy approach to SF control, focusing on exergy optimization and control of the SF. Thereby, it is assumed that the process is as a heater that offers thermal energy in a network. The process model reference is the ACUREX SF because it is a benchmark for control techniques evaluations [25]. Fig. 1 depicts the process.

The solar collector heats Therminol oil [26] as Heat Transfer Fluid (HTF) using mirrors to direct and concentrate solar beams in a receiver tube. The HTF is pumped at low temperatures in the inlet, heating along the receiver tube and exiting the process at a higher temperature. Note that on Fig. 1 several CSC loops compose the solar field. The control problem is to maintain a desired outlet temperature (T_{out}) manipulating the flow ($\dot{V}$), considering disturbances on solar irradiance (I), inlet temperature (T_{in}), ambient temperature (T_{amb}) and operational constraints. The optimization problem is to define the best operation point (T_{out}) accordingly to an objective function subject to variables and operational constraints.

2.2. Modeling

This work is based on phenomenological modeling of ACUREX SF based on an energy balance given by

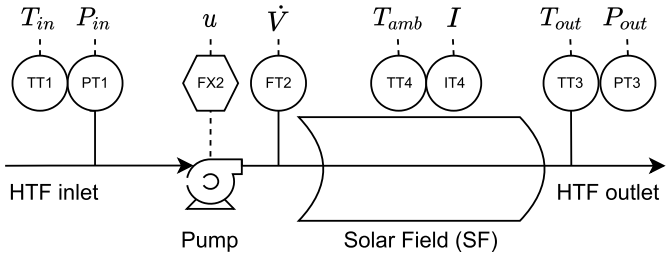

Fig. 1. Process (based on ACUREX SF). Several loops compose the solar field, which is lumped here in one unique solar field representation.

$$\overbrace{\frac{dE_{total}}{dt}}^{\text{accumulation}} = \underbrace{\overbrace{\dot{Q}_{sun}}^{\text{sunheat}} - \overbrace{\dot{E}_C}^{\text{internal-collectorenergy}} - \overbrace{\dot{Q}_{amb}}^{\text{ambientheatloss}}}_{\text{thermalenergy}} + \underbrace{\overbrace{\dot{E}_f}^{\text{flowenergy}} + \overbrace{\dot{E}_k}^{\text{kinecticenergy}} + \overbrace{\dot{W}_{PD}}^{\text{pressuredrop}} - \overbrace{\dot{W}_P}^{\text{pumppower}}}_{\text{mechanicalenergy}}, \tag{1}$$

where the derivative notation is $\dot{y} = dy/dt$ and control volume balance is $Y = Y_{out} - Y_{in}$ of a hypothetical variable Y, all subindices and variables are defined in the Nomenclature. The balance sign convention considers that thermal energy that enters the system is positive and the one that exits the system is negative. Also, considers that mechanical power done to the system is negative and by the system is positive. The left-hand side accumulation term of Equation (1) contains both thermal and mechanical contributions of energy. Next, right-hand side terms of Equation (1) are explained.

Thermal energy is composed of three terms. Sun heat ($\dot{Q}_{sun}$) is related to incident solar irradiance that is concentrated in absorber tubes by mirrors. Internal energy balance, forward called collector energy ($\dot{E}_C$), is associated with the incident solar irradiance that is transferred to the HTF flow and leads to temperature gain between inlet and outlet streams of the solar field. Lastly, ambient heat loss ($\dot{Q}_{amb}$) is referred to as the energy leak to the ambient in which is a function of tubes thermal insulation [27].

Mechanical energy is composed of four terms. Flow energy balance ($\dot{E}_f$) is associated with work done by pressure forces moving fluid through the SF boundary; kinetic energy balance ($\dot{E}_k$) is associated with the flow velocity; pressure drop power ($\dot{W}_{PD}$) is referred to fluid friction losses on the tube walls. The gravitational energy was not considered in this balance [27].

Considering SF objectives of energy optimization, safety, outlet temperature tracking, and disturbance rejection, the internal energy balance ($\dot{E}_i$) and the pump power ($\dot{W}_P$) are the terms of interest on Equation (1). Thus, the energy balance Equation (1) is divided in two to calculate both variables, one based on thermal and another on mechanical energy balances.

2.2.1. Thermal energy balance

Thermal energy balance is given by set of Equation (2),

$$\overbrace{\frac{dE_{thermal}}{dt}}^{\text{thermal accumulation}} = \frac{d(\rho c A L T_{out})}{dt} = \underbrace{\overbrace{\dot{Q}_{sun}}^{\text{sun heat}} - \overbrace{\dot{E}_C}^{\text{collector energy}} - \overbrace{\dot{Q}_{amb}}^{\text{ambientheat loss}}}_{\text{thermal energy}}, \tag{2a}$$

$$\dot{Q}_{sun} = \alpha G L I(t), \tag{2b}$$

$$\dot{E}_C = \dot{V}(t)\rho c(T_{out}(t) - T_{in}(t)), \tag{2c}$$

$$\dot{Q}_{amb} = 1980(\overline{T}(t) - T_{amb}(t)) - 34.651. \tag{2d}$$

The left hand side of equation depicts only the thermal part of accumulated energy, $\overline{T} = (T_{out} + T_{in})/2$ is the mean collector temperature, $\rho = 903 - 0.672\overline{T}(t)$ is the specific mass, $c = 1820 + 3.478\overline{T}(t)$ is the sensible heat, and $\dot{V} = \dot{m}/\rho$ is the volumetric flow. It is important to highlight that the HTF is an incompressible liquid therefore the specific heat(c) is a function only of temperature.

The oulet temperature (T_{out}) is the variable of interest. Thus, the final thermal model is obtained substituting the right hand side terms Equations (2c), (2b) and (2d) on Equation (2a) considering each SF active loop, and adding the transport delay (t_d) on inlet temperature,

$$\rho c A \frac{dT_{out}}{dt} = \alpha G I(t) + \rho c \frac{\dot{V}(t)}{n_{loop}} \frac{(T_{out}(t) - T_{in}(t - t_d))}{L} - \frac{\dot{Q}_{amb}}{L_t}, \tag{3}$$

note that Equation (3) is the same SF model described in Refs. [25,28], which have further detailed explanation of thermal balance.

Equation (4) [29] describes the fluid transportation time delay (t_d) at variable flow

$$L = \int_0^{t_d} v(t)dt \approx \frac{t_s}{A} \sum_{i=0}^{i=n} \dot{V}(i). \tag{4}$$

The time delay is the time that a flow with a given velocity $v(t)$ takes to travel through absorber length (L). Since only the flow ($\dot{V}$) measurement is available for this process, and automation systems use discrete calculations, the time delay interpretation is approximated by the number of samples n of one hydraulic residence time ($LA/\dot{V}$), which is the number of samples which a given flow $\dot{V}$ takes to replace all internal absorber volume L A. For a constant flow it becomes $n = LA/\dot{V}t_s$, where t_s is the sample time.

2.2.2. Mechanical energy balance

Mechanical energy balance is given by set of Equation (5),

$$\overbrace{\frac{dE_{mechanical}}{dt}}^{\text{mechanical accumulation}} = \underbrace{\overbrace{\dot{E}_f}^{\text{flow energy}} + \overbrace{\dot{E}_k}^{\text{kinectic energy}} + \overbrace{\dot{W}_{PD}}^{\text{pressure drop}} - \overbrace{\dot{W}_P}^{\text{pump power}}}_{\text{mechanical energy}}, \tag{5a}$$

$$\dot{E}_f = \dot{V}(t)(P_{out} - P_{in}), \tag{5b}$$

$$\dot{E}_k = \dot{V}(t)\rho\frac{v_{out}^2(t) - v_{in}^2(t)}{2}, \tag{5c}$$

$$\dot{W}_{PD} = \dot{V}(t)P_{PD}n_{loop}, \tag{5d}$$

$$P_{PD} = f_f\frac{\rho v^2 L}{2D}, \tag{5e}$$

$$\frac{1}{\sqrt{f_f}} = -2\log\left(\frac{\varepsilon}{3.7D} + \frac{2.51}{Re\sqrt{f_f}}\right), \tag{5f}$$

$$\mathrm{Re} = (vD\rho)/\mu. \tag{5g}$$

This balance considers steady-state operation and fully developed turbulent flow. The extra pump power needed to sustain flow because pressure drop loss is described by Equation (5d), which is calculated by Darcy - Weisbach Equation (5e). The latter is an empirical equation that correlates internal flow friction losses to velocity, specific mass, and tube geometry. Dimensionless friction factors describe the friction correlations, here is used the Colebrook-White Equation (5f) because it covers a wide range of conditions, being a function of readily available tube geometry and Reynold's number, equation (5g). For further details of pressure drop calculations refers to Ref. [30][p. 522].

Now, the steady state final mechanical model to calculate pump power is stated on Equation (6) It is obtained evidencing the pump power (W_P), adding to it an electro-mechanical efficiency (η_P) and substituting Equations (5b), (5c) and (5e) on Equation (5a),

$$\eta_P\dot{W}_P = \dot{V}\rho\frac{v_{out}^2}{2} + \dot{V}(P_{out} - P_{in}) + \dot{W}_{PD}. \tag{6}$$

The pump accelerates the fluid from rest to v_{out}, thus, $v_{in} = 0$. Therminol oil is the HTF and its dynamic viscosity is $\mu = 1.41\times 10^{-2} - 1.6\times 10^{-4}\overline{T} - 273 + 6.41\times 10^{-7}\overline{T}^2 - 8.66\times 10^{-10}\overline{T}^3$, lastly, absorber tubes of Schott PTR 70 model parameteres were hypothetically used for pressure drop calculations.

2.3. Nonlinear model predictive control - NMPC

MPC family predicts the process output at a future horizon for $k = N_1$ to N_2 considering a model, calculates a sequence of control actions that minimize a cost function (J) subject to constraints, applies just the first control signal (u) of the sequence and updates the procedure at each sample, resulting in a receding horizon algorithm. Because of the non-linear nature of solar collectors, there are incentives to develop NMPC control strategies [4,25]. compile works and applications of such questions. Several authors propose simplification techniques to avoid the Non-Linear Problem. One way is to use linear approximations of the model in each time step, which is the technique called Practical Non-linear Model Predictive Control (PNMPC) proposed by Ref. [31] and used in this work.

The idea of PNMPC is to approximate the non-linear predictions with a new linearized model at each sampling time to avoid a non-linear relationship between the manipulated and controlled variables. So, PNMPC calculates in each sampling time the free non-linear response of the system and then the jacobian matrix using small steps on incremental control vector along the control horizon. Thus, the free-response, the linearized forced response, and the system's jacobian matrix, are obtained. This work discretizes the continuous models using the Backward Euler method. The result is the following classic MPC optimization problem formulation described by Equation (7).

$$\begin{aligned} \min_{\Delta u} \quad & \textstyle\sum_{j=N_1}^{N_2}\gamma_j(\tilde{y}(k+j|k) - w(k+j|k))^2 + \sum_{i=0}^{N_u-1}\lambda_i\Delta u(k+i)^2 \\ \text{s.t.} \quad & y_{min} \le \tilde{y}(k+j|k) \le y_{max}\; j = N_1,\ldots,N_2, \\ & u_{min} \le u(k+i|k) \le u_{max}\; i = 0,\ldots,N_u-1, \\ & \Delta u_{min} \le \Delta u(k+i) \le \Delta u_{max}\; i = 0,\ldots,N_u-1. \end{aligned} \tag{7}$$

The cost function considers the errors between the predicted model outputs $\tilde{y}(k+j|k)$ and reference trajectory $w(k+j|k)$ and also the future incremental control actions $\Delta u(k+i)$ at a given instant k. The prediction horizon is from N_1 to N_2 and the control horizon is N_u; while γ and λ are respectivelly the error and control movement weighting factors. More details of the PNMPC algorithm can be found in Refs. [31,32].

3. Hierarchical control

This section defines the SF hierarchical control. First, the optimization layer problems are set. Next, the PNMPC control layer is described. Fig. 2 depicts the general hierarchy layout. The optimization layer is responsible for finding the decisions variables to maximize one objective function. The control layer is responsible for tracking a given optimal decision variable and reject disturbances. In this paper, the collector outlet temperature is the interest variable send from the optimization layer to the control layer as T_{ref}.

Two simulation tests are strategically designed to evaluate the optimizations, pump power and constraints effects, firstly, on optimization layer and, later, on whole hierarchical control. Test 1 addresses the combination of different objective functions in steady-state on optimization layer. Then, test 2 considers the dynamic simulation of the whole hierarchical control, thus operating the optimization and control layers simultaneously.

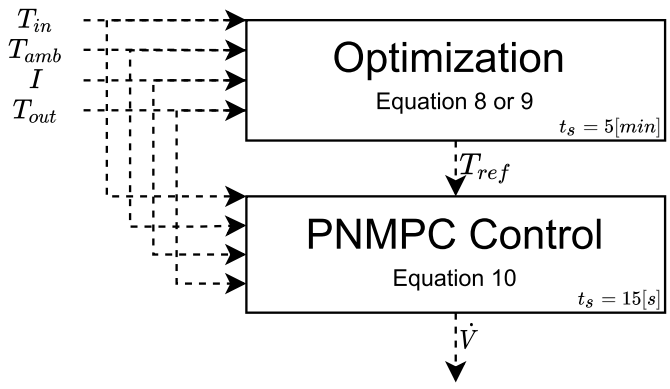

Fig. 2. The hierarchical control layout and sampling times detail. Note that the sampling time of the optimization layer is 5[*min*] and of the control layer is 15[*s*].

3.1. Optimization layer

Five objective functions are defined. Case 1 maximizes collector energy rate ($\dot{E_C} = \rho\dot{V}c(T_{out} - T_{in})$), Case 2 maximizes net energy rate production ($\dot{E} = \dot{E}_C - \dot{W}_P$), and Case 3 maximizes outlet temperature (T_{out}). Cases 1 to 3 are the common literature approaches. Case 4 maximizes collector exergy rate ($\dot{X_C} = \rho\dot{V}c(T_{out} - T_{in} - T_{amb}\ln(T_{out}/T_{in}))$. Note that exergy objective function is the energy term ($\rho\dot{V}c(T_{out} - T_{in})$ less the entropy term given by ($\dot{S_C} = \ln(T_{out}/T_{in})$). This term represent irreversibilities that must occur to transform thermal energy (not fully available) to mechanical energy (fully available) [27]. Therefore, the exergy rate optimization is an energy rate optimization that uses the second law of thermodynamics penalty or weight. Note that this penalty is phenomenological, well-defined, and dimensionally consistent. Lastly, Case 5 maximizes net exergy rate ($\dot{X} = \dot{X}_C - \dot{W}_P$). Cases 4 and 5 are the proposed optimization approaches. The Equation (8) states the above mentioned exergy/energy rate optimization problems with the outlet temperature and the flow as the decision variables

$$\max_{\dot{V},T_{out}} \sigma_1\rho\dot{V}c(T_{out} - T_{in}) - \sigma_2\rho\dot{V}c\left(T_{amb}\ln\frac{T_{out}}{T_{in}}\right) - \sigma_3\dot{W}_P, \tag{8a}$$

$$\text{s.t.} 0 = \alpha GI(t) - \rho c\frac{\dot{V}(t)}{n_{loop}}\frac{(T_{out}(t) - T_{in}(t - t_d))}{L} - \frac{\dot{Q}_{amb}(\overline{T}(t), T_{amb}(t))}{L_t}, \tag{8b}$$

$$2 \times 10^{-3}[m^3/s] \leq \dot{V} \leq 12 \times 10^{-3}[m^3/s], \tag{8c}$$

$$175[^\circ C] \leq T_{out} \leq 290[^\circ C]. \tag{8d}$$

Equation (9) defines the outlet temperature optimization problem, for this case the only decision variable is the volumetric flow.

$$\begin{aligned}&\max_{\dot{V}} T_{out}\\ &\text{s.t. } 0 = \alpha GI(t) - \rho c\frac{\dot{V}(t)}{n_{loop}}\frac{(T_{out}(t) - T_{in}(t - t_d))}{L} - \frac{\dot{Q}_{amb}(\overline{T}(t), T_{amb}(t))}{L_t},\\ &2 \times 10^{-3}[m^3/s] \leq \dot{V} \leq 12 \times 10^{-3}[m^3/s],\\ &175[^\circ C] \leq T_{out} \leq 290[^\circ C].\end{aligned} \tag{9}$$

The solutions are calculated every 5[*min*] by the nonlinear programming *fmincon* using an interior-point algorithm [33,34]. Equation (8b) is a constraint based on the energy conservation law ($0 = \dot{E}_{sun} - \dot{E}_C - \dot{Q}_{amb}$). Equation (8d) and Equation (8c) are operational constraints of ACUREX SF.

Summing up, five hierarchical control cases are set, each one switches between Equation (9), Equation (8) and σ_i. Sigma σ_i represents a boolean integer auxiliary variable used to combine terms of Equation (8a), therefore, vary simulations between cases depicted in Table 1.

The same model is used in the optimizer and PNMPC layers (the optimizer model is the static version of the dynamic model used in the PNPMC), and the static map ($\dot{V}$, T_{out}) is bijective. Thus, the operational points defined by the optimizer are achievable by the PNMPC using only T_{ref} as a target.

Table 1
Hierarchical Control simulation cases considered in the optimization layer.

Case	J	$max(\cdot)$	Eq.	σ_1	σ_2	σ_3
1		$\dot{E}_C$	(8)	1	0	0
2		$\dot{E}$	(8)	1	0	1
3		T_{out}	(9)	–	–	–
4		$\dot{X}_C$	(8)	1	1	0
5		$\dot{X}$	(8)	1	1	1

3.2. PNMPC control layer

As depicted in Fig. 2, the optimization layer sends the T_{ref} to the PNMPC defined by Equation (10)

$$\min_{\Delta\dot{V}} \sum_{j=N_1}^{N_2} \gamma(\tilde{T}_{out}(k+j|k) - T_{ref}(k+j|k))^2 + \sum_{i=0}^{N_u-1} \lambda\Delta\dot{V}(k+i|k)^2 \tag{10a}$$

$$\text{s.t.} 2 \times 10^{-3}[m^3/s] \leq \dot{V} \leq 12 \times 10^{-3}[m^3/s], \tag{10b}$$

$$175[^\circ C] \leq T_{out} \leq 290[^\circ C]. \tag{10c}$$

The decision variable is the flow, and the objective function is composed of two quadratic terms. The first term uses the difference between the predicted outlet temperature and the temperature reference along a simulation horizon from N_1 to N_2. The second term considers the flow variation itself along the control horizon Nu. The outlet temperature and flow constraints stated in Equation (10b) and Equation (10c) are the same used in the optimization layer. The objective function is solved using the quadprog quadratic programming algorithm [35].

The controller uses Equation (3) to compute the outlet temperature predictions $\tilde{T}_{out}$ as described in section 2.3 and has I, T_{in}, T_{amb} as inputs and $\dot{V}$ as output. The prediction and control horizon are set on $N_2 = 15$ and $N_u = 1$ with sampling time of 15[s]. Tuning is set with $\lambda = 1$ and $\gamma = 1$ (the model normalization uses upper operation limits). Note that the static operation point optimization takes place at each 5[*min*] and the control action, with the respective internal linearization, is done each 15[s] as depicted in Fig. 2.

4. Results

This section presents Test 1 and Test 2 results. Test 1 runs only the optimization layer using five objective functions depicted in Table 1. Test 2 runs the hierarchical control with both layers for the most suitable approaches of Test 1, resulting in six simulations presented in Fig. 5. Lastly, the start-up and shut-down phases are presented and discussed in section 4.3.

4.1. Test 1 - steady state optimal operation maps

The optimal operation maps are obtained running the optimization problems summarized on Table 1 for values of solar radiance from 0 to 1000[W/m^2]. Fig. 3 depicts the results of unconstrained steady-state optimization considering solar irradiance. The optimal operation points for outlet temperature are in Fig. 3.a and for flow in Fig. 3.b. Limits were widen by a factor of 10 of the limits defined in Equation (8) to prevent numerical problems.

Fig. 3.a shows that collector energy approach (solid blue) has the lowest outlet temperature values, followed by net energy (dashed orange), exergy (purple and dashed green) and maximum outlet

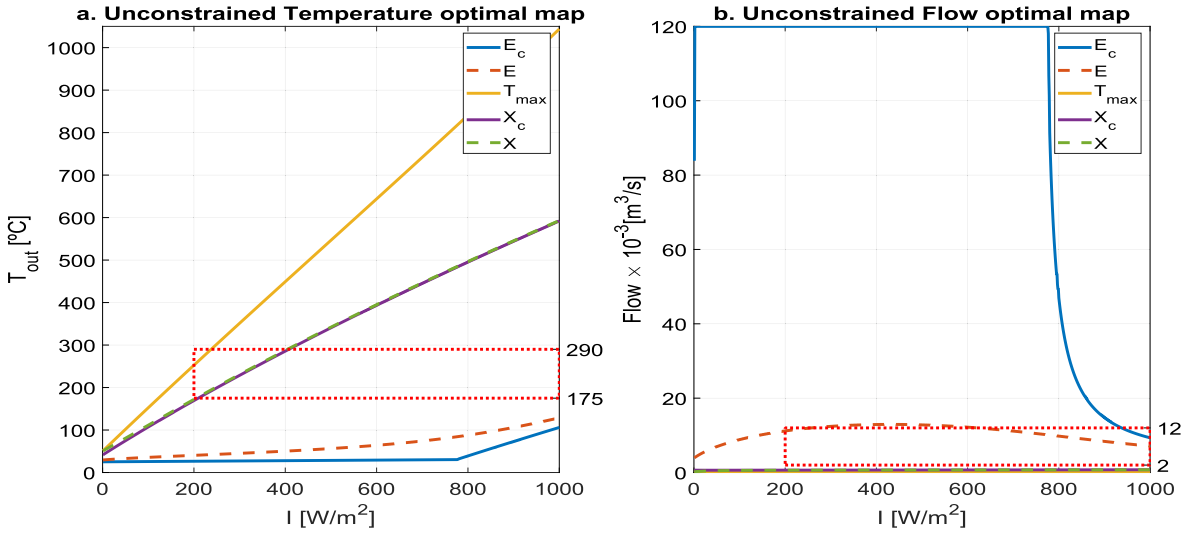

Fig. 3. Test 1. Optimal Temperature (a) and flow (b) operation points for unconstrained optimizations. $\dot{E}, \dot{X}$ are the net production rate (- - -) and $\dot{E}_C, \dot{X}_C, T_{out}$ are the collector production rate and maximum outlet temperature (——) optimizations.

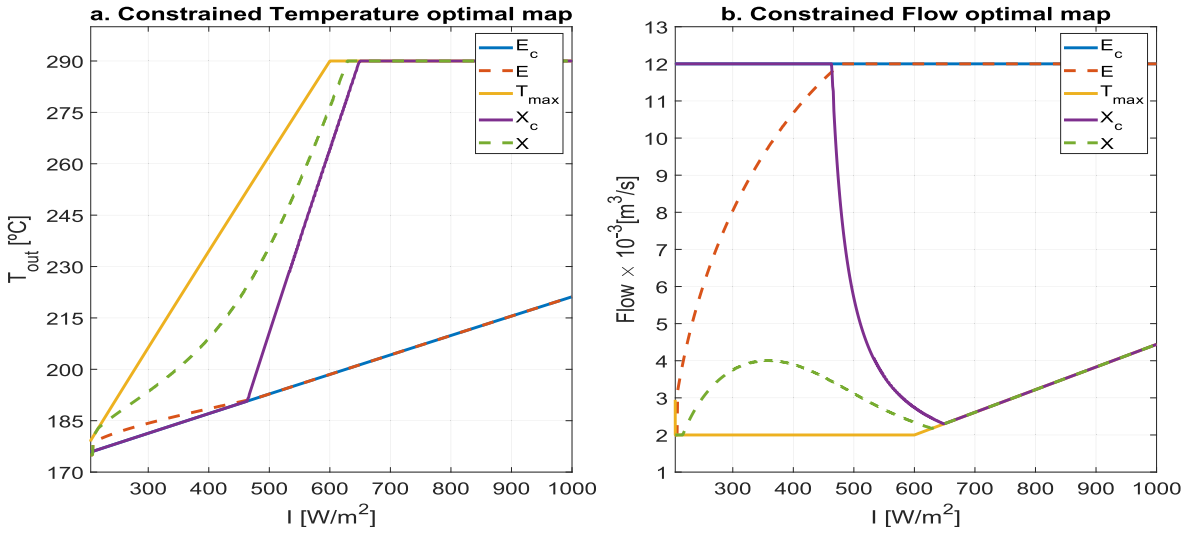

Fig. 4. Test 1. Optimal Temperature (a) and flow (b) operation points for constrained optimizations. $\dot{E}, \dot{X}$ are the net production rate (- - -) and $\dot{E}_C, \dot{X}_C, T_{out}$ are the collector production rate and maximum outlet temperature (——) optimizations.

temperature (yellow) approaches.

Consider the analysis of literature optimization results. On the one hand, the maximum outlet temperature approach results in temperature maximization with the minimum possible flow, $\dot{V} \rightarrow 0$. On the other hand, the collector energy optimization ($\dot{E}_C$) leads to the minimum outlet temperature where ambient losses are minimized because the flow is maximum.

The flow profile changes significantly if we consider the pump consumption, compare Fig. 3.a, orange dashed ($\dot{E}$) and blue lines ($\dot{E}_C$). This result is obvious since increasing flow results in increasing pump consumption, yet, the optimization procedure was able to find an optimum, considering the trade-off between pump consumption and ambient losses.

Next, we discuss the collector exergy-based optimization cases (purple and dashed green lines) of Fig. 3. First, exergy-based profiles follow the irradiance and seem to balance exergy ambient losses and production. Note that purple and dashed green lines are not coincident with the other lines. Second, the pump consumption does not change the exergy-based solutions because there are no appreciable differences between dashed green and purple lines. The explanation that the temperature is not constrained, and temperature variation has more weight on exergy production than the pump power for high temperatures.

Now lets discuss the constrained results depicted in Fig. 4. Note that the dotted red boxes in Fig. 3 represent the SF operational regions defined in Equations (8) and (9), and the axes limits of Fig. 4a and 4.b. Is worth to say that despite the dotted red rectangle on Fig. 3 define the Fig. 4 axes limits, the optimization results are not the same since the optimization conditions are different.

The outcomes are valid for $I > 200[W/m^2]$ because of minimum outlet temperature condition. The net exergy optimal profile (dashed green) is followed closely by the maximum temperature (yellow) until $650[W/m^2]$, when they become coincident. Although the maximum outlet temperature strategy has similar results to the optimal exergy, the approaches are not the same.

A comparison between lines with irradiances from 200 to 600

$[W/m^2]$ is used to deliver a physical explanation about Fig. 4 results. Note that maximum temperature T_{out} (yellow) and collector energy rates $\dot{E}_C$ (blue) optimal profiles define the bounds of outlet temperatures solutions, and the exergy profiles are inside these bounds. Now, if the pump power consumption is not considered in the objective function ($\dot{X}_C$) for $I < 450[W/m^2]$, flow is saturated, and temperature is low, this means that ambient exergy loss term is greater than the exergy production. However, when $I > 450[W/m^2]$ the exergy ambient loss becomes less than the exergy production gain, leading to temperature and exergy production increase, explaining why there is a sudden drop in flow and an increase in temperature profiles (purple). If the pump power is considered ($\dot{X}$), the pump exergetic cost is responsible for smoothing the collector exergy profile (purple line) into the net exergy production line (dashed green).

In the following the exergy and energy rate results are discussed. The impact of pump power on net exergy optimization is greater than on net energy due to the quality aspect of electrical or mechanical power used by the pump and low-quality thermal energy generated at low irradiance values. Also, the results indicate that considering the pump power on optimization leads to a smooth flow profile from $200 \leq I \leq 550[W/m^2]$ depicted in Fig. 4.b. For high irradiation levels only the exergy optimization reaches the upper limit temperature.

Now, comparing exergy rate and maximum temperature optimizations, both converge to the upper temperature operation limit for $I > 600[W/m^2]$. Considering collector exergy production $\dot{X}_C = \dot{E}_C - T_{amb}\dot{S}_C$, this function can be seen as an energy objective plus a second law of thermodynamics weight of $T_{amb}\dot{S}_C$ to penalize low temperatures and irreversibilities. In comparison, the maximum temperature strategy cannot consider the pump power in the objective function without losing dimensional consistency, although, in order to reach the maximum temperature it implicitly maintain the lowest flow, therefore, the pump power is the minimum.

The pump power effect is evidenced by comparing the flows (continuous lines) and net (dashed lines) Fig. 4.b. By inspection it can be seen that the pump power has an appreciable impact on the energy (blue, orange) and exergy (purple, green) optimal static maps.

4.2. Test 2 - hierarchical control

Test 2 runs the hierarchical control considering two input scenarios depicted on Fig. 5, Scenario 1 uses a near-ideal clear day depicted in Fig. 5.a, and Scenario 2 considers a cloudy day depicted in Fig. 5.b. Because of the appreciable impact of the pump power consumption and constraints, the hierarchical control simulations of this section consider only constrained cases 2, 3, and 5 depicted in Table 1.

Ambient temperatures and irradiances are validated measurements [36]. The data are linearly interpolated to generate points with $t_s = 15[s]$ since the raw inputs sampling time is $15[min]$ and the controller and optimizer operates at sampling times of $15[s]$ and $5[min]$, respectively. Both scenarios are composed by an all-day data set in a wide range of Irradiance ($200 < I < 1100[W/m^2]$) with inlet temperatures of $T_{in} \approx 175[^\circ C]$ and $T_{amb} \approx 19[^\circ C]$.

Fig. 5 shows the closed-loop performance for a 12 h period. The hierarchical control simulation is the following. First, the optimization layer is executed and finds the optimal outlet temperature and flow pair as discussed in Section 3.1. Next, at every $5[min]$, the outlet temperature reference T_{ref} is sent from the optimization layer to the PNMPC control layer. Then, the control layer executes the PNMPC algorithm and finds the best sequence of flows that minimizes the error between the set-point sent by the optimization layer and the measured outlet temperature along the horizon with sampling times of 15[s]s. Next, the flow is updated and actuates to drive the plant towards the optimal temperature. These steps are continuously updated at each sampling time with measured inputs.

To evaluate PNMPC performance on reference tracking and disturbance rejection the Integral of Absolute Error ($IAE = \int |T_{out}(t) - T_{ref}(t)|dt$) index is used along simulated period of 12h. PNMPC shows good reference tracking and disturbance rejection as can be seen on IAE values of Table 2. Note that the exergy hierarchical control gives references to which control layer tracks better if compared to the maximum outlet temperature hierarchical control (see IAE).

The energy optimization case shows more significant flow variation and pump saturation. This behavior is due to the model nonlinearity, which has a static gain proportional to the collector temperature — resulting in a more significant control effort and actuator saturation for low collector temperature. Pump energy (W_p) in Table 2 corroborate the results.

Outlet temperature maximization (Fig. 5e and 5.f) and exergy optimization (Fig. 5g and 5.h) show similar responses according to steady-state optimal maps of Fig. 4.a. By inspection, the temperature maximization and exergy approaches show appreciable differences in start-up and shutdown phases. Thus, both operate at the collector's upper-temperature limit at high irradiance values, but for low values, differences appear.

Table 2 and Fig. 5 depict the pump/control effort. Comparatively, energy optimization uses up to 3 times more pumping energy than the other cases. Meanwhile, the temperature maximization saturates the pump in the lower limit leading to the lowest pump consumption. The exergy hierarchical control uses almost the same low pump energy as Case 3. Moreover, the exergy approach conciliates irradiance and temperature resulting in intermediate temperature set points on start-up and shutdown. Section 4.3 presents a further investigation on start-up and shut down.

Table 2 resumes the daily production and performance for each scenario and each case concerning Test 2. The total production calculation integrates the energy rate ($\dot{E}$), exergy rate ($\dot{X}$), and pump power ($\dot{W}_P$) in time. The results are the produced energy (E), exergy (X), and consumed pump work (W_P). The energy efficiency calculation considers outlet collector and inlet sun energy ratio while the exergy efficiency counts on collector outlet and sun irradiation exergy ratio. Petela's exergy of heat radiation equation [37] defines the sun exergy upper limit used here.

Table 2 inspection shows that the energy rate optimization has the worst exergy production and uses almost three times more pump work than the others. Despite having the best energy, or first law of thermodynamics, production, energy rate optimization is not a good approach since it has the lowest exergy production and efficiency. Thus, it has the worst result from the second law of thermodynamics perspective.

Exergy rate optimization, in its turn, gives the highest net exergy productions with the highest efficiencies, followed closely by the maximum temperature strategy in all cases. Comparing temperature maximization and exergy approaches, both have practically the same results for both scenarios. It also was found that the sampling time has an important influence on results. For example, if the optimization layer has $t_s < 5[min]$, the exergy approach gives better results than temperature maximization for all cases. For $t_s > 5[min]$ case 3 shows better performance in cloudy days' (Scenario 2).

Since the maximum temperature case sends the maximum achievable value at a given instant, the system would operate seeking the upper limit, leading to more significant energy

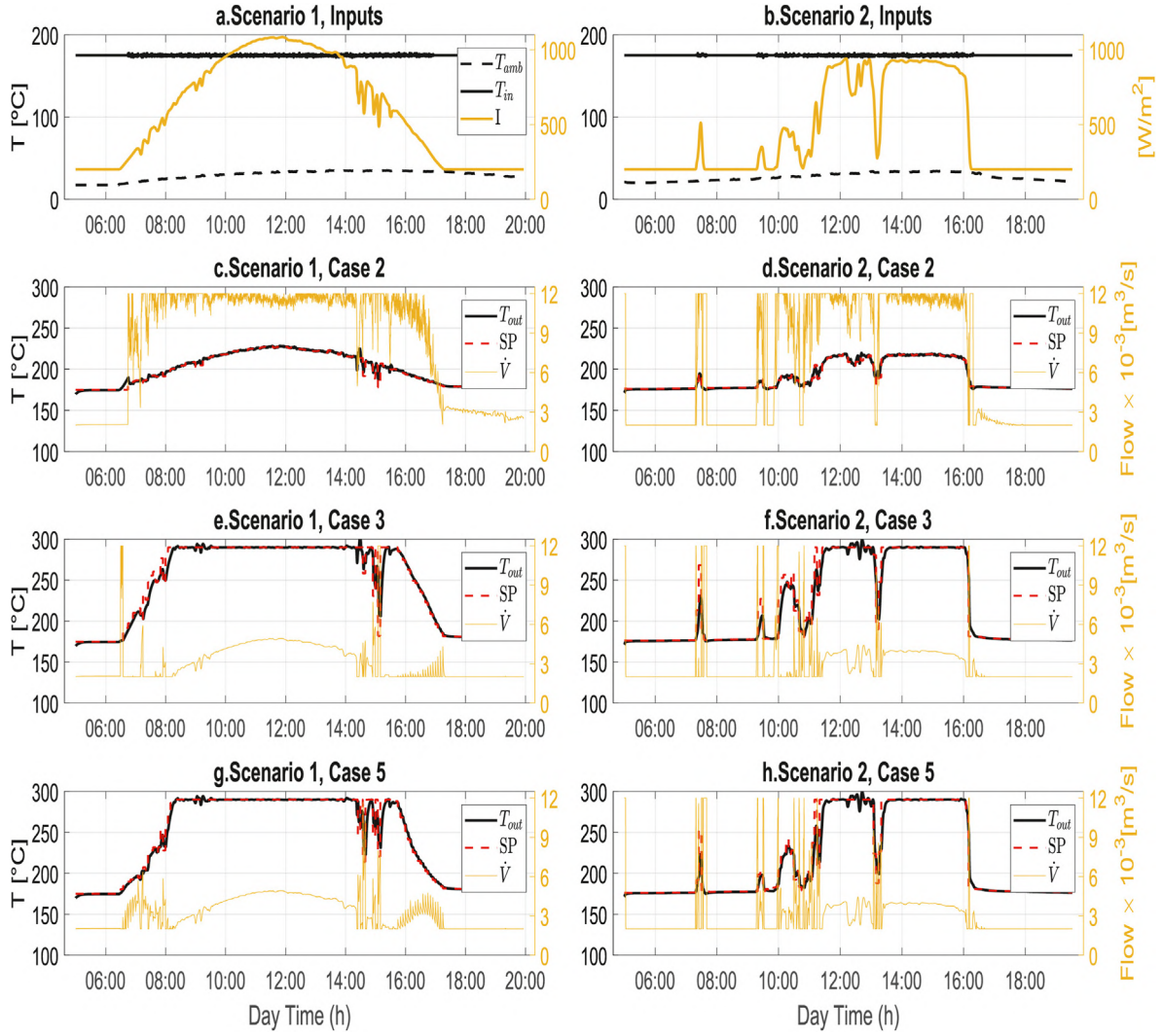

Fig. 5. Test 2 results. Scenario 1 considers a clear day inputs (a) while Scenario 2 considers a cloudy day inputs (b). c,d- Net energy rate optimization. e,f Maximum outlet temperature optimization. g,h- Net exergy rate optimization.

Table 2
Test 2 production/consumption results. Normalized values are referred for each E, X, W_p, η_E, η_X and IAE performances, that are the net energy, net exergy produced, pump consumption, energetic efficiency, exergetic efficiency and Integral of absolute error, respectively.

Case	E	X	W_p^1	η_E	η_X	IAE^2
Production (MJ) - Scenario 1						
1. $\dot{E}$	28823	9745	440	0.292	0.103	3606
2. $\dot{T}_3$	27902	10778	158	0.280	0.110	10464
3. $\dot{X}$	28029	10787	166	0.282	0.110	9131
Normalized production - Scenario 1						
1. $\dot{E}$	1.000	0.903	2.774	1.000	0.930	1.000
2. $\dot{T}_3$	0.968	0.999	1.000	0.959	0.999	2.902
3. $\dot{X}$	0.972	1.000	1.049	0.964	1.000	2.532
Production (MJ) - Scenario 2						
1. $\dot{E}$	17324	5664	321	0.241	0.084	3702
2. $\dot{T}_3$	16663	6312	143	0.232	0.091	13000
3. $\dot{X}$	16751	6324	150	0.233	0.091	11120
Normalized production - Scenario 2						
1. $\dot{E}$	1.000	0.896	2.237	1.000	0.924	1.000
2. $\dot{T}_3$	0.962	0.998	1.000	0.962	0.997	3.512
3. $\dot{X}$	0.967	1.000	1.043	0.967	1.000	3.004

[1,2]Normalization considers the lower value.
[2][^oC min].

gathering than exergy considering changes and uncertainties between sampling times. This maximum temperature advantage increases whatever increasing the sampling time. However, it leads to more significant IAE values and tracking errors, as shown in Table 2.

4.3. Test 2 - start-up and shut-down

Fig. 6 presents in detail start-up and shut-down operations which are depicted in Fig. 5.e around 6:30 to 8:00, Fig. 5.f around 15:30 to 17:00, Fig. 5.g around 10:00 to 11:00, and Fig. 5.h around 16:10 to 16:20. The energy-based control result is suppressed since it is not satisfactory considering Table 2 results.

By inspection of the first line of figures, the exergy (orange) and maximum temperature (blue) approaches are different until they reach maximum or minimum temperature constraint at 290 [^oC] and 175 [^oC], respectively. The flow behavior is depicted in the second line of figures, showing a more considerable control effort of exergy case (orange). A strong actuation happens because the setpoints (dotted lines) sent by the optimization layer with low irradiance values, which occurs in the morning and evening, have differences as depicted in the optimal maps and discussed in section 3. The net exergy production is depicted in the third line of

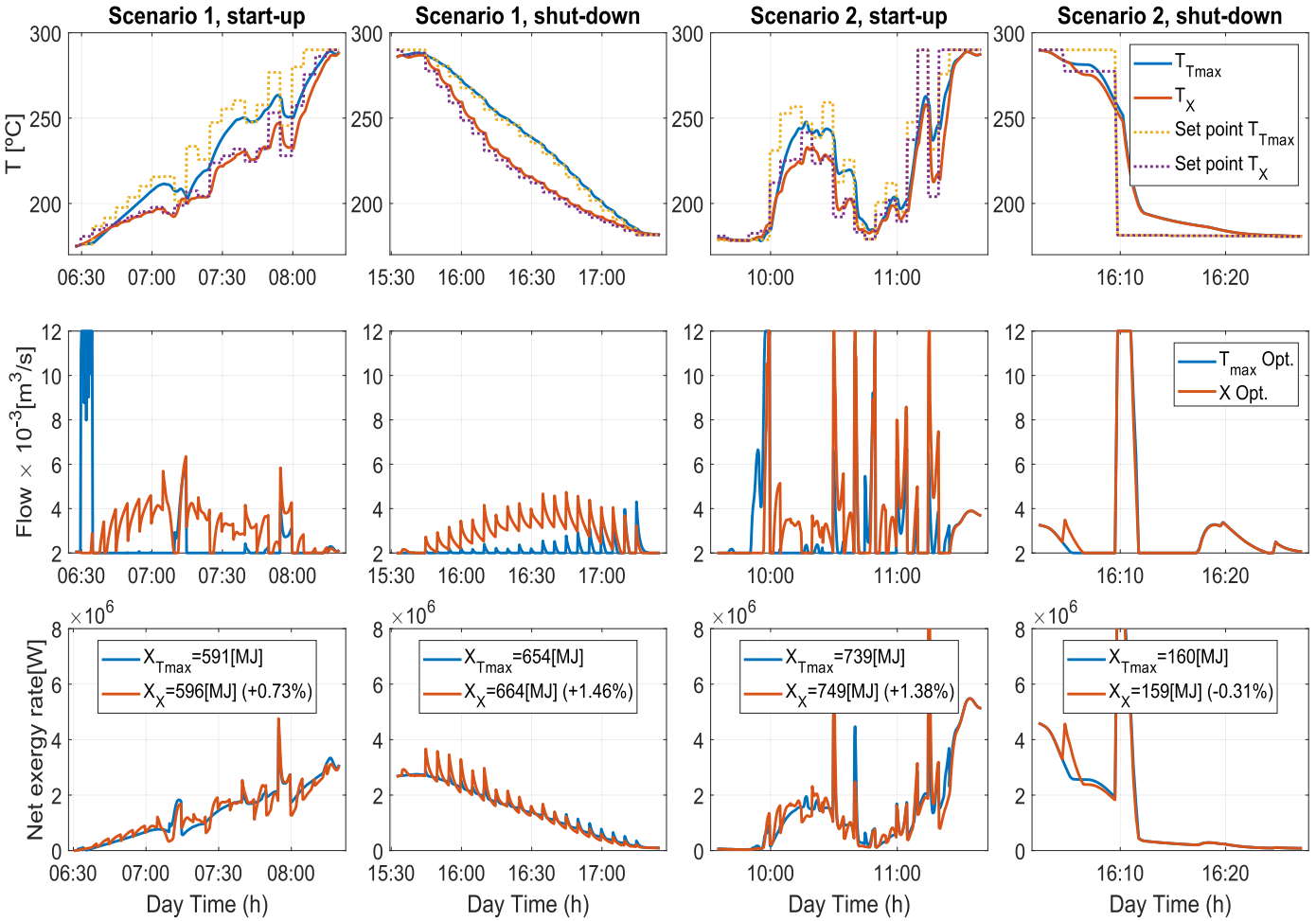

Fig. 6. SF start-up and shut-down. The graphics overlaps the simulations of Fig. 5e to .f for each Scenario. The third line presents the exergy production were total production and exergy percentage gain are available in the box.

figures, and the total exergy produced is presented in the box. Net exergy production presents advantages of the order of 1% for Scenario 1 and Scenario 2, start-up. Note that the start-up and shut down times are almost the same for the two strategies.

5. Conclusion

This work presents an optimal exergy-based hierarchical control capable of operating a solar field and clarifies its performance together with literature approaches. The proposed control is aware of the thermodynamic production limits considering the system's constraints and intermittency. In practice, it is found that the maximum temperature approach operates almost at the same points that the exergy optimization; therefore, seeking maximum temperature is a quasi-optimal strategy for the ACUREX SF case. The following conclusions emerge from the hierarchical control simulations:

- The proposed exergy-based hierarchical control can provide satisfactory reference tracking and disturbance rejection considering process intermittency, constraints, and pump power.
- The energy-based, or thermal power, hierarchical control performance is insufficient to increase thermal energy production from the second law of thermodynamics perspective.
- The proposed exergy-based hierarchical control performance is the most favorable considering the second law of thermodynamics therm in the objective function. It has a marginal production increase concerning the maximum outlet temperature strategy across an entire day simulation. Despite the low advantage, the controller implementation is desirable since it increases production and efficiency while not implying any investment or hardware change.
- The exergy-based approach has more advantages on start-up and shut-down phases, showing gains of the order of 1%.

It is worth noting that the maximum temperature strategy has very close results to the exergy-based approach because of the ACUREX operational constraints. So, assuming that the strategies have the same results is not valid for other SF using different fluids, materials, and equipment. In contrast, the exergy-based approach will lead to optimal results from the second law of thermodynamics point of view for any SF. Also, note that as new SF and HTF technologies are developed, the SF operational constraints region and the exergy-based application advantages increase.

Future work is interesting to consider exergy-based control-oriented solutions such as Real-Time Optimization procedures or merge useful energy concepts to economic MPC techniques and integrate both optimization and control layers in one technique.

Credit author statement

Diogo Ortiz Machado: Conceptualization, Investigation and writing. Gustavo Artur de Andrade: Software, review, Supervision. Julio Normey-Rico: Project administration, Resources, Supervision, Writing – review & editing. Carlos Bordons: Writing – review & editing.

Funding

This works was suported in part by the Coordenação de Aperfeiçoamento de Pessoal de Nível Superior (CAPES), Finance Code 001, in part by the Conselho Nacional de Desenvolvimento Científico e Tecnológico (CNPq), under grant 304032/2019–0, in part by the Agencia Estatal de Investigación (AEI) of the Spanish Ministry of Science and Innovation, under grant PID2019-104149RB-I00/10.13039/501100011033 (project SAFEMPC), and in part by the Fundación Carolina. D. O. Machado thanks the Instituto Federal de Educação, Ciência e Tecnologia (IFRS), Campus Rio Grande, for capacitation suport, and Secretaría General Iberoamericana (SEGIB) together with PrInt/UFSC for the international mobility scholarships.

Declaration of competing interest

The authors declare that they have no known competing financial interests or personal relationships that could have appeared to influence the work reported in this paper.

References

[1] A. S. Alsagri, A. A. Alrobaian, S. A. Almohaimeed, Concentrating solar collectors in absorption and adsorption cooling cycles: an overview (nov 2020). doi: 10.1016/j.enconman.2020.113420.
[2] Sharma AK, Sharma C, Mullick SC, Kandpal TC. Solar industrial process heating: a review. oct 2017. https://doi.org/10.1016/j.rser.2017.04.079.
[3] Goswami DY. Principles of solar engineering. third ed., vol. 1; 2015. https://doi.org/10.1017/CBO9781107415324.004. arXiv:arXiv:1011.1669v3 https://books.google.com/books?id=v4GbBgAAQBAJ&pgis=1.
[4] Camacho E, Bordons C. Model predictive control. Springer; 2007.
[5] Cirre CM, Valenzuela L, Berenguel M, Camacho EF. Control of solar plants with automatic set-point generation (in Spanish). Revista Iberoamericana de Automática e Informática Industrial 2004;1(1):50–6.
[6] Cirre CM, Berenguel M, Valenzuela L, Klempous R. Reference governor optimization and control of a distributed solar collector field. Eur J Oper Res 2009;193(3):709–17. https://doi.org/10.1016/j.ejor.2007.05.056.
[7] Berenguel M, Cirre CM, Klempous R, Maciejewski H, Nikodem M, Nikodem J, Rudas IJ, Valenzuela L. Hierarchical control of a distributed solar collector field. In: EUROCAST; 2005.
[8] Camacho EF, Gallego AJ. Optimal operation in solar trough plants: a case study. Sol Energy 2013;95:106–17. https://doi.org/10.1016/j.solener.2013.05.029.
[9] Alsharkawi A. Automatic control of a Parabolic trough solar thermal power plant. Ph.D. thesis. The University of Sheffield; 2017.
[10] J. R. D. Frejo, reportModel predictive control for freeway traffic networks, Ph.D. thesis.
[11] Bejan A, Kearney DW, Kreith F. Second law analysis and synthesis of solar collector systems. Journal of Solar Energy Engineering, Transactions of the ASME 1981;103(1):23–8. https://doi.org/10.1115/1.3266200.
[12] Bejan A. Extraction of exergy from solar collectors under time-varying conditions. Int J Heat Fluid Flow 1982;3(2):67–72. https://doi.org/10.1016/0142-727X(82)90002-9.
[13] Manfrida G. The choice of an optimal working point for solar collectors. Sol Energy 1985;34(6):513–5. https://doi.org/10.1016/0038-092X(85)90025-8.
[14] Fiaschi D, Manfrida G. Improvement of energy conversion/utilization by exergy analysis: selected cases for non-reactive and reactive systems. Entropy 2010;12(2):243–61. https://doi.org/10.3390/e12020243. http://www.mdpi.com/1099-4300/12/2/243.
[15] Manfrida G, Gerard V. Maximum exergy control of a solar thermal plant equipped with direct steam collectors. Int J Therm 2008;11(3):143–9. https://doi.org/10.5541/ijot.222.
[16] Grosu L, Mathieu A, Rochelle P, Feidt M, Ahmadi MH, Sadeghzadeh M. Steady state operation exergy-based optimization for solar thermal collectors. Environ Prog Sustain Energy 2019;(October):1–8. https://doi.org/10.1002/ep.13359.
[17] Ceylan I, Ergun A. Thermodynamic analysis of a new design of temperature controlled parabolic trough collector. Energy Convers Manag 2013;74:505–10. https://doi.org/10.1016/j.enconman.2013.07.020.
[18] Sciubba E, Wall G. A brief commented history of exergy from the beginnings to 2004. Int J Therm 2007;10(1):1–26. https://doi.org/10.5541/ijot.1034000184.
[19] James C, Kim TY, Jane R. A review of exergy based optimization and control. 2020. p. 1–15. https://doi.org/10.3390/pr8030364.
[20] Reddy CR, Razmara M, Shahbakhti M, Robinett RD. Optimal exergy-wise predictive control for a combined microcsp and hvac system in a building. In: 2019 American control conference (ACC); 2019. p. 235–40. https://doi.org/10.23919/ACC.2019.8815205.
[21] Sangi R, Müller D. Application of the second law of thermodynamics to control : a review. Energy 2019;174:938–53. https://doi.org/10.1016/j.energy.2019.03.024.
[22] Sayadi S. Dynamic exergy-based methods for improving the operation of building energy systems. Ph.D. thesis. Technische Universitat Berlin - TU; 2020.
[23] de Prada C. Overview: control hierarchy of Large processing plants. 2014.
[24] Findeisen W, Bailey FN, Brdys M, Malinowski K, Wozniak PA. Control and coordination IN hierarchical systems. John Wiley & Sons; 1980.
[25] Camacho EF, Berenguel M, Rubio FR, Martínez D. Control of solar energy systems. Springer Verlag; 2012.
[26] Eastman Co. Therminol vp-1 heat transfer fluid. Tech. rep. 2016 https://www.therminol.com/product/71093459.
[27] Moran MJ, Shapiro HN. Fundamentals of engineering thermodynamics. fifth ed., vol. 181; 2006. https://doi.org/10.1038/1811028b0. http://www.nature.com/doifinder/10.1038/1811028b0.
[28] Cirre CM, Valenzuela L, Berenguel M, Camacho EF. Feedback linearization control for a distributed solar collector. field 2005;38(1):356–61. https://doi.org/10.3182/20050703-6-CZ-1902.01788. 16th IFAC World Congress, http://www.sciencedirect.com/science/article/pii/S1474667016378004.
[29] Normey-Rico JE, Bordons C, Berenguel M, Camacho EF. A robust adaptive dead-time compensator with application to A solar collector field 1. IFAC Proceedings Volumes 1998;31(19):93–8. https://doi.org/10.1016/s1474-6670(17)41134-7.
[30] Incropera FP, DeWitt DP, Bergman TL, Lavinne AS. Fundamentals of heat and mass transfer. seventh ed. John Wiley & Sons, Inc.; 2011.
[31] Plucenio A. Desenvolvimento de técnicas de controle não linear para elevação de fluidos multifásicos. Ph.D. thesis. Programa de Pós-Graduação em Engenharia de Automação e Sistemas, DAS, Universidade Federal de Santa Catarina - UFSC; 2010.
[32] Andrade GA, Pagano DJ, Álvarez JD, Berenguel M. A practical nmpc with robustness of stability. applied to distributed solar power plants 2013;92:106–22.
[33] Byrd RH, Gilbert JC, Nocedal J. A trust region method based on interior point techniques for nonlinear programming. Mathematical Programming, Series B 2000;89(1):149–85. https://doi.org/10.1007/PL00011391.
[34] Waltz R, Morales J, Nocedal J, Orban D. An interior algorithm for nonlinear optimization that combines line search and trust region steps. Math Program 2006;107(3):391–408. https://doi.org/10.1007/s10107-004-0560-5. http://link.springer.com/10.1007/s10107-004-0560-5.
[35] Coleman TF, Li Y. A reflective Newton method for minimizing a quadratic function subject to bounds on some of the variables. SIAM J Optim 1996;6(4):1040–58. https://doi.org/10.1137/S1052623494240456.
[36] SONDA Project. Cachoeira paulista meteorological station (in Portuguese), Tech. rep. 2020. URL, http://sonda.ccst.inpe.br/basedados/cachoeira.html.
[37] Petela R. Exergy of heat radiation. J Heat Tran 1964;86(2):187–92. https://doi.org/10.1115/1.3687092.

9 RESULTS DISCUSSION AND CONCLUSION

This thesis integrates exergy, MPC, and renewable energy systems in a hierarchical control structure. The **research question** is answered using a hierarchical structure that separates the supervisory and process regulation problems into two layers that operate in distinct sampling periods. Such a structure allows proper optimization and control to find the optimal exergetic plant operation reference and define the appropriate control actions to follow the set points. Hierarchical exergy-based control mainly differs from the others when deciding the timing and sequence of plant start-up and shutdown. The problem is that the available models in the literature are limited in describing the processes around an operating point.

In this context and pursuing **specific objective 1**, an ANFIS model of an absorption machine was trained and validated with actual day and night operating data to test the plant's start-up and shutdown. Such a model is suitable for simulating the intermittency of the process operation as it expands the validated region of the dynamic description of the process. In addition, the ANFIS and PDE models of a Fresnel solar collector were properly validated. The referred models are adaptive and designed to be used as digital twins. The first is faster for its simulation and adaptation, despite having more significant errors than the PDE. Furthermore, these are the first results published in the literature that address the validation of system defocus.

Regarding regulatory control and **specific objective 2**, it is concluded that it is possible to geometrically operate the set of mirrors of a Fresnel solar collector, emulating the optical operation of a parabolic cylinder collector with variable focal point and directrix. Thus, the solar tracking system can proportionally vary the position of the mirrors by changing the focal point of the sun's rays concerning the absorber tube and the respective energy input in the system. The result is a new continuous manipulated variable available to the designer of control systems for this process. It is concluded that a PNMPC controller using this concept, manipulating both the defocus and the flow, prevents overheating and safety events, can reduce the generated thermal power while preserving the desired output temperature value, and has lower IAE. It is also concluded that a split-range controller using the same idea has similar performance, with the advantage of being simpler, easily implementable, and known in the industrial context. Furthermore, the main conclusion of Part II is that defocus is a necessary actuator in the control layer for concentrating solar plants with solar multiples greater than 1. That is, it should not be treated as a safety device only.

Regarding supervisory control and **specific objectives 2 and 3**, it is concluded that a hierarchical control is capable of integrating an optimization layer of the net exergy production of a concentrating solar collector. A PNMPC controller in the regulatory layer can receive the reference temperatures from the supervisory layer and follow them,

rejecting possible disturbances. Comparing the proposed approach to the literature's energy maximization or outlet temperature shows that the exergy-based control has the most favorable performance. Due to the thermal and mechanical limitations of materials and collector designs, the proposed approach has similar results to maximizing the outlet temperature. The difference is that the exergy-based hierarchical control design applies to any collector while maximizing the outlet temperature is a heuristic solution that does not necessarily result in the best useful energy production for any collector.

Finally, the **general objective** was to study exergy-based MPC controls. In this sense, a review of exergy-based MPC controllers was carried out and concluded that there are few publications on the subject. The publications mainly deal with the dynamic modeling of exergy, the cost function using exergy destruction, and the MPC structure that best fits each case. As for applying the technique in renewable energy systems, only two articles were published, indicating the relevance and opportunity to develop this thesis and the proposal of hierarchical control seeking to maximize the net production of exergy.

9.1 FUTURE WORKS

Integrate and validate the complete ETSI absorption plant model, then couple the absorption machine and solar collector models, and model the long pipes that connect such systems and test in the simulation.

Use the complete and validated model of the plant with the regulatory control proposed in Chapter 7.

Implement a supervisory control layer with an exergy-based PNMPC to define an optimal sequence of output temperatures and send them to regulatory control. Make comparisons between the proposed control and the original rule-based and energy-based control.

Implement a cost-effective MPC controller that integrates the regulatory and supervisory layers, evaluating its performance.

Develop a methodology for designing and tuning split-range and MPC controllers for concentrating solar collectors capable of handling both flow and defocus.

10 DISCUSIÓN DE RESULTADOS Y CONCLUSIONES

Esta tesis integra la exergía, el MPC y los sistemas de energía renovable en una estructura de control jerárquica. La **pregunta de investigación** se responde utilizando una estructura jerárquica que separa los problemas de supervisión y regulación de procesos en dos capas que operan en diferentes períodos de muestreo. Esta estructura permite la optimización y el control adecuado tanto para encontrar la referencia óptima de funcionamiento exergético de la planta, como para definir las acciones de control adecuadas para seguirlas. El control jerárquico basado en la exergía se difiere principalmente por decidir el tiempo y la secuencia de puesta en marcha y parada de la planta. El problema es que los modelos disponibles en la literatura son limitados en la descripción de los procesos alrededor de un punto de operación.

En este contexto, y buscando el **objetivo específico 1**, se entrenó y validó un modelo ANFIS de una máquina de absorción con datos reales de funcionamiento a lo largo del día y la noche para probar el accionamiento, arranque y parada de la planta. Dicho modelo es adecuado para simular la intermitencia de la operación del proceso porque expande la región de descripción dinámica validada del proceso. Además, los modelos ANFIS y PDE de un colector solar Fresnel fueron validados adecuadamente. El primero, a pesar de tener errores mayores que el PDE, es más rápido tanto por su simulación como por su adaptación. Los modelos mencionados son adaptativos y diseñados para ser utilizados como gemelos digitales. Además, estos son los primeros resultados publicados en la literatura que abordan la validación del sistema de desenfoque.

Con respecto al control de supervisión y al **objetivo específico 2**, se concluye que es posible operar geométricamente el conjunto de espejos de un colector solar Fresnel emulando el funcionamiento óptico de un colector cilindro parabólico con punto focal y directriz variables. Por lo tanto, el sistema de seguimiento solar puede variar proporcionalmente la posición de los espejos cambiando el punto focal de los rayos del sol en relación con el tubo absorbente y la respectiva entrada de energía en el sistema. El resultado es una nueva variable manipulada continua a disposición del diseñador del sistema de control de este proceso. Se concluye que un controlador PNMPC que utiliza este concepto, manipulando tanto el desenfoque como el flujo, evita el sobrecalentamiento y los eventos de seguridad, es capaz de reducir la potencia térmica generada preservando el valor de temperatura de salida deseado y presenta un IAE más bajo. También se concluye que un controlador de rango dividido que utiliza la misma idea tiene un rendimiento similar, con la ventaja de ser más simple, fácilmente implementable y conocido en el contexto industrial. Además, la principal conclusión de la Parte II es que el desenfoque es un actuador necesario en la capa de control para plantas de concentración solar con múltiplos solares mayores que 1. Es decir, no debe

tratarse solo como un dispositivo de seguridad.

Caixa de TextoEn cuanto al control supervisor y los **objetivos específicos 2 y 3**, se concluye que un control jerárquico es capaz de integrar una capa de optimización de la producción neta de exergía de un colector de concentración solar. Un controlador PNMPC en la capa reguladora es capaz de recibir temperaturas de referencia de la capa de supervisión y seguirlas, rechazando posibles interrupciones. Comparando los enfoques de la literatura de maximización de energía o temperatura de salida con la propuesta, se concluye que el control basado en la exergía tiene el rendimiento más favorable. Debido a las limitaciones térmicas y mecánicas de los materiales y los diseños de colectores, el enfoque propuesto tiene resultados similares a la maximización de la temperatura de salida. La diferencia es que el diseño de control jerárquico basado en la exergía es aplicable a cualquier colector, mientras que maximizar la temperatura de salida es una solución heurística que no necesariamente resulta en la mejor producción de energía útil para cualquier colector.

Finalmente, el **objetivo general** fue estudiar los controles MPC basados en exergía. En este sentido, se realizó una revisión y estado del arte de los controladores MPC basados en la exergía y se concluyó que existen pocas publicaciones sobre el tema. Las publicaciones encontradas tratan principalmente del modelado dinámico de la exergía, la función de costo utilizando la destrucción de la exergía, así como la estructura MPC que mejor se adapta a cada caso. En cuanto a la aplicación de la técnica en sistemas de energías renovables, sólo se publicaron dos artículos, indicando la relevancia y oportunidad de desarrollar esta tesis y la propuesta de control jerárquico de control buscando maximizar la producción neta de exergía.

10.1 TRABAJOS FUTUROS

Integrar y validar el modelo completo de la planta de absorción ETSI. Acoplar los modelos de la máquina de absorción, el colector solar, así como modelar las tuberías largas que conectan dichos sistemas, probando y validando la planta en simulación.

Utilizar el modelo completo y validado de la planta con el control regulatorio propuesto en Capítulo 5.

Implementar una capa de control de supervisión con un PNMPC basado en exergía para definir una secuencia óptima de temperaturas de salida y enviarlas al control reglamentario. Hacer comparaciones entre el control propuesto y el original basado en reglas, y el control basado en energía.

Implementar un controlador MPC económico basado en exergía que integre las capas regulatoria y supervisora, evaluando su desempeño.

Desarrollar una metodología de diseño y sintonía de controladores de rango dividido y MPC para colectores solares de concentración con la capacidad de manipular tanto el flujo como el desenfoque.

11 DISCUSSÃO DE RESULTADOS E CONCLUSÕES

Esta tese integra exergia, MPC e sistemas de energias renováveis em uma estrutura hierárquica de controle. A **pergunta de pesquisa** é respondida utilizando uma estrutura hierárquica que separa os problemas supervisórios e de regulação do processo em duas camadas que operam em períodos de amostragens distintas. Tal estrutura permite a otimização e o controle de maneira apropriada tanto para encontrar a referência ótima de operação exergética da planta, quanto para definir as ações de controle adequadas para segui-las. O controle hierárquico baseado em exergia diferencia-se principalmente decidindo o momento e a sequência de arranque e parada da planta. O problema é que os modelos disponíveis na literatura são limitados em descrever os processos em torno de um ponto de operação.

Neste contexto, e buscando-se o **objetivo específico 1**, um modelo ANFIS de uma máquina de absorção foi treinado e validado com dados reais de operação ao longo do dia e da noite para testar o ligamento, arranque e parada da planta. Tal modelo é adequado para simular a intermitência da operação do processo pois expande a região validada de descrição dinâmica do processo. Em adição, os modelos ANFIS e PDE de um coletor solar Fresnel foram devidamente validados. O primeiro, apesar de possuir erros maiores que o PDE, é mais rápido tanto para sua simulação quanto para sua adaptação. Os modelos referidos são adaptativos e projetados para serem utilizados como gêmeos digitais. Além disso, estes são os primeiros resultados publicados na literatura que abordam a validação do desfoque do sistema.

Com relação ao controle regulatório e o **objetivo específico 2**, conclui-se que é possível operar geometricamente o conjunto de espelhos de um coletor solar do tipo Fresnel emulando o funcionamento óptico de um coletor cilindro parabólico com ponto focal e diretriz variáveis. Assim, o sistema de rastreamento solar pode variar proporcionalmente a posição dos espelhos mudando o ponto focal dos raios solares em relação ao tubo absorvedor, e a respectiva entrada de energia no sistema. O resultado é uma nova variável manipulada contínua disponível para o projetista de sistemas de controle desse processo. Conclui-se que um controlador PNMPC utilizando esse conceito, manipulando tanto o desfoque quanto a vazão, previne sobreaquecimento e eventos de segurança, é capaz de reduzir a potência térmica gerada preservando o valor desejado de temperatura de saída, e apresenta menores IAE. Conclui-se ainda que um controlador split-range utilizando a mesma ideia, possui performance similar, com a vantagem de ser mais simples, facilmente implementável e conhecido no contexto industrial. Ademais, a principal conclusão da Parte II é que o desfoque é um atuador necessário na camada de controle para plantas de concentração solares com múltiplos solares maiores que 1. Isto é, não deve ser tratado somente como um dispositivo de segurança.

Caixa de TextoNo que tange o controle supervisório e os **objetivos específicos 2 e 3**, conclui-se que um controle hierárquico é capaz de integrar uma camada de otimização da produção líquida de exergia de um coletor solar de concentração. Um controlador PNMPC na camada regulatória é capaz de receber as temperaturas de referências oriundas da camada de supervisão e segui-las, rejeitando possíveis perturbações. Comparando-se as abordagens da literatura de maximização de energia ou da temperatura de saída com a proposta, conclui-se que o controle baseado em exergia possui a performance mais favorável. Devido às limitações térmicas e mecânicas dos materiais e projetos de coletores, a abordagem proposta tem resultados similares à maximização da temperatura de saída. A diferença é que o projeto do controle hierárquico baseado em exergia é aplicável a quaisquer coletores, enquanto maximizar a temperatura de saída é uma solução heurística que não necessariamente resulta na melhor produção de energia útil para quaisquer coletores.

Por fim, o **objetivo geral** residia em estudar controles MPC baseados em exergia. Nesse sentido, uma revisão e estado-da-arte de controladores MPC baseados em exergia foi realizada e concluiu-se que há escassas publicações sobre o tema. As publicações encontradas tratam principalmente da modelagem dinâmica da exergia, da função custo usando a destruição de exergia, bem como da estrutura MPC que melhor se ajusta para cada caso. Quanto à aplicação da técnica em sistemas de energias renováveis, havia somente dois artigos publicados, indicando a relevância e a oportunidade em desenvolver essa tese e a proposta de controle hierárquica de controle buscando maximizar a produção líquida de exergia.

11.1 TRABALHOS FUTUROS

Integrar e validar o modelo completo da planta de absorção da ETSI. Acoplar os modelos da máquina de absorção, do coletor solar, bem como modelar as longas tubulações que ligam tais sistemas e testar na simulação.

Utilizar o modelo completo e validado da planta com o controle regulatório proposto no Capítulo 5.

Implementar uma camada de controle supervisório com um PNMPC baseado em exergia para definir uma sequência ótima de temperaturas de saída e enviá-las ao controle regulatório. Realizar comparações entre o controle proposto e o original baseado em regras, e o baseado em energia.

Implementar um controlador MPC econômico que integre as camadas regulatória e supervisória, avaliando seu desempenho.

Desenvolver uma metodologia de projeto e sintonia de controladores split-range e MPC para coletores solares de concentração com capacidade de manipulação tanto da vazão quanto do desfoque.

REFERENCES

APPAVOU, Fabiani et al. **REN21 - 2019 Global Status Report**. [S.l.: s.n.], 2019. P. 336. ISBN ISBN 978-3-9818911-7-1.

BARANSKI, Marc; FÜTTERER, Johannes; MÜLLER, Dirk. Distributed exergy-based simulation-assisted control of HVAC supply chains. **Energy and Buildings**, Elsevier Ltd, v. 175, p. 131–140, Sept. 2018. ISSN 03787788.

BARANSKI, Marc; FÜTTERER, Johannes; MÜLLER, Dirk; SANGI, Roozbeh. An Algorithm for Stepwise Exergy-based Model Predictive Control of Building HVAC Supply Chains. In: KITANOVSKI, Andrej; POREDOŠ, Alojz (Eds.). **Proceedings of the 29th International Conference on Efficiency, Cost, Optimization, Simulation and Environmental Impact of Energy Systems - ECOS 2016**. Portorož Slovenia: Curran Associates, Inc., June 2016. University of Ljubljana - Faculty of Mechanical Engineering.

BEJAN, Adrian. **Entropy Generation Minimization**: The method of thermodynamic optimization of finite-size systems and finite-time processes. 1st. [S.l.]: CRC press, 1995. ISBN 0-8493-9651-4.

BLOOMBERGNEF. **Corporate clean energy buying surged to new record in 2018**. Jan. 2019. Available from: https://about.bnef.com/blog/corporate-clean-energy-buying-surged-new-record-2018/.

BROCKWAY, Paul E.; STEINBERGER, Julia K.; BARRETT, John R.; FOXON, Timothy J. Understanding China's past and future energy demand: An exergy efficiency and decomposition analysis. **Applied Energy**, Elsevier Ltd, v. 155, p. 892–903, 2015. ISSN 03062619.

CARNOT, Nicolas Léonard Sadi. **Reflections on the Motive Power of Heat**. 2nd. [S.l.]: Chapman & Hall, Limited, 1824.

CLIMATE CHANGE IPCC, The Intergorvernamental Panel on. **Climate Change 2013: The Physical Science Basis**: Technical Summary. Cambridge, 2013. Available from: https://www.ipcc.ch/site/assets/uploads/2018/02/WG1AR5_TS_FINAL.pdf.

DINCER, Ibrahim; ROSEN, Marc A. **EXERGY: Energy, Enviroment and Sustainable Development**. 1. ed. Amsterdam: Elsevier, 2007. ISBN 978-0-08-044529-8.

EUROPE, Science. **A Common Scale for Our Common Future: Exergy, a Thermodynamic Metric for Energy**. [S.l.]: Zenodo, Sept. 2015. Available from: https://doi.org/10.5281/zenodo.7022853.

EUROPE, Science. **In a Resource-constrained World: Think Exergy, not Energy**. [S.l.]: Zenodo, June 2016. Available from: https://doi.org/10.5281/zenodo.5060174.

HADIAN, Mohsen; ASHERI, M. H.; SALAHSHOOR, Karim. A novel exergy-event based model predictive control strategy for energy saving. **Journal of Natural Gas Science and Engineering**, Elsevier B.V, v. 21, p. 712–717, 2014. ISSN 18755100.

HERNANDEZ, Ana Gonzalez; CULLEN, Jonathan M. Exergy: A universal metric for measuring resource efficiency to address industrial decarbonisation. **Sustainable Production and Consumption**, Elsevier, v. 20, p. 151–164, Oct. 2019. ISSN 2352-5509.

INTERNATIONAL RENEWABLE ENERGY AGENCY (IRENA). **Global Energy Transformation: A Roadmap to 2050**. [S.l.: s.n.], 2018. P. 76.

JAIN, Neera; ALLEYNE, Andrew. Exergy-based optimal control of a vapor compression system. **Energy Conversion and Management**, Elsevier Ltd, v. 92, p. 353–365, 2015. ISSN 01968904.

JAMES, Corey; KIM, Tae Young; JANE, Robert. A Review of Exergy Based Optimization and Control. **Processes**, v. 8, n. 3, 2020. ISSN 2227-9717.

JONIN, Matthieu; KHOSRAVI, Mohammad; EICHLER, Annika; VILLASMIL, Willy; SCHUETZ, Philipp; JONES, Colin N.; SMITH, Roy S. Exergy-based model predictive control for design and control of a seasonal thermal energy storage system. **Journal of Physics: Conference Series**, v. 1343, n. 1, 2019. ISSN 17426596.

KANG, Chul Goo. Origin of Stability Analysis: "On Governors" by J.C. Maxwell [Historical Perspectives]. **IEEE Control Systems**, IEEE, v. 36, n. 5, p. 77–88, 2016. ISSN 1066033X.

KJELSTRUP, Signe; DEWULF, Jo; NORDÉN, Bengt. A thermodynamic metric for assessing sustainable use of natural resources. **International Journal of Thermodynamics**, v. 18, n. 1, p. 66–72, 2015. ISSN 13019724.

KOTAS, Tadeusz Josef. **The Exergy Method of Thermal Plant Analysis**. London: Butterworth, 1985. ISBN 0-408-01350-8.

LAITNER, John A. Linking energy efficiency to economic productivity: Recommendations for improving the robustness of the U.S. economy. **Wiley Interdisciplinary Reviews: Energy and Environment**, v. 4, n. 3, p. 235–252, 2015. ISSN 2041840X.

MACFARLANE, Alistair G.J. The Development of Frequency-Response Methods in Automatic Control. **IEEE Transactions on Automatic Control**, v. 24, n. 2, p. 250–265, 1979. ISSN 15582523.

MACHADO, Diogo O.; NORMEY-RICO, Julio; ANDRADE, Gustavo A. de. A 2DOF thermosolar concentrator proposal: Solar tracking and disturbance rejection using proportional defocus. **ISES Solar World Congress 2019 and IEA SHC International Conference on Solar Heating and Cooling for Buildings and Industry Proceedings**, p. 32–42, 2020.

MACHADO, Diogo O.; SANCHEZ, Adolfo J.; ANDRADE, Gustavo A. de; NORMEY-RICO, Julio; BORDONS, Carlos; CAMACHO, Eduardo F. Fresnel Solar Collector Control With Active Defocus. **European Control Conference (ECC) Proceedings**, IEEE, p. 1804–1809, July 2022.

MACHADO, Diogo Ortiz; ANDRADE, Gustavo Artur; NORMEY-RICO, Julio Elias; BORDONS, Carlos. Optimal operation of Concentrating Solar Collector fields using exergy-based hierarchical control. **Energy**, Pergamon, v. 239, p. 122462, Jan. 2022. ISSN 0360-5442.

MACHADO, Diogo Ortiz; SÁNCHEZ, Adolfo J.; GALLEGO, Antonio J.; ANDRADE, Gustavo A. de; NORMEY-RICO, Julio E.; BORDONS, Carlos; CAMACHO, Eduardo F. Split-range control for improved operation of solar absorption cooling plants. **Renewable Energy**, Pergamon, v. 192, p. 361–372, June 2022. ISSN 0960-1481.

MORAN, Michael J.; SHAPIRO, Howard N. **Fundamentals of Engineering Thermodynamics, 5th Edition**. [S.l.: s.n.], 2006. v. 181, p. 1–107. ISBN 978-87-7681-670-4.

OFFICE OF ENERGY EFFICIENCY & RENEWABLE ENERGY. **2016-2020 Strategic Plan and Implementing Framework**. 2016. Available from: https://energy.gov/eere/downloads/eere-strategic-plan.

RAZMARA, Meysam; BIDARVATAN, Mehran; SHAHBAKHTI, Mahdi; ROBINETT, Rush D. Optimal exergy-based control of internal combustion engines. **Applied Energy**, 2016. ISSN 03062619.

RAZMARA, Meysam; MAASOUMY, Mehdi; SHAHBAKHTI, Mahdi; ROBINETT, Rush D. Optimal exergy control of building HVAC system. **Applied Energy**, Elsevier Ltd, v. 156, p. 555–565, Oct. 2015. ISSN 03062619.

RAZMARA, Meysam; MAASOUMY, Mehdi; SHAHBAKHTIY, Mahdi; ROBINETT, Rush D. Exergy-based model predictive control for building HVAC systems. **Proceedings of the American Control Conference**, 2015-July, p. 1677–1682, 2015. ISSN 07431619.

REDDY, Chethan R.; RAZMARA, Meysam; SHAHBAKHTI, Mahdi; ROBINETT, Rush D. Optimal Exergy-wise Predictive Control for a Combined MicroCSP and HVAC System in a Building. **American Control Conference (ACC) Proceedings**, p. 235–240, 2019.

REDDY, Chethan R.; SHAHBAKHTI, Mahdi; ROBINETT, Rush D.; RAZMARA, Meysam. Exergy-wise predictive control framework for optimal performance of MicroCSP systems for HVAC applications in buildings. **Energy Conversion and Management**, Elsevier Ltd, v. 210, p. 112711, Apr. 2020. ISSN 01968904.

ROMERO, José Carlos; LINARES, Pedro. Exergy as a global energy sustainability indicator. A review of the state of the art. **Renewable and Sustainable Energy Reviews**, Elsevier, v. 33, p. 427–442, 2014. ISSN 13640321.

ROSEN, Marc A. Can exergy help us understand and address environmental concerns? **Exergy, An International Journal**, 2002. ISSN 11640235.

SALAHSHOOR, Karim; ASHERI, M. H. A new exergy-based model predictive control methodology for energy assessment and control. **Journal of Natural Gas Science and Engineering**, Elsevier B.V, v. 21, p. 489–495, 2014. ISSN 18755100.

SALAZAR, William Chicaiza; MACHADO, Diogo Ortiz; GALLEGO, Antonio Javier; GONZALEZ, Juan Manuel Escaño; ALBA, Carlos Bordons; ANDRADE, Gustavo Artur de; NORMEY-RICO, Julio Elias. Neuro-Fuzzy Digital Twin of a High Temperature Generator. **IFAC-PapersOnLine**, Elsevier, v. 55, p. 466–471, 9 Jan. 2022. ISSN 2405-8963.

SANGI, Roozbeh; FUETTERER, Alexander Kuempel Johannes; MUELLER, Dirk. A linear model predictive control for advanced building energy systems. **2017 25th Mediterranean Conference on Control and Automation, MED 2017**, p. 496–501, 2017.

SANGI, Roozbeh; KÜMPEL, Alexander; MÜLLER, Dirk. Real-life implementation of a linear model predictive control in a building energy system. **Journal of Building Engineering**, Elsevier Ltd, v. 22, p. 451–463, Mar. 2019. ISSN 23527102.

SANGI, Roozbeh; MÜLLER, Dirk. A novel hybrid agent-based model predictive control for advanced building energy systems. **Energy Conversion and Management**, Elsevier Ltd, v. 178, p. 415–427, Dec. 2018. ISSN 01968904.

SANGI, Roozbeh; MÜLLER, Dirk. Application of the second law of thermodynamics to control : A review. **Energy**, Elsevier Ltd, v. 174, p. 938–953, 2019. ISSN 0360-5442.

SAYADI, Saeed; TSATSARONIS, George; MOROSUK, Tatiana; BARANSKI, Marc; SANGI, Roozbeh; MÜLLER, Dirk. Exergy-based control strategies for the efficient operation of building energy systems. **Journal of Cleaner Production**, 2019. ISSN 09596526.

SCIUBBA, Enrico. Beyond thermoeconomics? The concept of Extended Exergy Accounting and its application to the analysis and design of thermal systems. **Exergy, An International Journal**, Elsevier BV, v. 1, n. 2, p. 68–84, Jan. 2001. ISSN 11640235.

SCIUBBA, Enrico; WALL, Göran. A brief commented history of exergy from the beginnings to 2004. **International Journal of Thermodynamics**, v. 10, n. 1, p. 1–26, 2007. ISSN 13019724.

TRINKLEIN, Eddy H.; PARKER, Gordon G.; MCCOY, Timothy J. Modeling, optimization, and control of ship energy systems using exergy methods. **Energy**, Elsevier Ltd, v. 191, p. 116542, Jan. 2020. ISSN 03605442.

TSATSARONIS, Georgios; WINHOLD, Michael. Exergoeconomic analysis and evaluation of energy-conversion plants-I. A new general methodology. **Energy**, Pergamon, v. 10, n. 1, p. 69–80, Jan. 1985. ISSN 03605442.

UNDP, United Nations Development Program. **Sustainable Development Goals**. 26 Nov. 2019. Available from: `https://www.undp.org/content/undp/en/home/sustainable-development-goals.html`.

UNITED Nations. **Paris Agreement - United Nations Treaty Collection, Chapter XXVII 7. d**, 2015.